

https://dspace.org/

# Synthesis and characterization of zn(ii) and co(ii) pyrrole-aldiminato complexes and their catalytic activity in carbon dioxide/ carbon disulphide coupling with propylene oxide

**Mapetla, Sabetha Makoma**

**2021**

https://hdl.handle.net/10539/36639

Downloaded from a DSpace repository. https://dspace.org/

**Molecular Science Institute, School of Chemistry**
**University of the Witwatersrand**

# Synthesis and Characterization of Zn(II) and Co(II) Pyrrole-aldiminato Complexes and their Catalytic activity in Carbon Dioxide/ Carbon Disulphide Coupling with Propylene Oxide

By: Sabetha Makoma Mapetla
Student number: 604060

A research Dissertation submitted to the Faculty of science, University of the Witwatersrand, in Partial fulfilment of the Requirement for the Degree. Master of Science (MSc) in Chemistry

By: Sabetha Makoma Mapetla

604060

Signature: Date: 22 October 2021

Student: Miss S.M Mapetla

Signature: Date: 22 October 2021

Supervisor: Dr J.L van Wyk

## ABSTRACT

Pyrrole-aldimine ligands **L1** – **L4** were successfully prepared following the Schiff base condensation reaction using the respective primary amines with pyrrole-2-carboxaldehyde. The ligands were isolated as powders and the yields were in the range 75 % - 95%. The neutral ligands were then used in the preparation of their respective bis-(pyrrole-aldiminato) Zn(II) and Co(II) complexes, **C1** – **C4** and **C5** – **C8**, respectively. The Zn(II) and Co(II) complexes were isolated as solids with varying consistencies and low yields in the range 30 % - 60 %. The ligands and their respective bis-(pyrrole-aldiminato) Zn(II) and Co(II) complexes were characterized using $^{1}$H NMR, $^{13}$C NMR, 2D NMR, FT-IR and UV-Vis spectroscopy. Mass spectrometry and elemental analysis were also used. The bis-(pyrrole-aldiminato) Co(II) complexes were not characterized by NMR spectroscopy due to their paramagnetic nature. The catalytic activity of the Zn(II) and Co(II) complexes was evaluated in the coupling of $CS_2$ and PO. **C1** was used to establish the baseline reaction conditions for this coupling reaction, which were then applied in screening the activity of all 8 metal complexes. In the absence of a co-catalyst and solvent-less conditions, **C1** was found to show no activity for the coupling of $CS_2$ and PO at room temperature over 24 hours. The introduction of co-catalysts (TBAC, DMAP, [PPN]Cl and MeIm) under the same reaction conditions resulted in the formation of a mixture of 3 cyclic products, which were identified as 5-methyl-1,3-oxathiolane-2-thione, 4-methyl-1,3-dithiolane-2-thione and 5-methyl-1,3-oxathiolan-2-one, with the highest conversion rate being 2.32 % for **C1**/TBAC. In the presence of MeOH, **C1**/MeIm resulted in the highest conversion rate and MeOH on its own resulted in the lowest conversion rate. These were found to be 61 % and 3.80 % respectively. Although a drastic improvement in catalytic activity was observed compared to when the reactions were carried out neat, a coupling product different to products obtained for neat reactions which was identified to be a methoxylated species of 4-methyl-1,3-dithiolane-2-thione was obtained as the major product. It was shown that after 6 hours, the selectivity for the methoxylated species of 4-methyl-1,3-dithiolane-2-thione is hampered as signals suggesting the presence of an additional cyclic product which could not be qualified were observed in the $^{1}$H-NMR spectrum. The intensity of the additional signals was observed to increase with an increase in reaction time. The conversion rate was seen to increase with an increase in reaction time. The catalytic activity of all 8 metal complexes was then evaluated in the coupling of $CO_2$/PO under mild conditions over 12 hours. **C5**/[PPN]Cl showed the highest activity, with a conversion rate of 1.05 % and **C2**/[PPN]Cl resulted in the lowest conversion rate of 0.27 %. This was found to be lower than that achieved with [PPN]Cl on its own and under the same reaction conditions, which was 0.38 %. Increasing the reaction

time to 24 hours and increasing the pressure to 25 bar of $CO_2$ resulted in a slight increase in conversion rate, however not by a significant margin. The addition of organic solvents was shown to impede the activity of **C5**/[PPN]Cl in this coupling process. The influence of ligand architecture on the catalytic activity of the Zn(II) and Co(II) complexes could not be established and this was attributed to their differences in degrees of stability in solution.

## DECLARATION

I declare that the thesis "S*ynthesis and characterization of Zn(II) and Co(II) pyrrole-aldiminato complexes and their catalytic activity in carbon dioxide/ carbon disulphide coupling with propylene oxide*" is my own work, and that it has not been submitted for any degree in any other university before, and that any sources used or quoted have been indicated and acknowledged as complete references.

Signature: 

Date: 22 October 2021

## ACKNOWLEDGEMENTS

I would like to thank Dr Juanita van Wyk for entrusting me with a research project of this magnitude and for her guidance throughout the course of this project. I would like to thank my mother for her continuous emotional and financial support. I would like to extend my deepest gratitude to my siblings for their encouragement throughout the duration of this project. Many thanks to the University of the Witwatersrand and the school of chemistry for granting me the opportunity to pursue my MSc at this institution. lastly, I would like to thank the NRF for their financial support.

## TABLE OF CONTENTS

Abstract……..…. ii
Declaration……... iii
Acknowledgements……..... iv
Table of contents……..... v
List of figures……vi
List of schemes…….…... ix
List of tables……xi
Abbreviations…….…. xii
Symbols……xv

**Chapter 1:** *Catalytic carbon dioxide coupling with propylene oxide: An overview*
**Chapter 2:** *Synthesis and characterization of pyrrole-aldimine ligands*
**Chapter 3:** *Synthesis and characterization of bis-(pyrrole-aldiminato) Zn(II) and Co(II) complexes*
**Chapter 4:** *Evaluation of the catalytic activity of Bis-(pyrrole-aldiminito) Zn(II) and Co(II) complexes for the coupling of carbon dioxide/ carbon disulphide with propylene oxide*
**Chapter 5:** *Summary*

## LIST OF FIGURES

### Chapter 1

**Figure 1.1:** Cyclic carbonates; a. ethylene carbonate (EC), b. propylene carbonate (cPC), c. diphenyl carbonate (DPC)…… 3

**Figure 1.2:** Double metal cyanide complex for the coupling of carbon dioxide and propylene oxide…… 17

**Figure 1.3:** Zinc(II) phenoxide catalysts for the copolymerization of $CO_2$ and epoxides…… 18

**Figure 1.4:** Homogeneous chromium salen complexes as catalysts in the coupling reaction of carbon dioxide and epoxides……19

**Figure 1.5:** Heterogeneous chromium salen complexes as catalysts in the coupling reaction of carbon dioxide and epoxides……20

**Figure 1.6:** Aluminium tetraphenylporphyrin catalyst for the coupling of propylene oxide and carbon dioxide.…… 21

**Figure 1.7:** Tetraphenylporphinatoaluminum chloride catalyst for the coupling of propylene oxide and carbon dioxide……..22

**Figure 1.8:** Highly efficient Cr(III) salen complexes as catalysts for the coupling reaction of epoxides with carbon dioxide……... 23

**Figure 1.9:** Highly active bifunctional Salen(AlX) catalysts for the coupling reaction of epoxides with carbon dioxide...…… 23

**Figure 1.10:** Novel salphen Co(III) complexes for the copolymerization of epoxides with $CO_2$ 24

**Figure 1.11:** New zinc catalysts based on $N_4$-chelating ligands for the coupling reaction of epoxides with carbon dioxide……... 25

**Figure 1.12:** Novel titanium complexes comprising of two non-symmetric bidentate pyrrole-imine chelate ligands…… 26

**Figure 1.13:** Palladium(II) complexes bearing non-symmetric bidentate pyrrole-iminato chelate ligands.…… 27

**Figure 1.14:** Vanadium complexes comprising of iminopyrrolide chelating ligand..……..27

**Figure 1.15:** Aluminum alkyl complexes supported by pyrrole-aldimine ligands.....……..28

**Figure 1.16:** Bis(pyrrole-aldiminato)aluminum methyl complexes……29

### Chapter 2

**Figure 2.1** Schiff base compound general structure……37

**Figure 2.2** Pyrrole-aldiminato and salicylaldiminato metal complexes general structure..…... 37

**Figure 2.3** $^1$H NMR spectrum for pyrrole-aldimine ligand **L1**……42

**Figure 2.4** COSY spectrum for pyrrole-aldimine ligand **L1**..... 46
**Figure 2.5** NOESY spectrum for ligand pyrrole-aldimine ligand **L1**.....47
**Figure 2.6** $^{13}$C NMR spectrum for pyrrole-aldimine ligand **L1**..48
**Figure 2.7** HSQC spectrum for pyrrole-aldimine ligand **L1**..... 50
**Figure 2.8** HMBC spectrum for pyrrole-aldimine ligand **L1**..... 51
**Figure 2.9** FT-IR spectrum for pyrrole-aldimine ligand **L1**.....52
**Figure 2.10** Electrospray ionization mass spectrum for pyrrole-aldimine ligand **L1**.....53
**Figure 2.11** Mass spectrometry isotopologue pattern for pyrrole-aldimine ligand **L1**.....53
**Figure 2.12** UV-Vis spectra for pyrrole-aldimine ligands **L1**, **L2**, **L3** and **L4**.....54

**Chapter 3**

**Figure 3.1** Iminoalkyl bis(pyrrole-aldiminato) metal complexes of Co, Ni, Pd, Cu and Zn.....63
**Figure 3.2** $^{1}$H NMR spectrum for the sodium ligand salt of pyrrole-aldimine ligand **L1**.....64
**Figure 3.3** $^{1}$H NMR spectrum for bis-(pyrrole-aldiminato) Zn(II) complex **C1**.....67
**Figure 3.4** COSY spectrum for bis-(pyrrole-aldiminato) Zn(II) complex **C1**.....70
**Figure 3.5** NOESY spectrum for bis-(pyrrole-aldiminato) Zn(II) complex **C1**.....71
**Figure 3.6** $^{13}$C NMR spectrum for bis-(pyrrole-aldiminato) Zn(II) complex **C1**.....73
**Figure 3.7** HSQC spectrum for bis-(pyrrole-aldiminato) Zn(II) complex **C1**.....76
**Figure 3.8** HMBC spectrum for bis-(pyrrole-aldiminato) Zn(II) complex **C1**.....77
**Figure 3.9** FT-IR spectra for ligand **L1**, metal complexes **C1** and **C5**.....79
**Figure 3.10** Full mass spectrum for bis-(pyrrole-aldiminato) Zn(II) complex **C1**.....80
**Figure 3.11** Expanded mass spectrum for bis-(pyrrole-aldiminato) Zn(II) complex **C1**.....80
**Figure 3.12** Full mass spectrum for bis-(pyrrole-aldiminato) Co(II) complex **C5**.....81
**Figure 3.13** Expanded mass spectrum for bis-(pyrrole-aldiminato) Co(II) complex **C5**.....82
**Figure 3.14** Stacked UV-Vis spectra for ligand L1 and bis-(pyrrole-aldiminato) Zn(II) and Co(II) complexes, **C1** and **C5**.....83
**Figure 3.15 Stacked** UV-Vis spectra showing the decline in the LMCT band for. bis-(pyrrole-aldiminato) Co(II) complex, **C7** with time.....84
**Figure 3.16** UV-Vis spectrum showing the d-d band for bis-(pyrrole-aldiminato) Co(II) complex, **C7**.....84

**Chapter 4**

**Figure 4.1** Salen- Al(III), Cr(III) and Co(III) complexes for the coupling of carbon disulphide and epoxides……96

**Figure 4.2** Bis-(pyrrole-aldiminato) Zn(II) and Co(II) complexes…… 98

**Figure 4.3** $^{1}$H NMR spectrum of the residue obtained using **C1** as a catalyst in the coupling of $CS_2$/PO in the absence of a co-catalyst (Entry **1**, **Table 4.1**)……..…99

**Figure 4.4** Aluminium salen complex for the coupling of propylene oxide and carbon disulphide…….… 100

**Figure 4.5** Representative $^{1}$H NMR spectrum for the yellow oil-like products obtained in investigating effect of co-catalysts (Entry **2**, **Table 2.1**)…..……102

**Figure 4.6** Effect of co-catalysts on conversion rate in the coupling of carbon disulphide and propylene oxide…… 103

**Figure 4.7** $^{1}$H NMR spectrum for the yellow oil-like products obtained using **C1** and TBAC for $CS_2$/PO coupling with MeOH as solvent, (Entry **2**, **Table 4.2**)……104

**Figure 4.8** Methoxylated species of 4-methyl-1,3-dithiolane-2-thione (**a**), 5-methyl-1,3-dithiolane-2-thione (**b**) and 4-methyl-1,3-oxathiolan-2-one (**c**)……105

**Figure 4.9** Solvent effect on the conversion rate in the coupling of carbon disulphide and propylene oxide…… 107

**Figure 4.10** Stacked $^{1}$H NMR spectra obtained for the yellow oil-like products obtained in the time study……. 108

**Figure 4.11** $^{1}$H NMR spectrum for the reaction residue obtained in using **C1** and [PPN]Cl in $CS_2$/$CO_2$ coupling using 0.5 mL MeOH for 6 hours (Entry **1**, **Table 4.4**)……..…110

**Figure 4.12** Effect of solvent volume on conversion rate in the coupling of carbon disulphide and propylene oxide……..….111

**Figure 4.13** Effect of catalyst in the coupling of carbon disulphide and propylene oxide……..…112

**Figure 4.14** $^{1}$H NMR spectrum for the reaction residue obtained in using **C5** and [PPN]Cl in carbon dioxide and propylene oxide coupling for 12 hours (Entry **6**, **Table 4.6**) ……115

**Figure 4.15** Effect of catalyst in the coupling of carbon dioxide and propylene oxide……116

**Figure 4.16** $^{1}$H NMR spectrum for the reaction residue obtained in using **C5** and [PPN]Cl in PO/$CO_2$ coupling for 12 hours (Entry **2**, **Table 4.6**) ……118

**Figure 4.17** $^{1}$H NMR spectrum for the reaction residue obtained in using **C5** and [PPN]Cl in PO/$CO_2$ coupling for 24 hours (Entry **3**, **Table 4.8**……...119

**Figure 4.18** Effect of solvent in the coupling of carbon dioxide and propylene oxide..……..…120

## LIST OF SCHEMES

**Chapter 1**

**Scheme 1.1** Synthesis of dimethyl carbonate from the transesterification of propylene carbonate with methanol……..…….. 4
**Scheme 1.2** Synthesis of propylene carbonate from phosgene and propylene glycol……..…. 5
**Scheme 1.3** Synthesis of propylene carbonate from the oxidative carboxylation of olefins; a. two-step, b. one-step reaction……... 5
**Scheme 1.4** Synthesis of propylene carbonate from propylene glycol and carbon dioxide.…….. 6
**Scheme 1.5** Synthesis of propylene carbonate from propylene glycol and urea…… 7
**Scheme 1.6** The coupling of carbon dioxide and propylene oxide…… 7
**Scheme 1.7** Proposed mechanism for the coupling of propylene oxide and carbon dioxide to yield propylene carbonate……. 8
**Scheme 1.8** Synthesis of poly(propylene carbonate)…… 13
**Scheme 1.9** Proposed mechanism for the synthesis of PPC……. 15
**Scheme 1.10** Formation of cyclic carbonates through alkoxide back-biting and carbonate back-biting of poly(propylene carbonate)…….. 16

**Chapter 2**

**Scheme 2.1** Synthetic scheme for pyrrole-aldimine ligand **L1**……. 39
**Scheme 2.2** General synthetic scheme for pyrrole-aldimine ligands **L2** – **L4**……. 40

**Chapter 3**

**Scheme 3.1** Preparation of sodium ligand salts of pyrrole-aldimine ligands **L1** – **L4**……... 65
**Scheme 3.2** General synthetic scheme for the preparation of bis-(pyrrole-aldiminato) Zn(II) and Co(II) metal complexes **C1** – **C8**…… 65

**Chapter 4**

**Scheme 4.1** The coupling of propylene oxide and carbon disulphide to yield either the polymeric or cyclic product……. 94
**Scheme 4.2** The coupling of carbon dioxide and propylene oxide to yield propylene carbonate and poly(propylene carbonate).…… 95
**Scheme 4.3** Formation of cyclic products from the coupling of propylene oxide and carbon disulphide……. 95

**Scheme 4.4** Proposed mechanism for the formation of the methanol adducts of-methyl-1,3-oxathiolane-2-thione, 4-methyl-1,3-dithiolane-2-thione and 5-methyl-1,3-oxathiolan-2-one…. 106

## LIST OF TABLES

### Chapter 2

**Table 2.1** $^{1}$H NMR data for ligands **L1** – **L4**……44
**Table 2.2** $^{13}$C NMR data for ligands **L1** – **L4**...……49
**Table 2.3** UV/Vis spectroscopy data for pyrrole-aldimine ligands **L1** – **L4**.……55
**Table 2.4** Yield, HR-MS, FT-IR and elemental analysis data for ligands **L1** – **L4**.……56

### Chapter 3

**Table 3.1** $^{1}$H NMR data for metal complexes **C1** – **C4**.……68
**Table 3.2** $^{13}$C NMR data for metal complexes **C1** – **C4**.……74
**Table 3.3** UV/Vis data for metal complexes **C1** – **C8**.……85
**Table 3.4** HR-MS, FT-IR and elemental analysis data for metal complexes **C1** – **C8**.……86

### Chapter 4

**Table 4.1**: Effect of co-catalyst in the coupling of $CS_2$ and PO reaction data……101
**Table 4.2** Effect of solvent in the coupling of $CS_2$ and PO reaction data.……105
**Table 4.3** Effect of reaction time in the coupling of $CS_2$ and PO reaction data.……109
**Table 4.4** Effect of solvent volume in the coupling of $CS_2$ and PO reaction data.……110
**Table 4.5** Effect of catalyst in the coupling of $CS_2$ and PO reaction data.……113
**Table 4.6** Effect of catalyst in the coupling of PO/$CO_2$ reaction data……117
**Table 4.7** Effect of increasing reaction time in the coupling of carbon dioxide and propylene oxide reaction data……118
**Table 4.8** Effect of solvent in the coupling of $CO_2$/PO reaction data……121
**Table 4.9** Effect of $CO_2$ pressure in the coupling of $CO_2$/PO reaction data……...122

## ABBREVIATIONS

| | |
|---|---|
| $^{1}H$ | Proton |
| $^{13}C$ | Carbon-13 |
| 2D | Two dimensional |
| Al | Aluminium |
| alt-PPC | Alternating poly(propylene carbonate) |
| APC | Aliphatic polycarbonate |
| Atm | Atmosphere |
| B.M | Bohr magneton |
| Br | Bromine |
| C1 | Chlorine |
| $CDCl_3$ | Deuterated chloroform |
| CHO | Cyclohexene oxide |
| $cm^{-1}$ | Per centimetre |
| Co | Cobalt |
| $CoCl_2$ | Cobalt chloride |
| $CO_2$ | Carbon dioxide |
| $CS_2$ | Carbon disulphide |
| COSY | Homonuclear correlation spectroscopy |
| cPC | Cyclic propylene carbonate |
| Cr | Chromium |
| Da | Dalton |
| DCM | Dichloromethane |
| DMAP | Dimethylaminopyridine |
| DMC | Dimethyl carbonate |
| DMF | Dimethylformamide |
| DMSO | Dimethyl sulphoxide |
| DMSO-d6 | Deuterated dimethylsulphoxide |
| DOX | Doxorubicin |
| DPC | Diphenyl carbonate |
| EC | Ethylene carbonate |
| ESI-MS | Electro spray ionization mass spectrometry |
| Et | Ethyl |

| | |
|---|---|
| Fe | Iron |
| FT-IR | Fourier transform infrared |
| h | Hour |
| $H_2$ | Hydrogen gas |
| HCl | Hydrochloric acid |
| HMBC | Heteronuclear Multiple Bond Correlation |
| HSQC | Heteronuclear single quantum coherence |
| i-Pr | Isopropyl |
| Kg | Kilograms |
| M | Metal |
| Me | Methyl |
| MeIm | Methylimidazole |
| MeOH | Methanol |
| min | Minute |
| mg | Milligram |
| Mg | Magnesium |
| mol | Mole |
| Mn | Number average molecular weight |
| Mpa | Mega pascals |
| MS | Mass spectrometry |
| m/z | Mass-to-charge ratio |
| NaH | Sodium hydride |
| nm | Nanometres |
| NMR | Nuclear magnetic resonance |
| NOESY | Nuclear Overhauser Effect |
| PDI | Polydispersity index |
| PEG | Poly(propylene glycol) |
| PO | Propylene oxide |
| PPC | Poly(propylene carbonate) |
| [PPN]Cl | Bis(triphenylphosphine)iminium chloride |
| TBAB | Tetrabutylammonium bromide |
| TBAC | Tetrabutylammonium chloride |
| Ti | Titanium |

| | |
|---|---|
| Tg | Glass transition temperature |
| TGA | Thermogravimetric analysis |
| THF | Tetrahydrofuran |
| TOF | Turn over frequency |
| ROP | Ring opening polymerization |
| tpp | Tetraphenylporphyrin |
| UV-Vis | Ultraviolet visible |
| Zn | Zinc |
| ZnEt2 | Diethyl zinc |
| Zno | Zinc oxide |

## SYMBOLS

| | |
|---|---|
| ʎmax | Absorption maximum |
| δ | Chemical shift |
| °C | Degrees Celsius |
| > | Greater than |
| Δ | Heat |
| < | Less than |
| % | Percentage |

# Catalytic carbon dioxide coupling with propylene oxide: An overview

CONTENT

1.1 INTRODUCTION……..2
1.2 AN OVERVIEW OF CYCLIC CARBONATES..……3
1.2.1 Applications of propylene carbonate……3
1.3 AN OVERVIEW OF ALIPHATIC CARBONATES.…….……...8
1.3.1 Properties of poly(propylene carbonate).……..9
1.3.2 Applications of poly(propylene carbonates……..11
1.3.3 Synthetic routes to the formation of poly(propylene carbonate)…..……13
1.4 TRANSITION METAL COMPLEXES AS CATALYSTS FOR THE COUPLING OF CARBON DIOXIDE AND PROYLENE OXIDE..…….……...16
1.4.1 Heterogenous catalysts for carbon dioxide and propylene oxide coupling……17
1.4.2 Homogeneous catalysts for carbon dioxide and propylene oxide coupling..……20
1.5 PYROLLE-ALDIMINITO COMPLEXES IN CATALYIC PROCESSES.…..……25
1.6 PROBLEM STATEMENT…… 29
1.7 AIMS AND OBJECTIVES……30
1.8 REFERENCES……...31

## 1.1 INTRODUCTION

Sustainable chemistry, which can be defined as the reduction or complete elimination of the negative impact the chemical industry has on the natural environment is a concept that research interest is increasingly leaning towards [1]. The accumulation of waste and hazardous chemicals in the natural environment has motivated researchers and the chemical manufacturing industry to consider green alternatives to conventional methods which contribute to the destruction of the environment. This has seen research efforts being directed towards achieving synthetic goals following green chemistry protocols. One example of sustainable chemistry is the utilization of feedstocks such as carbon dioxide ($CO_2$) in the formation of value added products [2].

There are many ways in which the green character of a chemical product can be improved and one of which is replacing non-sustainable starting reagents with more sustainable alternatives. What makes $CO_2$ an attractive one carbon (C1) feed stock is its abundance. The burning of fossil fuels is known as one of the leading contributors in the emission and accumulation of $CO_2$ in the atmosphere [3]. The rate at which carbon dioxide is emitted far outweighs the rate at which it is utilized. As such, the amount of carbon dioxide present in the atmosphere is constantly increasing. Although the use of $CO_2$ in chemical manufacturing processes is not capable of reducing $CO_2$ levels in the environment, it is worth exploring chemical processes that can add value to $CO_2$.

$CO_2$ is a cheap, renewable and non-toxic C1 feedstock. However, it suffers from poor reactivity as it is the most oxidized form of carbon. This can be overcome by pairing it with energy rich cyclic ether substrates such as isobutylene oxide, cycloheptene oxide, cyclopentene oxide, cyclohexene oxide, as well as with other cyclic oxides. The resulting product can either be polycarbonates or the respective cyclic carbonates. This is dependent on the reaction conditions and type of catalyst used in the coupling reaction [4]. Both classes of products are valuable intermediates in chemical manufacturing processes. Polycarbonates find uses in the production of biodegradable plastic materials, which are potential replacements for non-biodegradable plastic materials that are currently widely used [5]. Due to their biodegradability and low toxicity, cyclic carbonates are attractive alternatives to traditional polar aprotic solvents [6].

This chapter is a review of the coupling of $CO_2$ and epoxides. It covers the history and strides that have been made since its inception by looking at various catalyst systems that have been

developed and optimized for this process. Although there is a variety of epoxides that have been coupled with $CO_2$ to produce either the respective polycarbonates, cyclic carbonates or a mixture of both, this chapter will be focused specifically on carbonates derived from PO, as they are the most common and this study focuses on PO.

## 1.2 AN OVERVIEW OF CYCLIC CARBONATES

Cyclic carbonates are a class of compounds related to esters. They can be classified as either organic or inorganic. The three industrially viable cyclic carbonates are; diphenyl carbonate (DPC), ethylene carbonate (EC) and propylene carbonate (cPC) illustrated in (**Figure 1.1**) [7]. Due to their varying properties, they have a variety of uses and have the potential to be used in a wide range of applications. DPC finds uses as an additive in lithium-ion batteries [8]. Similar to cPC, EC is a polar aprotic solvent that finds uses as a plastisizer, a component in lithium ion batteries and as a monomer in ring opening polymerization reactions to produce linear carbonates [9]. cPC and EC are the most used cyclic carbonates with cPC in particular being known for its attractive properties that include low toxicity, low vapour pressure and a high flash point. As such, it has the potential to replace harmful polar aprotic solvents such as dimethylformamide (DMF) and acetonitrile in the synthesis of commercially viable products following green chemistry protocols [10]. As a solvent, cPC can also be used as a paint stripper for cleaning or as a degreasing agent.

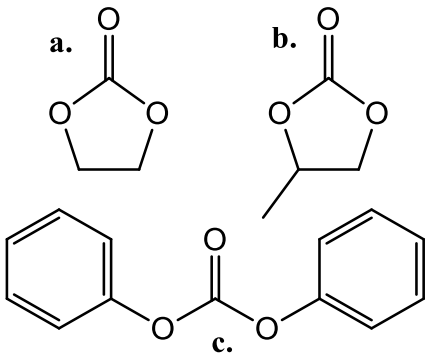



**Figure 1.1** *Cyclic carbonates; a. ethylene carbonate (EC), b. propylene carbonate (cPC), c. diphenyl carbonate (DPC)* [7]

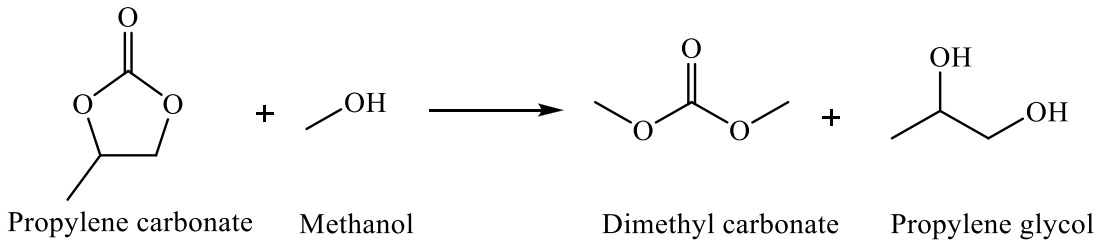
### 1.2.1 Applications of propylene carbonate

cPC has a high dielectric constant, which allows it to act as a high-permittivity component of electrolytes in lithium batteries. It has the potential to be used in lithium-ion batteries because of its high polarity, which is responsible for creating an effective solvation shell around lithium

ions. The consequence of this is the creation of a conductive electrolyte. At present, cPC is not used in lithium-ion batteries because it is destructive to graphite [11].

The solvency power of cPC makes it an ideal solvent for the removal of $CO_2$ from synthesis gas and natural gas in the Fluor solvent process. For this process to be efficient, hydrogen disulphide should not be present as the gas removal process shows greater selectivity for $HS_2$ over $CO_2$ [12]. In order to increase analyte charging in electrospray ionization mass spectrometry, cPC is doped into low surface tension solutions [13]. The low toxicity of cPC enables it to be used as a thickener in cosmetics and personal care products [14].

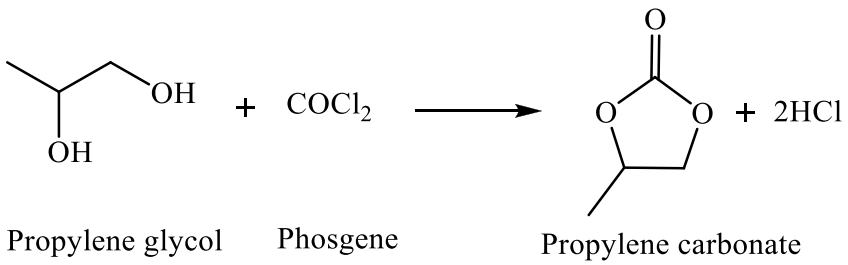
cPC is used in the transesterification process with methanol to produce dimethyl carbonate (DMC) (**Scheme 1.1**). DMC has many attractive properties, one of which is its non-toxicity. It finds uses as a methylating agent, which can be used in place of dimethyl sulphate and phosgene, known for their corrosiveness and high-toxicity. DMC also has the potential to be used as a fuel additive. However, its large scale usage is hampered by the high cost associated with its production [15]. In order to make DMC commercially viable for this particular application, its production cost would need to be reduced by at least 30 %. The reduction in the production cost of the starting material cPC can help achieve that.



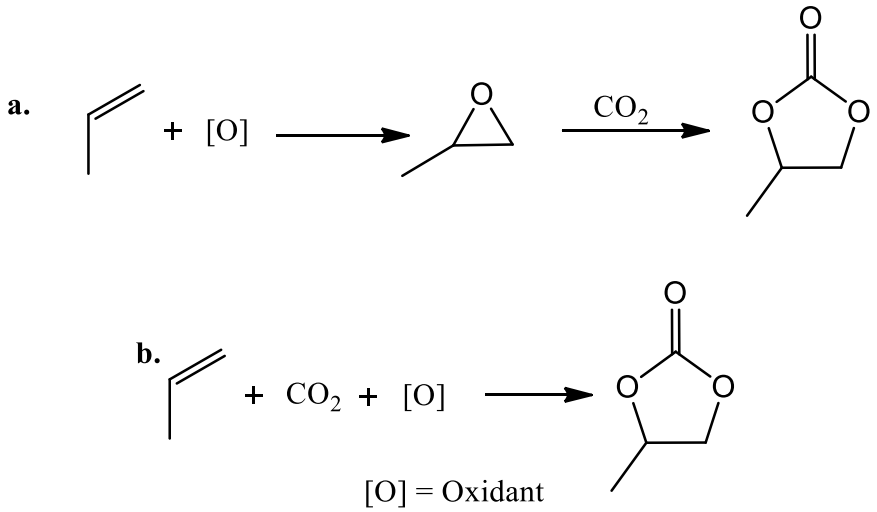

**Scheme 1.1** *Synthesis of dimethyl carbonate from the transesterification of propylene carbonate with methanol* [15]

There are a number of ways in which cPC can be prepared. These include the phosgenation method, direct oxidation of olefins with $CO_2$, transesterification of propylene glycol with DMC, from propylene glycol and $CO_2$ and a new route that makes use of propylene glycol and urea.

The phosgenation method is simple and affords cPC under mild reaction conditions (**Scheme 1.2**) [16]. It makes use of phosgene, which is known to be toxic and the disposal of the corrosive HCl by-product is an environmental concern. These drawbacks in addition to the poor selectivity for cPC in the reaction makes this method undesirable for large scale applications.




**Scheme 1.2** *Synthesis of propylene carbonate from phosgene and propylene glycol* [16]

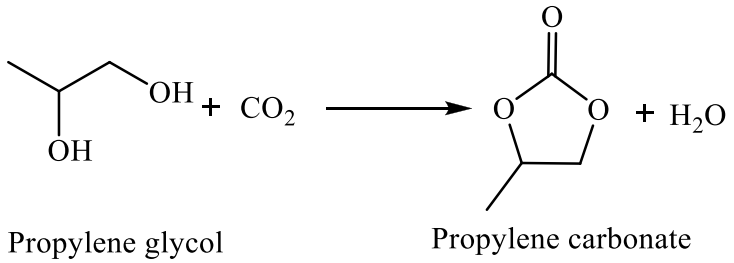



**Scheme 1.3** *Synthesis of propylene carbonate from the oxidative carboxylation of olefins; a. two-step, b. one-step reaction* [17]

The oxidative carboxylation of olefins to produce cPC can either proceed by a one-step (**Figure 4.a**) or two-step one-pot (**Figure 1.3 b**) reaction. The two-step reaction begins with the oxidation of the alkene to yield PO, which is then followed by the cycloaddition of $CO_2$ to yield cPC. This is very similar to the coupling of $CO_2$ and PO to produce cPC, the only difference is that this reaction avoids the work-up step that comes with first separately preparing the epoxide, prior to carrying out the cycloadding of $CO_2$ [17]. Although this route to cPC is environmentally friendly, it is not economical as some of the oxidants used in the alkene epoxidation step are very expensive. These include iodosobenzene, tetrabutyl-hydro

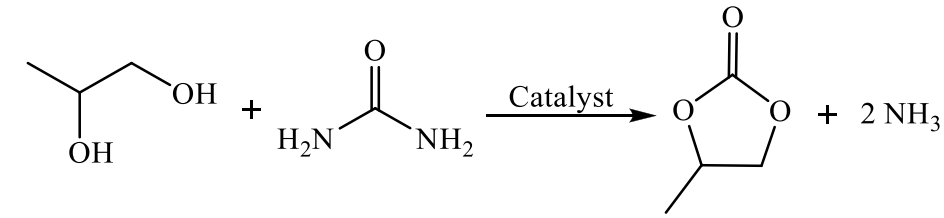
peroxide and peroxy acetic acid. The few homogeneous and heterogenous catalysts that have been evaluated for this reaction suffer from a number of issues. These include poor activity, require harsh reaction conditions, short-lifetime and difficulty with separation [17].

The first mention of the synthesis of cPC from PG and $CO_2$ as depicted in (**Scheme 1.4**) was reported in 2004 by Tomishige *et al*. This reaction was catalysed by a ceria based catalyst. In this reaction, low yields were obtained as a result of the equilibrium state reached because of the $H_2O$ produced. In the reaction, a mixture of cPC, the co-polymer- PPC and other side-products were expected. However, this was not the case as the $CeO_2$–$ZrO_2$ catalyst showed high selectivity towards the production of cPC. Although the catalyst showed high selectivity for PC, low yields remain a concern [18].



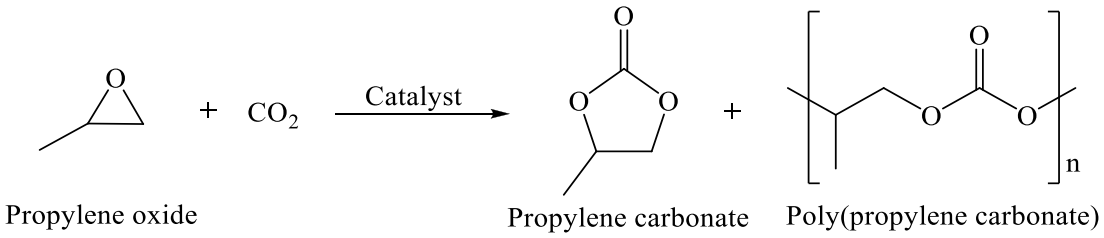

**Scheme 1.4** *Synthesis of propylene carbonate from propylene glycol and carbon dioxide* [18]

The synthesis of cPC using urea and propylene glycol (**Scheme 1.5**) is carried out in the presence of a suitable catalyst, typically a metal oxide catalyst. This is a multistep reaction with multiple side reactions. This route makes use of relatively reasonable reaction conditions and easily accessible raw materials, making it an affordable way to produce cPC. In addition to this, the by-product ammonia can be used in the production of the starting reagent, urea. Although promising, the commercialization of this route to cPC is limited by a number of factors. These include cost associated with extra consumption of energy with having to assemble vacuum equipment as the reaction is carried out under reduced pressure. Another drawback to this route to cPC is the need to use PG in excess. An increase in PG to urea ratio was shown to increase the yield of cPC. However, having PG in high excess is undesirable for industry as this means loss of raw material in addition to a tedious separation process [19].



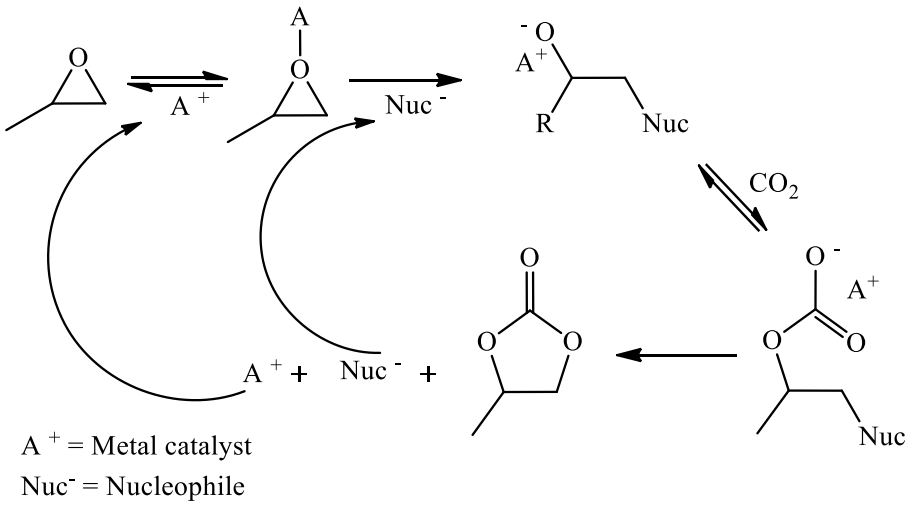

**Scheme 1.5** *Synthesis of propylene carbonate from propylene glycol and urea* [19]

A more environmentally benign and atom economical route to afford cPC is via the coupling reaction of PO and $CO_2$, in the presence of a suitable catalyst system (**Scheme 1.6**). This reaction was pioneered by Inoue *et al*. in the late 1960's using heterogeneous zinc catalysts in organic solvents [20]. Since then, a great deal of studies have been dedicated towards improving the efficiency and selectivity of this reaction. The products from this reaction can either be exclusively aliphatic- or cyclic carbonates or a mixture of both. They vary in properties, thereby widening the range of applications they can potentially be used in.




**Scheme 1.6** *The coupling of carbon dioxide and propylene oxide* [20]

The proposed mechanism for the synthesis of cPC is depicted in (**Scheme 1.7**). It begins with the activation of the epoxide by the catalyst. The activation of the epoxide is induced by the epoxide coordinating to the metal catalyst. This is followed by a nucleophilic attack on the least hindered site on the activated epoxide by the catalyst. This results in the ring opening of the activated epoxide leading to the formation of a metal alkoxide intermediate. The cycloaddition of $CO_2$ to the alkoxide intermediate yields an alkylcarbonate anion. The alkylcarbonate anion undergoes carbonate intermolecular cyclic elimination to yield cPC. The key requirement for a nucleophile provided by the catalyst is that it must be a good leaving group as in the final step of the mechanism, the nucleophile is displaced intramolecularly by the carbonate to form the five–membered ring and regenerate the catalyst [21].




**Scheme 1.7** *Proposed mechanism for the coupling of propylene oxide and carbon dioxide to yield propylene carbonate* [21]

cPC can be formed as a side product in the copolymerization of PO and $CO_2$ as depicted in (**Scheme 1.6**) [20]. This usually occurs when the reaction is carried out under forcing conditions, that is; high temperatures and high pressures of $CO_2$. This can also happen as a result of the catalyst showing selectivity for the formation of cPC over the copolymer (PPC). Another way in which cPC can be formed in the copolymerization of PO and $CO_2$ is through alkoxide back-biting (**Scheme 1.11**). This occurs when the reaction is carried out under high temperatures. At temperatures over 150–180 °C, the cyclic product is thermodynamically favoured over the copolymer [22].

## 1.3 AN OVERVIEW OF ALIPHATIC CARBONATES

Aliphatic carbonates (APCs) are polymers with backbones containing repeating carbonate (-O-C(O)-O-) linkages. APCs were first prepared in the 1930s but never rose in popularity when compared to polymers such as polyester and polyamide. Their undesirable low melting points and susceptibility to hydrolysis meant that research efforts were not directed towards studying APCs and their application for commercial purposes was overlooked, as a result [23].

Poly(propylene carbonates) (PPC) in particular, is a thermoplastic material which is soluble in polar solvents, but insoluble in solvents like alcohols, water, and aliphatic hydrocarbons. It is known for its low glass transition temperature ($T_g$) and poor thermal stability [24]. PPC as the product of the alternating copolymerization of PO and $CO_2$ is a broad term used to classify polymers with repeating carbonate linkages as the degree of alternation between PO and $CO_2$

varies. A host of factors in the conditions applied in their preparation is responsible for this variation. Aliphatic carbonates with 10 % or less repeating ether linkages along the polymer backbone are referred to as alternating PPC (alt-PPC).

### 1.3.1 Properties of poly(propylene carbonate)

Studying the physical and chemical properties of polymers is important in determining applications they are best suited for. This is especially important for polymers such as PPC because of the number of factors such as degree of alternation along the polymer backbone, average molecular weight and regioregularity drastically affect the properties of the polymer and hence the applications they can be utilized in. Understanding these properties is also important in the blending or reinforcement of PPC to make composites [25].

Thermal decomposition studies of PPC have revealed that it decomposes to cPC through backbiting or unzipping between 150–180 °C. Higher thermal decomposition values, up to 278 °C have been reported. The broad range of thermal decomposition values is attributed to the degree of PO and $CO_2$ alternation in the polymer backbone and differences in the number-average molecular weight (Mn). The accuracy of values below 200 °C obtained using thermogravimetric analysis (TGA) are questionable because of the poor sensitivity of TGA assessments below that temperature. Anything above 240 °C is also questionable as that is the temperature at which cPC is reported to decompose at [26].

PPC products are known to be similar but never identical as a result of differences in regioregularity in addition to the percentage of ether linkages in the polymer backbone. This is supported by the broad range of glass transition temperatures ($T_g$) reported for PPC products. These values range from 25 °C to about 45 °C. The relation between regioregularity and PPC $T_g$ was highlighted when Quan *et al*. synthesized polymers with 70 – 77% head-to-tail dyads which were reported to have a $T_g$ between 37 – 42 °C [27]. Lu *et al*. synthesized perfectly alternating PPC with more than 95% head-to-tail dyads had a $T_g$ of 40 °C [28]. In summary, the greater the concentration of head-to-tail linkages, the higher the $T_g$.

Chen *et al*. reinforced PPC with glass fibre (GF) and compared the mechanical and thermal properties of pure PPC with those of reinforced PPC at various loadings of GF. The tensile strength of the pure PPC used for this study was determined to be 17.32 MPa. At 20WT% GF loading, a critical point in the tensile strength was reached. It improved by 71.77% to a value

of 29.75 Mpa and beyond this GF loading, the tensile strength started to decrease. The tensile modulus increased with an increase in GF loading, at 10 WT%, a tensile modulus value of 1279 Mpa was obtained, which is an 87 % increase from that determined for pure PPC. Reinforcing PPC with glass fibre increased the hardness of the material, this is seen with the reduction of elongation at break percentage. Whereby, an increase in GF loading resulted in the drastic reduction of that value. This indicates that the incorporation of GF increased both mechanical strength and stiffness [29].

The decomposition of PPC due to the elements has been extensively studied and studies show that the rate of biodegradation is highly dependent on the conditions PPC is subjected to. These studies were conducted in water, soil, in the presences of enzymes and in aqueous solutions as standards. What can be noted is that water plays a crucial role in the biodegradation of PPC because of its poor compatibility with water. It was found that the degradation of PPC in water starts from the surface by erosion.

To study the degradation of PPC in the presence of enzymes, Zhou *et al*. prepared PPC from PO and $CO_2$ adopting a synthetic procedure reported by Inoue *et al*. For the degradation study, films of the copolymer were prepared from chloroform solutions following the solvent casting method. *Rhizopus arrhizus* lipase and *Rhizopus delemar* lipase are the two enzymes that were used as catalysts for the hydrolysis of the copolymer. It was found that PPC prepared from PO and $CO_2$ degrades in the presence of *Rhizopus delemar* lipase at 37°C in an acetate buffer solution, however, in *Rhizopus arrhizus* lipase, hydrolysis cannot be induced [30].

PPC pellets were prepared from PPC synthesized from PO and $CO_2$ to investigate the *in vivo* degradation and toxicity in rats. The pellets were surgically implanted into the peritoneal cavity of the rats after which the incisions were closed. The pellets prepared from PPC showed no degradation even after a period of 2 months. It is suspected that the surface area may have been too small for significant degradation. There were no signs of tissue damage in the area where the pellets were implanted, which suggests that PPC is non-toxic [31].

Kim *et al*. investigated the *in vivo* and *in vitro* degradation of PPC synthesized by the copolymerization of $CO_2$ with PO. The adhesion of bacteria and Hep-2 cells to PPC films was also investigated. To study the mechanism of PPC biodegradation in mice, in vitro oxidative degradation measurements were carried out for PPC films that were treated in an oxidative

solution of 20% hydrogen peroxide ($H_2O_2$) in aqueous 0.1 M cobalt chloride. The *in vivo* experiments were conducted by implanting PPC pellets into the mice. Along with surrounding tissue, the implanted pellets were removed at 1, 4, 8 and 12 weeks after implantation. The results suggest that PPC is biodegradable in mice by surface erosion, which is induced by enzymatic hydrolysis and oxidative degradation processes. Of the five bacterial strains used for the adhesion experiments, *Pseudomonas aeruginosa* and *Enterococcus faecalis* showed the highest levels of adhesion, whereas *Escherichia coli* and *Staphylococcus aureus* had the lowest levels, and *Staphylococcus epidermidis* showed intermediate adhesion. As a result of hydrophobicity and dimensional instability of the surface of the PPC films, there was no adhesion of human cells (cell line Hep-2) to the PPC films [32].

In order to investigate the degradation of PPC films buried in soil, Du *et al.* prepared perfectly alternating PPC form PO and $CO_2$. As a standard, PPC films which were prepared from chloroform solutions were immersed in a buffer solution at pH 6. The PPC films immersed in the buffer solutions showed a more rapid weight loss compared to the films buried in soil after a period of 6 months. For the soil buried PPC films, the weight loss rate was at its highest in the first two months of burial and reached its maximum weight loss value of 6.32% after 6 months exposure [33].

### 1.3.2 Applications of poly(propylene carbonates)

The wide use of PPC at an industrial scale is restricted by its low $T_g$ temperature and poor thermal stability. This is overcome by blending PPC with other materials to achieve properties required for a designated application without adversely hampering its desirable properties. Another way to utilize PPC is by blending it with other polymers. Although this has been shown to improve properties such as toughness and adhesion, it has been found that the mechanical properties of the individual polymers are compromised in the process. In any case, for applications that are not affected by this drawback, the blending of polymers remains an attractive means to achieve a balance in properties for a particular use [34], [35].

Chen *et al*. prepared PPC for the toughening of epoxy thermosets. PPC was used as an initiator for the ring opening copolymerization of ε-caprolactone and PPC to produce the poly(ε-caprolactone)-block-poly(propylenecarbonate)-block-poly(ε-caprolactone) (PCL-PPC-PCL) triblock copolymer. Incorporating 30 wt% PCL-PPC-PCL modifier into the thermoset resulted in an increase of more than 320% and 180% in the tensile elongation and the area under the

stress–strain curves, respectively, when compared to pure epoxy. The results from this study show that PPC is an excellent toughening agent [36].

A PPC/cloisite 20B (clay) nanocomposite was prepared by Khan *et al.* for the detection and quantification of ethanol in the environment. Comparing the thermal and mechanical properties of pure PPC and the nanocomposite, it was observed the thermal decomposition temperature was increased by 43 °C and the $T_g$ increased from 21 to 32 °C. Both elastic modulus and hardness showed a drastic increase from pure PPC to nanocomposite. In terms of sensitivity, PPC on its own is known as a good ethanol sensor, the sensitivity was improved by a factor of 3.24, from 0.2543 mA $cm^{-2}mM^{-1}$ for pure PPC to 0.8231 mA $cm^{-2}mM^{-1}$ for the nanocomposite. This shows that clay plays an important role in enhancing the thermal, mechanical and ethanol sensing properties of PPC [37].

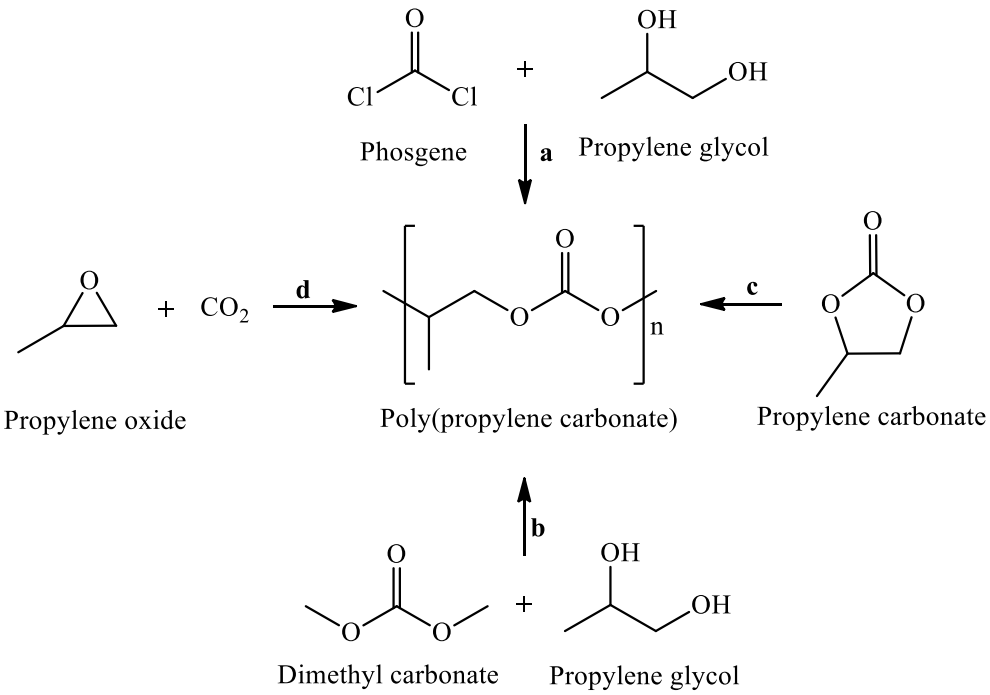
The biodegradable component of PPC is useful in the production of biodegradable plastic materials for packaging applications. Zinc oxide(ZnO)/PPC nanocomposite films were shown to have the potential to be used in the packaging industry when Seo *et al.* investigated the effect on the properties of the nanocomposite by varying the ZnO content. Solution blending method was used to prepare PPC/ZnO nanocomposite films with PPC/ZnO weight ratios of 100/0, 99/1, 97/3, 95/5, and 90/10. An increase in ZnO content resulted in a decrease in the diffusion coefficient, water uptake and oxygen transmission rate of the prepared films. Furthermore, the antibacterial properties of the films were enhanced as a result of the presence of ZnO in the nanocomposite. With improvements in compatibility and dispersion of the PPC matrix polymer and inorganic ZnO filler nanoparticles, this material has the potential to be used for packaging applications [35].

As a result of its biocompatibility, PPC can be used in drug delivery systems which work on the basis of hydrophobic interactions between the drug and the polycarbonate segments. A series of amphiphilic block polymer PEG-PPC-PEG with varying hydrophobic block length of PPC segments were prepared by Li and Niu to investigate their potential for drug delivery. Doxorubicin (DOX) was used as a model drug and supported on nanoparticles prepared with PEG-PPC-PEG. An increase in the hydrophobic block length of PPC resulted in an increase in the particle size of the nanoparticles. An inverse relation between particle size and the rate of drug release was observed. This is attributed to the wrapping of DOX by the hydrophobic block

length. The results of this study show that amphiphilic polymers PEG-PPC-PEG have the potential to be used as drug carries for drug delivery applications [38].

### 1.3.3 Preparation of poly(propylene carbonate)

There are four ways in which PPC can be prepared. The first report of their preparation involved polycondensation of phosgene or its derivatives and aliphatic diols (**Scheme 1.8 a**). The polymers produced showed a broad molecular weight distribution as a result of poor control. This, in addition to the use of phosgene, which is known to be toxic made this route non-ideal [39].

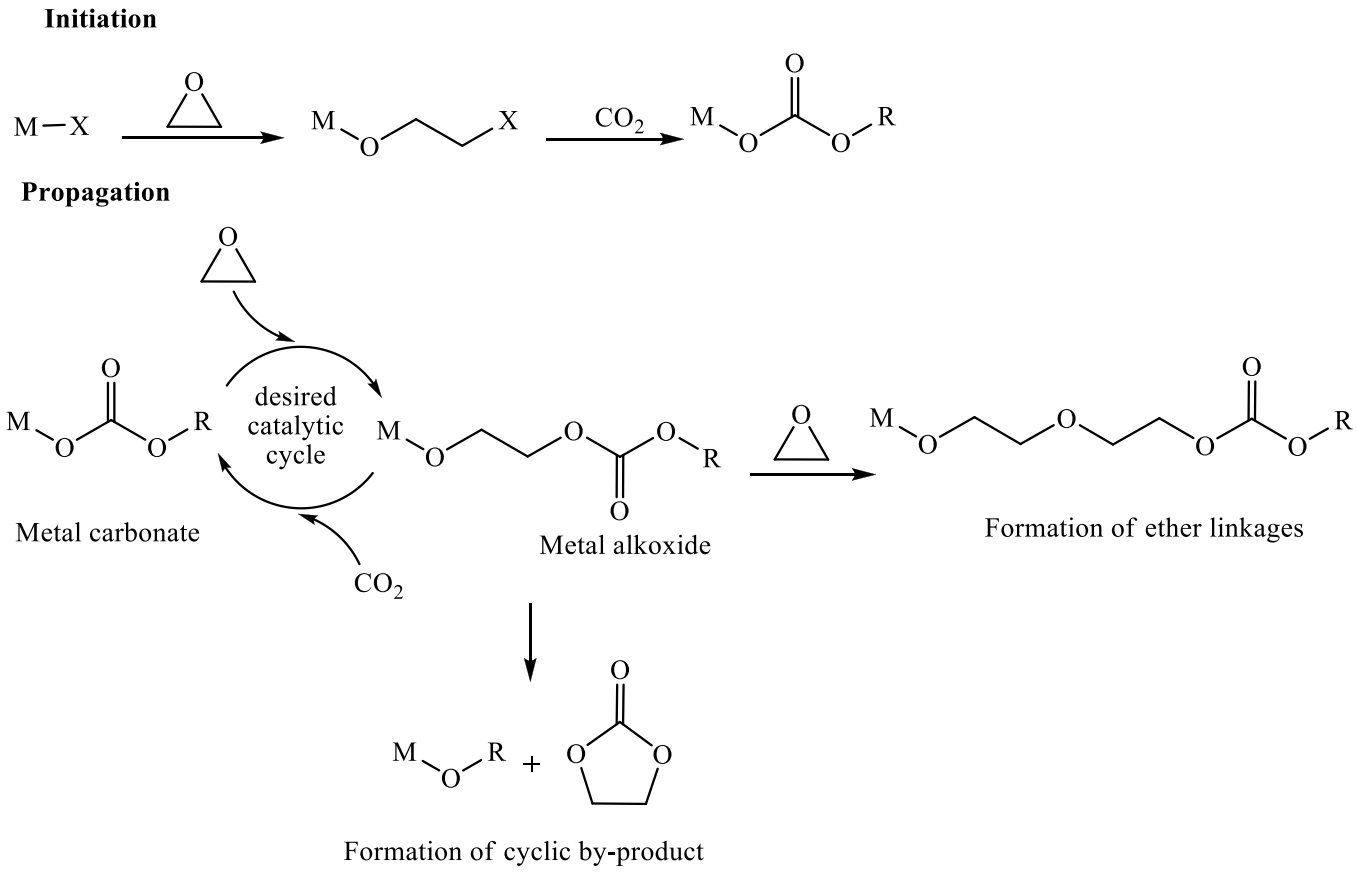



**Scheme 1.8** *Synthesis of poly(propylene carbonate)* [20], [39]–[41]

In order to eliminate the use of phosgene, a non-phosgene PPC preparation route was developed. Dialkyl carbonates were used in place of phosgene to birth the non-phosgene polycarbonate synthetic route (**Scheme 1.8 b**). This is a two-step reaction that begins with condensation, which is followed by transesterification between the –OH and –OC(O)R end-groups. The second step is responsible for the subsequent chain growth. It requires the use of a transesterification catalyst, which plays a key role in the properties of the APCs produced. The other factors reported to influence the properties of the polymers produced include; reaction temperature and the ratio of dialkyl carbonate to diol [40].

PPC can also be prepared from cyclic carbonate monomers via ring opening polymerization (ROP) of cPC (**Scheme 1.8 c**). Early reports of this route showed that the polymers produced suffered from undesired decarboxylation when potassium carbonate was used as a catalyst. Over time, catalysts efficient for the industrial production of PPC following this route have been developed. Known catalysts for this process include; transition metal catalysts, alkyl halides, basic and acidic organocatalysts, as well as enzyme catalyst. ROP of cyclic carbonates can be carried out in melt or in solutions by varying mechanisms including cationic, anionic, coordination-insertion, monomer activation, monomer and initiator dual activation, and enzymatic activation [41].

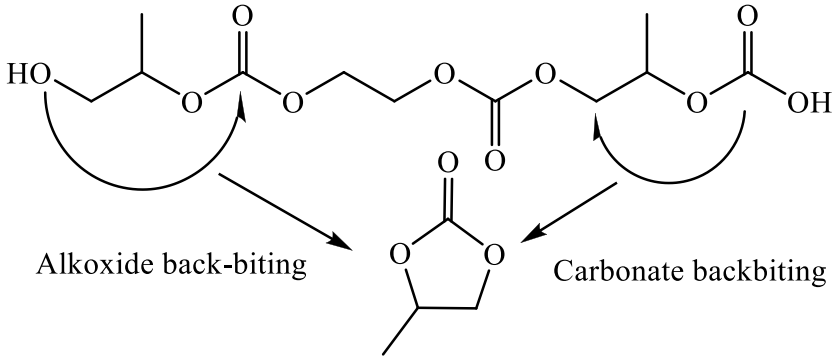
A more sustainable route to the preparation of aliphatic carbonates is the ring opening copolymerization of epoxides and $CO_2$ (**Scheme 1.8 d**) [20]. The proposed mechanism for the ring opening copolymerization of PO and $CO_2$ to afford PPC is depicted in (**Scheme 1.9**) is best described as a living step growth polymerization, which grows only one chain per metal centre. This is in contrast to the immortal type polymerization proposed by Inoue, which allows for multiple chains to propagate from one metal centre. It consists of an initiation, propagation, chain transfer and side product formation steps. The initiation step is signalled by the coordination of the epoxide molecule, which subsequently ring opens the epoxide molecule by the nucleophilic attack of the carbonate group. This is the initiation step, leading to the formation of an alkoxide intermediate. The initiation step is followed by chain propagation, whereby the insertion of $CO_2$ into the metal alkoxide intermediate to form a metal carbonate species takes place. Another molecule of epoxide is coordinated to the metal centre, followed by the nucleophilic attack by the carbonate group, which leads to the ring opening of the coordinated epoxide molecule to form the metal alkoxide intermediate. This process is repeated several times, eventually leading to the formation of polymers of various molecular weights. Therefore, chain propagation can be thought of as a step which involves the cycling between metal alkoxide and carbonate intermediates. The final step is chain termination, hydrolysis of the growing chain and end capping with a hydroxyl group is achieved by exposure to suitable conditions and reagents [42].




**Scheme 1.9** *Proposed mechanism for the synthesis of PPC* [42]

Several challenges are encountered with the ring opening copolymerization of $CO_2$ and PO. Contamination can occur from the formation of the undesired five-membered cyclic polycarbonate (cPC) side-product. The formation of cPC is favoured under forcible conditions since these are thermodynamic products of the reaction between $CO_2$ and epoxides. The formation of cPC takes place through a process known as a back-biting or de-polymerization reaction, which is caused by thermal decomposition (**Scheme 1.10**). cPC can also form off-metal when the reaction is carried out in the presence of ionic addictive and co-polymers. The off-metal chains produced undergo cyclization to form cPC. These off metal-chains exist in equilibrium between metal coordination and 'free' anionic polymer chains [22].

Depending on the application PPC produced are intended for, the formation of ether linkages in the polymer chain can either be a problem or of benefit as it has drastic effects on the properties of the polymers produced. This happens when the metal alkoxide attacks an epoxide molecule instead of inserting a $CO_2$ unit thereby reducing $CO_2$ inserted in the polymer backbone [43].




**Scheme 1.10** *Formation of cyclic carbonates through alkoxide back-biting and carbonate back-biting of poly(propylene carbonate)* [22]

## 1.4 TRANSITION METAL COMPLEXES AS CATALYSTS FOR THE COUPLING OF CARBON DIOXIDE AND PROPYLENE OXIDE

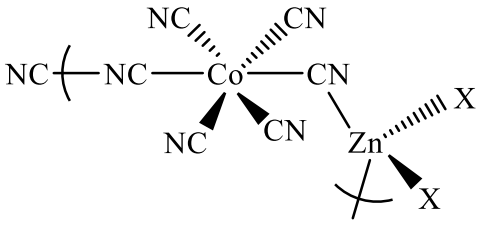
In 1969, Inoue *et al*. reported the successful preparation of PPC from the novel coupling reaction of PO and $CO_2$ using mixtures of diethyl zinc and organic solvents in varying ratios as the catalysts. The group achieved the highest turnover frequency (TOF) of 0.12 $h^{-1}$ (mol. epoxide consumed per mol. catalyst per hour) when 20–50 atm $CO_2$ and a temperature of 80 °C were used with diethyl zinc and water in 1:1 ratios as the catalyst. Although the reaction showed success, the polymers produced had 88% ether linkages, meaning that the reaction suffered from consecutive PO enchainment and a poor uptake of $CO_2$ [20]. One of the factors known to affect the properties of the products produced from this coupling reaction is the nature of catalyst used.

To build on the foundation laid by Inoue *et al*. a great deal of catalyst systems for this type of reaction have been studied and the most common are those that consist of metals such as Zn(II), Co(III) and Cr(III) [28], [44], [45]. These include both homogeneous and heterogenous systems.

### 1.4.1 Heterogenous catalysts for carbon dioxide and propylene oxide coupling

Very often, homogeneous catalysts that have been evaluated for their activity in the coupling of PO and $CO_2$ are transformed into heterogeneous catalysts by means of anchoring on supports such as silica. The benefit of this modification include an increase in the number of active sites on the catalyst by increasing the surface area, which would otherwise not be possible in a homogeneous state as a result of agglomeration. This translates to an improvement in the catalytic activity from homogeneous to heterogeneous state. Another benefit to this is the ease with which the catalyst can be separated from the products formed [46]. Another way in which homogeneous catalysts are transformed to heterogenous catalysts is by use of ionic liquids. This creates a biphasic system, which enables easy recovery of the catalyst upon catalysis [47].

Heterogenous catalysts possess attractive features including ease of recovery compared to their homogenous counterparts. One of the drawbacks associated with this class of catalyst systems is that they contain multiple active sites that result in the production of polymers with broad polydispersity indices (PDIs) and composition distributions. Very often, only a small percentage of the metal sites are active, and residual catalyst remains in the polymeric product as a result [48].



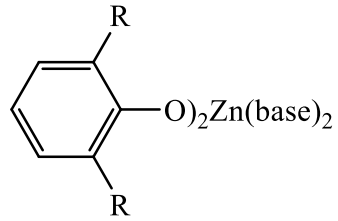

X = $H_2O$, Cl, Br, ROH

**Figure 1.2** *Double metal cyanide complex for the coupling of carbon dioxide and propylene oxide* [49]

The two major classes of heterogeneous catalysts that have been extensively studied and reported on are based on zinc glutarate ($[Zn(O_2C(CH_2)_3CO_2)]_n$) and double metal cyanides (**Figure 1.2**) [50]. Although these catalysts have been shown to be efficient for the homopolymerization of epoxides, to an extent that they are utilized for this transformation at an industrial scale, they have proven to be inefficient when compared to their homogeneous counterparts in the coupling of $CO_2$ and PO as they show poor activity for this coupling process. In order to compare to homogeneous catalyst systems, the use of high pressures of $CO_2$ is

required, which is not ideal as there is a high cost associated with systems operated at high pressures. Their poor uptake of $CO_2$ means that the polymers produced in the presence of these catalysts lack perfectly alternating ether linkages in the polymer back-bone [51].

Early studies showed that dialkyzinc-carboxylic acid catalyst systems are active for the copolymerization of $CO_2$ and PO. Diethylzinc-cyclic carboxylic systems were found to be more active than systems reported in earlier studies, however, reaction times of upto 7 days were required to obtain optimal yields. At 35 °C, $CO_2$ pressure of 40 atm and a reaction time of 277 hours, a PPC yield of 21.29 g was obtained when $ZnEt_2$ and L-mandelic acid were used as the catalyst system in 1:1 molar ratios. $ZnEt_2$-aliphatic carboxylic acid catalyst systems performed poorly compared to $ZnEt_2$-cyclic catalysts systems in this study. The highest yield of PPC of 1.61 g was achieved when $ZnEt_2$ and muconic acid in 1:1 molar ratios were used as the catalyst system at 35 °C, $CO_2$ pressure of 40 atm and a reaction time of 44 hours. Results of this study revealed that the catalytic activity of these systems is highly dependent on the R-group on the acid species generated upon reacting with $ZnEt_2$. That is, $ZnEt_2$ paired with cyclic acids showed higher catalytic activities compared to their aliphatic counterparts [52].




R = $C_6H_5$, *i*-Pr, $^t$Bu
Base = THF, pyridine, $Et_2O$

**Figure 1.3** *Zinc*(II) *phenoxide catalysts for the copolymerization of $CO_2$ and epoxides* [53]

Darensbrough *et al*. prepared a series of Zn(II) phenoxides for the copolymerization of $CO_2$ and epoxides. When complex (R= $C_6H_5$, base= THF) (**Figure 1.3**) was used as a catalyst in the absence of strongly coordinating solvents, high activities for the copolymerization of cyclohexene oxide (CHO) and $CO_2$ were achieved. However, when the epoxide was varied from CHO to PO while keeping the reaction conditions constant, cPC was produced [53]. The temperature dependence on the major product formed in this reaction being either cPC or PPC was corroborated when the coupling reaction was carried out at 40 °C with complex **2** (**Figure 1.3**) as the catalyst. It was found that the formation of PPC was more favoured to the formation

of cPC. Another key finding was the lack of influence of sterics on the major product formed [53].

Ramin *et al*. prepared a series of chromium salen complexes (**Scheme 1.12**) and investigated their activity in the solvent-less and co-catalyst free coupling reaction of $CO_2$ and epoxides. The most active catalysts were immobilised on a silica support (**Scheme 1.13**) using different immobilisation methods, and their activities were compared to those of the free metal complexes. Catalyst **4** showed the highest activity, reaching a TOF of 170 $h^{-1}$ at a conversion of 70% and a PC selectivity greater than 98% [46].

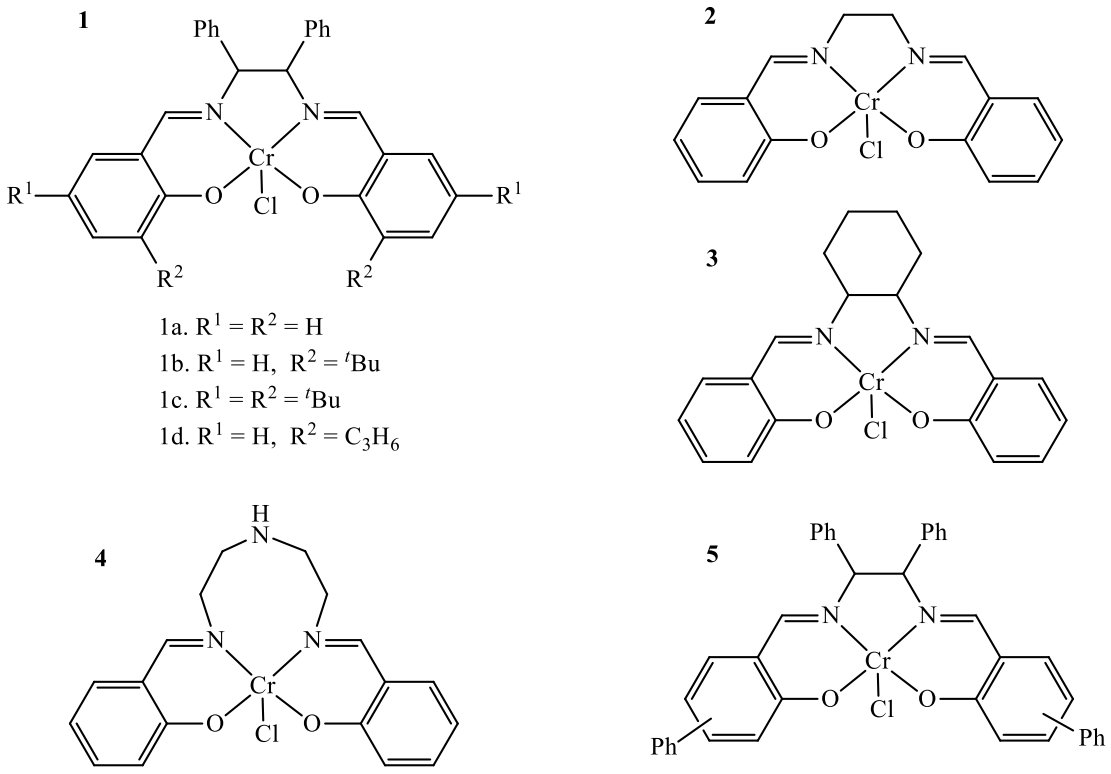



**Figure 1.4** *Homogeneous chromium salen complexes as catalysts in the coupling reaction of carbon dioxide and epoxides* [46]

Catalyst **9**, which is a heterogenous derivative of catalyst **4** was prepared by anchoring the metal to a modified silica surface by coordination of the $Cr^{3+}$ centre to an amine group. In evaluating the catalytic activity of catalyst **9**, a TOF of 330 $h^{-1}$ was achieved. Catalyst **10**, which was prepared by covalently binding the metal complex to the silica support, showed higher catalytic activity compared to its homogeneous derivative, catalyst **1**. The superior

performance of the silica supported catalysts is attributed to the isolation of active sites on the catalyst, which would otherwise be hampered by the agglomeration of the homogenous catalysts. Results of the reusability study revealed the importance of the method used to anchor the catalysts to the silica support by showing that covalently-bound complexes are more stable than coordinated complexes [46].

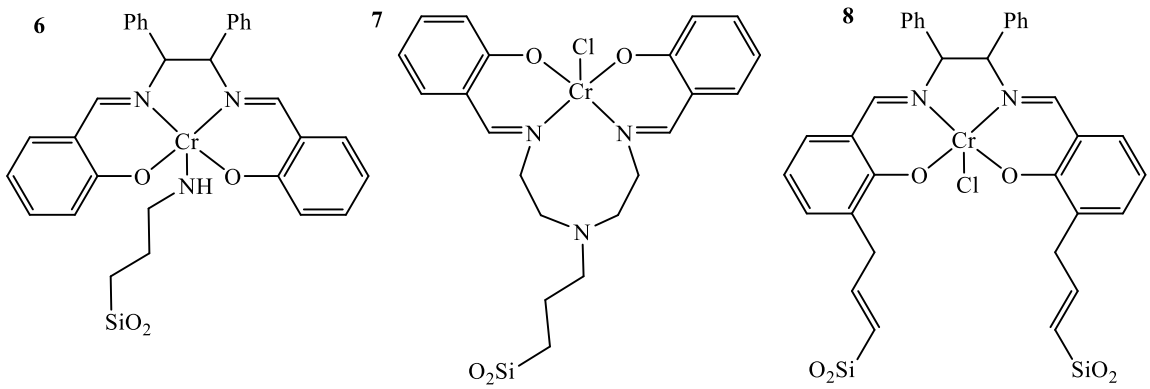



**Figure 1.5** *Heterogeneous chromium salen complexes as catalysts in the coupling reaction of carbon dioxide and epoxides* [46]

### 1.4.2 Homogeneous catalysts for carbon dioxide and propylene oxide coupling

Homogeneous catalysts, in contrast to heterogenous catalysts have been reported to result in highly alternating copolymers as a result of their relatively high uptake of $CO_2$. Moderate to high pressures of $CO_2$ are required for this process in the presence of these catalysts systems [48]. With recent studies focused on improving the reaction conditions these systems are active under, perfectly alternating aliphatic carbonates have been produced under low pressures of carbon dioxide using newly developed and highly active homogenous catalysts [54].

The most reported homogeneous catalysts are generally classified as either bicomponent binuclear or catalyst systems. Biocomponent catalysts are usually metal complexes comprising of Co(III), Cr(III), Mn(III) or Al(III), stabilized by salen or porphyrin ligands. These tend to be applied in conjunction with ionic liquid co-catalysts, with the commonly used being bis(triphenylphosphine)iminium [55]–[58]. Dinuclear catalysts are made up of metal(II/III) complexes. These comprise of mononucleating ligands, such as Zn(II) β-diiminates, which bond the two metals to each other [59], [60]. Other examples include metal complexes of

Zn(II), Mg(II), Co(II/III) or Fe(III) with macrocyclic ligands, which are known as deliberately dinucleating ligand, coordinating to the metal ions [61]–[63].

The first report of a single-site homogenous catalyst for the copolymerization of carbon dioxide and epoxides was reported in 1978 by Inoue *et al*. where aluminium tetraphenylporphyrin (tpp) complexes (**Figure 1.6**) showed activity towards this reaction. When $EtPh_3PBr$ was used as a co-catalyst, the tpp complexes were found to be active for the coupling of $CO_2$ with either propylene oxide and cyclohexene oxide. Although active, longer reaction times (up to 13 days) were required for the reactions to reach completion. The copolymers produced were characterized by high molecular weights and low polydispersity indices [64].

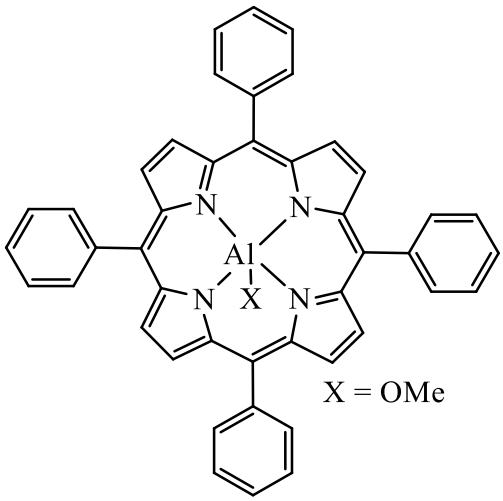



**Figure 1.6** *Aluminium tetraphenylporphyrin catalyst for the coupling of propylene oxide and carbon dioxide* [64]

The conversion rate of the tetraphenylporphinatoaluminum chloride (TPPAlCl) catalyst system (**Figure 1.7**) was improved when Jung *et al*. evaluated the catalytic activity of a PO adduct of this catalyst, ($TPPAl(PO)_2Cl$) for the coupling of $CO_2$ and PO. In the absence of a co-catalyst, TPPAlCl and its PO adduct resulted in a 64.8% and 63.6% product conversion rate, respectively. Although these catalyst systems favoured the production of oligomers over the cyclic product to a great extent, a poor $CO_2$ uptake was evidenced by the high degree of ether linkages observed along the oligomers backbone. The addition of a co-catalyst to both TPPAlCl and its PO adduct increased the conversion rate, a 100% conversion rate was achieved with the PO adduct. The oligomers produced had a lower degree of ether linkages compared to the oligomers produced in the absence of a co-catalyst. However, the presence of co-catalyst

enhanced the formation of cPC, that is, pairing the catalysts with a co-catalysts reduced the selectivity for the linear products to the cyclic products [65].

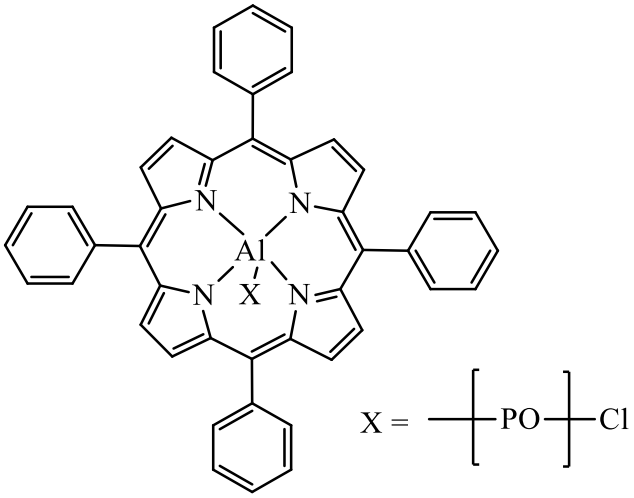
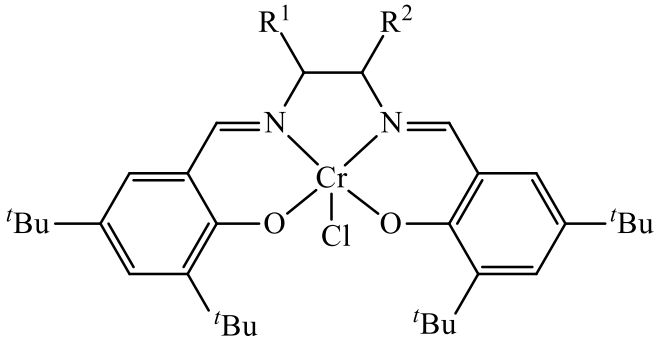



**Figure 1.7** *Tetraphenylporphinatoaluminum chloride catalyst for the coupling of propylene oxide and carbon dioxide* [65]

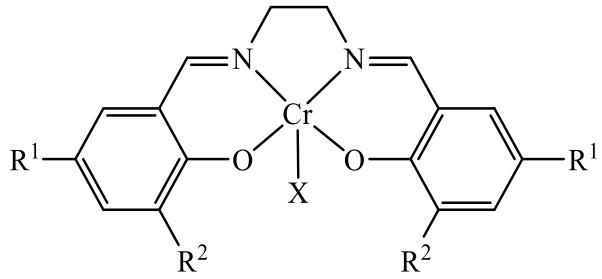
Inspired by the report by Kruper *et al*. on the activity of a Cr(III) porphyrin complex as a catalyst for the coupling of PO and $CO_2$ to produce cPC [66]. Robert *et al*. varied the coordination environment around the Cr metal centre from a porphyrin to a salen ligand. This was justified by the ease of synthesis, efficiency and ability to easily tune the steric and electronic properties of catalyst systems derived from salen ligands by changing the substituents on the ligand [56]. In the presence of (4-dimethylamino)pyridine (DMAP), catalyst **a** (**Figure 1.8**) showed activity towards the production of cPC. In the absence of a co-catalyst, no activity was observed. Complex 1.6d showed the highest activity of all four complexes. Looking into the effect of catalyst to co-catalyst ratio using catalyst **d** (**Figure 1.8),** it was found the optimal ratio is 1:2. Increasing the concentration of the co-catalyst beyond this resulted in the gradual deactivation of the catalyst, until a point where no activity was observed at 4 equivalents of DMAP [56].




a. $R^1 = R^2 =$ *trans* $(CH_2)_4$
b. $R^1 = CH_2$, $R^2 = H$
c. $R^1 = R^2 =$ *trans* $(C_6H_5)$
d. $R^1 = R^2 =$ *meso* $(C_6H_5)$

**Figure 1.8** *Highly efficient Cr(III) salen complexes as catalysts for the coupling reaction of epoxides with carbon dioxide* [56]

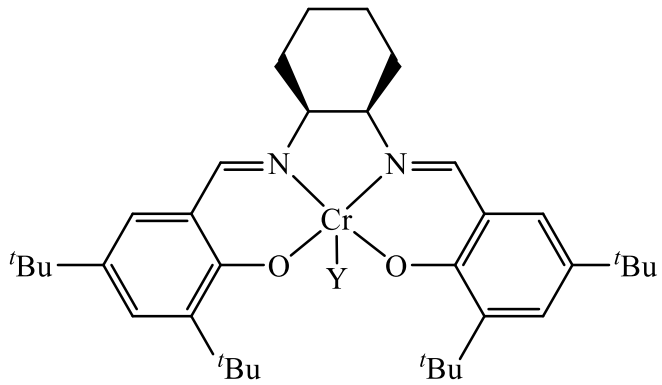
Lu *et al*. produced cPC at a TOF of up to 84.2 $h^{-1}$ at 35 °C when a bifunctional (Salen)AlX catalyst **a** (**Figure 1.9**) was used in the coupling reaction of PO and $CO_2$, in the presence of a quaternary ammonium salt (n-$Bu_4$NY) as the co-catalyst. The study investigated the effect of the leaving ability of the anion $Y^-$ of the quaternary ammonium salt (n-Bu4NY), electrophilicity of central metal ion and the steric factor of substituent groups on the aromatic rings of the (Salen)AlX metal complex on the efficiency and selectivity in this reaction. In the absence of the co-catalyst, catalyst **a** (**Figure 1.9**) showed poor activity and selectivity which was observed by the production of a mixture of cPC and PPC, evidenced by FTIR spectroscopy [67].



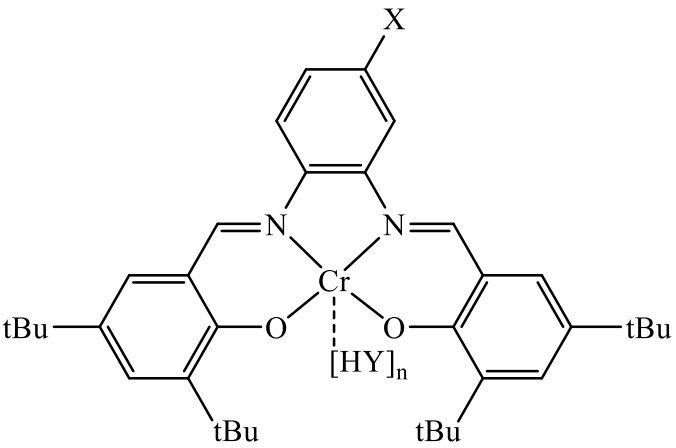

a. $R^1 = R^2 =$ H, X = Cl
b. $R^1 = R^2 =$ H, X = Et
c. $R^1 = {}^t$Bu, $R^2 =$ H, X = Et
d. $R^1 = R^2 = {}^t$Bu, X = Et
e. $R^1 = R^2 = NO_2$, X = Et

**Figure 1.9** *Highly active bifunctional Salen(AlX) catalysts for the coupling reaction of epoxides with carbon dioxide* [67]

Poor activity was observed for the rest of the catalyst systems when the coupling reaction was carried out in the absence of the quaternary ammonium salt. Order of activity as a result of the electrophilicity the prepared complexes was expected to be: **1.9 e** > **1.9 a** > **1.9 b** > **1.9 c** > **1.9 d**, however, it was found to be: **1.9 a** > **1.9 b** > **1.9 e** > **1.9 c** > **1.9 d**. what this means is that all the factors that were set out to be investigated play a significant role on the activity and selectivity of the metal complexes [67].




1a. Y = $OOCCCl_3$
1b. Y = DNP
1c. Y = $OBzF_5$



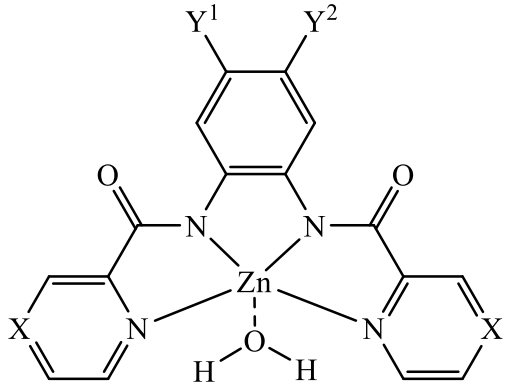

2. X = H, Y= 0, n = 0
2a. X = H, Y= $OOCCCl_3$, n = 1
2b. X = H, Y= DNP, n = 0
2c. X = H, Y= $OBzF_5$ , n = 1

3. X = Cl, Y= 0, n = 0
3a. X = Cl, Y= $OOCCCl_3$, n = 1
3b. X = Cl, Y= DNP, n = 1
3c. X = Cl, Y= OAc , n = 0

**Figure 1.10** *Novel salphen Co(III) complexes for the copolymerization of epoxides with $CO_2$* [68]

Zdeněk Hošťálek *et al*. prepared a series of novel symmetric and asymmetric salphen cobalt (III) complexes with different counter anions as catalysts for the copolymerization of $CO_2$ with PO. Salen complexes **1a** -**1c** (**Figure 1.10**) were used as references. These complexes have been shown to be efficient and selective (up to 99% selectivity for PPC with **1a**) for this coupling reaction. Mixtures of PPC and cPC were obtained in the case of the novel salphen complexes. Catalyst **2a** (**Figure 1.10**) showed the highest selectivity among the novel salphen complexes (up to 88% for PPC) with a TOF of 190 $h^{-1}$. This was achieved in 4 hours under ambient temperature and a $CO_2$ pressure of 1 Mpa. Increasing the temperature to 50 °C and 75 °C resulted in an increase in the TOF (190 $h^{-1}$ and 560 $h^{-1}$), however, selectivity for PPC over cPC was compromised, with a selectivity of 81% and 59% respectively. At elevated temperatures, selectivity for PPC is known to decrease as a result of the activation energy favouring the formation of cPC being reached [68].

These complexes have been shown to be efficient and selective (up to 99% selectivity for PPC with 1a) for this coupling reaction. Mixtures of PPC and cPC were obtained in the case of the novel salphen complexes. Catalyst **2a** (**Figure 1.10**) showed the highest selectivity among the novel salphen complexes (up to 88% for PPC) with a TOF of 190 $h^{-1}$. This was achieved in 4 hours under ambient temperature and a $CO_2$ pressure of 1 Mpa. Increasing the temperature to 50 °C and 75 °C resulted in an increase in the TOF (190 $h^{-1}$ and 560 $h^{-1}$), however, selectivity for PPC over cPC was compromised, with a selectivity of 81% and 59% respectively. At elevated temperatures, selectivity for PPC is known to decrease as a result of the activation energy favouring the formation of cPC being reached [68].




1a. X = CH, $Y^1 = Y^2 = H$
1b. X = CH, $Y^1 = Y^2 = Cl$
1c. X = CH, $Y^1 = H$, $Y^2 = NO_2$
1d. X = CH, $Y^1 = Y^2 = CH_3$
1e. X = N, $Y^1 = Y^2 = H$

**Figure 1.11** *New zinc catalysts based on $N_4$-chelating ligands for the coupling reaction of epoxides with carbon dioxide* [69]

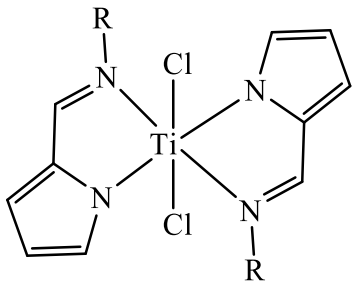
Adolph *et al*. demonstrated that tetrabutylammoniumiodide (TBAI) is the best co-catalyst when paired with an equimolar quantity of a zinc bpb complex **1e** (**Figure 1.11**) in the coupling of PO with $CO_2$ to produce cPC. A 92% yield of cPC was obtained in 20 h, a temperature of 80 °C and a $CO_2$ pressure of 35 bar. It is worth nothing that complex 8 on its own showed no activity for this reaction, however, the co-catalyst on its own showed very little activity (yielding 5% of cPC). When the halide ion was varied, a trend on activity as a result of the nature of the halide on the co-catalyst emerged: iodide (92% cPC) > bromide (39% cPC) > chloride (20% cPC). This observation is attributed to the leaving ability of the halide ions, where the iodide ion is a better leaving group compared to bromide and chloride ions [69].

## 1.5 PYRROLE-ALDIMINATO COMPLEXES IN CATALYTIC PROCESSES

Numerous Schiff base metal complexes have been synthesized, characterized and shown to be active in various catalytic applications including the ring opening copolymerization of carbon

dioxide ($CO_2$) and e-caprolactone and olefin oligomerization [70], [71]. These metal complexes are either prepared from transition metals and main group metals and stabilized by pyrrole-imine ligands bearing the desired functionalities [72], [73].

Novel titanium complexes (**Figure 1.12**) comprising of two non-symmetric bidentate pyrrolide-imine chelate ligands, [2-(RNCH)$C_4H_3N]_2TiCl_2$] were synthesized and characterized by Yoshida *et al.* and their catalytic activity in the polymerization of ethylene was investigated. In the presence of methylalumoxane (MAO) as a co-catalyst, these catalysts displayed reasonable activities to produce high-molecular-weight polyethylenes. The highest activity (14 100 kg of polymer/((mol of Ti) h) was observed for complex **4**, which is similar to that observed for the $Cp_2TiCl_2$ complex. The polymers produced had very high molecular weight (Mv) value of up to 2 601 000. When $Ph_3CB(C_6F_5)4$/i-$Bu_3Al$ was used in place of MAO as a cocatalyst, lower activities (1500-2000 kg of polymer/((mol of Ti)/h). were observed. However, the polyethylenes produced had greater molecular weight (Mv > 4 000 000) [74].




1.R= $C_6H_5$
2.R= Et
3.R= $nC_6H_{13}$
4.R= $C_6H_{11}$

**Figure 1.12** *Novel titanium complexes comprising of two non-symmetric bidentate pyrrole-imine chelate ligands* [74]

Liang *et al.* prepared and characterized a series of neutral palladium(II) complexes bearing non-symmetric bidentate pyrrole-iminato or salicylaldiminato chelate ligands (**Figure 1.13**). Their catalytic activity in the polymerization of norborene was investigated. These complexes showed Catalytic activity of up to 8.52 x $10^3$ kg/molPd h. and produce non-crystalline vinyl-addition polynorborenes [75].

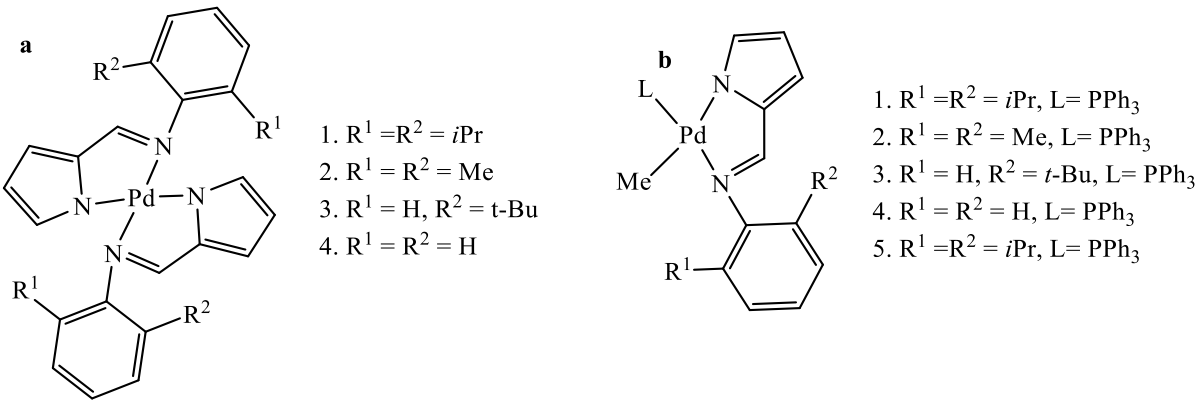



**Figure 1.13** *Palladium(II) complexes bearing non-symmetric bidentate pyrrole-iminato chelate ligands* [75]

Bao-Chang Xu *et al.* synthesized and characterized a series of vanadium complexes comprising of iminopyrrolide chelating ligands [2-(RN=CH)$C_4H_3N$]V(THF)2$Cl_2$ (**Figure 1.14**). High catalytic activities up to 48.6 kg PE mmol$V^{-1}$ $h^{-1}$ $bar^{-1}$ for ethylene polymerization were observed in the presence of $Et_2AlCl$ as a co-catalyst. This in addition to the production of polymers with high molecular weights. The single-site behaviour of all 5 metal complexes was evidenced by their tolerance to elevated temperatures (70 ◦C) and the production of unimodal polyethylenes. The efficient incorporation of the functional alpha-olefin 10-undecen-1-ol can be into polyethylene chains can be achieved by pre-treating with equimolar quantities of alkylaluminums [76].

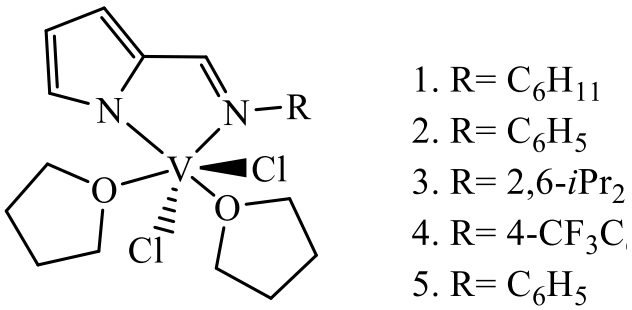



**Figure 1.14** *Vanadium complexes comprising of iminopyrrolide chelating ligand* [76]

Tabthong *et al.* prepared two series of aluminum alkyl complexes supported by pyrrolylaldiminate ligands, $LAlMe_2$ (**1a** – **7a**) (**Figure 1.15**) and $L_2AlMe$ (**1b** – **7b**) (**Figure 1.15**). These were successfully synthesized by reacting trimethylaluminum with the corresponding pyrrolylaldiminate ligands in the molar ratios of 1 : 1 and 1 : 2 resulting in

dimethylaluminum pyrrolylaldiminates (**1a**–**7a**) (**Figure 1.15**) and monomethylaluminum pyrrolylaldiminates (**1b** – **7b**) (**Figure 1.12**), respectively, in good yields [77].

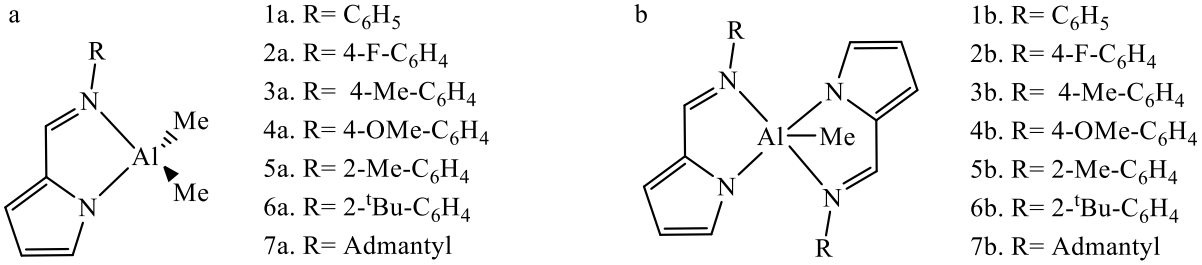
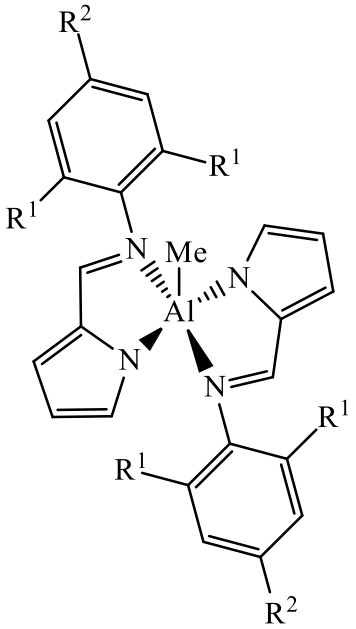



**Figure 1.15** *Aluminum alkyl complexes supported by pyrrolylaldiminate ligands* [77]

In the presence of 1 equivalence of benzyl alcohol, all complexes facilitated the living ring-opening polymerization of rac-lactide and showed good control over molecular weights and polydispersities. However, the addition of an excess of benzyl alcohol (up to 5 equivalents) an improved efficiency with complexes **6a** and **7a** (**Figure 1.15**) was observed. This was evidenced by the narrow PDI values and the good agreement between the experimental Mn values and monomer/benzyl alcohol ratios. A key observation that was made is the influence of steric and electronic properties of the prepared metal complexes on the living ring-opening polymerization of rac-lactide as well as the polymer microstructure. Generally, the monomethylaluminum complexes performed slightly better than the dimethylaluminum complexes [77].

Pracha *et al.* reported the synthesis of seven bis(pyrrolylaldiminato)aluminum methyl complexes with varying steric and electronic demands. The synthesis of these metal complexes was achieved from the reactions of $AlMe_3$ with two molar equivalents of the respective pyrrolylaldimine ligands (**Figure 1.16**), for the polymerization of lactide. The polymerization reactions were carried out using benzyl alcohol as an initiator. The rate of polymerization was found to be highly dependent on the steric and electronic demands induced by the substituents on the benzyl group. The rate of polymerization was found to increase with a decrease in steric bulk and increased with a decrease in the electron withdrawing capabilities of the substituents on the benzyl group [78].




1. $R^1 = R^2 = H$
2. $R^1 = Me$, $R^2 = H$
3. $R^1 = R^2 = Me$
4. $R^1 = Et$, $R^2 = H$
5. $R^1 = i$Pr, $R^2 = H$
6. $R^1 = H$, $R^2 = CF_3$
7. $R^1 = H$, $R^2 = OMe$

**Figure 1.16** *Bis(pyrrolylaldiminato)aluminum methyl complexes* [78]

## 1.6 PROBLEM STATEMENT

The coupling of PO and $CO_2$ to produce the biodegradable aliphatic polycarbonate (PPC) or cyclic propylene carbonate (cPC) is an attractive chemical transformation. This is because of its sustainability, owing to the abundance of $CO_2$ which is employed as a C1 feedstock in this reaction [20]. Several catalysts for the coupling of PO and $CO_2$ have been developed and modified in order to enhance their catalytic activity and selectivity for the production of either aliphatic polycarbonate or cyclic propylene carbonate product [56], [58], [69], [79], [80].

For the purpose of this study, a range of pyrrole-aldimine ligands will be prepared and employed in the synthesis of their corresponding bis(pyrrole-aldiminato) complexes, with Zn(II) and Co(II) metal centres [81]. Porphyrin ligand systems, which have a similar architecture to that of pyrrole-aldimine ligands have been extensively studied for the coupling of $CO_2$ and PO, surprisingly, catalyst systems based on bis-(pyrrole-aldimine) ligands have not been reported for the coupling of $CO_2$ and PO [57], [62], [82]. In addition, metal complexes derived from pyrrole-aldimine ligands have been shown to be active in a range of catalytic processes which makes this class of compounds worth exploring in the coupling of PO and $CO_2$ [74], [77], [83]. The successfully synthesized metal complexes will be investigated in the coupling of $CO_2$ and PO. All the products synthesized will be characterized using various spectroscopic techniques.

## 1.7 AIMS AND OBJECTIVES

The main aim of this study is the synthesis and characterization of bis-(pyrrole-aldiminato) Zn(II) and Co(II) complexes and the investigation of these complexes as catalyst precursors for the coupling of $CO_2$ and PO. This aim will be achieved by synthesizing 4 pyrrole-aldimine ligands with varying electronic and steric demands following the Schiff base condensation method. The successfully synthesized ligands will then be used in the preparation of their corresponding bis-(pyrrole-aldiminato) Zn(II) and Co(II) complexes by exploring a number of synthetic routes to achieve this. Prior to evaluating the catalytic activity of the successfully prepared bis-(pyrrole-aldiminato) Zn(II) and Co(II) complexes in the coupling of $CO_2$ and PO, their activity will be evaluated in the coupling of $CS_2$ and PO, which is a chemical transformation similar to the former. This will be done in order to determine whether these complexes will yield similar results in both coupling transformations, as $CS_2$ is an analogue of $CO_2$, even though the two C1 feedstocks vary in their reactivities.

The successfully prepared ligands and their corresponding bis-(pyrrole-aldiminato) Zn(II) complexes will be characterized by $^{1}H$ NMR-, $^{13}C$ NMR-, 2D NMR-, FT-IR and UV-Vis-spectroscopy. ESI-MS will be used to confirm the preparation of the compounds, and elemental analysis will be used to confirm their purity. The same characterization techniques used for the ligands and their corresponding bis-(pyrrole-aldiminato) Zn(II) complexes will be used to characterize the bis-(pyrrole-aldiminato) Co(II) complexes, with the exception of $^{1}H$ NMR-, $^{13}C$ NMR- and 2D NMR- spectroscopy, as the bis-(pyrrole-aldiminato) Co(II) complexes are expected to be paramagnetic in nature, and therefore their magnetic susceptibilities will be determined using the Evans method. For the coupling of PO with either $CS_2$ or $CO_2$, $^{1}H$ NMR spectroscopy will be used as an analytical technique to evaluate if the metal complexes are active as well as to identify the nature of the products produced.

## 1.8 REFERENCES


[1] P. T. Anastas and J. C. Warner, *Oxford Univ. Press. New York*, 1998, 30.

[2] M. Aresta, *Wiley*, 2010, 3, 5, 631-632.

[3] R. J. Andres, T. A. Boden1, F.M. Bréon, P. Ciais, S. Davis, D. Erickson, J. S. Gregg, A. Jacobson, G. Marland, J. Miller, T. Oda, J. G. J. Olivier, M. R. Raupach, P. Rayner and K. Treanton1., *Biogeosciences*, 2012 9, 5, 1845–1871.

[4] X. B. Lu, W. M. Ren, and G. P. Wu, *Acc. Chem. Res.*, 2012, 45, 10, 1721–1735.

[5] J.K. Varghese, S.J. Na, J.H. Park, D. Woo, I. Yang, and B.Y. Lee, *Polym. Degrad. Stab.*, 2010, 95, 6, 1039-1044.

[6] H.L. Parker, J. Sherwood, A.J. Hunt, and J.H. Clark, *ACS Sustain. Chem. Eng.*, 2014, 2, 7, 1739-1742.

[7] H. Blattmann, M. Fleischer, M. Bähr, and R. Mülhaupt, *Macromol. Rapid Commun.,* 2014, 14, 35, 1238-1254.

[8] P. Karayaylali, Y. Zhang, L. Giordano, Y. Katayama, R. Tatara, Y. Yu, F. Maglia R. Jung and Y. Shao-Horn, *J. Electrochem. Soc.*, 2020, 167, 4.

[9] A. Chamú-Muñoz, O. Hernández-Meléndez, M. Hernández-Luna, J. Alcaraz-Cienfuegos, E. Vivaldo-Lima, and E. Bárzana, *Macromol. Mater. Eng.*, 2015, 300, 8, 810-822.

[10] J. S. Bello Forero, J. A. Hernández Muñoz, J. Jones Junior, and F. M. da Silva, *Curr. Org. Synth.*, 2016, 13, 6, 834-846.

[11] H. Jiang, Q. Zhang, Y. Zhang, L. Sui, G. Wu, K. Yuan and X. Yang OR., *Phys. Chem. Chem. Phys.*, 2019, 21, 10417-10422.

[12] R. Bucklin and R. Schendel, *Energy Prog.*, 1984, 4, 3, 137-142.

[13] C. A. Teo and W. A. Donald, *Anal. Chem.*, 2014, 86, 9, 4455–4462.

[14] "2: Final Report on the Safety Assessment of Propylene Carbonate," *J. Am. Coll. Toxicol.*,1987. 6, 1, 23–51.

[15] Z. Song, B. Subramaniam, and R. V. Chaudhari., *ACS Sustain. Chem. Eng.*, 2019, 7, 6, 5698–5710.

[16] H. Babad and A. G. Zeiler, *Chem. Rev.*, 1973, 73, 1, 75–91.

[17] J. Sun, L. Liang, J. Sun, Y. Jiang, K. Lin, X.Xu and R. Wang., *Catal. Surv. Asia*., 2011, 15, 1, 49-54.

[18] K. Tomishige, H. Yasuda, Y. Yoshida, M. Nurunnabi, B. Li, and K. Kunimori, *Catal. Letters*, 2004, 95, 1, 45-49.

[19] X. Zhao, N. Sun, S. Wang, F. Li, and Y. Wang., *Ind. Eng. Chem. Res.*, 2008, 47, 5,

1365–1369.

[20] S. Inoue, H. Koinuma, and T. Tsuruta., *J. Polym. Sci. Part C Polym. Lett.*, 1969, 130, 1, 210-220.

[21] J. W. Comerford, I. D. V. Ingram, M. North, and X. Wu, *Green Chem.,* 2015,17, 1966-1987.

[22] G. A. Luinstra, *Polym. Rev.*, 2008, 48, 1, 192–219.

[23] B. Lepoittevin and P. Roger, *Handbook of Engineering and Specialty Thermoplastics, Volume 3: Polyethers and Polyesters*. 2011.

[24] H. Yan, W. R. Cannon, and D. J. Shanefield, *Ceram. Int.*, 1998, 24, 6, 433-439.

[25] I. Manavitehrani, A. Fathi, Y. Wang, P. K. Maitz, and F. Dehghani, *ACS Appl. Mater. Interfaces 2015, 7, 40, 22421–22430*.

[26] S. J. Wang, L. C. Du, X. S. Zhao, Y. Z. Meng, and S. C. Tjong, *J. Appl. Polym. Sci.*, 2002. 85, 11, 2327 - 2334.

[27] Z. Quan, J. Min, Q.Zhou, D. Xie, J. Liu, X. Wang, X. Zhao and F. Wang., *Macromol. Symp.*, 2003, 195, 1, 281-286.

[28] X. B. Lu and Y. Wang, *Angew. Chemie - Int. Ed.*, 2004, 43, 27, 3574-3577.

[29] W. Chen, M. Pang, M. Xiao, S. Wang, L. Wen, and Y. Meng, *J. Reinf. Plast. Compos.*, 2010, 29, 10, 1545-1550.

[30] M. Zhou, M. Takayanagi, Y. Yoshida, S. Ishii, and H. Noguchi, *Polym. Bull.*, 1999, 42, 4, 419-424.

[31] T. Kawaguchi, M. Nakano, K. Juni, S. Inoue, and Y. Yoshida, *Chem. Pharm. Bull.*, 1983, 31, 4, 1400-1403.

[32] G. Kim, M. Ree, H. Kim, I. J. Kim, J. R. Kim, and J. I. Lee, *Macromol. Res.*, 2008, 6, 5, 473-480.

[33] L. C. Du, Y. Z. Meng, S. J. Wang, and S. C. Tjong, *J. Appl. Polym. Sci.*, 2004, 93, 3, 1840-1846.

[34] D. Han, Z. Guo, S. Chen, M. Xiao, X. Peng, S. Wang and Y. Meng, *Polymers (Basel).*, 2018, 10, 7, 771.

[35] J. Seo, G. Jeon, E. S. Jang, S. Bahadar Khan, and H. Han, *J. Appl. Polym. Sci.*, 2011, 122, 2, 1101-1108.

[36] S. Chen, B. Chen, J. Fan, and J. Feng, *ACS Sustain. Chem. Eng.*, 2015, 3, 9, 2077–2083.

[37] S. B. Khan, K. Akhtar, J. Seo, H. Han, and M. A. Ru, *Chinese J. Polym. Sci. (English Ed).*, 2012, 30, 735–743.

[38] H. Li and Y. Niu, *Mater. Sci. Eng. C*, 2018, 89, 160-165.

[39] H. Schnell, L. Bottenbruch, and H. Krimm, "Thermoplastic Aromatic Polycarbonates And Their Manufacture," 1962.

[40] P. U. Naik, K. Refes, F. Sadaka, C.H Brachais, G. Boni, J.P Couvercelle, M. Picquet and L. Plasseraud., *Polym. Chem.,* 2012,3, 1475-1480.

[41] R. Abdul-Karim, A. Hameed, and M. I. Malik, *Eur. Polym. J.*, 2018, 105, 95-106.

[42] M. R. Kember, A. Buchard, and C. K. Williams*, Chem. Commun*., 2011, 47, 141-163.

[43] F.Gao, Q. Zhou, Y. Dong, Y. Qin, X. Wang, Z. Xiaojiang, W. Fosong, *J. Polym. Res.*, 2012, 19, 5, 1-5.

[44] S. S. Wua, X.W Zhanga, W.LDaia, S.F Yina, W.S Lia, Y.Q Rena and C.T Aub, *Appl. Catal. A Gen.*, 2008, 341, 1-2, 106-111.

[45] D. J. Darensbourg, M. Ulusoy, O. Karroonnirum, R. R. Poland, J. H. Reibenspies, and B. Çetinkaya, *Macromolecules*, 2009, 42, 18, 6992–6998

[46] M. Ramin, F. Jutz, J. D. Grunwaldt, and A. Baiker, *J. Mol. Catal. A Chem.*, 2005, 242, 1-2, 32-39.

[47] J. K. Lee, Y.J. Kim, Y.S Choi, H. Leeb, J. S Lee, J. Hong, E.K Jeong, H.S Kim and M. Cheong, *Appl. Catal. B Environ.*, 2012, 111-112, 621-627.

[48] G. W. Coates and D. R. Moore, "*Angew. Chemie Int. Ed.*, 2004, 43, 48, 6618–6639.

[49] N. J. Robertson, Z. Qin, G. C. Dallinger, E. B. Lobkovsky, S. Lee, and G. W. Coates, *J. Chem. Soc. Dalt. Trans.*, 2006, 341, 1–2, 106-111.

[50] I. Kim, M. J. Yi, K. J. Lee, D. W. Park, B. U. Kim, and C. S. Ha, *Catalysis Today*, 2006, 111, 3, 292-296.

[51] D. J. Darensbourg and M. W. Holtcamp, *Macromolecules*, 1995, 28, 22, 7577–7579.

[52] M. Kobayashi, S. Inoue, and T. Tsuruta, *J. Polym. Sci. Polym. Chem. Ed.*, 1973, 11, 9 2383-2385.

[53] D. J. Darensbourg M.W. Holtcamp, G.E. Struck, M.S. Zimmer, S.A. Niezgoda, P. Rainey, J.B. Robertson, J.D. Draper, and J.H. Reibenspies, *J. Am. Chem. Soc.*, 1999, 121, 1, 107–116.

[54] Y. Xiao, Z. Wang, and K. Ding, *Chem. - A Eur. J.*, 2005, 11, 12, 3668-3678.

[55] L. N. Saunders, N. Ikpo, C.F. Petten, U.K Das, L.N. Dawe, C.M. Kozak and F.M. Kerton, *Catal. Commun.*, 2012, 18, 165-167.

[56] R. L. Paddock and S. T. Nguyen, *J. Am. Chem. Soc.,* 2001, 123, 46, 11498–11499.

[57] J. L. S. Milani, A.M. Meireles, B.N. Cabral, W.A. Bezerra, F.T. Martins, D.C.S. Martins. and R.P. Chagas, *J. CO2 Util.*, 2019, 30, 100-106.

[58] W. M. Ren, Y. Liu, and X. B. Lu, *J. Org. Chem.*, 2014, 79, 20, 9771–9777.

[59] P. K. Saini, C. Romain, and C. K. Williams, *Chem. Commun.*, 2014, 50, 32, 4164-4167.

[60] A. Thevenon, J. A. Garden, A. J. P. White, and C. K. Williams, *Inorg. Chem*., 2015, 54, 24, 11906–11915.

[61] G. Trott, J. A. Garden, and C. K. Williams, *Chem. Sci.*, 2019, 10, 4618-4627.

[62] C. E. Anderson, S. I. Vagin, M. Hammann, L. Zimmermann, and B. Rieger, *ChemCatChem*, 2013, 5, 11, 3269-3280.

[63] F. D. Monica, S.V. C. Vummaleti, A. Buonerba, A.D. Nisi, M. Monari, S. Milione, A. Grassi, L. Cavallo and C. Capacchione, *Adv. Synth. Catal.*, 2016, 358, 20, 3231-3243.

[64] N. Takeda and S. Inoue, *Die Makromol. Chemie*, 1978, 179, 5, 1377-1381.

[65] J. H. Jung, M. Ree, and T. Chang, *J. Polym. Sci. Part A Polym. Chem.*, 1999, 37, 16, 3329-3336.

[66] W. J. Kruper and D. V. Dellar, *J. Org. Chem.*, 1995, 60, 3, 725–727.

[67] X. B. Lu, Y. J. Zhang, B. Liang, X. Li, and H. Wang, *J. Mol. Catal. A Chem.*, 2004, 210, 1-2, 31-34.

[68] Z. Hošt'álek, R. Mundil, I. Císařová, O. Trhlikova, E. Grau, F. Peruch, H. Cramail and J. Merna, *Polymer (Guildf).*, 2015, 63, 52-61.

[69] M. Adolph, T. A. Zevaco, C. Altesleben, S. Staudt, and E. Dinjus, *J. Mol. Catal. A Chem.*, 2015, 400, 104-110.

[70] H. Vignesh Babu and K. Muralidharan, *J. Chem. Soc. Dalt. Trans.*, 2013, 42, 1238-1248.

[71] S. Matsui, T. P. Spaniol, Y. Takagi, Y. Yoshida, and J. Okuda, *J. Chem. Soc. Dalt. Trans.*, 2002, 24, 4529-4531.

[72] A. Mohamadou, J.-P. Barbier, and R. P. Hugel, *Polyhedron*, 1992, 11, 20, 2697–2702.

[73] C.S.B. Gomes, M.T. Duarte, and P.T. Gomes, *J. Organomet. Chem.*, 2014, 760, 167-176.

[74] Y. Yoshida, S. Matsui, Y. Takagi, M. Mitani, T. Nakano, H. Tanaka, N. Kashiwa, and T. Fujita, *Organometallics*, 2001, 20, 23, 4793–4799.

[75] H. Liang, J. Liu, X. Li, and Y. Li, *Polyhedron*, 2004, 23, 9, 1619-1627.

[76] B. C. Xu, T. Hu, J. Q. Wu, N. H. Hu, and Y. S. Li, *Dalt. Trans.*, 2009, 41, 41, 8854-8863.

[77] S. Tabthong, T. Nanok, P. Kongsaeree, S. Prabpai, and P. Hormnirun, *Dalt. Trans.*,

2014, 43, 1348-1359.

[78] S. Pracha, S. Praban, A. Niewpung, G. Kotpisan, P. Kongsaeree, S. Saithong, T. Khamnaen, P. Phiriyawirut, S. Charoenchaidet and K. Phomphrai, *Dalt. Trans.*, 2013, 42, 15191-15198.

[79] H. V. Babu and K. Muralidharan, *RSC Adv.*, 2014, 4, 6094-6102.

[80] M. Ree, Y. Hwang, J. S. Kim, H. Kim, G. Kim, and H. Kim, *Catal. Today*, 2006, 115, 1-4, 134-145.

[81] Y. Kobuke and K. Ogawa, *Bull. Chem. Soc. Jpn.*, 2003, 76, 2, 689-708.

[82] L. Jin, H. Jing, T. Chang, X. Bu, L. Wang, and Z. Liu, *J. Mol. Catal. A Chem.*, 2007, 261, 2, 262-266.

[83] J. S. Mu, Y. X. Wang, B. X. Li, and Y. S. Li, *Dalt. Trans.*, 2011, 40, 14, 3490-3497.

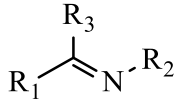
# Chapter 2
# Synthesis and characterization of pyrrole-aldimine ligands

CONTENT

2.1 INTRODUCTION…….…… 37
2.2 RESULTS AND DISCUSSION.…….... 38
2.2.1 Synthesis and characterization of pyrrole-aldimine ligands..…… 38
2.2.1.1 Characterization of pyrrole-aldimine ligands **L1** – **L4** with $^{1}$H NMR, COSY and NOESY spectroscopy……...…….…… 40
2.2.1.2 Characterization of pyrrole-aldimine ligands **L1** – **L4** with $^{13}$C NMR, HSQC and HMBC spectroscopy……..…… 46
2.2.1.3 Characterization of pyrrole-aldimine ligands **L1** – **L4** with FT-IR spectroscopy, mass spectrometry and elemental analysis……..…… 52
2.2.1.4 Characterization of pyrrole-aldimine ligands **L1** – **L4** with UV/Vis spectroscopy…….…… 54
2.3 CONCLUSION…..……..... 58
2.4 EXPERIMENTAL……. 58
2.4.1 Materials and instrumentation……. 58
2.4.2 Ligand synthesis……...…… 59
2.4.2.1 Synthesis of **L1** (E)-N-((1H-pyrrol-2-yl) methylene)aniline……...…… 59
2.4.2.2 Synthesis of **L2** (E)-N-((1H-pyrrol-2-yl)methylene)-2,6-dimethylaniline……... 59
2.4.2.3 Synthesis of **L3** (E)-N-((1H-pyrrol-2-yl)methylene)-2,6-diisopropylaniline……... 59
2.4.2.4 Synthesis of **L4** (E)-N1-((1H-pyrrol-2-yl)methylene)-N4,N4-diethylbenzene-1,4-diamine……... 60
2.5 REFERENCES…….…… 61

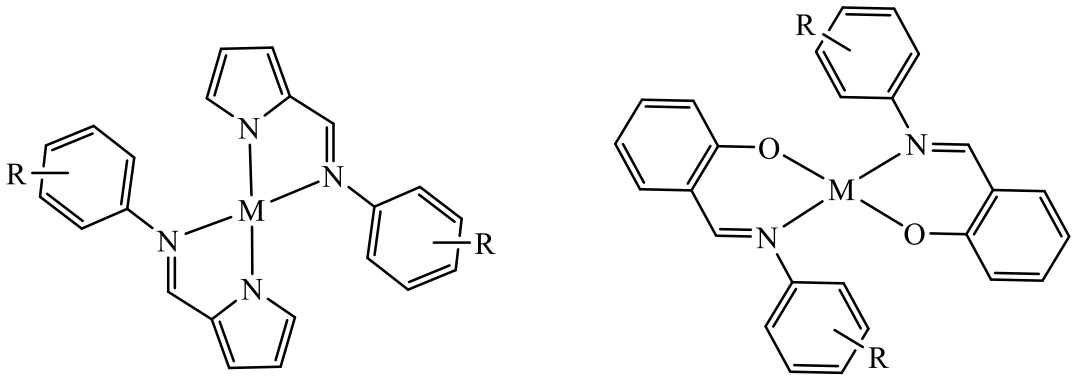
## 2.1 INTRODUCTION

Schiff base ligands (**Figure 2.1**) are a class of compounds that have been thoroughly studied and reported [1]–[3]. Pyrrole-aldimine ligands in particular have recently seen a rise in popularity due to their ease of synthesis and ease with which their electronic and steric properties can be varied. The presence of an imine and a pyrrole ring donor moiety makes this class of bidentate chelating ligands of interest in the area of coordination chemistry, as this allows them to stabilize metal ions in high oxidation states [4].




$R_1$, $R_2$ = aryl or alkyl
$R_3$ = H, alkyl

**Figure 2.1** *Schiff base compound general structure* [1]




Pyrrolylaldiminato complex

Salicylaldiminato complex

R = H, aryl, alkyl
M = Metal ion

**Figure 2.2** *Pyrrolylaldiminato and salicylaldiminato metal complexes general structures* [5]

Pyrrole-aldimine ligands are monoanionic bidentate nitrogen-based ligands with a pyrrole ring moiety which is substituted in the 2-position by a neutral imine donor moiety. This class of ligands is structurally similar to salicylaldimine ligands but differ in the manner in which they bind to metal ions. That is, salicylaldimine ligands form 6-membered ring chelates with metal ions through N,O donor atoms whereas pyrrole-aldimine ligands form five-membered ring chelates with metal ions through N,N donor atoms (**Figure 2.2**). Their ability to bind to metal

ions is afforded by the deprotonation of the acidic pyrrole-ring N-H proton in the presence of a strong base such as NaH or BuLi [5].

The ease with which their steric and electronic properties can be tuned is allowed by the ability to vary the substituents on the imine donor moiety [6]. This property widens the range of applications metal complexes derived from this class of ligands can potential be used in [7]–[9]. The synthesis and characterization of various pyrrole-aldimine ligands in which the imine moiety contains either alkyl or aryl substituents have been widely reported. Their synthesis proceeds via the condensation reaction of pyrrole-2-carboxaldeyde with the respective primary amine in the presence of an acid or base catalyst. With aryl amines, these reactions are usually carried out in the presence of an acid catalyst. Although this has been shown to speed up the reactions, product discoloring which may be a result of decomposition are observed as a result of the presence on an acid [3].

In this chapter, the synthesis and characterization of a range of pyrrole-aldimine ligands derived from pyrrole-2-carboxaldehyde and aryl amines, namely; aniline, 2,6-dimethylaniline, 2,6-diisopropylaniline and N,N-diethylanililine exploring different synthetic routes adapted from literature is reported.

## 2.2 RESULTS AND DISCUSSION

### 2.2.1 Synthesis and characterization of pyrrole-aldimine ligands

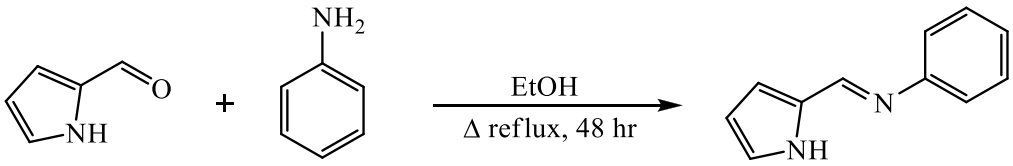
Three attempts at the synthesis of **L1** were carried out prior to finding the ideal synthetic route to **L1**. The first attempt involved reacting pyrrole-2-carboxaldehyde with aniline in the presence of MeOH as a solvent and formic acid as a catalyst. The reaction was carried out over a period of 24 hours at room temperature. In this attempt, product discoloring which could be a sign of decomposition as a result of the presence of acid was observed [10]. **L1** was obtained as a deep-red colored oil which was worked up to yield a deep red powder. A combined low yield of 35 % was isolated upon purification. In order to improve product yield and to find the cause of product discoloring, a different synthetic route was explored.

In the second attempt, the reactions conditions were kept the same as in the first attempt, however, acetic acid was used as a catalyst in place of formic acid. Changing the catalyst to acetic acid resulted in a deep-red colored oil, as with the first attempt, which was worked up to yield a deep red colored solid product. In both formic acid and acetic acid approaches, low

product yields were obtained. **L1** was isolated as deep red powders in yields of 35 % and 44 %, respectively.

In order to investigate if the presence of an acid catalyst could be the cause of product discoloring which could be a sign of decomposition, a third attempt at the synthesis of **L1** involved reacting pyrrole-2-carboxaldehyde and aniline in ethanol in the absence of a catalyst at room temperature over a period of 12 hours. This reaction resulted in poor conversion of starting material to **L1**. Although less product discoloring which is speculated to be a sign of decomposition was observed, very low yields of **L1** were obtained upon purification. **L1** was isolated as an off-white powder at a yield of 46 %.

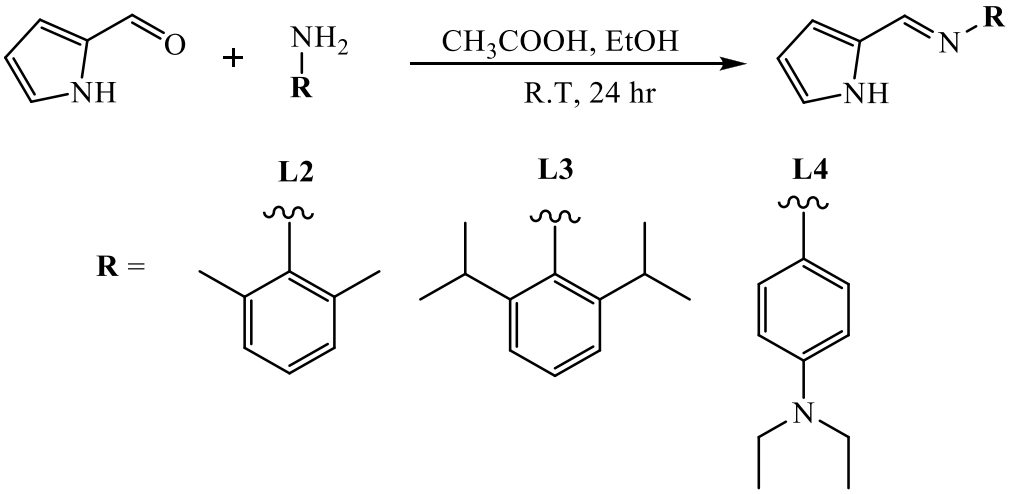
Upon realizing that the absence of an acid catalyst results in less product discoloring, pyrrole-aldimine ligand **L1** was synthesized by reacting pyrrole-2-carboxaldehyde and aniline under refluxing conditions as depicted in (**Scheme 2.1**). This reaction was carried out in the absence of an acid catalyst. Refluxing the pyrrole-2-carboxaldehye, aniline and ethanol reaction mixture greatly improved conversion of starting material to **L1** whilst avoiding product decomposition which is caused by the presence of an acid catalyst. Following this route, **L1** was isolated as a pure off-white powder in a yield of 75 %. **L1** was found to be soluble in both polar and nonpolar organic solvents and insoluble in water.




**Scheme 2.1** *Synthetic scheme for pyrrole-aldimine ligand **L1***

Two attempts at the synthesis of **L2** – **L4** were carried out. The first attempt, which was adapted from literature involved using methanol as a solvent and formic acid as a catalyst [10]. Carrying out the reactions in this manner resulted in product discolouring for **L2** and **L4**, which may be a result of product decomposition. **L2** and **L4** were obtained as bright yellow and dark brown oils, respectively. The yellow and dark brown oils were observed to solidify over a period of 24 hours when exposed to the atmosphere at room temperature. The yellow and dark brown solid crude products were then purified by recrystallization in MeOH. Activated charcoal was added in the recrystallization process in order to minimize the discoloring of the products. This

yielded **L2** and **L4** as light yellow and brown crystals in yields of 56 % and 39 %, respectively. Unlike with **L2** and **L4**, after 24 hours, **L3** precipitated out of solution as white precipitate. The white precipitate was isolated from the mother liquor by vacuum filtration. This yielded **L3** as a fine white powder in a yield of 66 %.




**Scheme 2.2** *General synthetic scheme for pyrrole aldimine ligands **L2** – **L4*** [10]

In an effort to improve the product yields of **L2** – **L4**, a second attempt, which is a modification of the first synthetic route was explored. The purpose of this was to also investigate whether changing the catalyst from formic acid to acetic acid would minimize product discoloring of **L2** and **L4**. This attempt resulted in satisfactory results as the yields were greatly improved to 85 %, 91 % and 90 %, for **L2**, **L3** and **L4**, respectively. This involved reacting pyrrole-2-carboxaldehyde with the respective amine in ethanol as depicted in (**Scheme 2.2**). Acetic acid was used to catalyze the reactions. Less product discoloring was observed and **L2** – **L4** were isolated in respectable yields. **L1** and **L2** were found to ne soluble in both polar and nonpolar organic solvents and insoluble in water. In the synthesis of all four ligands, the reactions do not reach completion. As such, tedious and extensive work-up processes are required to obtain the target ligands as pure products [10].

#### 2.2.1.1 Characterization of pyrrole-aldimine ligands L1 – L4 with $^1$H NMR, COSY and NOESY spectroscopy

All four ligands were characterized by proton nuclear magnetic resonance ($^1$H NMR) spectroscopy. Their $^1$H NMR chemical shifts as well as their atom labels are shown in (**Table 2.1**). All four ligands contain the pyrrole moiety as well as the HC=N functional group as a

result of the successful condensation of pyrrole-2-carboxaldehyde and the respective amine. The HC=N proton, which is labelled **5** is observed as a singlet in the range 7.91 – 8.31 ppm. This proton appears the most de-shielded in ligands **L1** and **L4** than it is in ligands **L2** and **L3** (**Table 2.1**). This is attributed to the presence of the $-CH_3$ and $-CH(CH_3)_2$ substituents on the phenyl rings of **L2** and **L3**, respectively. These sterically shield the imine protons, thereby resulting in their chemical shift positions appearing slightly up-field. The $-CH_3$ and $-CH(CH_3)_2$ substituents on the phenyl rings of **L2** and **L3** are electron donating groups, this contributes to their imine protons appearing more deshielded than those for **L1** and **L4**. The pyrrole ring proton labelled **1** is the most de-shielded of the three pyrrole ring protons. It resonates between 6.60 – 6.98 ppm as a doublet of doublet. Proton **2** is the most shielded of the three pyrrole ring protons. It resonates between 6.21 – 6.31 ppm as a doublet of doublet. Proton **3** appears as a doublet of doublet between 6.47 – 6.70 ppm.

Ligands **L1** and **L4** have no substituents in the ortho- position of the phenyl ring, the protons in this position are labelled **7** and **8**. They overlap and appear as a single signal between 7.01 – 7.41 ppm and are observed as a multiplet. All 4 ligands have no substituents in the meta position of the phenyl ring. The protons in this position are labelled **9** and **10**. For ligands **L1**, **L2** and **L3**, these protons overlap and appear as a single signal in the range 7.10 – 7.40 ppm. For ligands **L4**, these protons resonate between 6.65 – 6.58 ppm and appear as a multiplet. Ligands **L1**, **L2** and **L3** have no substituents in the para- position of the phenyl ring. The proton in this position is labelled **11**. For **L1**, this proton signal overlaps with the proton signal for the protons in positions **7** & **8**, which appears at 7.14 – 7.19 ppm. For **L2**, the signal for this proton is observed between 6,86 and 6.91 ppm. For **L3**, this proton signal overlaps with the proton signal assigned to the proton labelled **1**, which is observed at 7.01 – 7.06 ppm.

**L2** has methyl ($-C\underline{H}_3$) groups in the ortho position of the phenyl ring which appear as a singlet at 2.17 ppm. Ligand **L3** has isopropyl ($-CH(CH_3)_2$) groups in the ortho position of the phenyl ring. The C<u>H</u> protons, which are labelled **12** and **13** appear as a multiplet at 3.05 ppm. The $C\underline{H}_3$ protons which are labelled **14, 15, 16** and **17** appear as a doublet at 1.12 – 1.14 ppm. **L4** contains the N,N-diethyl [$-N(CH_2)_2(CH_3)_2$] group in the para position of the phenyl ring. Due to free rotation along the phenyl carbon and N,N-diethyl nitrogen (C-N) bond the $C\underline{H}_2$ protons labelled **12** and **13** overlap at 3.37 ppm and are observed as a quartet. The $\underline{CH}_3$ protons labelled **14** and **15** overlap at 1.18 ppm and are observed as a triplet. The $^1$H NMR spectrum of ligand **L1** (**Figure 2.3**) is shown as an example of the $^1$H NMR spectra obtained for ligands all 4 ligands.

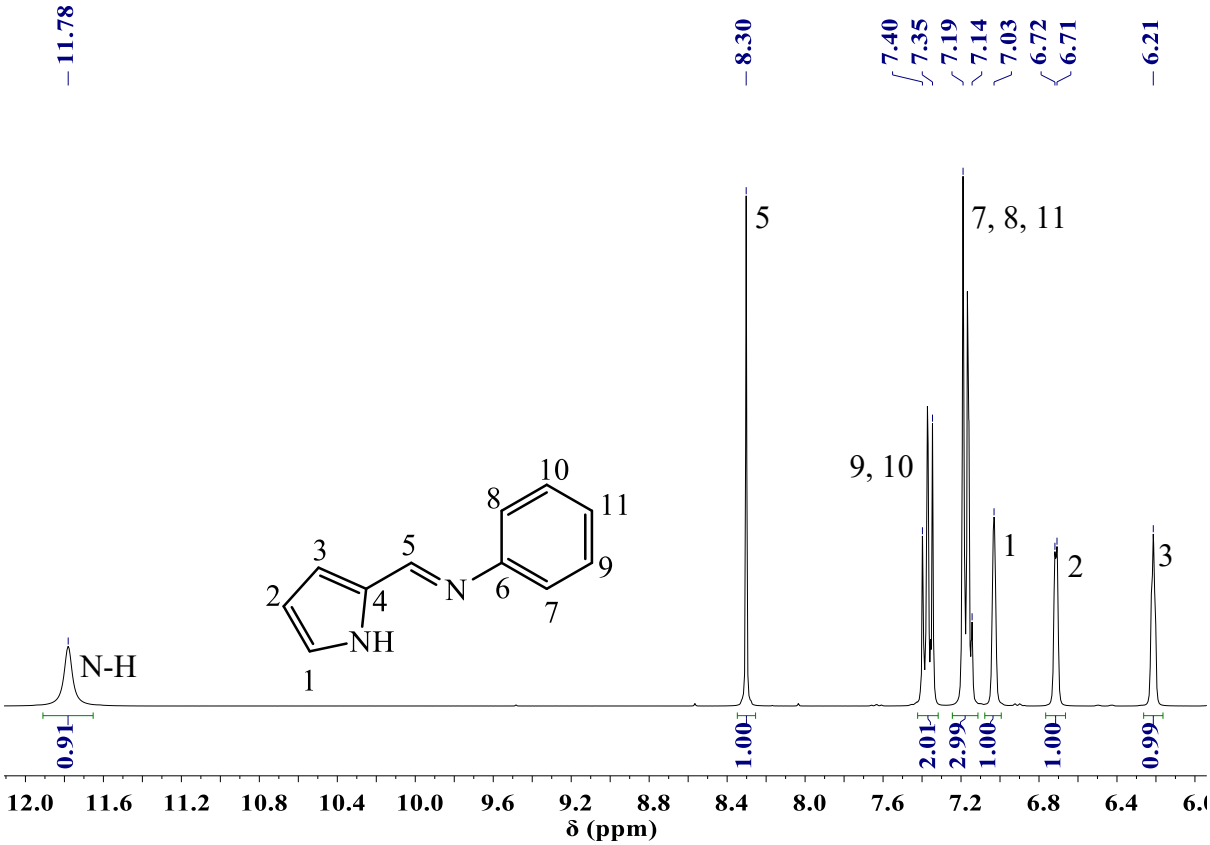



**Figure 2.3** *$^{1}$H NMR spectrum for pyrrole-aldimine ligand **L1** ( **DMSO**-d6, 300 K )*

Homonuclear correlation (COSY) spectroscopy was used to conclusively assign all protons on the basis that they will interact with any other proton that is up to 3 bonds away. All four ligands have three pyrrole ring protons labelled **1**, **2** and **3**, as they all contain the pyrrole moiety. The expected interaction between **2** with **1** and **3**, through three bonds was observed. No interaction between **1** and **3** is observed as they are four bonds away from each other. The imine proton does not interact with any other protons as there are no protons 2 or 3 bonds away. **L1** and **L4** contain no substituents in the ortho- position of the phenyl ring, as such **7** & **8** interact with **9** & **10** through three bonds. **L1**, **L2** and **L3** do not have substituents on the meta- position of the phenyl ring, as such **11** interacts with **9** & **10** through three bonds. **L2** contains $CH_3$ groups in the ortho position of the phenyl ring, as a result, **11** and **12** do not interact with any protons as there are none 2 or 3 bonds away. **L3** contains (-$CHCH_3$) groups in the ortho position on the phenyl ring, as a result, **11&12** interact with **13**, **14**, **15** & **16** through three bonds. **L4** contains the N,N-diethyl [-$N(CH_2)_2(CH_3)_2$] group in the para position of the phenyl ring. The $C\underline{H}_2$ protons labelled **12** & **13** interact with **14** & **15** through three bonds. The COSY spectrum

(**Figure 2.4**) obtained for ligand **L1** is illustrated as an example of the COSY spectra obtained for all 4 ligands.

**Table 2.1** *$^{1}H$ NMR data for ligands **L1** – **L4***

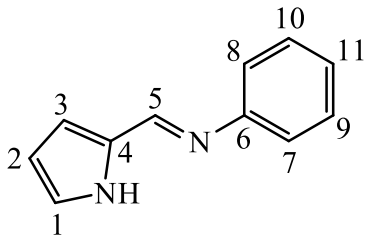
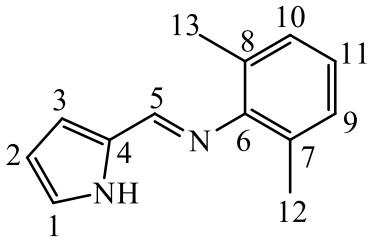
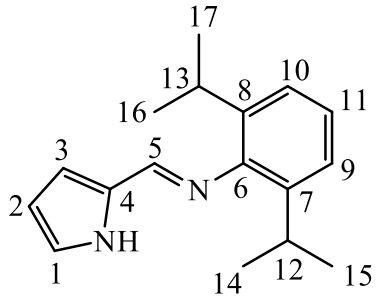
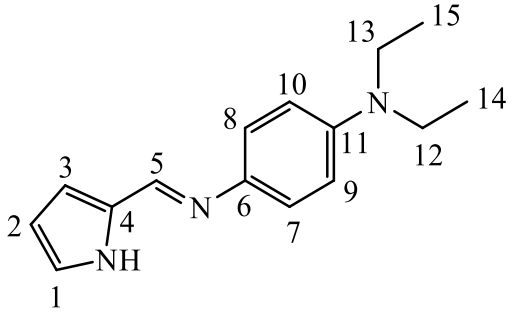
| Structure | N-H | HC=N | Pyrrole | Imino substituents |
|---|---|---|---|---|
|  | 11.79 | 8.30 (s, 1H) | **1:** 7.07 – 6.95 (m, 1H)<br>**2:** 6.21 (t, J = 3.1 Hz, 1H)<br>**3:** 6.71 (dt, J = 3.2, 1.4 Hz, 1H) | **7,8,11:** 7.04 (d, J = 7.3 Hz, 3H)<br>**9,10:** 7.41 – 7.33 (m, 2H) |
|  | 11.80 | 7.97 (s, 1H) | **1:** 6.89 (dd, J = 8.0, 6.9 Hz, 1H)<br>**2:** 6.22 (t, J = 2.0 Hz, 1H)<br>**3:** 6.65 (dt, J = 3.4, 1.6 Hz, 1H) | **9,10&11:** 7.18- 7.24 (m, 3H)<br>**12&13:** 2.10 (s, 6H) |

**Table 2.1 (continued)** *$^{1}$H NMR data for ligands **L1** – **L4***

| Structure | N-H | HC=N | Pyrrole | Imino substituents |
|---|---|---|---|---|
|  | 11.83 | 7.97 (s, 1H) | **1:** 7.07 – 6.99 (m, 1H)<br>**2:** 6.20 (t, J = 2.0 Hz, 1H)<br>**3:** 6.66 (dt, J = 3.4, 1.6 Hz, 1H) | **9,10:** 7.15 – 7.08 (m, 2H)<br>**11:** 7.07 – 6.99 (m, 1H)<br>**12&13:** 2.99 (hept, J = 6.9 Hz, 2H)<br>**14,15,16,17:** 1.11 (d, J = 7.0 Hz, 12H) |
|  | 11.55 | 8.31 (s, 1H) | **1 & 3:** 6.77 – 6.68 (m, 2H)<br>**2:** 6.15 (dd, J = 3.3, 1.7 Hz, 1H) | **7 & 8:** 7.23 (d, J = 9.0 Hz, 2H)<br>**9 & 10:** 6.62 (d, J = 9.1 Hz, 2H)<br>**12 & 13:** 3.29 – 3.36 (q, 2H)<br>**14 & 15:** 1.06 (t, J = 7.0 Hz, 7H) |

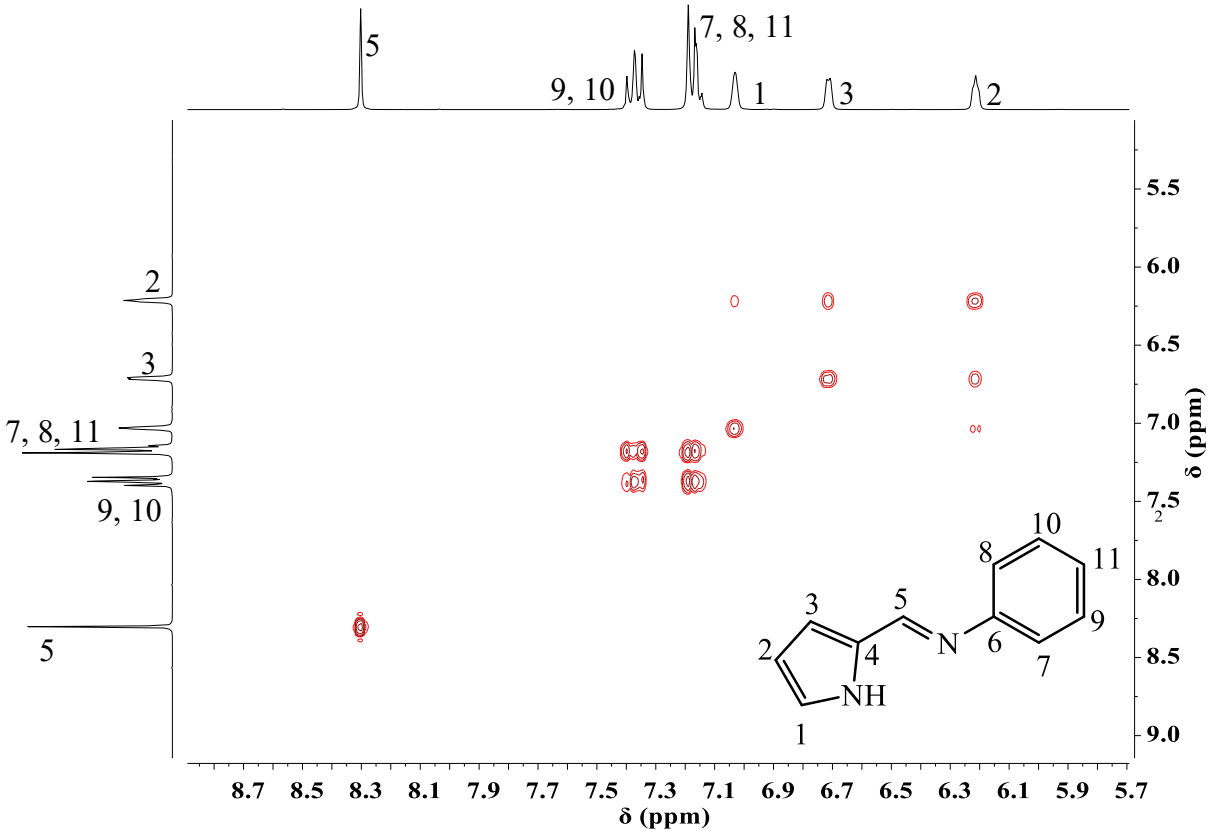



**Figure 2.4** *COSY spectrum for pyrrole-aldimine ligand **L1** ( **DMSO**-d6, 300 K )*

Nuclear overhauser effect (NOESY) spectroscopy was used to corroborate the assignment of the three pyrrole ring protons, this was done on the basis that protons that are close to each other through space will interact. Using the imine signal labelled **5** as a starting point, an interaction through space between the proton signal labelled **3** and the imine proton signal is observed. The proton labelled **3** interacts with **2** through space. An interaction between **2** with both **1** and **3** through space is observed. The interaction through space between the imine signal and protons in position **7** & **8** was used to distinguish and assign the phenyl ring protons labelled **7** & **8** and **9** & **10**. **L1** and **L4** do not have substituents in the **7** and **8** positions, the protons in these positions interact with the imine proton through space. **L2** contains $CH_3$ groups in the ortho- position. The $C\underline{H}_3$ protons interact with the imine proton labelled **5** and with the phenyl ring protons labelled **9** & **10** through space. **L3** contains isopropyl ($-CH(CH_3)_2$) groups in the ortho position of the phenyl ring, the $C\underline{H}_3$ protons labelled **13**, **14**, **15** and **16** interact with **5**, **9** & **10** through space. Ligands **L1**, **L2** and **L3** do not contain substituents in the para-position on the phenyl ring. The interaction between this proton with the protons in the meta-position through space was used to assign **11**. **L4** contains the N,N-diethyl [$-N(CH_2)_2(CH_3)_2$]

group in the para position of the phenyl ring. The $C\underline{H_2}$ protons labelled **12** & **13** interact with **9** & **10** as well as the alkyl $CH_3$ protons labelled **14** & **15** through space. The NOESY spectrum (**Figure 2.5**) obtained for ligand **L1** is illustrated as an example of the NOESY spectra obtained for all 4 ligands.

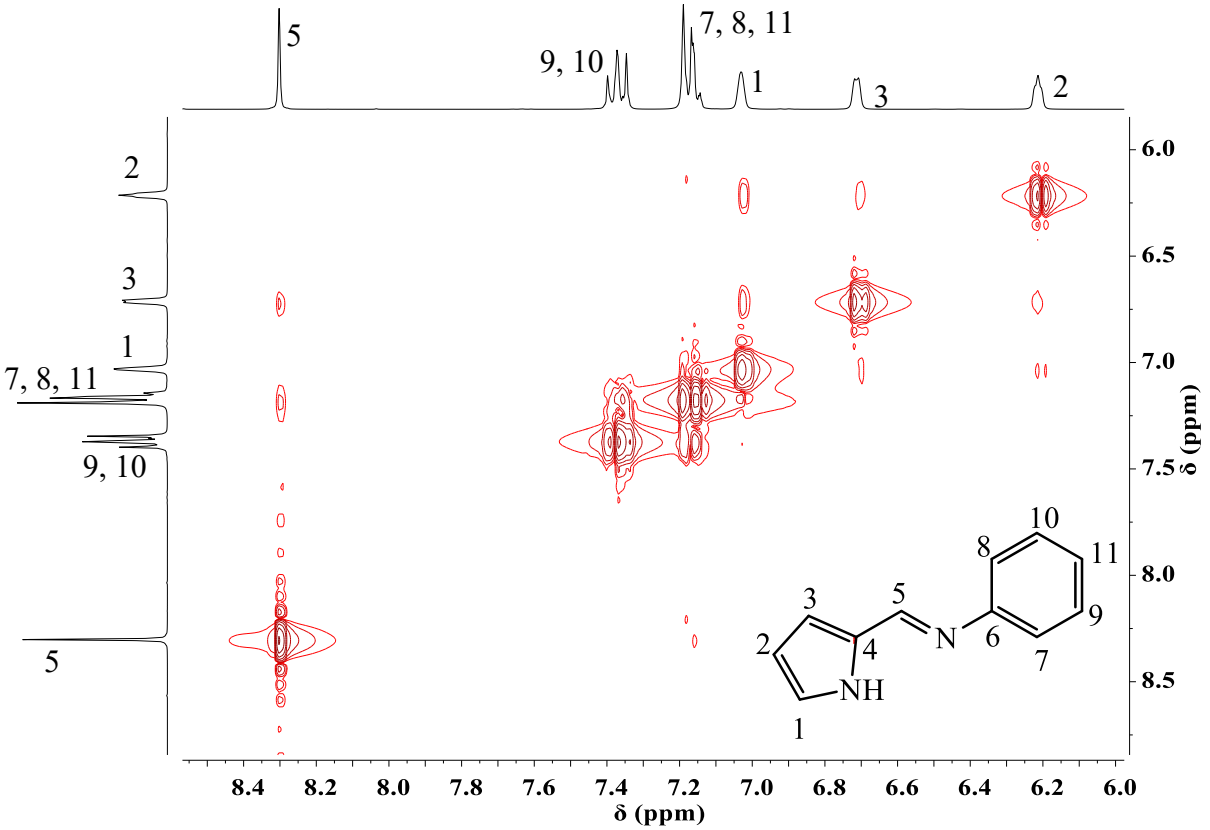



**Figure 2.5** *NOESY spectrum for pyrrole-aldimine ligand **L1** ( **DMSO**-d6, 300 K )*

### 2.2.1.2 Characterization of pyrrole-aldimine ligands L1 – L4 with $^{13}$C NMR, HSQC and HMBC spectroscopy

Heteronuclear single quantum coherence (HSQC) spectroscopy and heteronuclear multiple bond correlation (HMBC) spectroscopy were used to assign the $^{13}$C NMR signals for ligands all four ligands. This was done on the basis that each proton will interacts with the carbon atom that it is directly bonded to. The $^{13}$C NMR spectrum of ligand **L1** (**Figure 2.6**) is illustrated as an example of the $^{13}$C NMR spectra obtained for all four ligands. The most de-shielded signal observed in the range 145.63 – 152.43 ppm is assigned to the imine $H\underline{C}$=N carbon atom. This signal confirms the successful synthesis of all five ligands. The pyrrole moiety carbon signals labeled **1**, **2** and **3** are observed in the range 122. 63 – 123.83 ppm, 109.32 – 109.71 ppm and 114.55 – 116.45 ppm. The pyrrole ring quaternary carbon atom labeled **4** resonates between

130.08 - 131.14 ppm. The aromatic quaternary carbon atom labelled **6** shows a signal in the range 145.89 - 151.36 ppm.

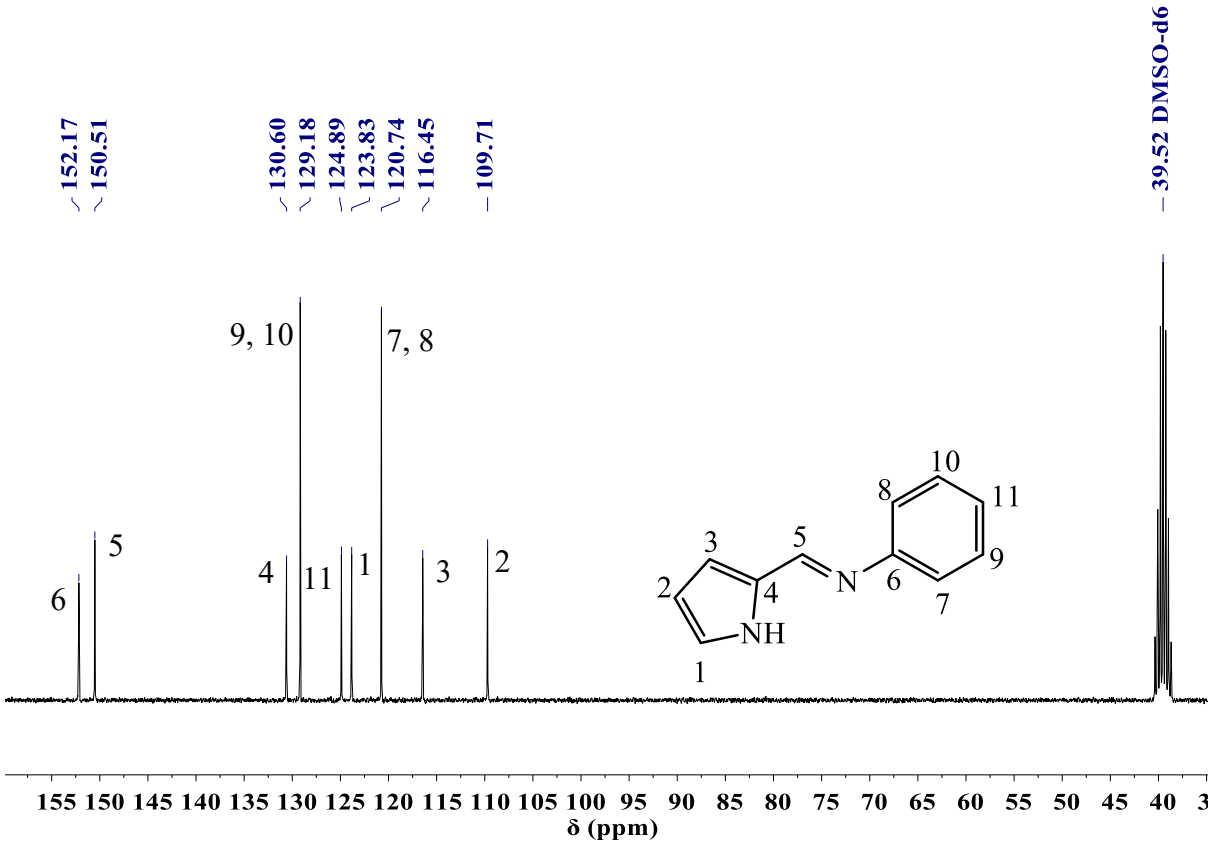



**Figure 2.6** *$^{13}$C NMR spectrum for pyrrole-aldimine ligand **L1** ( **DMSO**-d6, 300 K)*

Ligands **L1** and **L4** have no substituents in the ortho position of the phenyl ring labelled **7** & **8**, the carbon signals on this position are observed at 120.74 – 121.91 ppm, respectively. For **L2** and **L3**, these are quaternary carbon atoms and their signal is observed at 127.87 – 137.60 ppm, respectively. All four ligands contain no substituents on the meta position the phenyl ring, the carbon atoms in this position are labelled **9** & **10**. The signals assigned to these atoms are observed in the range 123.50 – 129.26 ppm. Ligands **L1- L3** contain no substituents in the para position on the phenyl ring, the phenyl carbon atom labelled **11** is observed between 122.70 – 139.90 ppm. The carbon atom in this position on **L4** is a quaternary carbon and the signal for this atom is observed at 114.55 ppm. Ligand **L2** contains methyl (-$CH_3$) groups in the ortho position on the phenyl ring. The carbon atoms labelled **12** and **13** are observed at 18.12 ppm. Ligand **L3** has isopropyl (-$CH(CH_3)_2$) groups in the ortho position on the phenyl ring. The C<u>H</u> carbon atoms which are labelled **12** and **13** appear at 20.05 ppm. <u>C</u>$H_3$ signal for carbon atoms labelled **14, 15, 16** and **17** appear at 23.73 ppm. **L4** contains the N,N-diethyl [-$N(CH_2)_2(CH_3)_2$]

group in the para position of the phenyl ring. Due to free rotation along the phenyl carbon and N,N-diethyl nitrogen (C-N) bond the $\underline{C}H_2$ carbon atoms labelled **12** and **13** are observed at 42.27 ppm whereas the $\underline{C}H_3$ labelled **14** and **15** are observed at 10.35 ppm.

**Table 2.2** *$^{13}$C NMR data for ligands **L1 – L4***

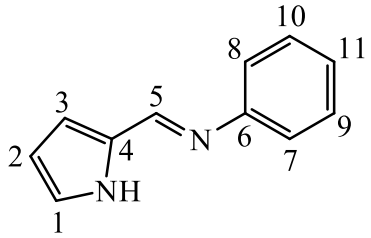
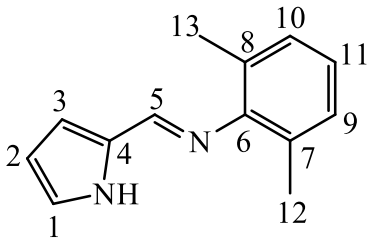
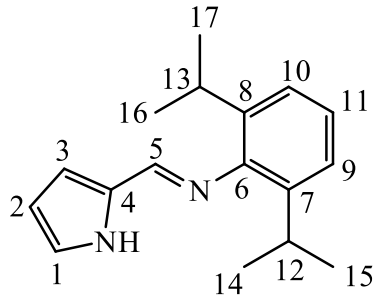
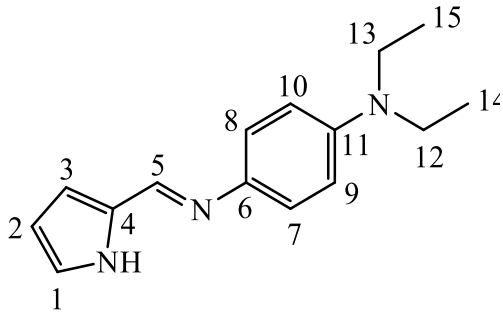
| Structure | HC=N | Pyrrole | Imino substituents |
|---|---|---|---|
|  | 152.17 | **1:** 116.45<br>**2:** 109.71<br>**3:** 123.83<br>**4:** 130.60 | **6:** 150.51<br>**7&8:** 120.74<br>**9&10:** 129.18<br>**11:** 124.89 |
|  | 153.08 | **1:**152.88<br>**2:** 109.64<br>**3:** 116.58<br>**4:** 129.63 | **6:** 150.36<br>**7&8:** 129.94<br>**9,10&11:** 7.18- 7.24 (m, 3H)<br>**12&13:** 18.12 |

**Table 2.2 (continued)** *$^{13}$C NMR data for ligands **L1 – L4***

| Structure | HC=N | Pyrrole | Imino substituents |
|---|---|---|---|
|  | 152.43 | **1:** 122.70<br>**2:** 109.45<br>**3:** 115.74<br>4: 130.08 | **6:** 149.26<br>**7&8:** 137.60<br>**9, 10:** 123.50<br>**11:** 122.70<br>**12&13:** 27.32<br>**14, 15, 16, 17:** 23.48 |
|  | 146.40 | **1:** 122.95<br>**2:** 109.98<br>**3:** 115.60<br>4: 131.30 | **6:** 146.06<br>**7 & 8:** 122.24<br>**9 & 10:** 112.38<br>**11:** 139.37<br>**12 & 13:** 42.27<br>**14 & 15:** 10.35 |

HSQC spectroscopy was used to assign carbon signals for all 4 ligands in the cases where the carbon atoms are directly bonded to protons. The imine proton labelled **5** correlates to the most de-shielded carbon signal which is observed in the range 145.63 – 152.43 ppm. the pyrrole ring protons labelled **1**, **2** and **3** are observed in the ranges 122.63 – 123.83 ppm, 109.32 – 109.71 ppm and 114,55 – 116,45 ppm. Ligands **L1** and **L4** contain no substituents in the ortho and meta positions on the phenyl ring. The proton signal assigned to **7** & **8**, correlates to the carbon signal observed in the range 120.74 – 121.91 ppm. The proton signal assigned to **9** & **10** correlate to the carbon signal observed between112.08 – 129.18 ppm. Ligands **L1**, **L2** and **L3** contain no substituents on the para position on the phenyl ring. The proton signal in this position correlates to the carbon signal observed between 122.70 – 139.90 ppm.

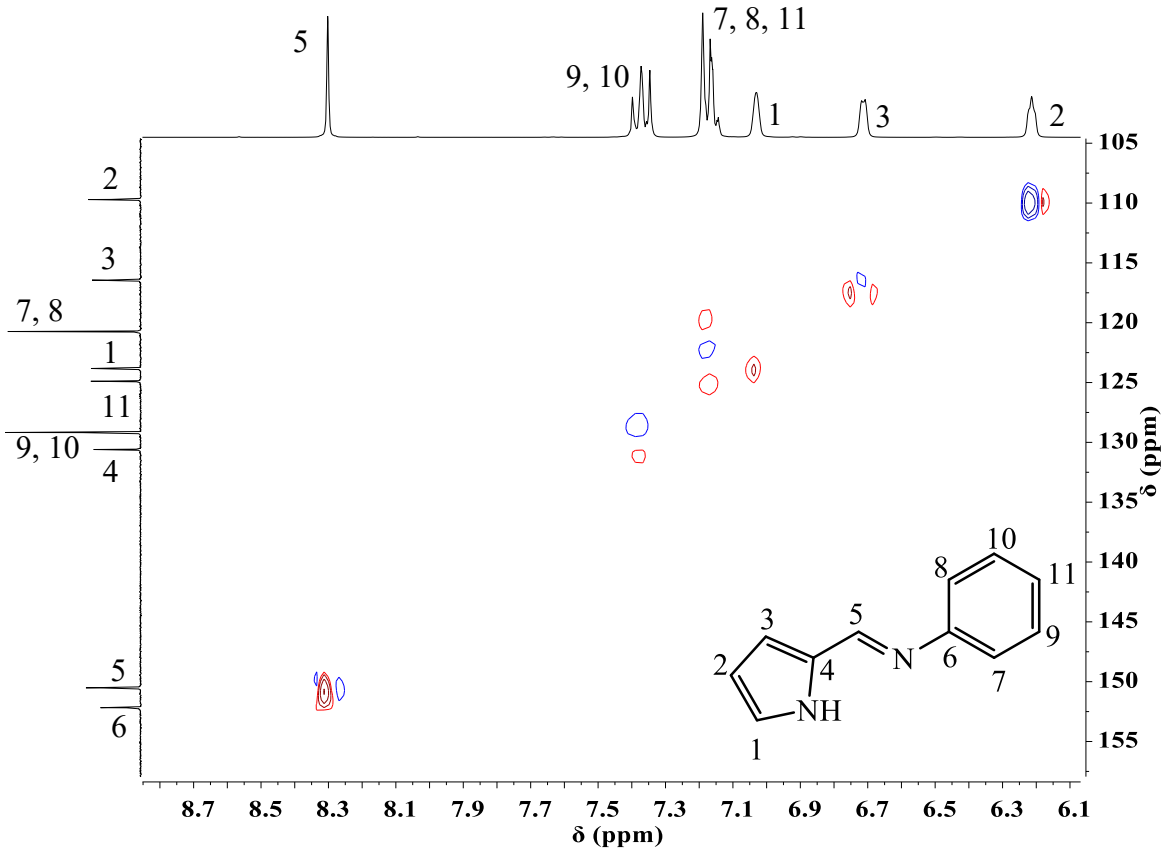



**Figure 2.7** *HSQC spectrum for pyrrole-aldimine ligand **L1** ( **DMSO**-d6, 300 K)*

Ligands **L2** and **L3** contain methyl (-$CH_3$) and isopropyl (-$CH(CH_3)_2$) groups on the ortho position on the phenyl ring, respectively. For **L2**, the $CH_3$ protons' signal correlated the carbon signal observed at 18.18 ppm. The CH proton signal correlates to a carbon signal observed at 27.32 ppm and the $CH_3$ proton signal correlates to the carbon signal observed at 23.48 ppm for **L3**. **L4** contains the N,N-diethyl [-$N(CH_2CH_3)$] group in the para position of the phenyl ring.

The $C\underline{H_2}$ proton signals correlate to carbon signal observed at 43.80 ppm and the $C\underline{H_3}$ proton signal correlates to the carbon signal observed at 12.51 ppm. Ligands **L2** and **L3** contain methyl ($-CH_3$) and isopropyl ($-CH(CH_3)_2$) groups on the ortho position on the phenyl ring, respectively. For **L2**, the $C\underline{H_3}$ protons' signal correlated the carbon signal observed at 18.18 ppm. The $C\underline{H}$ proton signal correlates to a carbon signal observed at 27.32 ppm and the $C\underline{H_3}$ proton signal correlates to the carbon signal observed at 23.48 ppm for **L3**. **L4** contains the N,N-diethyl [$-N(CH_2CH_3)$] group in the para position of the phenyl ring. The $C\underline{H_2}$ proton signals correlate to carbon signal observed at 43.80 ppm and the $C\underline{H_3}$ proton signal correlates to the carbon signal observed at 12.51 ppm. **Figure 2.7** shows the HSQC spectrum obtained for pyrrole-aldimine ligand **L1** and is shown as an example of the HSQC spectra obtained for all four ligands.

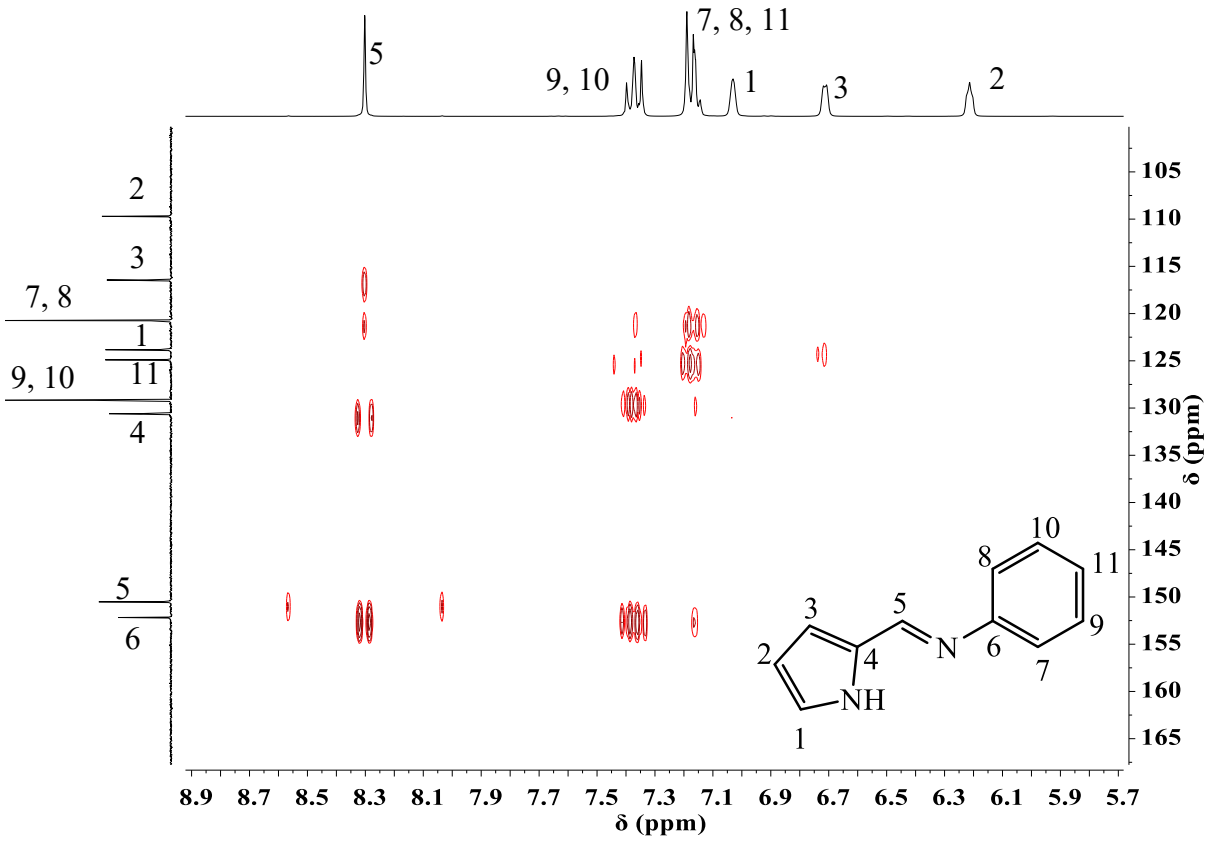



**Figure 2.8** *HMBC spectrum for pyrrole-aldimine ligand **L1** ( **DMSO**-d6, 300 K)*

HMBC spectroscopy was used to assign the quaternary carbon signals for ligands **L1** – **L4**. The proton signals for **3** and **5** correlate to a carbon signal observed in the range 130.08 – 131.14 ppm. This signal is assigned to the pyrrole ring quaternary carbon atom labelled **4** on the basis that it interacts with the proton signals for 3 and 5 through 2 bonds. The proton signal

assigned to **7** & **8** correlates to a carbon signal observed at 149.26 –145.89 ppm for **L1** and **L2**, respectively. These signals are assigned to the phenyl ring quaternary carbon atom labelled 6 on the basis that protons 7&8 interact with 4 through 2 bonds. Ligands **L1** and **L2** contain methyl (-$CH_3$) and isopropyl (-$CH(CH_3)_2$) groups on the ortho position on the phenyl ring, respectively. The methyl $C\underline{H}_3$ and isopropyl C<u>H</u> proton signals correlate to a carbon signals observed at 127.87 – 137.60 ppm, respectively. These signals are assigned to the phenyl ring quaternary carbon atoms labelled **7** & **8**, which bear the alkyl substituents. **Figure 2.8** shows the HMBC spectrum obtained for pyrrole-aldimine ligand **L1** and is shown as an example of the HMBC spectra obtained for all four ligands.

#### 2.2.1.3 FT-IR spectroscopy, mass spectrometry and elemental analysis characterization of pyrrole-aldimine ligands L1 – L4

All four ligands contain the pyrrole moiety, and as such their FT-IR spectra exhibit the ν(N-H) band which is observed in the range 3172 $cm^{-1}$ and 3240 $cm^{-1}$. The successful preparation of ligands **L1** – **L4** is corroborated by the presence of an intense sharp band in the range 1606 $cm^{-1}$ – 1631 $cm^{-1}$ and its shoulder peak in the range 1662$cm^{-1}$ – 1590 $cm^{-1}$ in the IR spectra of these ligands (**Figure 2.9**). These are assigned to the imine ν(HC=N) functional group. The aromatic ν(C-H) bands as a result of the aomatic component of the ligands are observed in the range 2275 $cm^{-1}$ – 3000 $cm^{-1}$. This is in-line with the FT-IR bands reported by Bengharez *et al*. when the group prepared a range of pyrrole-aldimine ligands for a hydrolysis kinetics study. The ligand derived from aniline, which is structurally identical to **L1** showed FT-IR bands at 1625 $cm^{-1}$ and 3220 $cm^{-1}$. These were assigned to ν(C=N) and ν(N–H) functional groups, respectively [6]. In the mass spectra obtained for ligands **L1** - **L4**, molecular ion peaks consistent with the calculated molecular weights of the four ligands as charged species, $[M+H]^+$ are observed (**Table 2.4**). This observation further confirms the successful preparation of all four ligands. The mass spectrum for ligand **L1** (**Figure 2.10**) is shown as an example of the mass spectra obtained for all 4 ligands. A match in the predicted isotopologue pattern with the isotopologue pattern observed in the mass spectrum obtained for ligand **L1** (**Figure 2.11**) is illustrated as an example of the isotopologue pattern match observed for all four ligands. Elemental analysis was used to confirm the purity of the 4 successfully synthesized ligands. The elemental analysis data obtained for ligands **L1** - **L4** are in agreement with the calculated elemental composition for these ligands as listed in (**Table 2.4**).

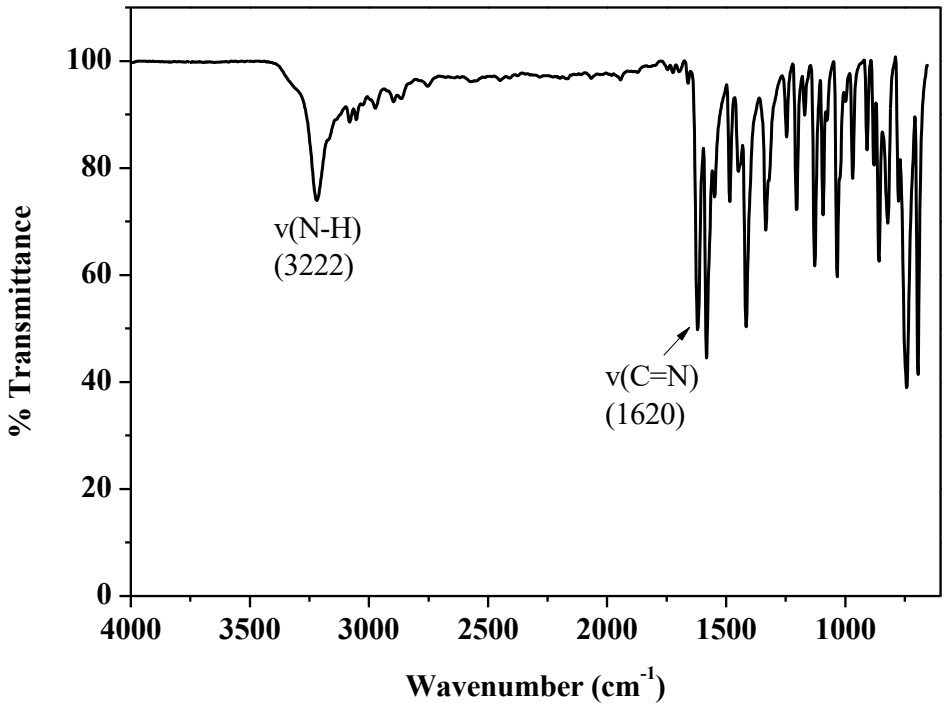



**Figure 2.9** *FT-IR spectrum for pyrrole-aldimine ligand* ***L1***

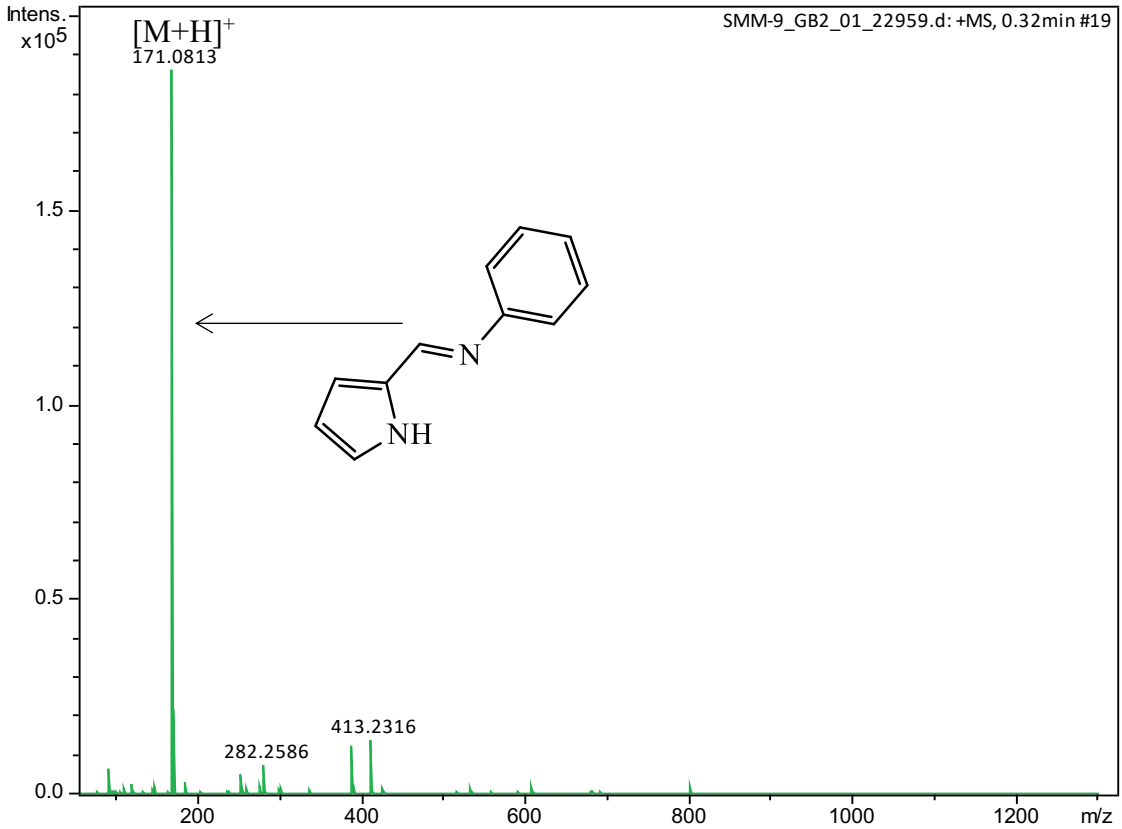



**Figure 2.10** *Electrospray ionization mass spectrum for pyrrole-aldimine ligand* ***L1***

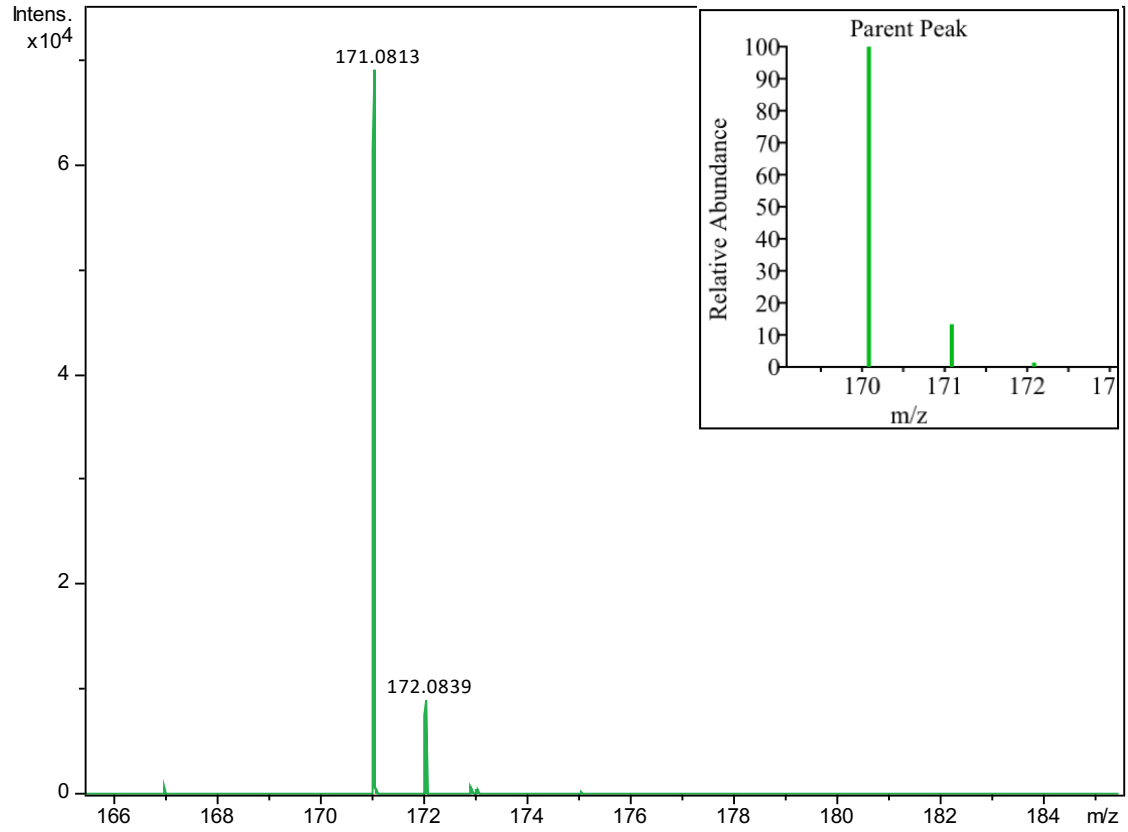



**Figure 2.11** *Mass spectrometry isotopologue pattern for pyrrole-aldimine ligand **L1***

### 2.2.1.4 Characterization of pyrrole-aldimine ligands L1 – L4 with UV-Vis spectroscopy

The absorption spectra for ligands **L1** – **L4** were recorded in toluene at a concentration of 0.0001 M (**Figure 2.12**). All four spectra exhibit a single absorption band in the range 300 nm – 378 nm as listed in (**Table 2.3**). These bands are assigned to intra-ligand transitions. The absorption bands for **L2** and **L3** are shifted to a lower wavelength relative to those for **L1** and **L4** because of the variance in the extension of π-orbital delocalization to the phenyl group. This is attributed to steric effects as a result of the methyl ($-CH_3$) and isopropyl ($-CH(CH_3)_2$) substituents in the ortho position on the phenyl rings of **L2** and **L3**, respectively. The presence of these groups results in larger dihedral angles of the substituents in relation to the iminopyrrole/yl backbone, which in turn results in the delocalization occurring to a lesser extent for **L2** and **L3** [11], [12].

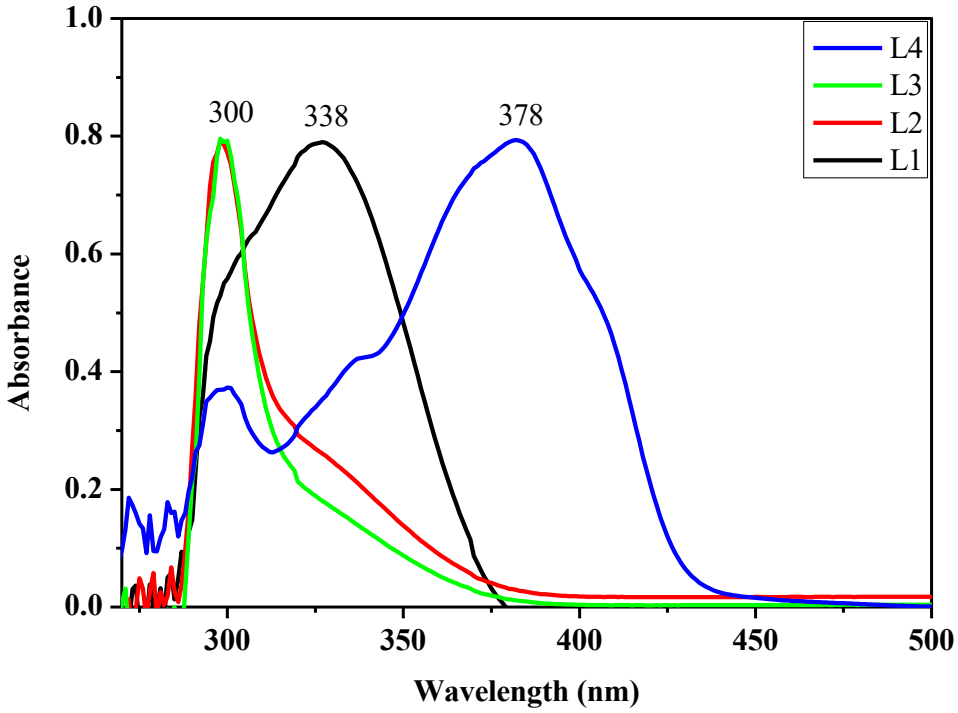



**Figure 2.12** *UV-Vis spectra (in toluene) for pyrrole-aldimine ligands **L1**, **L2**, **L3** and **L4***

**Table 2. 3** *UV/Vis spectroscopy data for pyrrole-aldimine ligands **L1** – **L4***

| **Ligand** | **Uv-vis (λMax/nm)** |
|---|---|
| | Intra-ligand band |
| **L1** | 338 |
| **L2** | 300 |
| **L3** | 300 |
| **L4** | 378 |

**Table 2.4** *Yield, HR-MS, FT-IR and elemental analysis data for ligands **L1** – **L4***

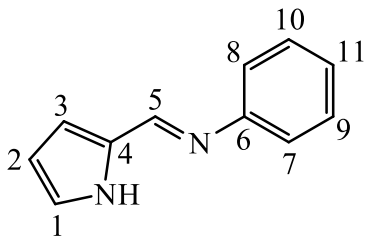
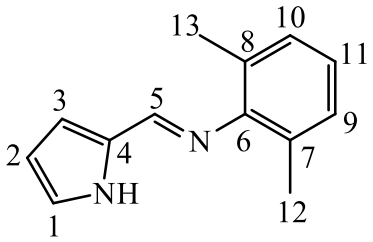
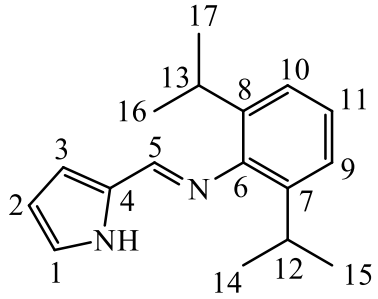
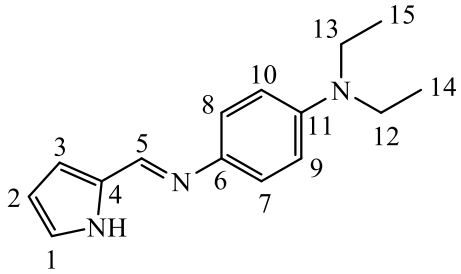
| **Structure** | **Yield %** | **Formula** | **ESI-MS [M+H]$^+$** | **FT-IR** | | **Elemental analysis Found (cal)** | | |
|---|---|---|---|---|---|---|---|---|
| | | | Found (Cal) | ν(N-H) | ν(C=N) | C | H | N |
|  | 75 | $C_{11}H_{10}N_2$ | 171.081 (171.091) | 3217 | 1622 1583 | 76.45 (77.62) | 5.94 (5.92) | 16.34 (16.46) |
|  | 85 | $C_{13}H_{14}N_2$ | 199.123 (199.122) | 3213 | 1627 1589 | 78.33 (78.75) | 7.16 (7.12) | 14.51 (14.13) |

**Table 2.3 (continued)** *Yield, HR-MS, FT-IR and elemental analysis data for ligands* ***L1 – L4***

| Structure | Yield % | Formula | ESI-MS $[M+H]^+$ | FT-IR | | Elemental analysis (calc) | | |
|---|---|---|---|---|---|---|---|---|
| | | | Found (Cal) | ν(N-H) | ν(C=N) | C | H | N |
|  | 91 | $C_{17}H_{22}N_2$ | 255.166 (255.185) | 3240 | 1631 | 79.97 (80.23) | 8.91 (8.72) | 11.12 (11.01) |
|  | 90 | $C_{15}H_{19}N_3$ | 242.148 (242.165) | 3201 | 1606 1571 | 74.54 (74.65) | 8.59 (7.94) | 17.56 (17.41) |

## 2.3 CONCLUSION

Four pyrrole-aldimine ligands with varying steric demands were successfully synthesized following the Schiff base condensation reaction in ethanol. The preparation of ligand **L1** was carried out in the absence of an acid catalyst as prior attempts at the synthesis of **L1** in the presence of acid led to product discoloring. Ligands **L2** – **L4** were synthesized in the presence of acetic acid as a catalyst. All four ligands were isolated as powders in respectable yields. The presence of the imine proton signal, which is observed in the range 7.91 – 8.31 ppm in the $^{1}$H NMR spectra of all four ligands confirmed the successful condensation of pyrrole-2-carboxablehyde and the respective amine. The conclusive assignments of the $^{1}$H NMR spectra chemical shifts were made using COSY and NOESY spectroscopy. The successful preparation of the ligands was corroborated the presence of the imine carbon, which is observed in the range 145.63 – 152.43 ppm in the $^{13}$C NMR spectra of all four ligands. The assignments of the $^{13}$C NMR spectra were conclusively made using HSQC and HMBC spectroscopy. In the FT-IR spectra of all four ligands, sharp intense bands observed in the range 1606 $cm^{-1}$ – 1631 $cm^{-1}$, which are assigned to the imine functional group as well as broad bands observed in the range 3172 $cm^{-1}$ and 3240 $cm^{-1}$ assigned to the pyrrole N-H functional group and aromatic C-H bands observed in the range 2275 $cm^{-1}$ – 3000 $cm^{-1}$ corroborate the successful condensation of pyrrole-2-carboxaldehye with the respective amines. Molecular ion peaks in the obtained mass spectra consistent with the expected m/z values predicted for all four ligands show that **L1** – **L4** were successfully synthesized. In the UV/Vis spectra, single bands at λmax of 338 nm, 300 nm, 300 nm and 378 nm and assigned to intra-ligand transitions further corroborates the preparation of **L1**, **L2**, **L3** and **L4** respectively. The obtained elemental analysis data was found to be consistent with the calculated elemental composition data for all four ligands. This observation confirmed purity of the successfully prepared ligand

## 2.4 EXPERIMENTAL

### 2.4.1 Materials and instrumentation

All chemical reactions and manipulations were performed on a dual vacuum/nitrogen line using standard Schlenk techniques unless otherwise stated. Reagent grade chemicals were obtained from Sigma Aldrich and used as received. All solvents were dried using appropriate drying reagents and distilled prior to use. $^{1}$H NMR, $^{13}$C NMR and 2D NMR spectra were recorded on a Varian 300 MHz spectrometer using tetramethyl silane as an internal standard. Chemical shifts are reported in ppm and referenced to the solvent signal (DMSO-d6). FT-IR spectra were

recorded on a Bruker TENSOR 27 spectrometer using ATR. Mass spectra of the ligands were recorded on Bruker compact ultimate 3000 HR-MS. Absorption measurements were recorded on a SpeCord 210 plus AnalytikJena UV-Vis spectrophotometer in toluene. Elemental analysis were performed in the micro analytical laboratory of the University of Stellenbosch.

### 2.4.2 Ligand synthesis

#### 2.4.2.1 Synthesis of L1 (E)-N-((1H-pyrrol-2-yl)methylene)aniline

Aniline (15.0 mmol, 1.3970 g) was added to a pale brown solution of pyrrole-2-carboxaldehyde (15.0 mmol, 1.4265 g) in ethanol (10.00 mL). The light brown solution was refluxed under magnetic stirring for 48 hours. The solvent was removed under vacuum to yield a pale-brown oil. The pale brown oil was observed to crystalize over 24 hours to yield light brown crystals. To purify the product, the crystals were crushed to obtain a light brown powder. The light brown powder was washed 3 times with distilled water and isolated from the water by vacuum filtration after each wash. This yielded an off-white powder. Isolated yield: 1.9238 g (75%).

#### 2.4.2.2 Synthesis of L2 (E)-N-((1H-pyrrol-2-yl)methylene)-2,6-dimethylaniline

To a stirring pale brown solution of pyrrole-2-carboxaldehyde (15.0 mmol, 1.4265 g) in ethanol (10.00 mL), acetic acid (5 drops) was added. The solution was stirred for 5 minutes prior to the dropwise addition of 2,6-dimethylaniline (15.0 mmol, 1.3970 g). The yellow solution was stirred for 18 hours during which an off-white solid precipitated from solution. The reaction mixture was further concentrated to increase the quantity of the solid produced. Vacuum filtration was used to isolate the off-white solid. To improve yield, the filtrate was concentrated until more ligand precipitated out of solution. The ligand was isolated from the mother liquor by vacuum filtration. This process was repeated 2 additional times to yield a white powder. Isolated yield: 2.5611 g (85%).

#### 2.4.2.3 Synthesis of L3 (E)-N-((1H-pyrrol-2-yl)methylene)-2,6-diisopropylaniline

**L3** was prepared following the same synthetic procedure used for **L2**. 2,6-diisopropylaniline (15.0 mmol, 1.3970 g) was added dropwise to a stirring solution of pyrrole-2-carboxaldehyde (15.0 mmol, 1.4265 g) and acetic acid (5 drops) in ethanol (10.00 mL). Magnetic stirring was used to stir the light pink solution for 18 hours during which a solid precipitated from solution. The reaction mixture was concentrated under vacuum in order to maximize the formation of the solid which was isolated from the reaction mixture by vacuum filtration. The filtrate was worked up by concentrating it under vacuum and the resulting white precipitate isolated by

vacuum filtration. This process was repeated 2 additional times to yield **L3** as a white powder. Isolated yield: 3.4621 g (91 %).

#### 2.4.2.4 Synthesis of L4 (E)-N1-((1H-pyrrol-2-yl)methylene)-N4,N4-diethylbenzene-1,4-diamine

**L4** was synthesized following the same synthetic procedure used for **L2** and **L3**. N,N-diethylylaniline (15.00 mmol, 1.3970 g) was added dropwise to a stirring light brown solution of pyrrole-2-carboxaldehyde (15.00 mmol, 1.4265 g) and acetic acid (5 drops) in ethanol (10.00 mL). Magnetic stirring was used to stir the dark brown solution for 18 hours. A solid precipitated out of solution without concentrating the reaction mixture under vacuum. However, to maximize yield, the reaction mixture was concentrated under vacuum. The solid was isolated from the reaction mixture by vacuum filtration. The filtrate was returned to the reaction flask and concentrated under vacuum until more product precipitated out of solution. The precipitate was separated from the reaction mixture by vacuum filtration. This process was repeated 2 additional times to yield **L4** as a mustard-yellow powder. Isolated yield: 2.8843 g (90 %).

## 2.5 REFERENCES


[1] H. Schiff, *Justus Liebigs Ann. Chem.*, 1864, 131, 1, 118 - 119.

[2] H. V. Babu and K. Muralidharan, *RSC Adv.*, 2014, 4, 12, 6094 - 6102.

[3] V. V. Grushin and W. J. Marshall, *Adv. Synth. Catal.*, 2004, 346, 12, 1457-1460.

[4] C. S. B. Gomes, M. T. Duarte, and P. T. Gomes, *J. Organomet. Chem.*, 2014, 760, 167-176.

[5] H. Hao, S. Bhandari, Y. Ding, J. Magull, H.G Schmidt, M. Noltemeyer and C. Cui, *Eur. J. Inorg. Chem.*, 2002, 2002, 5, 1060 - 1065.

[6] Z. Bengharez, Z. El Bahri, and A. Mesli, *Int. J. Chem. Kinet.*, 2013, 45, 6, 404 - 414.

[7] G. H. Chen, W. J. Leu, J. H. Guh, C. H. Lin, and J. H. Huang, *J. Organomet. Chem.*, 2018, 868, 122 - 130.

[8] Y. S. Li, Y. R. Li, and X. F. Li, *J. Organomet. Chem.*, 2003, 667, 1, 185-191.

[9] Z. Wu, Q. Chen, G. Yanga, C. Xiao, J. Liu, S. Yang, and J.S Ma, *Sensors Actuators, B Chem.*, 2004, 99, 2 - 3, 511 - 515.

[10] Y. Yoshida, S. Matsui, Y. Takagi, M. Mitani, T. Nakano, H. Tanaka, N. Kashiwa, and T. Fujita, *Organometallics*, 2001, 20, 23, 4793–4799.

[11] S.A. Carabineiro, L.C Silva, P.T Gomes, L.C.J Pereira, L.F Veiros, S.I Pascu, M.T Duarte, S. Namorado, and R.T Henriques, *Inorg. Chem.*, 2007, 46, 17, 6880 – 6890.

[12] C. S. B Gomes, P. T Gomes, M. T Duarte, R.E Di Paolo, A. L Maçanita, and M. J Calhorda, *Inorg. Chem.*, 2009, 48, 23, 11176 - 11186.

# Chapter 3:

# Synthesis and characterization of bis-(pyrrole-aldiminato) Zn(II) and Co(II) complexes

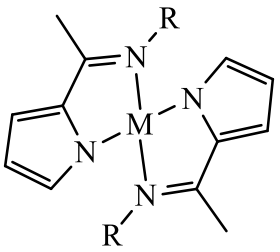
CONTENT

3.1 INTRODUCTION…… 63
3.2 RESULTS AND DISCUSSION…… 64
3.2.1 Synthesis and characterization of bis-(pyrrole-aldiminato) Zn(II) and Co(II) complexes……... 64
3.2.1.1 Characterization of bis-(pyrrole-aldiminato) Zn(II) **C1** – **C4** complex with $^{1}$H NMR, COSY and NOESY spectroscopy…….…….…….……... 66
3.2.1.2 Characterization of bis-(pyrrole-aldiminato) Zn(II) complexes **C1** – **C4** with $^{13}$C NMR, HSQC and HMBC spectroscopy…… 72
3.2.1.3 Characterization of bis-(pyrrole-aldiminato) Zn(II) and Co(II) complexes **C1** – **C8** with FT-IR spectroscopy, mass spectrometry and elemental analysis…… 77
3.2.1.4 Characterization of bis-(pyrrole-aldiminato) Zn(II) and Co(II) complexes **C1** – **C8** with UV/Vis spectroscopy…….……... 83
3.3 CONCLUSION…… 87
3.4 EXPERIMENTAL…… 82
3.4.1 Materials and instrumentation…… 87
3.4.2 Synthesis of the sodium ligand salts of **L1** – **L4**…… 87
3.4.3 Synthesis of bis-(pyrrole-aldiminato) Zn and Co complexes **C1** – **C8**…… 88
3.4 REFERENCES…...…… 92

.

### 3.1 Introduction

The first rational report of the preparation of bis-(pyrrole-aldiminato) metal complexes was by Holm *et al*. in the late 1960s. Iminoalkyl bis(pyrrole-aldiminato) metal complexes of Co, Ni, Pd, Cu and Zn, where the metal ions are in a 2+ oxidation state were synthesized (**Figure 3.1**). In the case of Co, it was found that steric hindrance plays a key role in stoichiometric control. In the case where less sterically demanding pyrrole-aldimine ligands were used, octahedral Co(III) metal complexes were obtained. The introduction of the sterically demanding tert-butyl substituent on the imine group resulted in a Co(II) metal complex (**Figure 3.1, 2a**) [1].




M= Ni
1a. R = *t*-$C_2H_5$
1b. R = *n*-$C_3H_7$
1c. R = *i*-$C_3H_7$
1d. R = *sec*-$C_4H_9$
1e. R = *t*-C4H9
1f. R = $CH(C_2H_5)_2$
1g. R = $C_6H_{11}$
1h. R = $CH_3CHCH_2OCH_3$
1i. R = *p*-$C_6H_4CH_3$
1j. R= $CH_3CHCH(CH_3)_2$

M= Co
2a. R= *t*-$C_4H_9$

M = Cu
3a. R = *i*-$C_3H_7$
3b. R = *n*-$C_4H_9$
3c. R = *t*-$C_4H_9$

M= Zn
4a. R = *i*-$C_3H_7$
4b. R = *n*-$C_4H_9$

M = Pd
5a. R = $CH_3$

**Figure 3.1** *Iminoalkyl bis(pyrrole-aldiminato) metal complexes of Co, Ni, Pd, Cu and Zn* [1]

Since then, the synthesis and characterization of a variety of bis(pyrrole-aldiminato) metal complexes has been reported [2]–[6]. Although a great deal of literature is available on transition metal complexes derived from pyrrole-aldimine ligands, limited information is available on the synthesis and characterization of bis(pyrrole-aldiminato) metal complexes of group 9 and group 12 transition metals.

Their easily tunable steric and electronic properties widen the range of applications in which they can be used. These include; both homogeneous and heterogeneous catalysis, in display technology due to their containment of chromophores that can emit visible light at various wavelengths and in biological applications as anti-bacterial, anti-microbial and anti-cancer agents [3]–[5], [7], [8].

In this chapter, the synthesis and characterization of bis(pyrrole-aldiminato) Zn(II) and Co(II) metal complexes derived from the pyrrole-aldimine ligands reported in chapter 2 is reported.

## 3.2 RESULTS AND DISCUSSION

### 3.2.1. Synthesis and characterization of bis-(pyrrole-aldiminato) Zn(II) and Co(II) complexes

Zinc complexes **C1** – **C4** and cobalt complexes **C5** – **C8** were synthesized following a synthetic procedure adapted from literature. This began with the preparation of the sodium ligand salt of the respective neutral ligand. This was carried out at room temperature by treating the neutral ligands with a slight excess of sodium hydride in THF to deprotonate the pyrrole ring N-H proton (**Scheme 3.1**) [5]. The successful preparation of the sodium ligand salts was confirmed by $^{1}$H NMR spectroscopy. An overlay of the $^{1}$H NMR spectrum of the sodium ligand salt of **L1** and the $^{1}$H NMR spectrum of **L1** obtained in DMSO-$_{d6}$ is shown to highlight the changes in chemical shift positions moving from neutral ligand to sodium ligand salt (**Figure 3.2**). The disappearance of the signal assigned to the N-H proton, which is observed between 11.55 – 11.83 ppm, in the neutral ligands' spectra confirms the successful deprotonation of the neutral ligands. This is further supported by a significant up-field shift in signals from neutral ligand spectra to the spectra obtained upon treatment of the neutral ligands with NaH in THF.

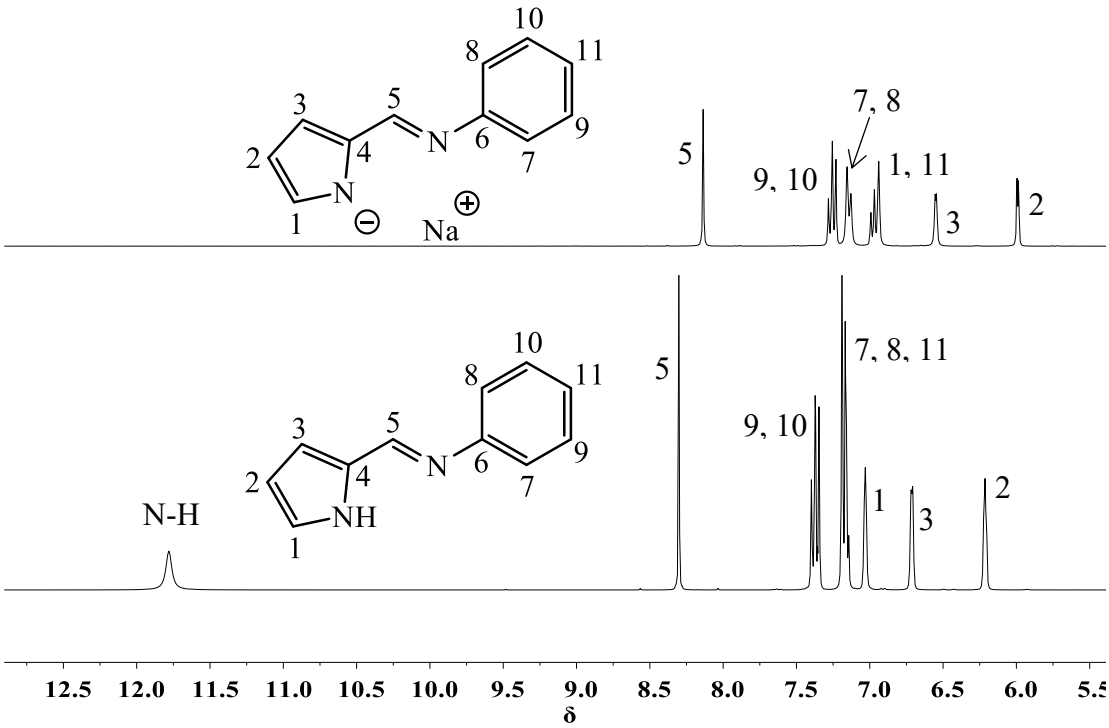
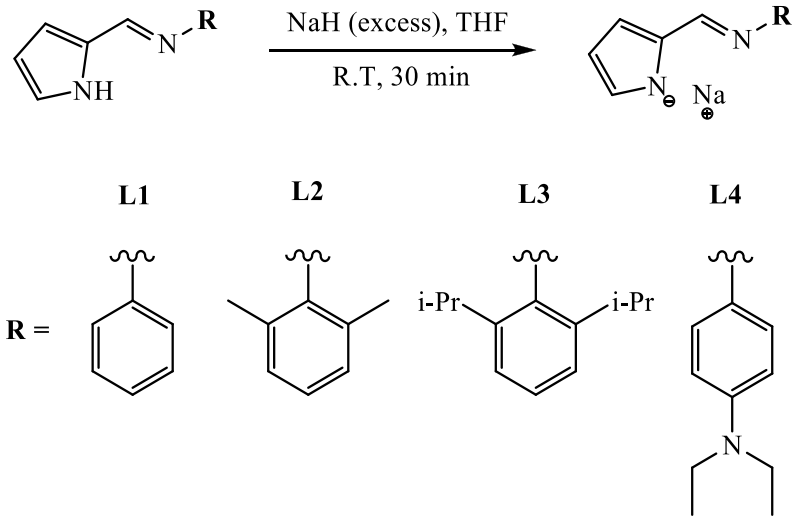
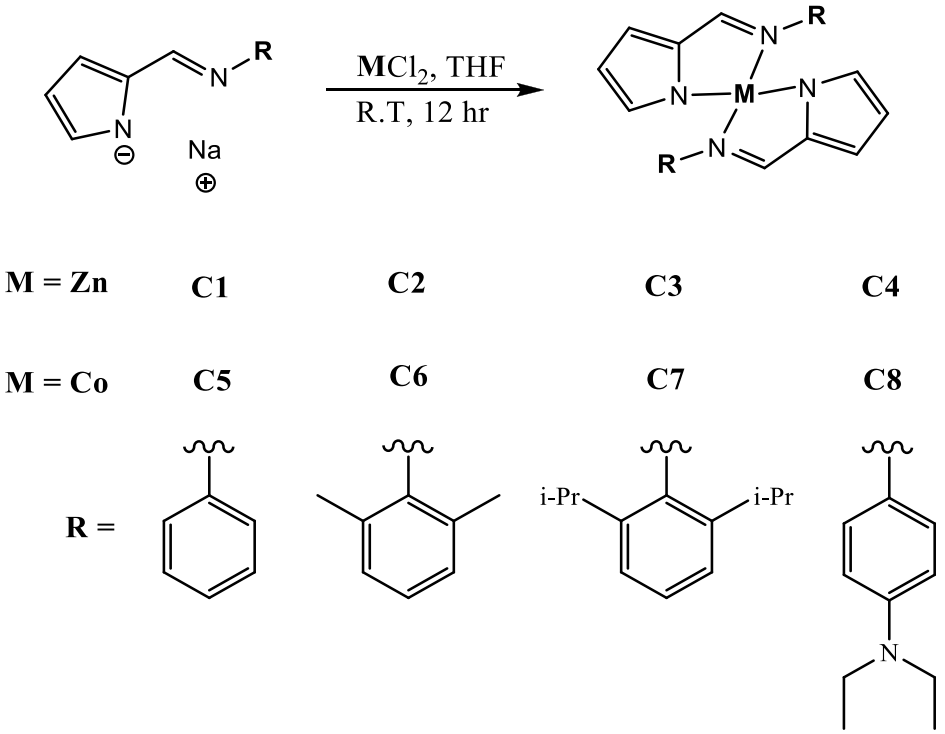



**Figure 3.2** *Stacked $^{1}$H NMR spectra for **L1** and the sodium ligand salt of pyrrole-aldimine ligand **L1** (DMSO-D6, 300 K)*




**Scheme 3.1** *Preparation of sodium ligand salts of pyrrole-aldimine ligands **L1** – **L4*** [5]




**Scheme 3.2** *General synthetic scheme for the preparation of bis-(pyrrole-aldiminato) Zn(II) and Co(II) metal complexes **C1** – **C8*** [5]

In a separate Schlenk tube, $ZnCl_2$ for **C1** - **C4** and $CoCl_2$ for **C5** - **C8** were suspended in THF and added dropwise to their respective sodium ligand salt solutions. The reaction mixtures were stirred for 12 hours at room temperature (**Scheme 3.2**) [5]. After 12 hours, all volatiles were

removed under vacuum. Upon work-up, the 8 metal complexes were obtained as powders in yield ranging from 30% - 60%.

### 3.2.1.1 Characterization of bis-(pyrrole-aldiminato) Zn(II) complexes with $^1$H NMR, COSY and NOESY spectroscopy

Only the four zinc complexes were characterized by $^1$H NMR because of the paramagnetism of the cobalt complexes. This technique was used to assign the proton chemical shifts of the prepared complexes. The disappearance of the N-H signal which is observed in the range 11.55 ppm – 11.80 ppm in the ligands' $^1$H-NMR spectra confirms the successful deprotonation of the N-H proton. A downfield shift for the signal assigned to the imine HC=N proton from ligand to complex spectra suggests a change in the chemical environment around the imine functional group as a result of coordination through the lone pair of electrons on the imine nitrogen to a zinc ion. This down field shift is observed for complexes **C1**, **C2** and **C4** from 8.20 ppm, 7.98 and 8.27 ppm to 8.63 ppm, 8.00 ppm and 8.60 ppm, respectively. An upfield shift from 7.94 ppm to 7.91 ppm is observed for complex **C3**. The imine proton for **C1** and **C4** appears more down-field than those for **C2** and **C3** as shown in (**Table 3.1**). This is attributed to steric shielding afforded by the -$CH_3$ and -$CH_2CH_3$ groups on the phenyl rings of **C2** and **C3**, respectively, which are not present in **C1** and **C4**. The most de-shielded pyrrole ring proton, which is labelled **1** resonates between 6.65 – 7.03 ppm. The least de-shielded pyrrole ring proton, in the position labelled **2** is observed in the range 5.70 ppm – 6.20 ppm. The third pyrrole ring proton, which is labeled **3** is observed between 5.82 ppm and 6.76 ppm. Complexes **C2** and **C3** have substituents in the ortho positions of the phenyl ring and no substituents in the meta and para positions on the phenyl rings. The protons on these positions are labelled **9**, **10** and **11** and they overlap between 6.98 ppm and 7.16 ppm as multiplets. Proton **11** in **C1** does not overlap with the protons in positions **9** and **10**. This proton is observed at 7.17 ppm and appears as a triplet. Complexes **C1**, **C4** and **C5** contain no substituents in the ortho and meta positions on the phenyl ring. The protons in positions **7** and **8** appear in the range 7.22 ppm and 7.47 ppm. The protons in positions **9** and **10** overlap with each other and are observed between 6.60 – 7.45 ppm. Complex **C2** contains methyl (-$CH_3$) groups in the ortho position of the phenyl ring. The C$\underline{H_3}$ protons are observed as a singlet at 1.98 ppm. Complex **C3** contains isopropyl (-$CH_3CH_2$) groups in the ortho positions on the phenyl ring. The C$\underline{H_2}$ protons in positions **12** and **13** appear at 3.00 – 3.07 ppm as a multiplet. The C$\underline{H_3}$ protons in positions **14**, **15**, **16** and **17** are observed as two doublets at 0.88 ppm and 1.05 ppm. Complex **C4** contains an N-diethyl (-$N(CH_2CH_3)_2$)) group in the para position on the phenyl ring. The C$\underline{H_2}$ protons in positions **12**

and **13** overlap with the water signal at 3.34 ppm. The $C\underline{H_3}$ protons labelled **14** and **15** resonate at 1.98 ppm and this signal is observed as a singlet. The $^1$H NMR spectrum of complex **C1** (**Figure 3.3**) is shown as an example of the $^1$H NMR spectra obtained for all four Zn complexes.

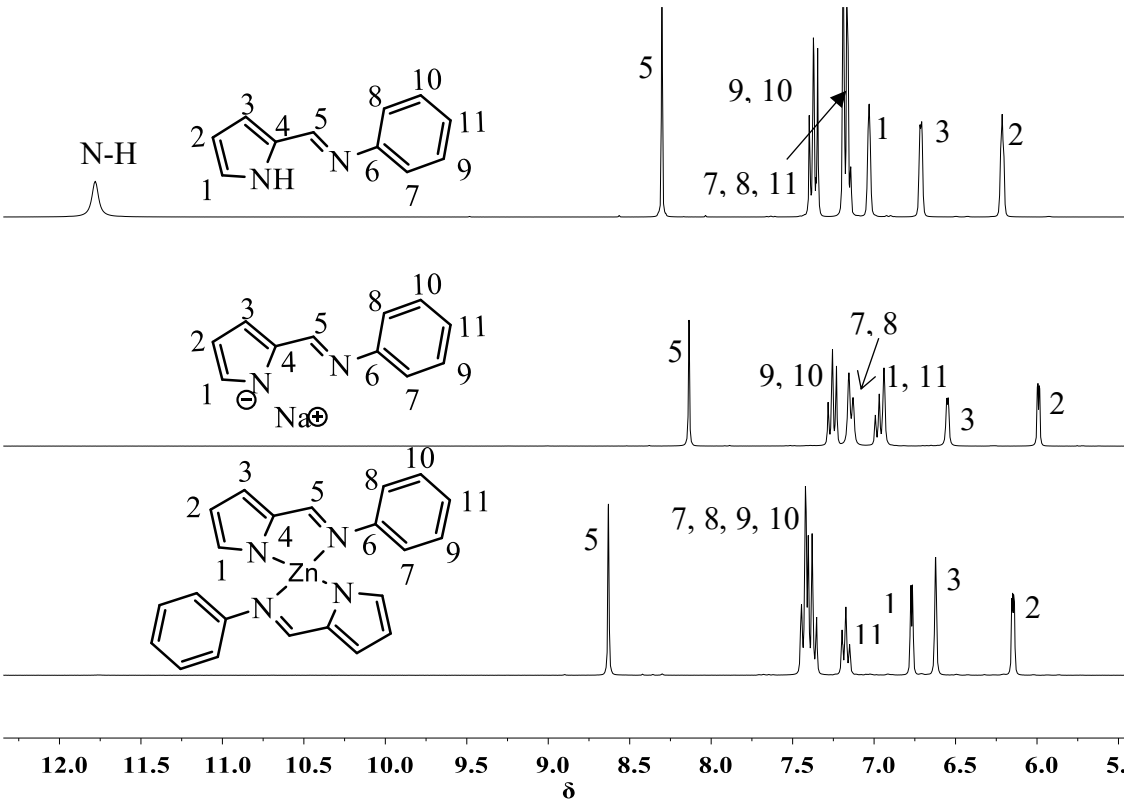



**Figure 3.3** Stacked *$^1$H-NMR spectra for **L1**, sodium ligand salt of **L1** and bis-(pyrrole-aldiminato) Zn(II) complex **C1** (**DMSO**-d6, 300 K)*

COSY spectroscopy was used to conclusively assign the $^1$H NMR signals on the basis that protons that are up to 3 bonds away from each other will interact. The imine proton labelled **5** interacts with the pyrrole-ring proton labelled **3** through 4 bonds. the pyrrole ring proton labelled **3** interact with the other 2 pyrrole ring protons labelled **1** and **2** through 4 and 3 bonds, respectively. Metal complexes **C1** and **C4** contain no substituents on the ortho- position labelled **7** and **8** on the phenyl ring, these protons interact with the protons on **9** and **10** on the phenyl ring through 3 bonds. for **C1**, **7** and **8** interact with **11** through 4 bonds. **C1**, **C2** and **C4** contain no substituents on **11**, this proton interacts with **9** and **10** through 3 bonds.

**Table 3.1** *$^{1}H$ NMR data for metal complexes* ***C1 – C4***

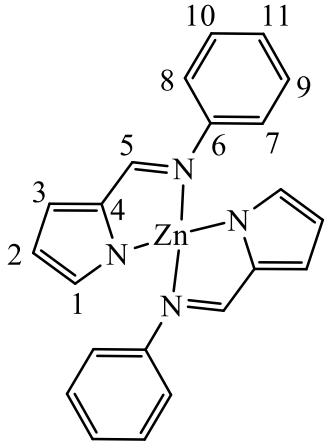
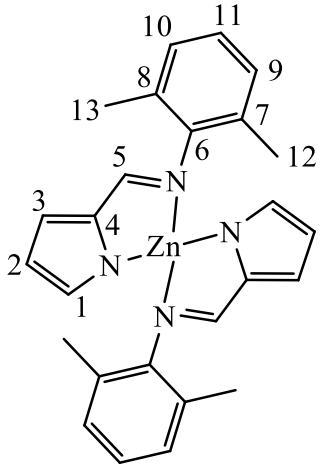
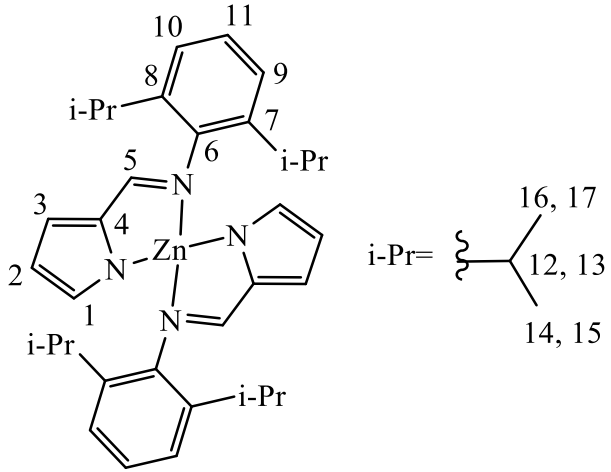
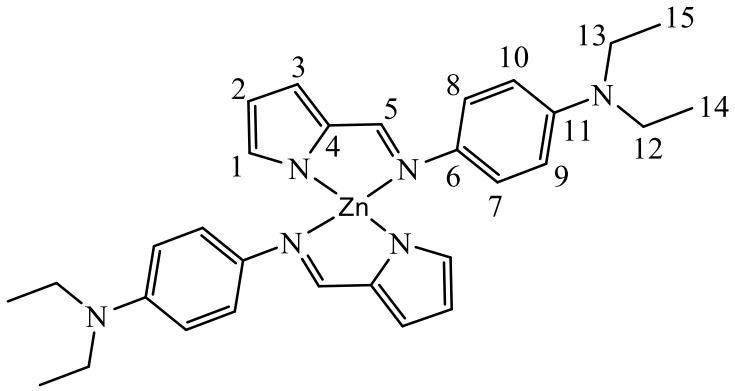
| Structure | HC=N | Pyrrole | Imino substituents |
|---|---|---|---|
|  | 8.63 (s, 1H) | **1:** 6.77 (dd, J = 3.5, 1.1 Hz, 1H)<br>**2:** 6.15 (dd, J = 3.5, 1.7 Hz, 1H)<br>**3:** 6.62 (q, J = 1.2 Hz, 1H) | **7,8,9,10:** 7.35-7.45 (m, 4H)<br>**11:** 7.15-7.20 (m, 1H) |
|  | 8.00 (s, 1H) | **1:** 6.64 (dt, J = 12.8, 0.0 Hz, 1H)<br>**2:** 6.08 (dd, J = 3.4, 1.7 Hz, 2H)<br>**3:** 6.41 (s, 1H) | **9,10 & 11:** 7.10 – 6.92 (m, 3H)<br>**12&13:** 1.98 (s, 6H) |

**Table 3.1 (continued)** *$^{1}$H NMR data for metal complexes* ***C1 – C4***

| Structure | HC=N | Pyrrole | Imino substituents |
|---|---|---|---|
|  | 7.91 (s, 1H) | **1:** 6.50 (d, J = 3.9 Hz, 1H)<br>**2:** 5.70 (s, 1H)<br>**3:** 5.82 (d, J = 4.9 Hz, 1H) | **9,10 & 11:** 7.12 (d, J = 30.7 Hz, 3H)<br>**12&13:** 3.03 (p, J = 6.8 Hz, 2H)<br>**14&15:** 0.88 (d, J = 6.8 Hz, 6H)<br>**16&17:** 1.05 (d, J = 6.8 Hz, 6H) |
|  | 8.59 (s, 1H) | **1&3:** 6.72 (d, J = 15.9 Hz, 2H)<br>**2:** 6.15 (d, J = 5.0 Hz, 1H) | **7 & 8:** 7.23 (d, J = 9.0 Hz, 2H)<br>**9 & 10:** 6.62 (d, J = 9.1 Hz, 2H)<br>**12 & 13:** 3.33 (d, J = 7.1 Hz, 4H)<br>**14 & 15:** 1.06 (t, J = 7.0 Hz, 6H) |

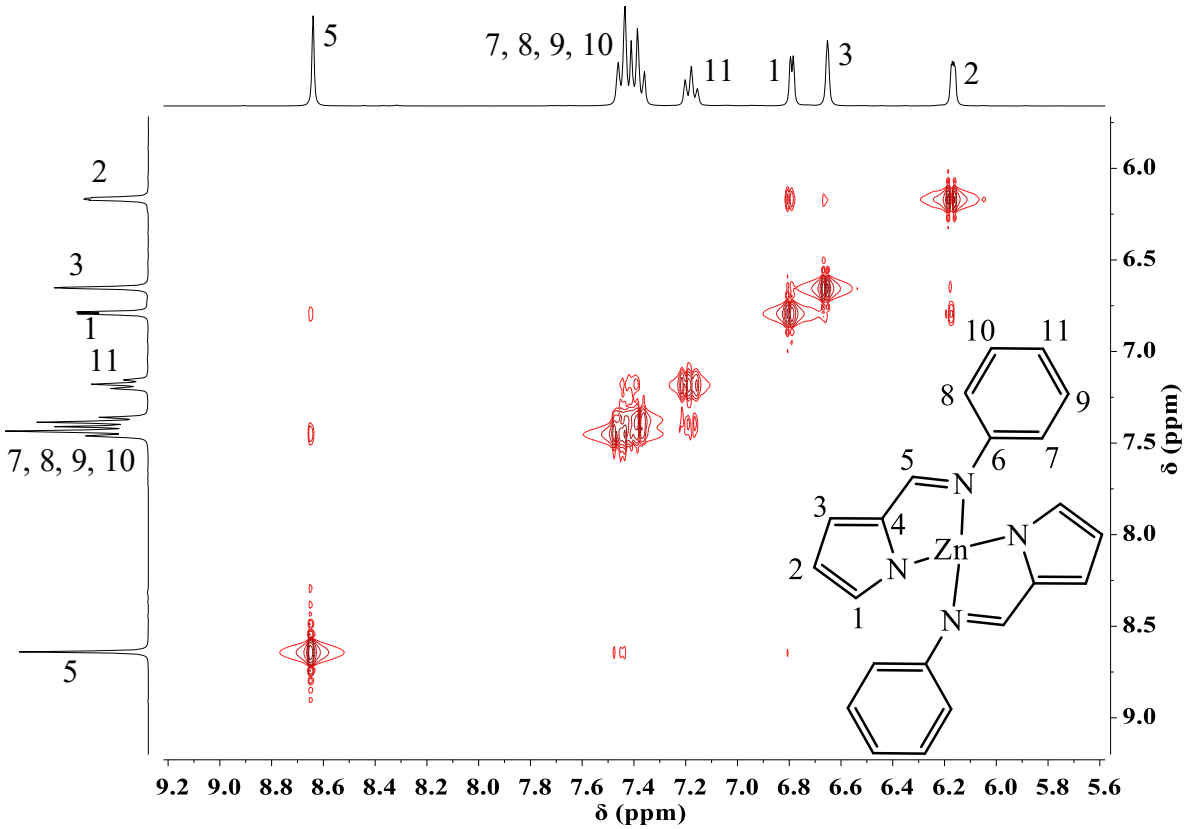



**Figure 3.4** *COSY spectrum for bis-(pyrrole-aldiminato) Zn(II) complex **C1** (**DMSO**-d6, 300 K)*

**C2** contains a methyl ($CH_3$) group in the ortho position on the phenyl ring, the protons in these positions are labelled **12** and **13** and do not interact with any other protons through bonds. **C3** contains isopropyl ($CHCH_3$) groups in the ortho position on the phenyl ring. The C<u>H</u> protons labelled **12** and **13** interact with the C<u>$H_3$</u> protons labelled **14**, **15**, **16** and **17** through 3 bonds. **C4** contains an N,N-diethyl ($(CH_2CH_3)_2$) on the para position on the phenyl ring. The C<u>$H_2$</u> protons labelled **12** and **13** interact with the C<u>$H_3$</u> protons labelled **14** and **15** through 3 bonds. The COSY spectrum of complex **C1** (**Figure 3.4**) is shown as an example of the COSY spectra obtained for all four Zn(II) complexes.

NOESY spectroscopy was used to conclusively assign the pyrrole ring protons and to distinguish between the phenyl ring protons labelled **7** & **8** and **9** & **10**. The conclusive assignments using this technique is based on the interaction of protons that are close to each other through space. The imine proton labelled **5** was used as a reference point. The imine proton interacts with the pyrrole ring proton labelled **3** and the phenyl ring protons labelled **7**

and **8** through space. The pyrrole ring proton labelled **2** interacts with the other pyrrole ring protons labelled **1** and **3** through space. **C1** and **C4** contain no substituents on **7** & **8** and **9** & **10**. The protons on **7** & **8** interact with **9**&**10** and **5** through space. **C1**, **C2** and **C3** contain no substituents on **11**, and as such, the proton in this position interacts with **9** and **10** through space. **C2** contains a methyl groups labelled **12** and **13**, the protons in these positions interact with **3**, **5**, **9** and **10** though space. **C4** contains isopropyl groups with the CH protons labelled **12** and **13** and the methyl protons labelled **14**, **15**, **16** and **17**. The $\underline{CH_3}$ protons interact with **1**, **2**, **3**, **5**, **9**,**10**, **11**, **12** and **13** through space. **C4** contains an N,N-diethyl ($(CH_2CH_3)_2$) on the para position on the phenyl ring with the $CH_2$ protons labelled **12** and **13** and the $\underline{CH_3}$ protons labelled **14** and **15**. **12** and **13** interact with **9** & **10** and **14** and **15** through space. The NOESY spectrum of complex **C1** (**Figure 3.5**) is shown as an example of the NOESY spectra obtained for all four Zn(II) complexes.

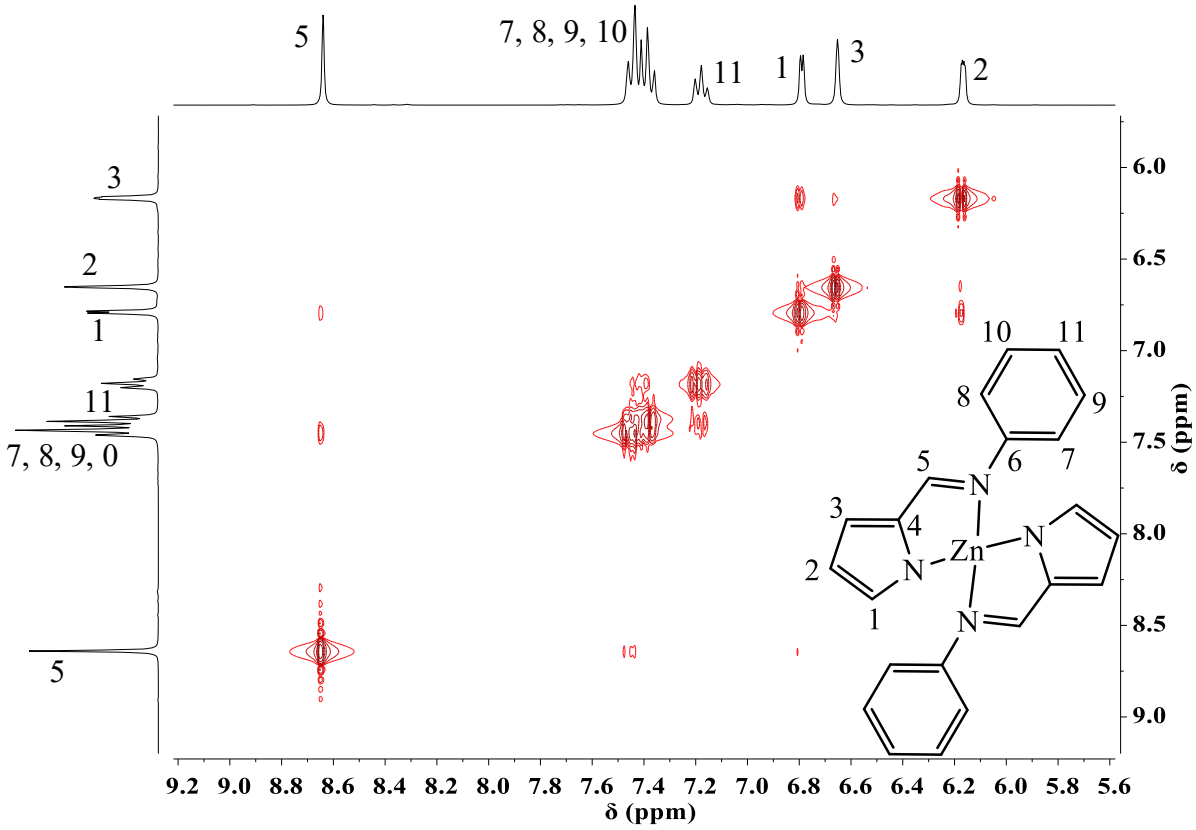



**Figure 3.5** *NOESY spectrum for bis-(pyrrole-aldiminato) Zn(II) complex* ***C1*** *(****DMSO****-d6,300 K)*

### 3.2.1.2 Characterization of bis-(pyrrole-aldiminato) Zn(II) C1 – C4 with $^{13}C$ NMR, HSQC and HMBC spectroscopy

$^{13}C$ NMR spectroscopy was used to assign the carbon atoms. The most de-shielded signal which is observed in the range 153.11 – 159 ppm is assigned to the imine carbon labelled **5**. The pyrrole carbons labelled **1**, **2** and **3** are observed in the ranges 118.41 – 124.49 ppm, 112.45 – 112.31 ppm and 117.78 – 135.06 ppm, respectively. The quaternary pyrrole ring carbon labelled **4** is observed in the range 134.28 – 136.88 ppm. The quaternary phenyl ring carbon atom labelled **6** is observed in the range 135.96 – 148.48 ppm and is the second most de-shielded signal. The phenyl ring protons labelled **7** & **8** and **9** & **10** appear in the ranges 129.25 – 129.97 ppm and 120.98 – 127.96 ppm, respectively. The carbon atom labelled **11** resonates between 124.99 – 125.77 ppm. **C2** contains methyl substituents in the ortho position on the phenyl ring. The signal as a result of the $\underline{C}H_3$ carbon atom is observed at 18.29 ppm. **C3** has isopropyl ($-CH(CH_3)_2$) groups in the ortho position on the phenyl ring. The $\underline{C}H$ carbon atoms which are labelled **12** and **13** appear at 20.05 ppm. $\underline{C}H_3$ signal for carbon atoms labelled **14, 15, 16** and **17** appear at 23.73 ppm. C4 contains the N,N-diethyl [$-N(CH_2)_2(CH_3)_2$] group in the para position of the phenyl ring. The $\underline{C}H_2$ carbon atoms labelled **12** and **13** are observed at 42.27 ppm whereas the $\underline{C}H_3$ carbon atoms labelled **14** and **15** are observed at 10.35 ppm. The $^{13}C$ NMR spectrum of complex **C1** (**Figure 3.6**) is shown as an example of the $^{13}C$ NMR spectra obtained for all four Zn complexes.

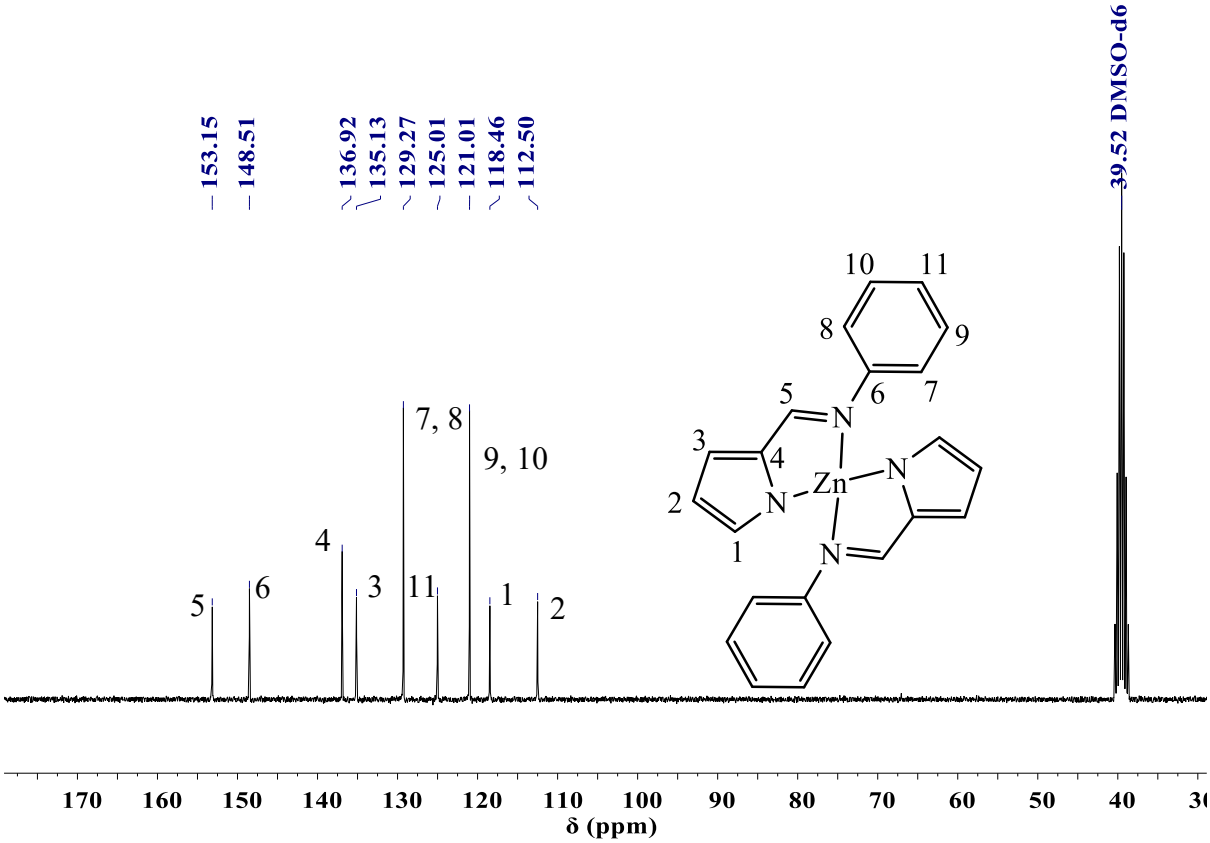



**Figure 3.6** *$^{13}$C NMR spectrum for bis-(pyrrole-aldiminato) Zn(II) complex **C1** (**DMSO**-d6, 300 K)*

**Table 3.2** *$^{13}$C NMR data for metal complexes **C1 – C4***

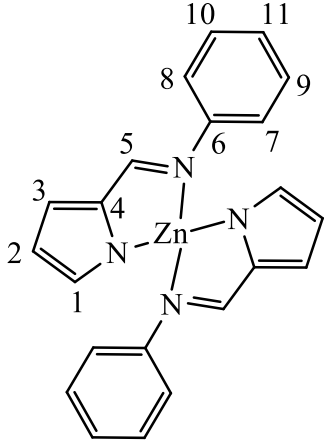
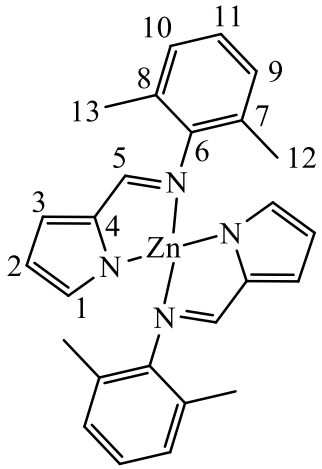
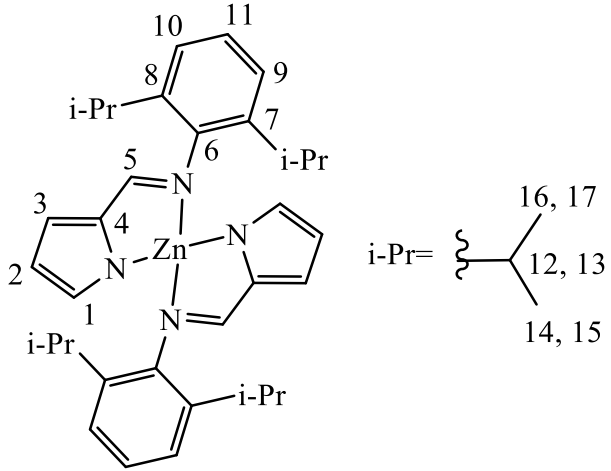
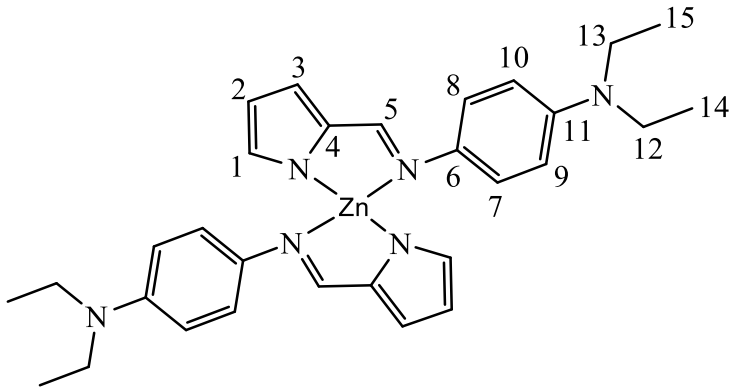
| Structure | HC=N | Pyrrole | Imino substituents |
|---|---|---|---|
|  | **5:** 153.15 | **1:** 118.46<br>**2:** 112.50<br>**3:** 135.13<br>4: 136.92 | **6:** 148.51<br>**7 & 8:** 124.27<br>**9 & 10:** 121.01<br>**11:** 125.01 |
|  | **5:** 159.67 | **1:** 124.49<br>**2:** 112.34<br>**3:** 117.78<br>**4:** 134.38 | **6:** 135.96<br>**7 & 8:** 129.97<br>**9, 10 &:** 127.96<br>**12&13:** 18.29 |

**Table 3.2 (continued)** *$^{13}$C NMR data for metal complexes **C1 – C4***

| Structure | HC=N | Pyrrole | Imino substituents |
|---|---|---|---|
|   | **5:** 152.88 | **1:** 123.70<br>**2:** 111.45<br>**3:** 117.74<br>**4:** 136.08 | **6:** 148.56<br>**7 & 8:** 127.94<br>**9,10 & 11:** 128.94<br>**12&13:** 29.05<br>**14,15,16 & 17:** 25.78 |
|   | **5:** 146.40 | **1:** 122.95<br>**2:** 109.98<br>**3:** 115.60<br>4. 131.30 | **6:** 146.06<br>**7 & 8:** 122.24<br>**9 & 10:** 112.38<br>**11:** 139.37<br>**12 & 13:** 42.27<br>**14 & 15:** 10.35 |

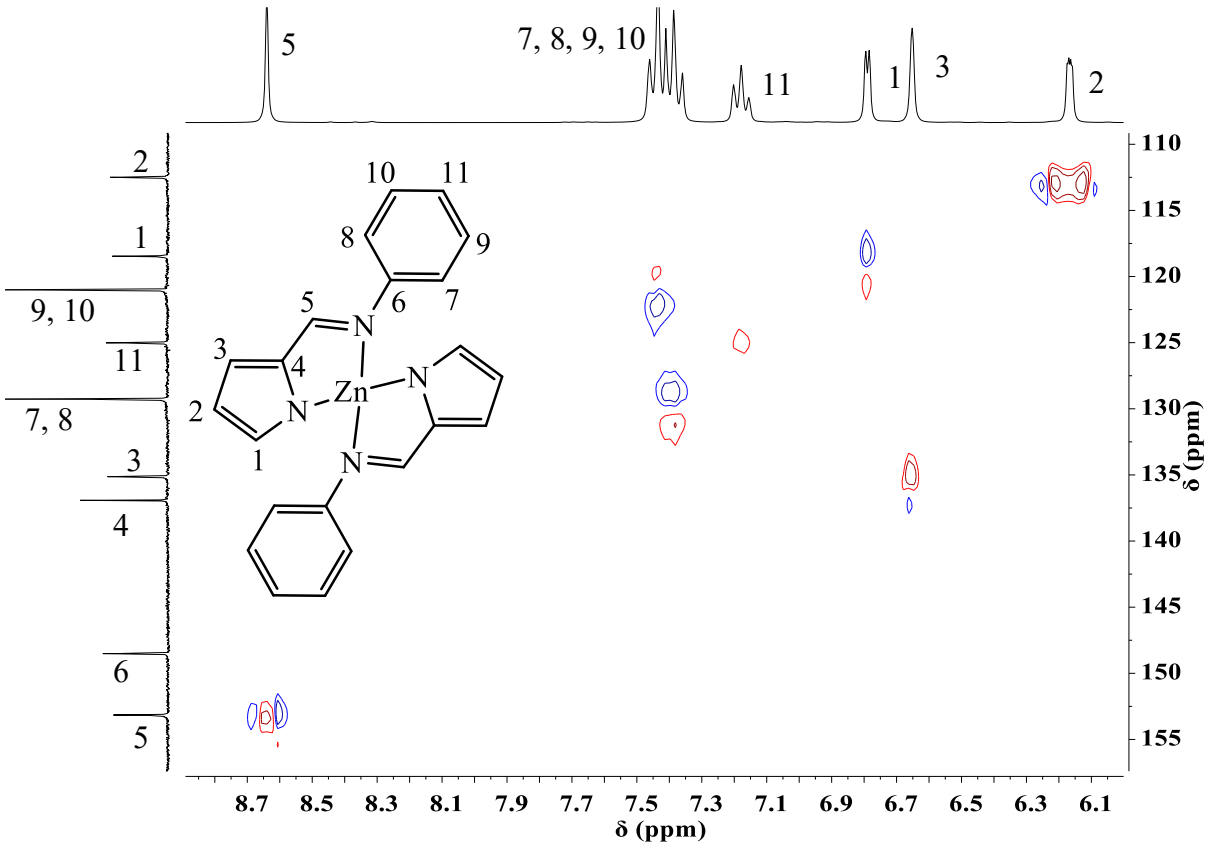



**Figure 3.7** *HSQC spectrum for bis-(pyrrole-aldiminato) Zn(II) complex **C1** (**DMSO**-d6, 300 K)*

HSQC spectroscopy was used to conclusively assign the $^{13}C$ NMR signals for the non-quaternary carbon atoms for **C1** – **C4**. The conclusive assignments were made on the basis that protons correlated to the signals of carbon atoms they are directly bonded to. The imine proton in position **5** correlates to the most de-shielded carbon signal. The pyrrole ring protons in positions **1**, **2** and **3** correlate to carbon signals in the ranges 118.41 – 124.49 ppm, 112.34 ppm –112.45 ppm and 117.78 ppm –135.06 ppm, respectively. The phenyl ring protons labelled **7** & **8** and **9** & **10** correlate to carbon signals observed between 129.25 – 129.97 ppm and 120.98 – 127.96 ppm, respectively. The carbon atom labelled **11** shows a correlation with the signal observed between 124.99 ppm and 125.77 ppm. **C2** contains methyl substituents in the ortho position on the phenyl ring. The proton signals in these positions correlate to the signal as a result of the carbon atom which is observed at 18.29 ppm. **C3** has isopropyl (-$CHCH_3$) groups in the ortho position on the phenyl ring. The protons in these position correlate to the C̲H carbon atoms which are labelled **12** and **13** and appear at 20.05 ppm. The protons in this position correlate to the C̲$H_3$ signal labelled **14, 15, 16** and **17** appear at 23.73 ppm. **C4** contains the

N,N-diethyl [-N($CH_2$)$_2$($CH_3$)$_2$] group in the para position of the phenyl ring. The $CH_2$ protons in this position correlate to the $\underline{C}H_2$ carbon atoms labelled **12** and **13** which are observed at 42.27 ppm whereas the $C\underline{H}_3$ protons in **14** and **15** correlate to the $\underline{C}H_3$ signal observed at 10.35 ppm. The HSQC spectrum of complex **C1** (**Figure 3.7**) is shown as an example of the HSQC spectra obtained for all four Zn complexes.

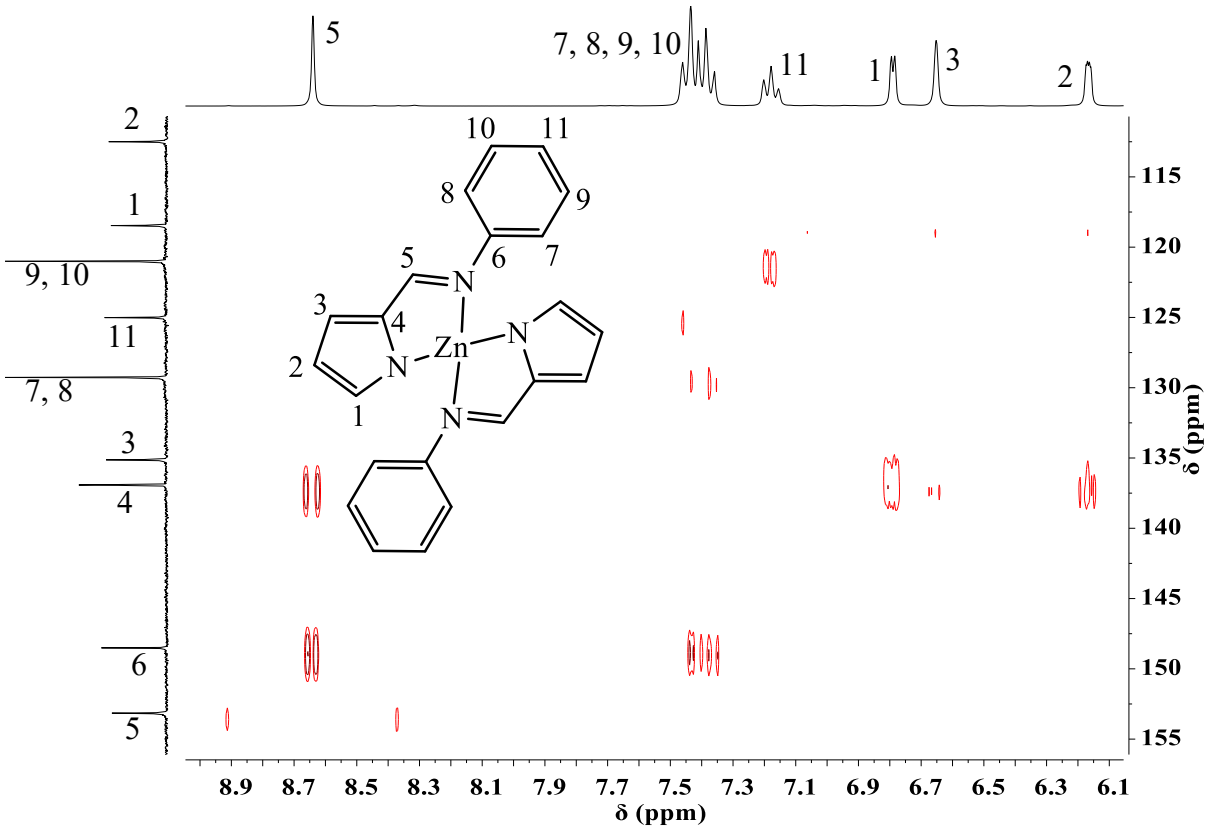



**Figure 3.8** *HMBC spectrum for bis-(pyrrole-aldiminato) Zn(II) complex **C1** (**DMSO**-d6, 300 K)*

HMBC spectroscopy was used to assign the $^{13}$C NMR signals for the quaternary carbons for **C1** - **C4**. The proton signals labelled **2**, **3** and **5** correlate to the signal observed in the range 134.38 ppm –136.88 ppm. The quaternary carbon labelled **4** was assigned on the basis that the protons labelled **2**,**3** and **5** correlate to this signal, which is 3, 2 and 2 bonds away, respectively. the carbon labelled **6** was assigned on the basis that the protons labelled **7** & **8** and **9** & **10** correlate to the signal observed in the range 147.89 ppm – 148.88 ppm. These protons are 2 and 3 bonds away from **6**. **C2** and **C3** contain methyl and isopropyl substituents in the ortho position on the phenyl ring. These positions are labelled **7** & **8**, and as such, the carbon atoms in these positions are quaternary carbons. These were assigned on the basis that the protons in

positions **9** & **10** and **11** correlate to the signal observed between 135.96 ppm and 148.87 ppm, and these protons are 2 and 3 bonds away from **7** & **8**. **C4** contains the N,N-diethyl [-$N(CH_2)_2(CH_3)_2$] group in the para position of the phenyl ring, which is labelled **11**. The signal for this carbon atom was assigned on the basis that the proton signals for **7** & **8** and **9** & **10** correlate to the signal observed at 139.37 ppm. this carbon atom is 3 and 2 bonds away from the proton signals assigned to **7** & **8** and **9** & **10**. The HMBC spectrum of complex **C1** (**Figure 3.8**) is shown as an example of the HMBC spectra obtained for all four Zn complexes.

#### 3.2.1.3 Characterization of bis-(pyrrole-aldiminato) Zn(II) and Co(II) complexes C1 – C8 with FT-IR spectroscopy, mass spectrometry and elemental analysis

In the FT-IR spectra obtained for complexes **C1** - **C8**, the disappearance of the pyrrole N-H band which is observed in the range 3172 $cm^{-1}$ to 3240 $cm^{-1}$ for their corresponding neutral ligands suggests the successful deprotonation of the N-H proton. A shift to a lower frequency value for the sharp intense ν(C=N) band and its shoulder peak is observed. The ν(C=N) band and its shoulder peak shifted from a range of 1606 $cm^{-1}$ – 1631 $cm^{-1}$ and 1662$cm^{-1}$ – 1590 $cm^{-1}$ to 1558 cm and 1562 $cm^{-1}$, respectively. This shift in the frequency position from neutral ligand to complex spectra suggests a delocalization in metal electron density to the π-system of the ligand, which indicates coordination of the nitrogen atom of the C=N moiety to the metal atoms [9]. This further confirms the successful preparation of all eight metal complexes. (**Figure 3.9**) shows the stacked IR spectra of ligand **L1** and the corresponding bis-(pyrrole-aldiminato) Zn(II) and Co(II) complexes' IR spectra to highlight the disappearance of the N-H band and the shift in the imine band, as observed for all 8 metal complexes.

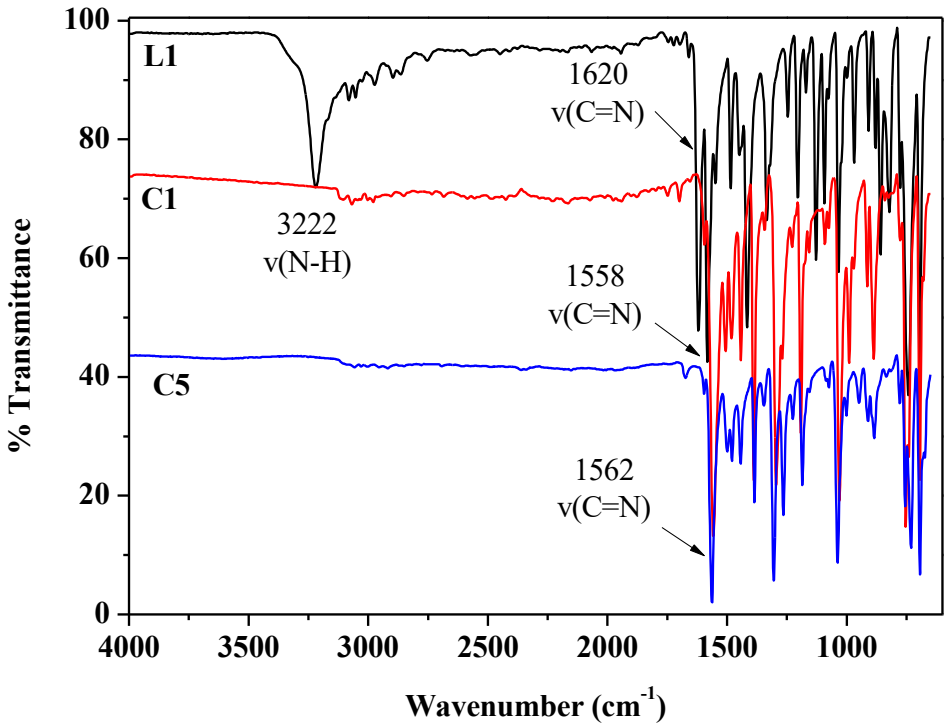



**Figure 3.9** *FT-IR spectra for ligand **L1**, metal complexes **C1** and **C5***

Mass spectrometry was used to confirm the successful preparation of all 8 metal complexes. 6 of the 8 mass spectra were obtained in HPLC grade MeOH. The other 2 were obtained in HPLC grade DMSO. The mass spectrum obtained for **C1** is shown in (**Figure 3.10**) and the expanded mass spectrum for **C1** (**Figure 3.11**), which shows the isotopololgue pattern match of the predicted and obtained spectra are illustrated as examples of the mass spectra obtained for bis-(pyrrole-aldiminato) Zn(II) complexes, **C1** – **C3**. In the mass spectrum for **C1** (**Figure 3.10**), a molecular ion peak with an m/z value of 403.0872 DA, is observed. This value is in agreement with the predicted m/z value for **C1**. The mass spectrum for **C4** was obtained in HPLC grade DMSO. A molecular ion peak consistent with the calculated molecular weight of **C4** could not be identified, however, molecular ion peaks consistent with fragments of **C4** were identified. These are shown in the appendix section. As such, the m/z value for **C4** is not listed in (**Table 3.4**).

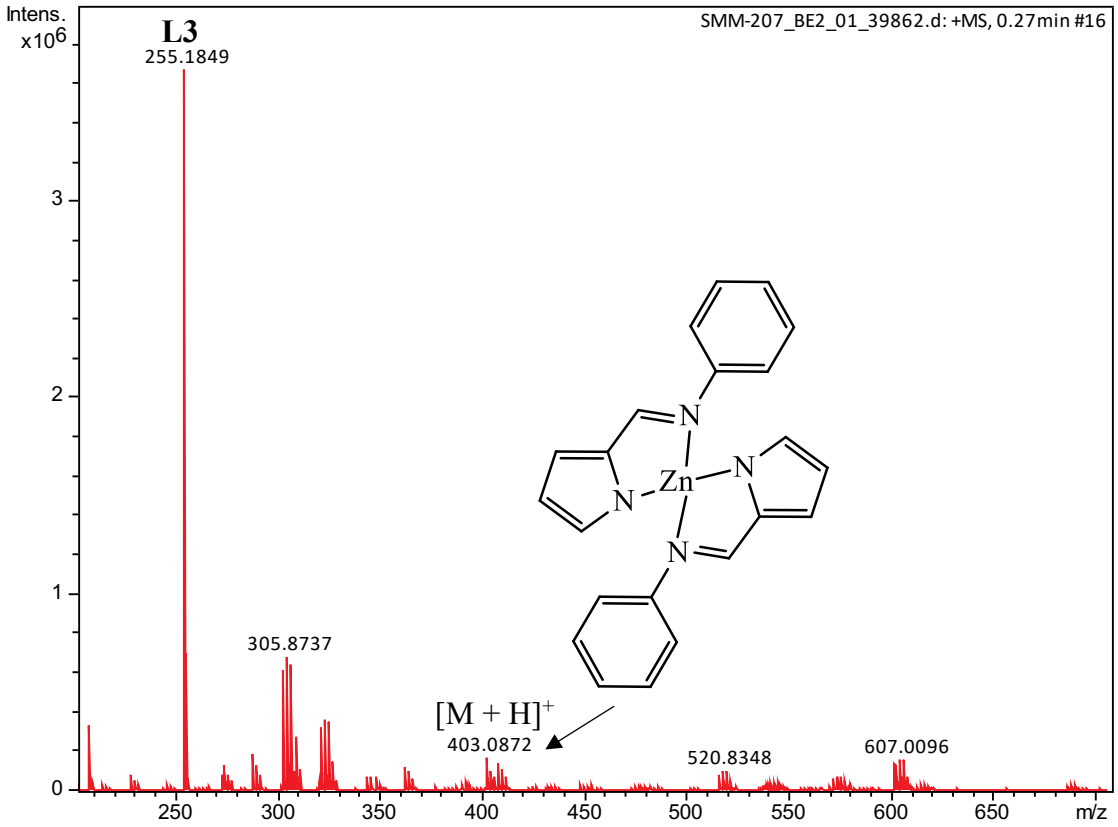



**Figure 3.10** *Full mass spectrum for bis-(pyrrole-aldiminato) Zn(II) complex* ***C1***

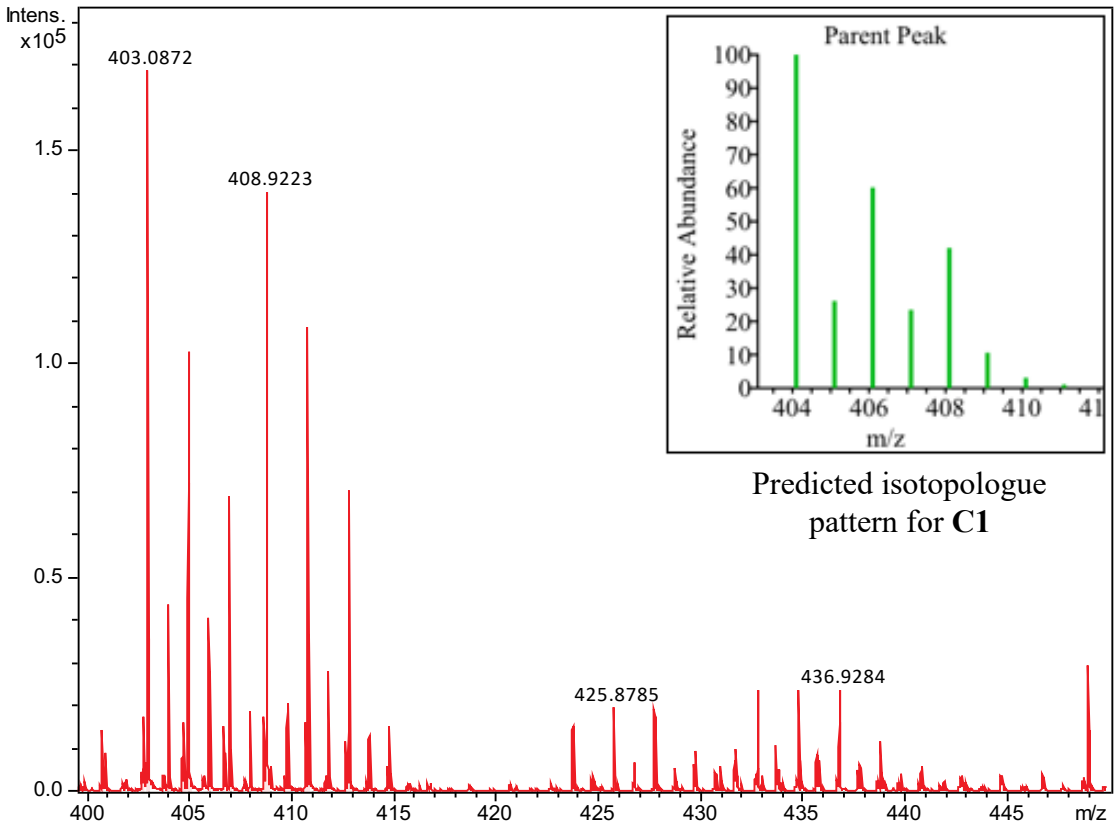



**Figure 3.11** *Expanded mass spectrum for bis-(pyrrole-aldiminato) Zn(II) complex* ***C1***

In the mass spectrum obtained for **C5**, a molecular ion peak consistent with the octahedral Co(III) complex is observed. This peak is identified as the peak with a mass-to-charge ratio of 567.1697 Da and it is labelled as $[M + H]^+$ + **L1** in the mass spectrum (**Figure 3.12**). The presence of this molecular ion peak suggests the preparation of the Co(III) metal complex, which fragments to the Co(II) complex **C5** $[M + H]^+$, with an m/z value of 397.0896 Da (**Figure 3.12**). In all eight mass spectra, molecular ion peaks consistent with the calculated molecular weights for all eight metal complexes (as listed in **Table 3.4**) were identified. In addition to this, the molecular ion peaks of **C1** – **C4** show an isotopologue pattern consistent with the presence of a Zn(II) ion and those for **C5** – **C8** show an isotopologue pattern consistent with the presence of a Co(II) ion. This observation further confirms the successful preparations of metal complexes **C1** – **C8**.

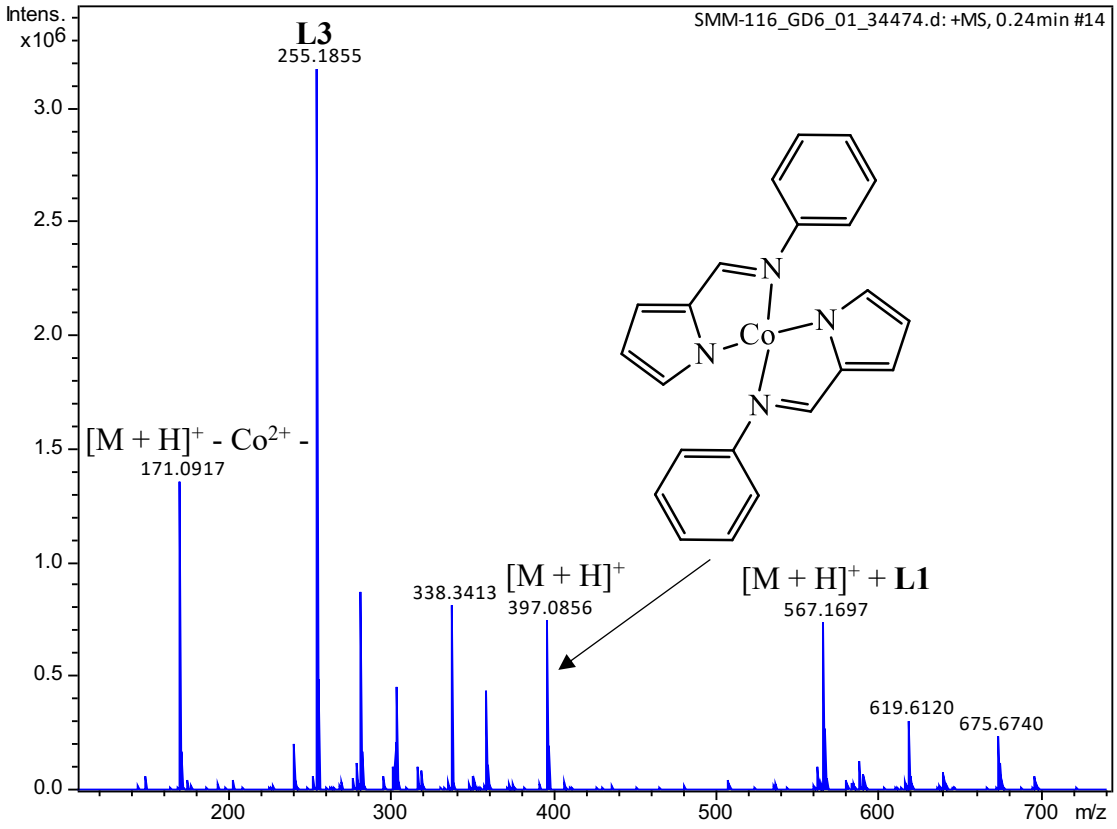



**Figure 3.12** *Full mass spectrum for bis-(pyrrole-aldiminato) Co(II) complex **C5***

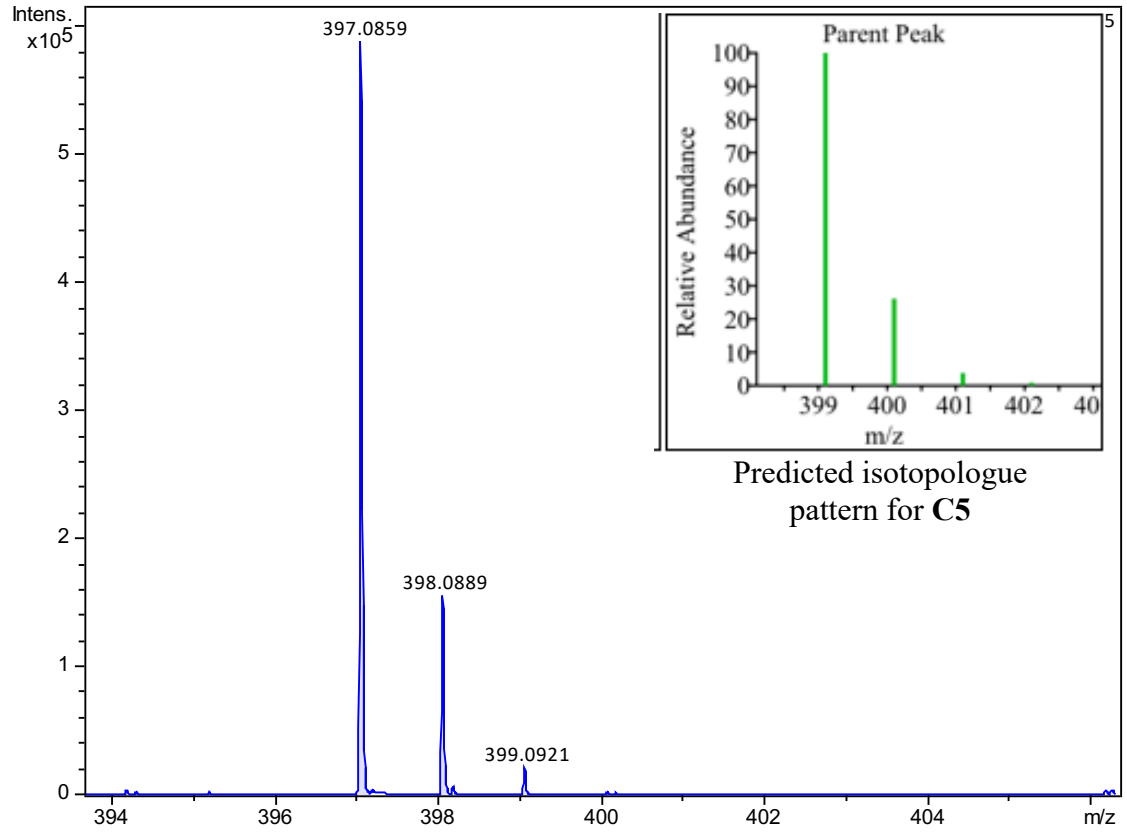



**Figure 3.13** *Expanded mass spectrum for bis-(pyrrole-aldiminato) Co(II) complex **C5***

Elemental analysis was used to confirm the purity of complexes **C1** – **C8**. The elemental analysis data obtained for complexes **C1**, **C2**, **C3**, **C5**, **C6** and **C7** (**Table 3.4)** is in-line with the calculated elemental composition data for these metal complexes. This further confirms the successful synthesis of these metal complexes and confirms that they were isolated as pure compounds. The elemental analysis data (**Table 3.4**) suggests that the presence of a molecular ion peak consistent with the octahedral Co(III) complex of **L1**, with an m/z value 567.1697 Da could be a result of oxidation of the Co(II) of **L1** complex to the Co(III) complex of **L1** taking place in the mass spectrometer and not the result of poor stoichiometry control as a result of the poor steric demands of **L1**. The values obtained for the elemental composition for complex **C4** are lower than the expected values, this suggests the presence of unreacted metal salt as a result of poor purification of **C4**. The elemental composition values obtained for **C8** deviate from the calculated elemental analysis data. These values are consistent with elemental composition values calculated with taking into account the presence of THF. This implies that **C8** was isolated as a solvated compound.

### 3.2.1.4 Characterization of bis-(pyrrole-aldiminato) Zn(II) and Co(II) C1 – C8 with UV/Vis spectroscopy

The absorption spectra (**Figure 3.14**) for **C1** – **C8** were recorded in toluene. In all 8 spectra, the intra-ligand transition bands, which are observed in the range 300 nm – 408 nm in the neutral ligand spectra are present (**Table 3.3**). The presence of this band is suspected to be a result of the decomposition of metal complex to neutral ligand as pyrrole-aldiminato complexes of Co(II) and Zn(II) have been reported to be sensitive to air and moisture, especially in solution. This speculation was confirmed by recording the electronic spectra of a sample of **C3** in toluene over 5 minutes in 1-minute intervals (**Figure 3.15**). With time, an increase in the intensity of the band assigned to IL transitions, which is observed at 300 nm and a decrease in the intensity of the band assigned to LMCT, which is observed at 366 nm was evident. This observation suggests a gradual loss in metal complex character to more neutral ligand character of the sample with time, which may be caused by the poor stability of bis-(pyrrole-aldiminato) complexes of Co(II) and Zn(II) when exposed to the atmosphere, especially in solution [5], [11].

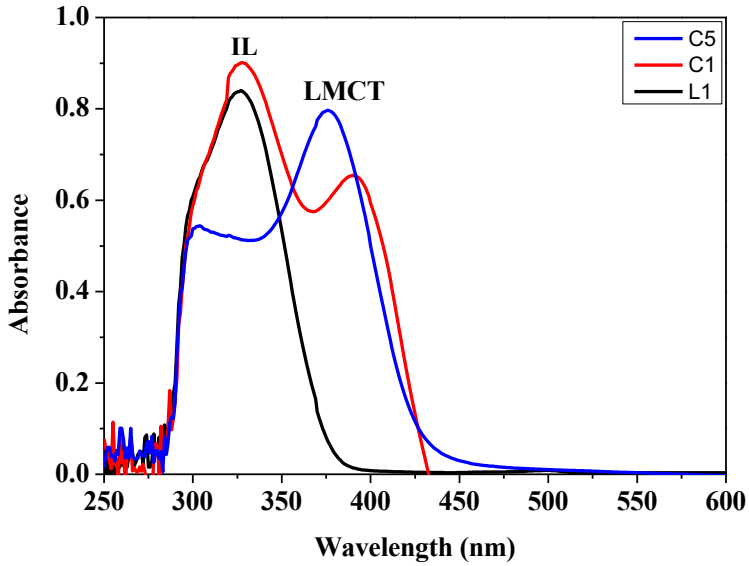



**Figure 3.14** *Stacked UV-Vis spectra for ligand **L1** and bis-(pyrrole-aldiminato) Zn(II) and Co(II) complexes, **C1** and **C5***

Unlike in the neutral ligand spectra, an additional band in the range 379 nm – 390 nm is observed for metal complexes **C1** – **C4**. This band is assigned to ligand to metal charge transfer. This observation is in-line with the observation made by Gomes *et al*. The group reported a

red-shift in the absorption spectra of bis-(pyrrole-aldiminato) Zn(II) complexes, which are structurally identical to **C1** and **C3** relative to their corresponding neutral ligand spectra.

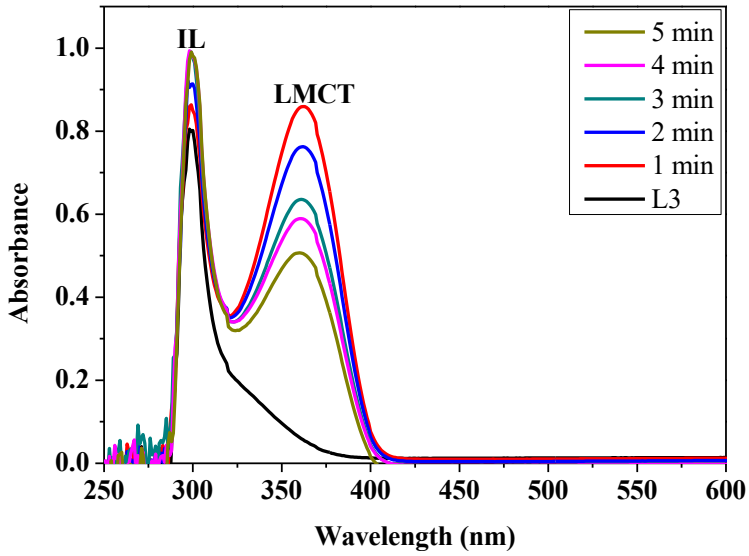



**Figure 3.15 Stacked** UV-Vis spectra showing the decline in the LMCT band for *bis-(pyrrole-aldiminato) Co(II) complex, **C7** with time*

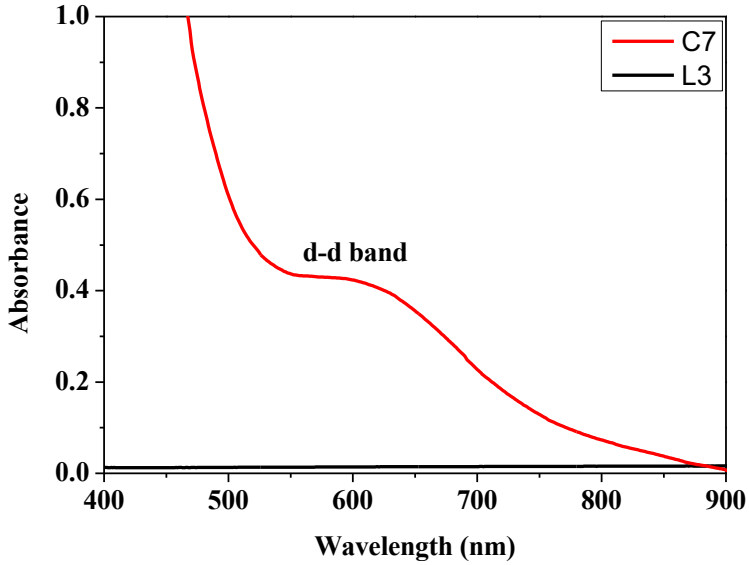



**Figure 3.16** *UV-Vis spectrum showing the d-d band for bis-(pyrrole-aldiminato) Co(II) complex, **C7***

The group attributed this observation to the enhancement of the π-conjugation due to the bidentate complexation of the ligand to the $d^{10}$ spectroscopically inactive $Zn^{2+}$ ion. A red shift

(35 nm - 65 nm) is observed for metal complexes **C1** – **C4** relative to their corresponding neutral ligand precursors [5].

In the absorption spectra obtained for **C5** – **C8**, bands in the range 379 nm – 390 nm are observed (**Figure 3.12**). These are assigned to LMCT. Additional bands are observed between 400 nm and 636 nm for **C6** and **C7** (**Figure3.16**). The presence of these bands is attributed transitions involving Co(II) ions and are assigned to d-d bands [10]. Efforts to obtain UV-Vis spectra showing the d-d bands for **C5** and **C8** proved to be elusive. This is attributed to challenges faced with getting the concentration to a point where the d-d bands become apparent.

**Table 3.3** *UV/Vis data for metal complexes **C1** – **C8***

| **Complex** | **Uv-vis (λMax/nm)** | |
|---|---|---|
| | LMCT band | d-d band |
| **C1** | 391 | - |
| **C2** | 359 | - |
| **C3** | 366 | - |
| **C4** | 409 | - |
| **C5** | 379 | - |
| **C6** | 390 | 492, 530, 636 |
| **C7** | 383 | 608 |
| **C8** | 379 | - |

**Table 3.4** *HR-MS, FT-IR and elemental analysis data for metal complexes* ***C1 – C8***

| Metal complex | Yield (%) | Formula | ESI-MS $[M+H]^+$ | FT-IR | Elemental analysis Found (calc) | | |
|---|---|---|---|---|---|---|---|
| | | | Found (cal) | ν(C=N) | C | H | N |
| **C1** | 60 | $C_{22}H_{11}N_4Zn$ | 403.0878 (403.0906) | 1558 | 65.43 (65.28) | 4.49 (3.98) | 13.87 (13.77) |
| **C2** | 43 | $C_{26}H_{26}N_4Zn$ | 459.1517 (459.1532) | 1562 | 67.90 (68.5) | 5.70 (6.4) | 12.18 (12.2) |
| **C3** | 57 | $C_{34}H_{42}N_4Zn$ | 571.2850 (571.2784) | 1560 | 71.38 (70.8) | 7.40 (8.7) | 9.87 (9.7) |
| **C4** | 38 | $C_{30}H_{36}N_4Zn$ | - | 1606 | 65.99 (61.75) | 6.65 (4.35) | 15.39 (13.62) |
| **C5** | 60 | $C_{22}H_{11}N_4Co$ | 397.0318 (398.0947) | 1564 | 66.50 (65.31) | 4.57 (4.28) | 14.10 (13.62) |
| **C6** | 55 | $C_{26}H_{26}N_4Co$ | 454.1477 (454.1573) | 1585 | 68.87 (67.5) | 5.78 (6.8) | 12.38 (11.9) |
| **C7** | 44 | $C_{34}H_{42}N_4Co$ | 565.2733 (565.2825) | 1568 | 72.19 (73.31) | 7.48 (6.94) | 9.90 (9.30) |
| **C8** | 58 | $C_{30}H_{36}N_4Co$•THF | 540.1712 (540.2417) | 1606 | 66.78 (66.77) | 6.73 (7.28) | 15.58 (14.74) |

## 3.3 CONCLUSION

The four sodium ligand salts of **L1** – **L4** (**LN**$^{-}$ Na$^{+}$, **N**= **1**, **2**, **3** or **4**) were prepared by the in *situ* deprotonation of their respective neutral ligands. This was done by treating the neutral ligands with a slight excess of NaH in THF to afford the respective sodium ligand salts as powders of varying colours. The successful preparation of **LN**$^{-}$ Na$^{+}$ was confirmed by $^{1}$H NMR spectroscopy. The successfully prepared sodium ligand salts were then used in the preparation of their respective bis-(pyrrole-aldiminato) Zn(II) and Co(II) complexes. The successful preparation of the bis-(pyrrole-aldiminato) Zn(II) and Co(II) metal complexes was confirmed by FT-IR spectroscopy, mass spectrometry and Uv-Vis spectroscopy. Elemental analysis and was used to confirm the purity of all 8 metal complexes as well as to further corroborate their successful preparation. The metal complexes were isolated in low yields, with the highest for **C1** and **C5**, which were around 60 % each. The low yields are attributed to the limited selectivity of the solvent extraction method of purification.

## 3.4 EXPERIMENTAL

### 3.4.1 Materials and instrumentation

All chemical reactions and manipulations were performed on a dual vacuum/nitrogen line using standard Schlenk techniques unless otherwise stated. Reagent grade chemicals were obtained from Sigma Aldrich and used as received. All solvents were dried under appropriate drying reagents and distilled prior to use. $^{1}$H NMR, $^{13}$C NMR and 2D NMR spectra were recorded on a Varian 300 MHz spectrometer using tetramethylsilane as an internal standard. Chemical shifts are reported in ppm and referenced to the solvent signal (DMSO-d6). FT-IR spectra were recorded on a Bruker TENSOR 27 spectrometer using ATR. Mass spectra of the complexes were recorded on Bruker compact ultimate 3000 HR-MS. Elemental analysis were performed in the micro analytical laboratory of the University of Stellenbosch. Absorption measurements were recorded on a SpeCord 210 plus AnalytikJena UV-Vis spectrophotometer in toluene.

### 3.4.2 Sodium ligand salt synthesis

#### 3.4.2.1 Synthesis of the sodium ligand salt of L1

To a stirring white suspension of NaH (1.50 mmol) in THF (10.00 mL), **L1** (1.00 mmol, 0.1701 g) was slowly added as a powder under a counter flow of $N_{2(g)}$. Upon addition of **L1** to the NaH suspension, vigorous bubbling, which signalled the evolution of $H_{2(g)}$ was observed. The reaction mixture turned yellow with the slow addition of **L1**. Once the bubbling had ceased,

the yellow reaction mixture was stirred under magnetic stirring for 30 min. All volatiles were removed under vacuum to yield the sodium ligand salt of **L1** as a yellow powder.

#### 3.4.2.2 Synthesis of the sodium ligand salt of L2

The ligand salt of **L2** was prepared following a synthetic procedure similar to that used for **L1**. **L2** (1.00 mmol, 0.1981 g) was slowly added as a powder to a stirring white suspension of NaH (1.50 mmol) in THF (10.00 mL), under the counter flow of $N_{2(g)}$. Upon addition of **L2** to the NaH suspension, vigorous bubbling, which signalled the evolution of $H_{2(g)}$ was observed. The reaction mixture turned light pink with the slow addition of **L2**. Once the bubbling had ceased, the light-pink reaction mixture was stirred under magnetic stirring for 30 min. All volatiles were removed under vacuum to yield the sodium ligand salt of **L2** as a light-pink powder.

#### 3.4.2.3 Synthesis of the sodium ligand salt of L3

The ligand salt of **L3** was prepared following a synthetic procedure similar to that used for **L1** and **L2**. **L3** (1.00 mmol, 0.2544 g) was slowly added as a powder to a stirring white suspension of NaH (1.50 mmol) in THF (10.00 mL), under the counter flow of $N_{2(g)}$. Upon addition of **L3** to the NaH suspension, vigorous bubbling, which signalled the evolution of $H_{2(g)}$ was observed. Unlike the sodium ligand salt reaction mixtures of **L1** and **L2**, the reaction mixture remained white with the slow addition of **L3**. Once the bubbling had ceased, the white reaction mixture was stirred under magnetic stirring for 30 min. All volatiles were removed under vacuum to yield the sodium ligand salt of **L3** as a white powder.

#### 3.4.2.4 Synthesis of the sodium ligand salt of L4

The sodium ligand salt of **L4** was prepared following a synthetic procedure similar to that used for **L1**, **L2** and **L3**. **L4** (1.00 mmol, 0.2143 g) was slowly added as a powder to a stirring white suspension of NaH (1.50 mmol) in THF (10.00 mL), under the counter flow of $N_{2(g)}$. Upon addition of **L4** to the NaH suspension, vigorous bubbling, which signalled the evolution of $H_{2(g)}$ was observed. The mustard yellow colour of **L4** intensified to a bright yellow colour as it reacted with NaH in THF. Once the bubbling had ceased, the bright yellow reaction mixture was stirred under magnetic stirring for 30 min. All volatiles were removed under vacuum to yield the sodium ligand salt of **L4** as a bright-yellow powder.

### 3.4.3 Synthesis of bis-(pyrrole-aldiminato) Zn(II) and Co(II) complexes C1 – C8

#### 3.4.3.1 Synthesis of bis-(pyrrole-aldiminato) Zn(II) complex C1

To a stirring solution of **L1**$^{-}$Na$^{+}$ (1.00 mmol, 0.1919 g) in THF (10.00 mL), a solution of $ZnCl_2$ (0.65 mmol, 0.08858 g) was added dropwise. The yellow colour solution of **L1**$^{-}$Na$^{+}$ intensified as the $ZnCl_2$ solution was added. The reaction mixture was stirred under magnetic stirring for 12 hours. After 12 hours, the reaction was stopped, and all volatiles were removed under vacuum to yield a yellow powder. Dry hexane was used to extract **C1** from the crude yellow power until the extract become colourless. The yellow hexane extract was concentrated under vacuum, and as this was carried out, yellow precipitate which was confirmed to be **C1** emerged. Vacuum filtration was used to isolate the precipitate from the mother liquor to yield **C1** as a light-yellow solid with a cotton consistency. Isolated yield: 0.1211 g (60 %).

#### 3.4.3.2 Synthesis of bis-(pyrrole-aldiminato) Zn(II) complex C2

To a stirring solution of **L2**$^{-}$Na$^{+}$ (1.00 mmol, 0.2210 g) in THF (10.00 mL), a solution of $ZnCl_2$ (0.65 mmol, 0.08858 g) was added dropwise. The light-pink colour of the solution of **L2**$^{-}$Na$^{+}$ turned white as the $ZnCl_2$ solution was added. The reaction mixture was stirred under magnetic stirring for 12 hours. After 12 hours, the reaction was stopped, and all volatiles were removed under vacuum to yield a white powder. Dry hexane was used to extract **C3** from the concentrated under vacuum, and as this was carried out, white precipitate which was confirmed to be **C2** emerged. Vacuum filtration was used to isolate the crude white power. This was repeated several times as the colour of the extract could not be used to determine when **C2** was completely extracted from the crude powder. The colourless hexane extract was precipitate from the mother liquor to yield **C2** as a white powder. Isolated yield: 0.09878 g (43 %).

#### 3.4.3.3 Synthesis of bis-(pyrrole-aldiminato) Zn(II) complex C3

To a stirring solution of **L3**$^{-}$Na$^{+}$ (1.00 mmol, 0.2764 g) in THF (10.00 mL), a solution of $ZnCl_2$ (0.65 mmol, 0.08858 g) was added dropwise. The white colour of the solution of **L3**$^{-}$Na$^{+}$ remained white as the $ZnCl_2$ solution was added. The reaction mixture was stirred under magnetic stirring for 12 hours. After 12 hours, the reaction was stopped, and all volatiles were removed under vacuum to yield a white powder. Dry hexane was used to extract **C3** from the concentrated under vacuum, and as this was carried out, white precipitate which was confirmed to be **C3** emerged. Vacuum filtration was used to isolate the crude white power. This was repeated several times as the colour of the extract could not be used to determine when **C3** was completely extracted from the crude powder. The colourless hexane extract was precipitate from the mother liquor to yield **C3** as a white crystalline solid. Isolated yield: 0.1627 g (57 %).

### 3.4.3.4 Synthesis of bis-(pyrrole-aldiminato) Zn(II) complex C4

To a stirring solution of **L4**$^{-}$Na$^{+}$ (1.00 mmol, 0.2633 g) in THF (10.00 mL), a solution of $ZnCl_2$ (0.65 mmol, 0.08858 g) was added dropwise. The bright yellow colour of the solution of **L4**$^{-}$Na$^{+}$ intensified as the $ZnCl_2$ solution was added. The reaction mixture was stirred under magnetic stirring for 12 hours. After 12 hours, the reaction was stopped, and all volatiles were removed under vacuum to yield a bright yellow powder. Dry hexane was used to extract **C4** from the crude bright yellow powder until the extract was colourless. The bright yellow extract was concentrated under vacuum, and as this was carried out, yellow-orange precipitate which was confirmed to be **C4** emerged. Vacuum filtration was used to isolate the yellow-orange filtrate from the mother liquor. This yielded **C4** as a yellow-orange powder. Isolated yield: 0.1107 g (38 %).

### 3.4.3.5 Synthesis of bis-(pyrrole-aldiminato) Co(II) complex C5

To a stirring solution of **L1**$^{-}$Na$^{+}$ (1.00 mmol, 0.1919 g) in THF (10.00 mL), a suspension of $CoCl_2$ (0.65 mmol, 0.08858 g) was added dropwise. The yellow colour of the **L1**$^{-}$Na$^{+}$ solution turned brown as the $CoCl_2$ suspension was added. The reaction mixture was stirred under magnetic stirring for 12 hours. After 12 hours, the reaction was stopped, and all volatiles were removed under vacuum to yield a dark brown powder. Dry hexane was used to extract **C5** from the dark-brown power until the extract become colourless. The brick-red hexane extract was concentrated under vacuum, and as this was carried out, brick-red precipitate which was confirmed to be **C5** emerged. Vacuum filtration was used to isolate the precipitate from the mother liquor to yield **C4** as a brick-red solid powder. Isolated yield: 0.1214 g (60 %).

### 3.4.3.6 Synthesis of bis-(pyrrole-aldiminato) Co(II) complex C6

To a stirring solution of **L2**$^{-}$Na$^{+}$ (1.00 mmol, 0.2210 g) in THF (10.00 mL), a suspension of $CoCl_2$ (0.65 mmol, 0.08858 g) was added dropwise. The light-pink colour of the solution of **L2**$^{-}$Na$^{+}$ turned brown as the $CoCl_2$ suspension was added. The reaction mixture was stirred under magnetic stirring for 12 hours. After 12 hours, the reaction was stopped, and all volatiles were removed under vacuum to yield a dark-brown powder. Dry hexane was used to extract **C6** from crude dark-brown powder until the extract became colourless. The brown extract was concentrated under vacuum, and as this was carried out, brown precipitate which was confirmed to be **C6** emerged. Vacuum filtration was used to isolate the brown precipitate from the mother liquor to yield C6 as a brown powder. Isolated yield: 0.1495 g (55 %).

### 3.4.3.7 Synthesis of bis-(pyrrole-aldiminato) Co(II) complex C7

To a stirring solution of **L3**$^{-}$Na$^{+}$ (1.00 mmol, 0.2764 g) in THF (10.00 mL), a suspension of $CoCl_2$ (0.65 mmol, 0.08858 g) was added dropwise. The white colour of the solution of **L3**$^{-}$Na$^{+}$ turned brown as the $CoCl_2$ suspension was added. The reaction mixture was stirred under magnetic stirring for 12 hours. After 12 hours, the reaction was stopped, and all volatiles were removed under vacuum to yield a dark-brown powder. Dry hexane was used to extract **C7** from crude dark-brown powder until the extract became colourless. The olive-green extract was concentrated under vacuum, and as this was carried dark-green precipitate which was confirmed to be **C7** emerged. Vacuum filtration was used to isolate the dark-green precipitate from the mother liquor to yield C7 as a dark-green powder. Isolated yield: 0.1251 g (44 %).

### 3.4.3.8 Synthesis of bis-(pyrrole-aldiminato) Co(II) complex C8

To a stirring solution of **L4**$^{-}$Na$^{+}$ (1.00 mmol, 0.2633 g) in THF (10.00 mL), a suspension of $CoCl_2$ (0.65 mmol, 0.08858 g) was added dropwise. The white colour of the solution of **L4**$^{-}$Na$^{+}$ turned brown as the $CoCl_2$ suspension was added. The reaction mixture was stirred under magnetic stirring for 12 hours. After 12 hours, the reaction was stopped, and all volatiles were removed under vacuum to yield a dark-brown powder. Dry hexane was used to extract **C8** from crude dark-brown powder until the extract became colourless. The brown extract was concentrated under vacuum, and as this was carried brown precipitate which was confirmed to be **C8** emerged. Vacuum filtration was used to isolate the brown precipitate from the mother liquor to yield **C8** as a brown powder. Isolated yield: 0.1652 g (58 %).

## 3.5 REFERENCES


[1] R. H. Holm, A. Chakravorty, and L. J. Theriot, *Inorg. Chem.*, 1966, 5, 4, 625–635

[2] A. Mohamadou, J.-P. Barbier, and R. P. Hugel, *Polyhedron*, 1992, 11, 20, 2697–2702

[3] H. Liang, J. Liu, X. Li, and Y. Li, *Polyhedron*, 2004, 23, 9, 1619-1627.

[4] Z. Wu, Q. Chen, G. Yanga, C. Xiaoa, J. Liu, S. Yang, J.S Maa, *Sensors Actuators, B Chem.*, 2004, 99, 2–3, 511-515.

[5] C. S. B. Gomes, P. T. Gomes, M. T. Duarte, R. E. Di Paolo, A. L. Maçanita, and M. J. Calhorda, *Inorg. Chem.*, 2009, 48, 23, 11176–11186.

[6] H. Vignesh Babu and K. Muralidharan, *J. Chem. Soc. Dalt. Trans.*, 2013,42, 1238-1248.

[7] C. N. Iverson, C. A. G. Carter, R. T. Baker, J. D. Scollard, J. A. Labinger, and J. E. Bercaw, "C-H Bond Activation by Unsymmetrical 2-(N-Arylimino)pyrrolide Pt Complexes: Geometric Effects on Reactivity," *J. Am. Chem. Soc.*, 2003.

[8] G. H. Chen, W. J. Leu, J. H. Guh, C. H. Lin, and J. H. Huang, *J. Organomet. Chem.*, 2018, 868, 122-130

[9] R. M. Ahmed, E. I. Yousif, and M. J. Al-Jeboori, *Sci. World J.*, 2013, 2013, 754868

[10] S. A. Carabineiro, L.C Silva, P.T Gomes, L.C.J Pereira, L.F Veiros, S.I Pascu, M.T Duarte, S. Namorado, and R.T Henriques*, Inorg. Chem.,* 2007, 46, 17, 6880–6890

[11] D. Suresh, P.S Lopes, B. Ferreira, C.A Figueira, C.S.B Gomes, P.T Gomes, R.E Di Paolo, A.L Maçanita, M.T Duarte, A. Charas, J. Morgado and M.J Calhorda, *Chem. - A Eur. J.*, 2014, 20, 14, 4126–4140

[12] T.H Crawford and J. swanson, *J. Chem. Educ.,* 1971, 48, 6, 382

[13] R, Kant, *IJSRP*., 2009, 9, 3, 87101

# Chapter 4:

# Evaluation of the catalytic activity of bis-(pyrrole-aldiminato) Zn(II) and Co(II) complexes for the coupling of carbon dioxide/ carbon disulphide with propylene oxide

CONTENT


4.1 INTRODUCTION……..94

4.2 RESULTS AND DISCUSSION…… 98

4.2.1 The coupling of propylene oxide and carbon disulphide in the presence of **C1** as a catalyst precursor……98

4.2.2 Effect of solvent in the coupling of carbon disulphide and propylene oxide ……103

4.2.3 Effect of reaction time in the coupling of carbon disulphide and propylene oxide……108

4.2.4 Effect of MeOH quantity on the nature of the products formed in the coupling of carbon disulphide and propylene oxide……..109

4.2.5 Effect of catalyst in the coupling of carbon disulphide and propylene oxide……112

4.2.6 Effect of neutral ligand and cobalt chloride as catalyst systems in the coupling of carbon disulphide and propylene oxide…….……114

4.2.7 Effect of catalyst in the coupling of carbon dioxide and propylene oxide……115

4.2.8 Effect of reaction time in the coupling of carbon dioxide and propylene oxide……117

4.2.9 Effect of solvent in the coupling of carbon dioxide and propylene oxide……..119

4.2.10 Effect of $CO_2$ pressure in the coupling of carbon dioxide and propylene oxide……120

4.3 CONCLUSION…….. 123

4.4 EXPERIMENTAL…… 124

4.4.1 Materials and instrumentation…….. 124

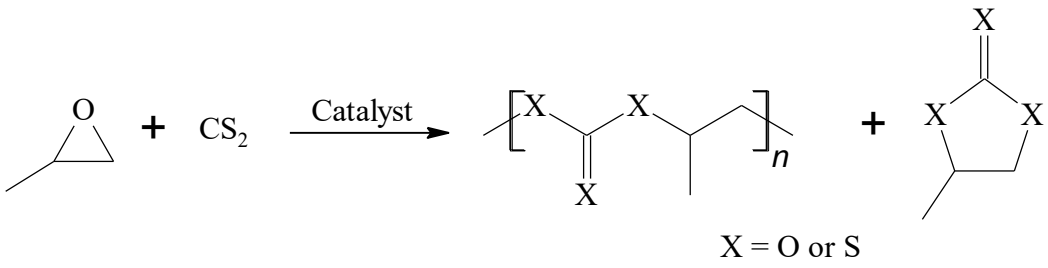
4.4.2 General procedure for the coupling of carbon disulphide and propylene oxide……124

4.4.3 General procedure for the coupling of carbon dioxide and propylene oxide…… 125

4.5 REFERENCES……... 126

## 4.1 INTRODUCTION

The coupling of carbon disulphide ($CS_2$) with epoxides (**Scheme 4.1**) is a chemical process similar to the coupling of $CO_2$ with epoxides (**Scheme 4.2**). As with the latter, the products can either be cyclic or polymeric, with the most common products being cyclic dithiocarbonates (**Scheme 4.3**) [1]–[3]. $CS_2$ is a cheap sulphur rich C1 feedstock which is an analogue of $CO_2$ [4]. $CS_2$ finds uses in a great deal of industrial processes, however, its detrimental effects on the environment are of concern. This makes the need to find chemical transformations that can add value to the excess $CS_2$ that could potentially be discharged into the natural environment of utmost importance [5].

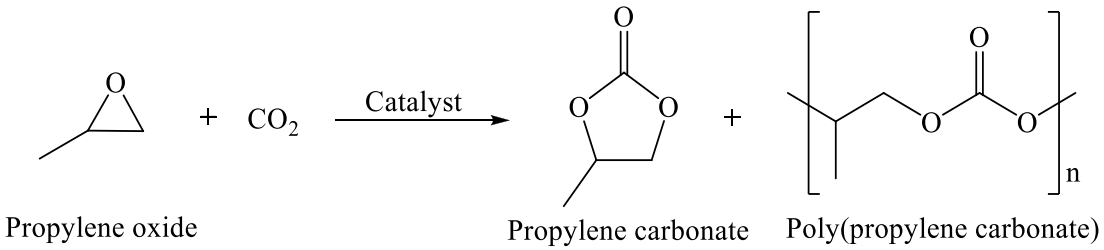



**Scheme 4.1** *The coupling of propylene oxide and carbon disulphide to yield either the polymeric or cyclic product* [1]

The ease with which $CS_2$ can be handled in the coupling reaction with epoxides compared to $CO_2$ has seen it being used to optimize $CO_2$/epoxides reaction conditions. However, applying identical reaction conditions to both coupling processes has been shown to not produce identical results as the chemical properties of the two monomers, $CS_2$ and $CO_2$ are not identical. This is attributed to the difference in the physical states of the two monomers. That is: $CS_2$ is a liquid, and as such, reactions with $CS_2$ can be carried out under standard Schlenk techniques, whereas $CO_2$ is a gas, and the reactions thereof require pressurized systems. Another factor which makes the coupling of epoxides with $CO_2$ different from the coupling of epoxides with $CS_2$ is the difference in the stability of the two C1 feedstocks. That is, $CO_2$ is the most oxidized form of carbon, which makes it more stable and less reactive than $CS_2$. The use of $CS_2$ to establish some sort of baseline is still a good starting point. [4], [6], [7].

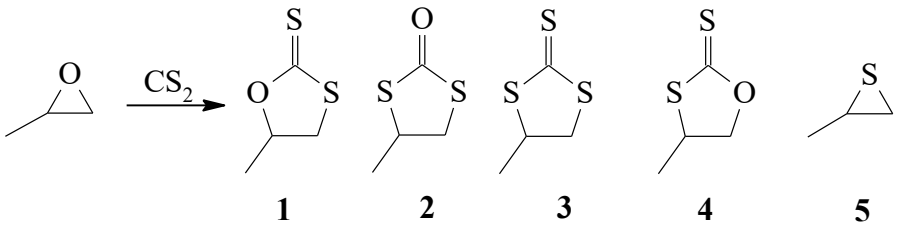
Reactions with $CS_2$ and epoxides are known to be more complex relative to reactions between $CO_2$ and epoxides because of the variety of cyclic products that can be produced with the former. The cyclic products that have been produced with the coupling of $CS_2$ and PO include

1,3-oxathiolane-2-thiones, 1,3-dithiolane-2-ones, 1,3-dithiolane-2-thiones, 1,3-oxathiolane-2-ones and thiiranes (**Scheme 4.3, 1 - 5**). With this reaction, a mixture of at least two cyclic products is usually obtained. 5-methyl-1,3-oxathiolane-2-thione and 4-methyl-1,3-dithiolane-2-thione (**Scheme 4.3 1 and 3**) have been reported to be favoured to form in this reaction. The reaction conditions applied as well as the nature of the catalyst and co-catalyst system are known to affect the ratios of cyclic products obtained in the product mixtures [3], [8]–[10].




**Scheme 4.2** *The coupling of carbon dioxide and propylene oxide to yield propylene carbonate and poly(propylene carbonate)* [2]

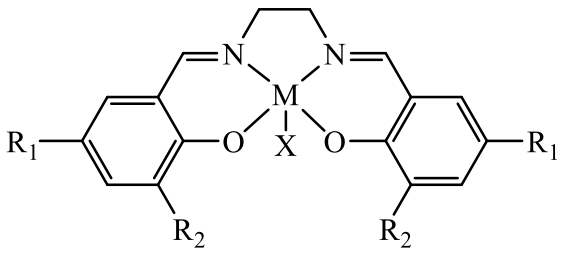
Cyclic thiocarbonates (**Scheme 4.3**, **1** – **4**) are useful intermediates in the chemical manufacturing industry. They find uses in the synthesis of tetrathiafulvalene derivatives, which are known for their excellent electrical properties. They are used in the preparation of crown thioethers, which are known to have the ability to coordinated to metal ions and have been shown to be capable extracting heavy metals in the remediation of heavy metal polluted water. Cyclic dithiocarbonate **2** (**Scheme 4.3**) is known for its biological activity as an anti-cancer agent. Cyclic dithiocarbonates also have been used as monomers in the preparation of poly-(thiocarbonates) [11]–[15].




**Scheme 4.3** *Formation of cyclic products from the coupling of propylene oxide and carbon disulphide* [3]

In the last few decades, an array of catalyst systems have been developed and evaluated for the coupling of $CS_2$ and PO. These include transition metal complexes, quaternary ammonium salts and alkali metal salts. Of the transition metal complexes that have been evaluated for this process, the most common are penta-coordinate $Al^{3+}$ complexes which are supported by salen ligands, with the ancillary ligand either being electron withdrawing halogen ions or electron donating alkyl groups. Catalysts previously evaluated in the coupling of $CO_2$ and PO have been applied to the coupling of $CS_2$ and PO and it has been shown that not every catalyst that is active in the former will yield similar results with the former [8], [16], [17].

Lu *et al*. demonstrated that metal complex catalyst systems active for the coupling of $CO_2$ and PO are also active for the coupling of $CS_2$ and PO. The group prepared a series of salen(AlX) complexes (**Figure 4.1**) and evaluated their catalytic activity in the coupling of $CO_2$ and PO at ambient temperature. 98 % yield of cPC was achieved when complex **5** (**Figure 4.1**) was used in conjunction with 18-crown-6–KI as the catalyst system over 12 hours. The group then applied the same complexes in the coupling of $CS_2$ and PO in the presence of tetrabutylammonium bromide (TBAB) as the co-catalyst and a reaction temperature of 100 °C. As with the coupling of $CO_2$ and PO, complex **5** (**Figure 4.1**) showed the highest activity and resulted in 99% yield of a mixture of 4-methyl-1,3-dithiolane-2-thione, 5-methyl-1,3-oxathiolane-2-thione and 4-methyl-1,3-oxathiolane-2thione [8], [18].




1. M = Al, X = Et, $R_1 = R_2 = H$
2. M = Al, X = Et, $R_1 = {}^tBu$, $R_2 = H$
3. M = Al, X = Et, $R_1 = R_2 = {}^tBu$
4. M = Al, X = Et, $R_1$ = Br, $R_2 = H$
5. M = Al, X = Cl, $R_1 = R_2 = H$
6. M = Cr, X = Cl, $R_1 = R_2 = {}^tBu$
7. M = Co, X = Cl, $R_1 = R_2 = {}^tBu$

**Figure 4.1** *Salen- Al(*III), Cr(III) and Co(III) *complexes for the coupling of carbon disulphide and epoxides* [8]

Contrary to the observations made when salen(AlX) complexes were evaluated in the coupling of PO with either $CO_2$ or $CS_2$, cobalt(III)–salen complex **6** (**Figure 4.1**) was found to be highly active for the coupling of $CO_2$ and PO and inactive for the coupling of $CS_2$ and PO. A similar observation was made for chromium(III)–salen complex **7** (**Figure 4.1**). It has been reported

to be highly active for the coupling of $CO_2$ and PO, however, low activity was observed for the coupling of $CS_2$ and PO. The little to no activity observed with chromium(III)–salen complex **7** and cobalt(III)–salen complex **16** (**Figure 4.1**) is suspected to be a result of sulphur poisoning from $CS_2$ [8], [10], [19]–[21].

In this chapter, the preliminary results obtained in evaluating the catalytic activity of bis-(pyrrole-aldiminato) Zn(II) and Co(II) complexes, which are discussed in chapter 3, for the coupling of $CS_2$ and PO as well as the coupling of $CO_2$ and PO is reported. The coupling of PO and $CS_2$ will be used to establish the baseline reaction conditions using bis-(pyrrole-aldiminato) Zn(II) complex **C1** prior to applying them across all 8 metal complexes. These reaction conditions will then be adapted in the coupling of PO and $CO_2$, as some metal complexes active for the coupling of PO and $CS_2$ have been reported to be active in the coupling of PO and $CO_2$. There are a few exceptions in this where metal complexes active in the coupling of PO and $CO_2$ showed little to no activity in the coupling of PO and $CS_2$.

## 4.2 RESULTS AND DISCUSSION

Bis-(pyrrole-aldiminato) Zn(II) and Co(II) complexes, **C1** – **C8** (**Figure 4.2**) reported in chapter 3 were evaluated for their catalytic activity in the coupling of $CS_2$ and PO as well as in the coupling of $CO_2$ and PO.

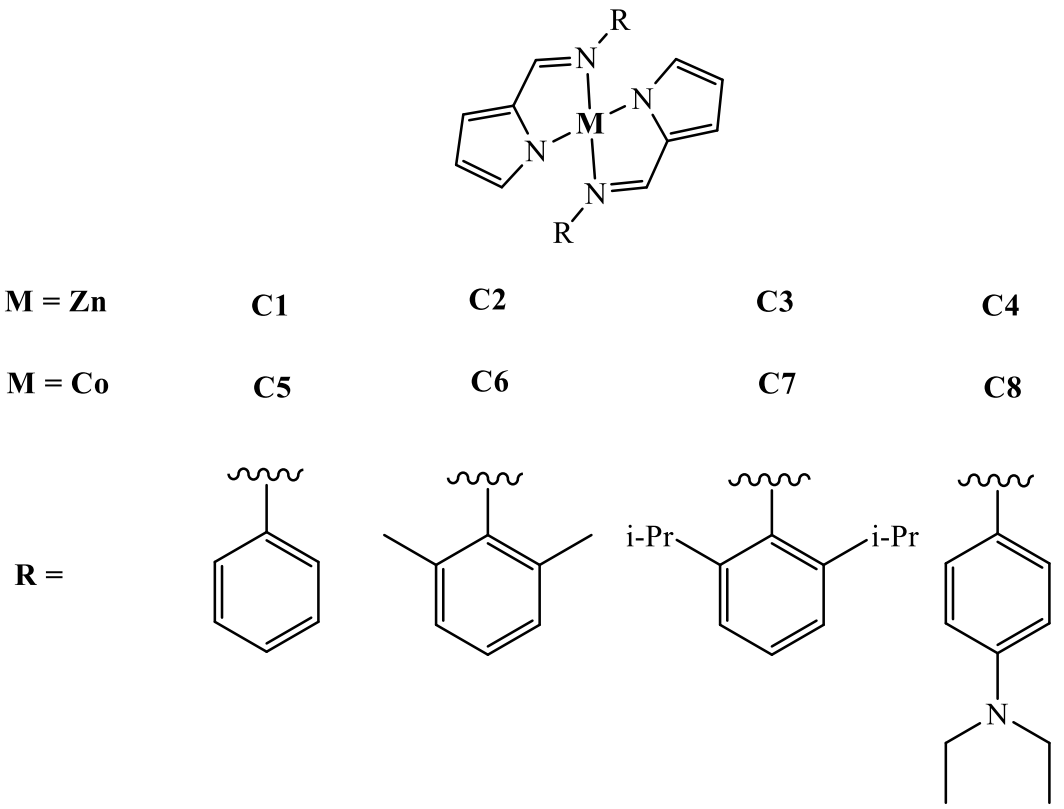



**Figure. 4.2** *Bis-(pyrrole-aldiminato) Zn(II) and Co(II) complexes,* ***C1*** *–* ***C8***

### 4.2.1 The coupling of propylene oxide and carbon disulphide in the presence of C1 as a catalyst precursor

A series of preliminary experiments were carried out with complex **C1** in order to establish baseline reaction conditions for the coupling process. The reactions were carried out following a procedure adapted from literature [22]. The general procedure is as follows; to a stirring solution of PO in which all 8 complexes are soluble in, the respective catalyst and co-catalyst, $CS_2$ was added. The reaction mixtures were stirred for the specified time period at room temperature. Once the reaction mixtures were stirred for the desired period of time, the reactions were stopped. All volatiles were removed under vacuum and the resulting residue was dissolved in DCM. The DCM solution was filtered through silica as means to remove the respective co-catalyst. as the co-catalysts have an affinity to silica. The DCM filtrate was then transferred to a round bottom flask and all volatiles were removed under vacuum. $^1$H NMR

spectra of the resulting residues or oil-like products were obtained in $CDCl_3$ to determine if the coupling reaction was successful and identify the coupling products observed. The masses of the products were determined by mass difference and used to quantify the % PO converted.

**C1** was used to investigate the best reaction conditions for the coupling of $CS_2$ and PO before the other metal complexes reported in chapter 3 were also evaluated. This complex was used because it contains no substituent groups on the imino phenyl ringing in addition, it is the easiest to synthesize and purify of all 8 metal complexes.

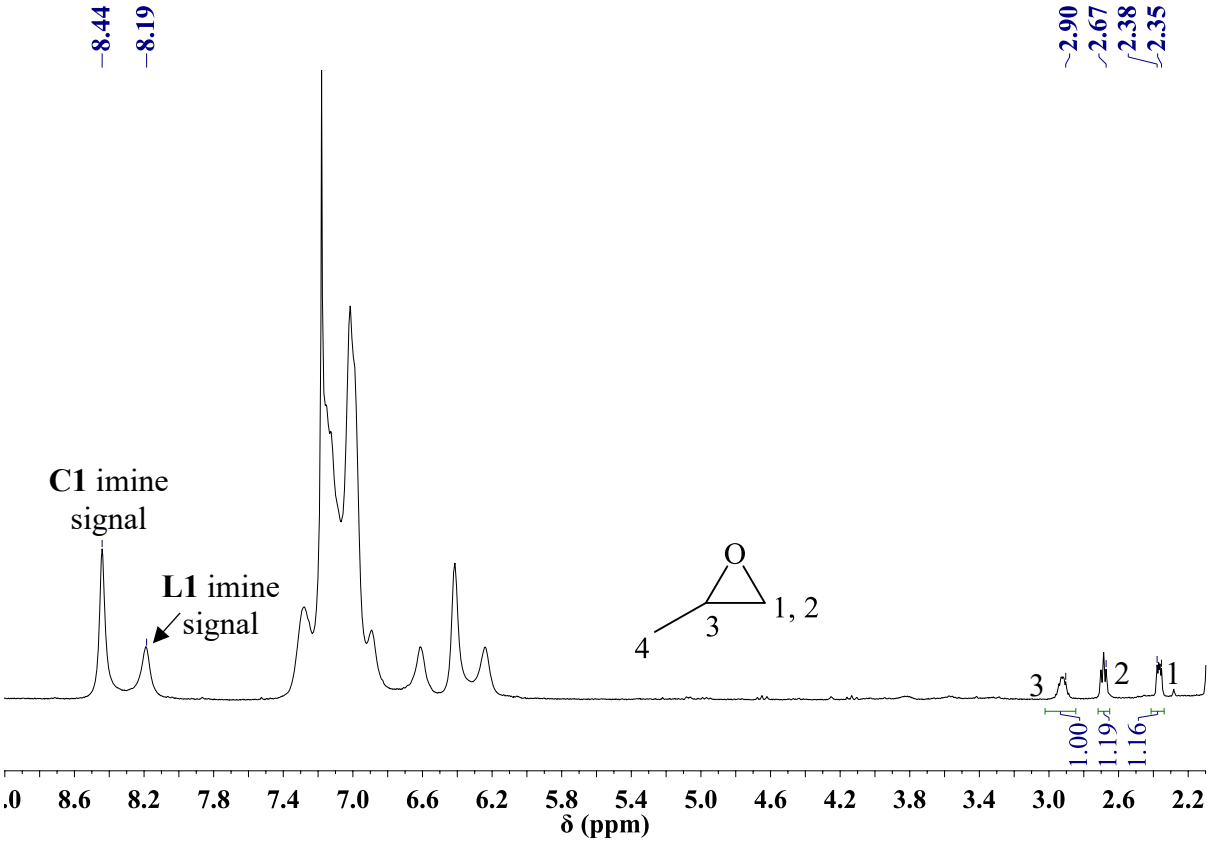



**Figure 4.3** *$^1$H NMR spectrum of the residue obtained using **C1** as a catalyst in the coupling of $CS_2$/PO in the absence of a co-catalyst (Entry **1**, **Table 4.1**) ($CDCl_3$, 300 K)*

A control experiment was performed investigating the performance of **C1** without addition of a co-catalyst. In this experiment no conversion of PO to cyclic product or polymer was observed as shown in the $^1$H NMR spectrum (**Figure 4.3**). This is similar to an observation made by North *et al*. when the group demonstrated that an aluminium salen complex (**Figure 4.4**) shows no activity for the coupling of PO and $CS_2$ in molar ratios 1:7, in the absence of co-catalyst, under solvent-less conditions, over 16 hours even when the reaction temperature was

raised to 50 °C [23]. An interesting observation is made in the aromatic region; two signals are observed in the imine region, the signal at 8.44 ppm is assigned to the metal complex imine proton, whereas the signal observed at 8.19 ppm is assigned to the neutral ligand imine proton.

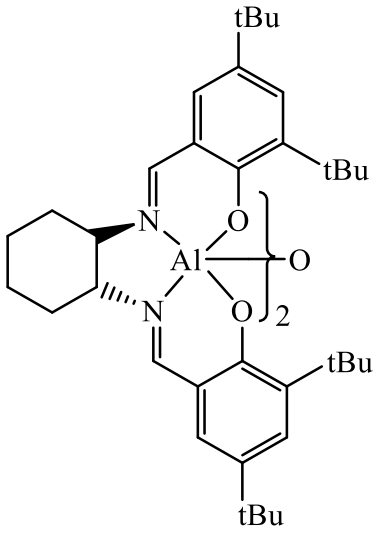



**Figure 4.4** *Aluminium salen complex for the coupling of propylene oxide and carbon disulphide* [23]

This observation suggests that **C1** decomposes to **L1** in the presence of PO and $CS_2$. This is in-line with reports that bis-(pyrrole-aldimine) Zn(II) complexes suffer from poor stability, especially in solution.

After observing that **C1** shows no activity for the coupling of PO and $CS_2$ at room temperature even after 24 hours, the activity of **C1** was evaluated in the presence of 4 different co-catalysts, namely, TBAC, [PPN]Cl, MeIm and DMAP. Control reactions were carried out in which the 4 co-catalysts were screened on their own for the coupling of PO and $CS_2$ under the same reaction conditions as the reactions carried out in the presence of **C1** paired with the co-catalysts (Entries **6** – **9**, **Table 4.1**). This was done in order to confirm that the activity achieved for the reactions in which **C1** is paired with either one of the co-catalysts is not induced by the co-catalysts on their own. The reactions were carried out following a method similar to that mentioned in **4.2.1**. To a stirring solution of PO, **C1** and the respective co-catalyst, $CS_2$ was added. The reaction mixtures were stirred for 24 hours at room temperature, after which the reactions were stopped. All volatiles were removed under vacuum. Upon work-up, $^1$H NMR spectra of the resulting yellow oil-like products were obtained in $CDCl_3$.

**Table 4.1**: *Effect of co-catalyst in the coupling of $CS_2$ and PO reaction data*

| Entry | Catalyst | Co-catalyst | Mass cyclic products (mg) | % PO conversion | Cyclic product % conversion | | |
|---|---|---|---|---|---|---|---|
| | | | | | a | b | c |
| **1** | **C1** | - | - | - | - | - | - |
| **2** | **C1** | TBAC | 83.8 | 2.32 | 55 | 9 | 36 |
| **3** | **C1** | [PPN]Cl | 42.5 | 1.04 | 50 | - | 50 |
| **4** | **C1** | DMAP | 22.6 | 0.56 | 14 | 15 | 71 |
| **5** | **C1** | MeIm | 34.9 | 0.80 | - | 20 | 80 |
| **6** | - | TBAC | 20 | 0.49 | - | - | 100 |
| **7** | - | [PPN]Cl | 22.10 | 0.54 | 67 | 5 | 28 |
| **8** | - | DMAP | 0.5 | 0.01 | - | - | - |
| **9** | - | MeIm | 1.14 | 0.03 | - | - | - |

Reactions performed solventless in PO (2.01 mL) and $CS_2$ (1.86 mL), mmol complex = co-catalyst = 30.00 mmol, ratio of complex:$CS_2$ = 1:1000:1000, temperature = 24 °C, time = 24 hours. a = 5-methyl-1,3-oxathiolane-2-thione, b = 4-methyl-1,3-oxathiolane-2-thione, c = 4-methyl-1,3-dithiolane-2-thione

The catalyst system pairs of **C1** with TBAC, [PPN]Cl and MeIm (Entries **2**,**3** and **5**, **Table 4.1**) resulted in the conversion of PO and $CS_2$ into three cyclic products, namely; 5-methyl-1,3-oxathiolane-2-thione, 4-methyl-1,3-dithiolane-2-thione and 5-methyl-1,3-oxathiolan-2-one (**Scheme 4.3, 1, 3 & 4**). **Figure 4.4** shows a representative $^1$H NMR spectrum obtained in $CDCl_3$ for the products obtained in this section. It is illustrated as an example of the spectra obtained for the products obtained in this co-catalyst study.

In the $^1$H NMR spectra obtained for the coupling reactions carried out in the presence of **C1** with TBAC and DMAP the presence of 5-methyl-1,3-oxathiolane-2-thione is confirmed by the observation of signals at 5.28 ppm, 3.56 ppm and 3.31 ppm. These are assigned to the C<u>H</u>, C<u>H$_2$</u> and C<u>H$_2$</u> protons, respectively. The C<u>H$_3$</u> protons appear between 1.56 ppm and 1.59 ppm and overlap with C<u>H$_3$</u> protons assigned to 4-methyl-1,3-dithiolane-2-thione as shown in the expanded spectrum (**Figure 4.5**). Proton signals as a result of the presence of 4-methyl-1,3-dithiolane-2-thione are observed at 4.44 ppm, 3.93 ppm, and 3.56 ppm. These are assigned to the C<u>H</u>, C<u>H$_2$</u> and C<u>H$_2$</u> protons, respectively. The C<u>H$_3$</u> protons appear between 1.56 ppm and 1.58 ppm. The third set of signals, which are assigned to 4-methyl-1,3-oxathiolane-2-thione are observed at 4.76 ppm, 3.42 ppm and 3.21 ppm. These are assigned to the C<u>H</u>, C<u>H$_2$</u> and C<u>H$_2$</u>

protons, respectively. The C<u>H$_3$</u> protons appear between 1.46 ppm and 1.49 ppm. A similar observation is made in the spectra obtained for products from the control reactions, in which the co-catalysts were screened on their own.

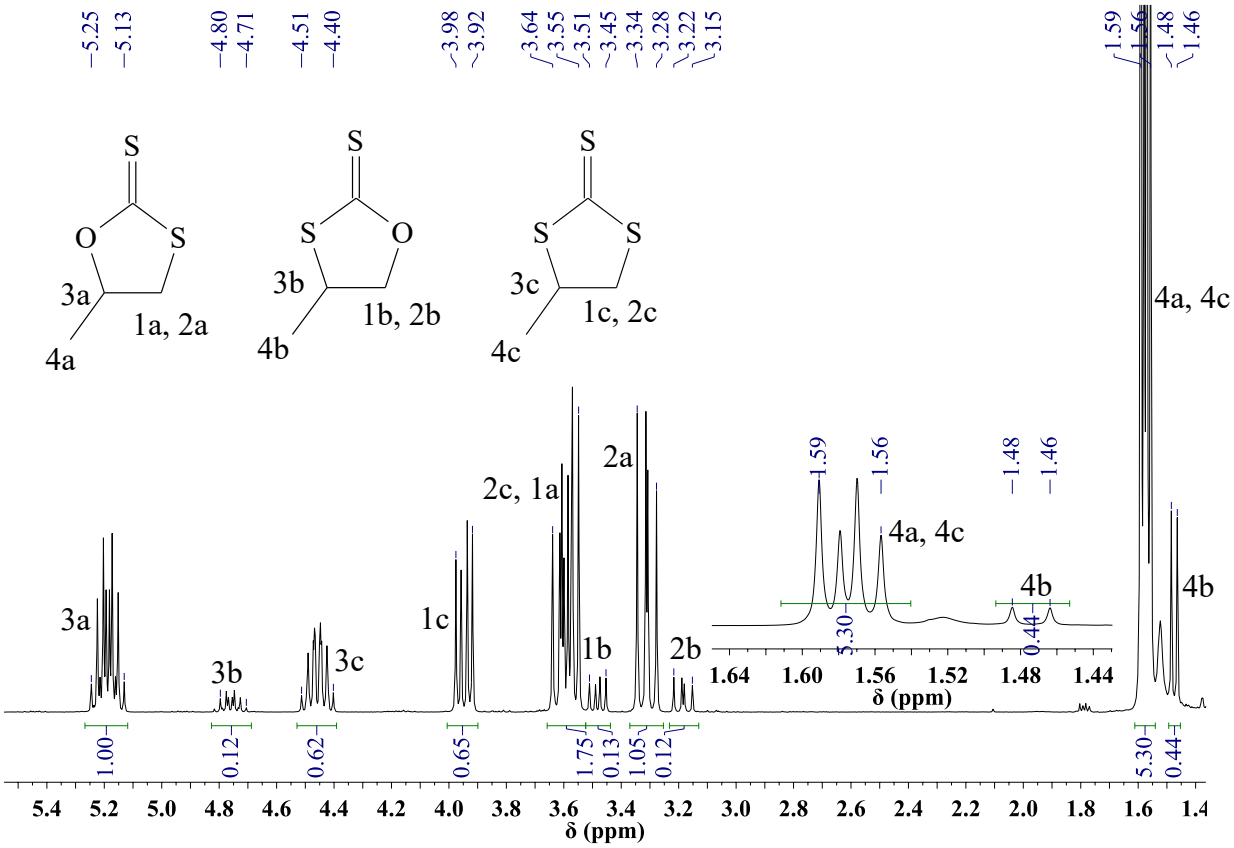



**Figure 4.5** *Representative $^1$H NMR spectrum for the yellow oil-like products obtained in investigating effect of co-catalysts (Entry **2**, **Table 2.1**) (CDCl$_3$, 300 K)*

**C1** paired with [PPN]Cl showed selectivity for two cyclic products in a 1:1 ratio. These were identified as 5-methyl-1,3-oxathiolane-2-thione and 4-methyl-1,3-dithiolane-2-one. **C1** paired with MeIm also showed selectivity for two cyclic products, however, in a 1:0.2 ratio. The cyclic products were identified as 4-methyl-1,3-dithiolane-2-thione and 4-methyl-1,3-oxathiolane-2-thione, respectively.

Although the presence of TBAC, DMAP, [PPN]Cl and MeIm improved the activity of **C1** in the coupling of PO and $CS_2$, the conversion rates were very poor. The highest conversion rate was found to be 2.32 %, of which 54 % was determined to be 5-methyl-1,3-oxathiolane-2-thione, 36 % 4-methyl-1,3-dithiolane-2-thione and 9 % 4-methyl-1,3-oxathiolane-2-thione. This was achieved for the reactions carried out using **C1** and TBAC as the catalyst system. The

lowest conversion rate was achieved with **C1** paired with DMAP. It resulted in a 0.56 % conversion of PO to three cyclic products of which 71 %, 15 % and 14 % were identified as 4-methyl-1,3-dithiolane-2-thione, 5-methyl-1,3-oxathiolane-2-thione and 5-methyl-1,3-oxathiolane-2-thione, respectively.

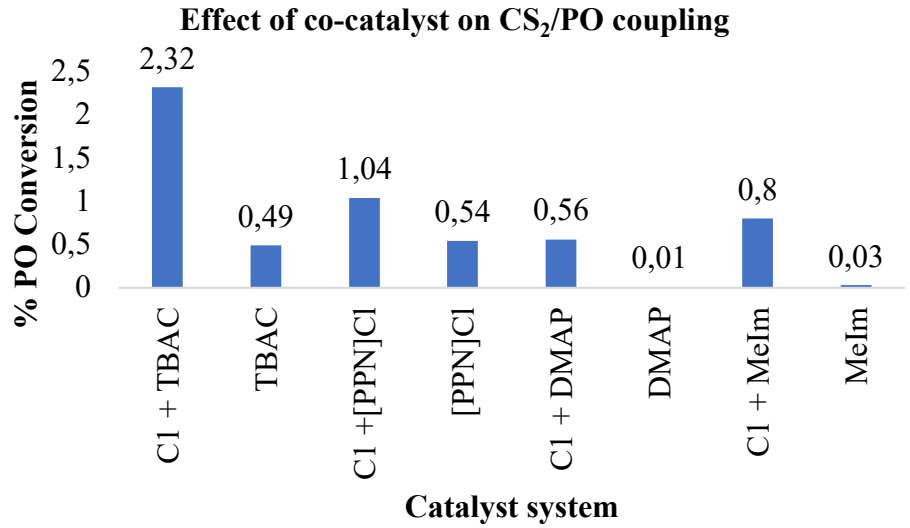



**Figure 4.6** *Effect of co-catalysts on conversion rate in the coupling of carbon disulphide and propylene oxide*

The co-catalysts on their own performed worse than when they were paired with **C1**. The highest conversion rate was found to be 0.54 % and this was achieved with [PPN]Cl. The lowest conversion rate achieved with DMAP and this was found to be 0.01 %. **Figure 4.6** shows a graphic comparison of the conversion rates achieved when catalyst system pairs of **C1** and the respective co-catalyst were used compared to when the co-catalysts were used on their own.

### 4.2.2 Effect of solvent in the coupling of PO/$CS_2$ in the presence of C1 and co-catalysts

After observing that catalytic performance for **C1** with a co-catalyst for the coupling of PO and $CS_2$, resulted in very low conversion, the experiments were repeated in the presence of MeOH (5.00 mL). The reactions were carried out following a similar procedure outline in **4.2.1**. To a stirring solution of **C1**, PO, $CS_2$ and the respective co-catalyst, MeOH was added. Two control reactions were also carried out. In the first, **C1** was used as a catalyst in the absence co-catalyst. In the second control reaction, both **C1** and co-catalyst were omitted. A second set of reactions were carried out in which the activity of the co-catalysts on their own was evaluated for the

coupling of PO and $CS_2$. This was done in order to confirm that the activity achieved for the reactions in which **C1** is used in conjunction with co-catalysts isn't induced by the co-catalysts on their own.

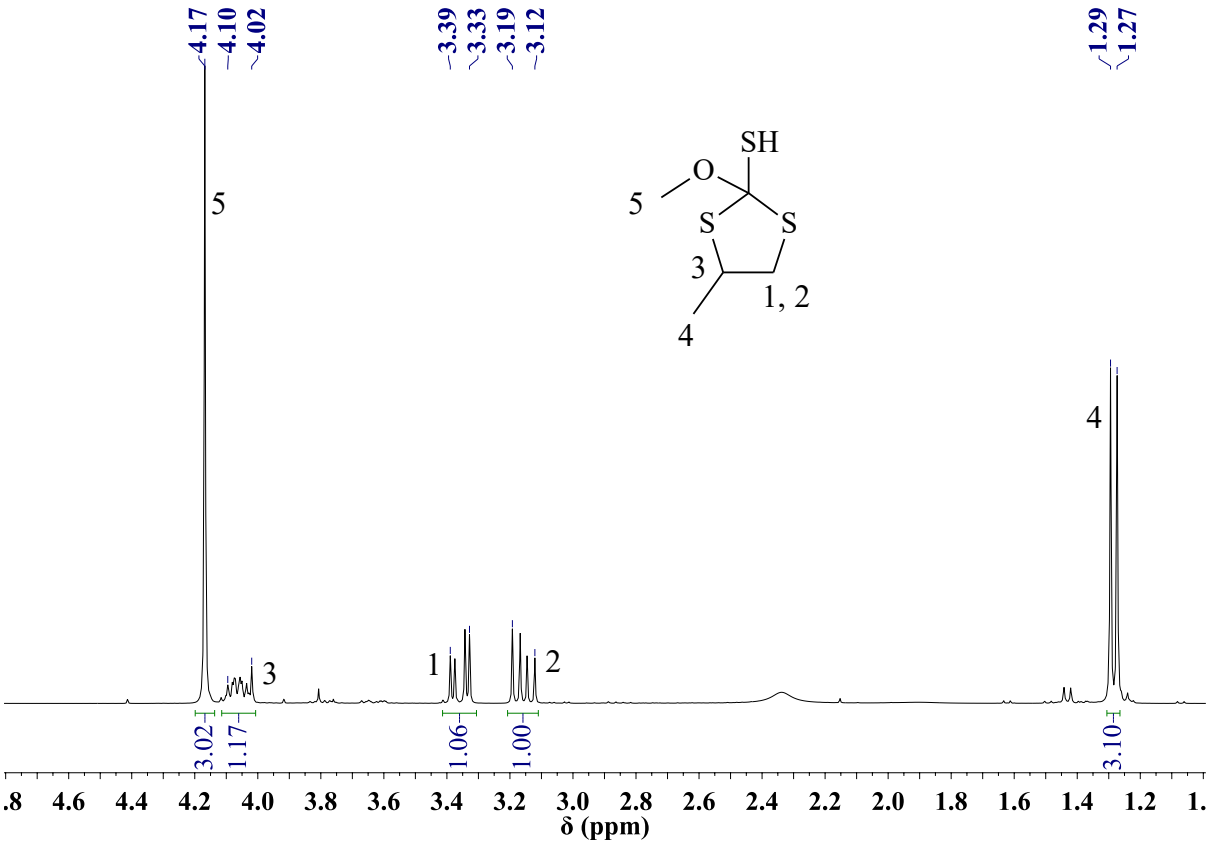



**Figure 4.7** *$^1$H NMR spectrum for the yellow oil-like products obtained using **C1** and TBAC for $CS_2$/PO coupling with MeOH as solvent, (Entry **2**, **Table 4.2**) ($CDCl_3$, 300 K)*

The reaction mixtures were stirred for 24 hours at room temperature. After 24 hours, the reactions were stopped, and all volatiles were removed under vacuum and the residues analysed with $^1$H NMR in $CDCl_3$.

In all the experiments perform the formation of cyclic coupling products were observed in the $^1$H NMR spectra of the residues of the catalytic experiments, however the signals corresponding to the cyclic products obtained when the coupling reaction were performed neat are not observed. Instead signals corresponding to what appears to be the methoxylated cyclic products reported in **4.2.1** are observed. In (**Figure 4.7**) the $^1$H-NMR spectrum of the residue obtained for Entry **3** (**Table 4.2**) is shown. In this spectrum signals appear at 4.13 ppm, 3.95 – 4.05 ppm, 3.35 – 3.30 ppm, 3.08 – 3.15 ppm and 1.21 – 1.23 ppm. These are assigned to the

methoxy O$\underline{CH_3}$, $\underline{CH_2}$, $\underline{CH_2}$ and the methyl $\underline{CH_3}$ protons, respectively. The SH and/or OH proton appears as a broad signal in some cases and as a doublet in other cases.

**Table 4.2** *Effect of solvent in the coupling of $CS_2$ and PO reaction data*

| Entry | Catalyst | Co-catalyst | Mass cyclic product (mg) | % PO conversion |
|---|---|---|---|---|
| **1** | **C1** | - | 413.60 | 7.56 |
| **2** | **C1** | TBAC | 1835.70 | 33.55 |
| **3** | **C1** | [PPN]Cl | 2021.50 | 36.95 |
| **4** | **C1** | DMAP | 3185.70 | 58.23 |
| **5** | **C1** | MeIm | 3310.05 | 60.50 |
| **6** | - | - | 209.10 | 3.80 |
| **7** | - | TBAC | 1699.70 | 31.07 |
| **8** | - | [PPN]Cl | 1247.74 | 22.80 |
| **9** | - | DMAP | 3174.01 | 58.01 |
| **10** | - | MeIm | 2468.93 | 45.19 |

Reactions performed in MeOH (5.00 mL), PO (2.01 mL) and $CS_2$ (1.86 mL), mmol complex = co-catalyst = 30.00 mmol, ratio of complex:$CS_2$ = 1:1000:1000, temperature = 24 °C, time = 24 hours

The chemical shift for the S$\underline{H}$ is not the same in all spectra (see appendix section, **Pages 168 - 171**). Additional signals are identified; however, they are not as intense as the major product signals. These are observed as a doublet between 1.39 ppm and 1.41 ppm, a multiplet between 3.73 ppm and 3.81 ppm, another multiplet is observed between 3.55 ppm and 3.65 ppm. The presence of these signals suggests the formation of isomers of the methoxylated cyclic products (**Figure 4.8**) produced to due to sulphur oxygen scrambling. However, the nature of the product as a result of the presence of the additional signals could not be conclusively determined, even with the use of HR-MS.

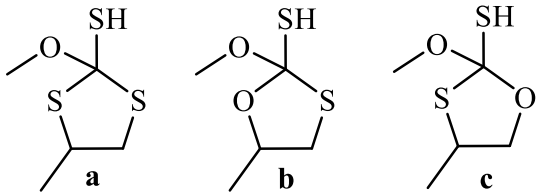
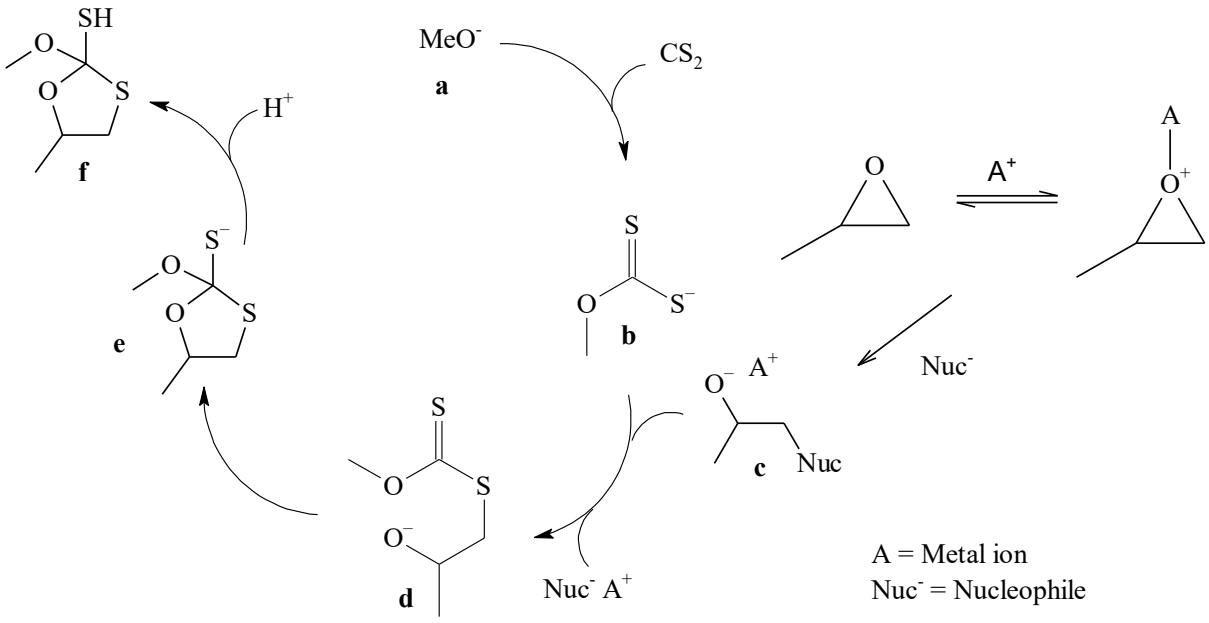



**Figure 4.8** *Methoxylated species of 4-methyl-1,3-dithiolane-2-thione (**a**), 5-methyl-1,3-dithiolane-2-thione (**b**) and 4-methyl-1,3-oxathiolan-2-one (**c**)*




**Scheme 4.4** *Proposed mechanism for the formation of the methanol adducts of-methyl-1,3-oxathiolane-2-thione, 4-methyl-1,3-dithiolane-2-thione and 5-methyl-1,3-oxathiolan-2-one* [24]

The formation of the methoxylated cyclic products is proposed in **Scheme 4.4** and is adapted from literature. It begins with the deprotonation of the mildly acidic MeOH proton to afford the methoxide ion (**a**). The methoxide ion reacts with $CS_2$ to yield (**b**). Upon activation and ring opening of PO, an alkoxide intermediate stabilized by a metal ion (**c**) is formed. Nucleophilic attack by (**b**) on the alkoxide intermediate (**c**) yields (**d**) which undergoes intramolecular ring closing to yield (**e**). Instead of the elimination of the methoxide to yield either one of- or a mixture of 5-methyl-1,3-oxathiolane-2-thione, 4-methyl-1,3-dithiolane-2-thione and 5-methyl-1,3-oxathiolan-2-one, the S- anions of (**e**) is protonated to yield (**f**). In the presence of a metal catalyst and or a co-catalyst, (**f**) is believed to undergo the scrambling reaction which can result in either one of the methanol adducts depicted in **Figure 4.8** (**a** - **c**). Based on the chemical shift positions of the signals in **Figure 4.6**, the major product is speculated to be the methanol adduct of 4-methyl-1,3-dithiolane-2-thione (cyclic product (**a**) **Figure 4.7**)). This speculation is supported by how close the two C$\underline{H_2}$ proton signals are to each other and it is corroborated by the up-field chemical shift position of the C$\underline{H}$ proton, which is bonded to the carbon atom with the methyl group is bonded to [24], [25].

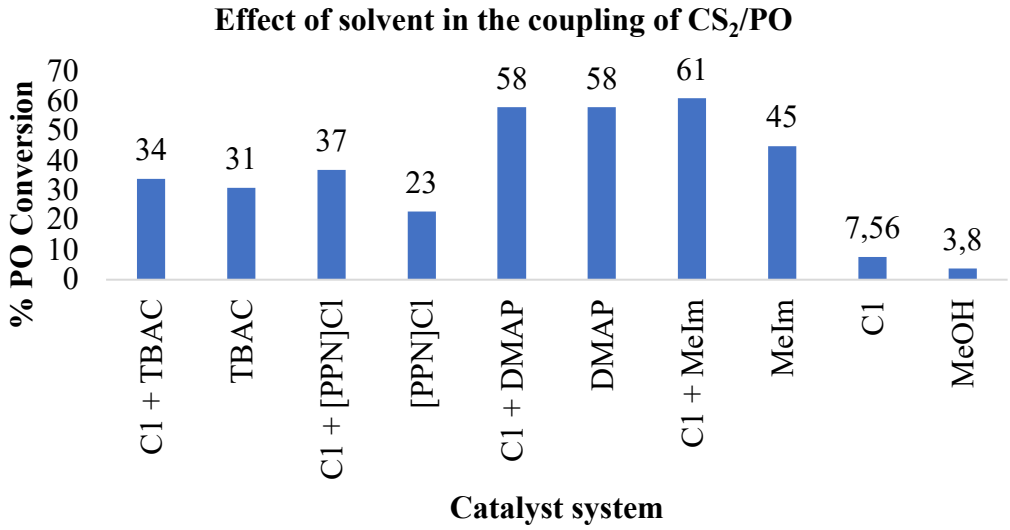



**Figure 4.9** *Solvent effect on the conversion rate in the coupling of carbon disulphide and propylene oxide*

Although the nature of the product obtained in the presence of MeOH is different to the mixture of products obtained in the reactions carried out in the absence of MeOH, the addition of MeOH showed a remarkable improvement in conversion rate. MeOH on its own was found to catalyse the coupling of PO and $CS_2$ to yield the methoxylated species of 4-methyl-1,3-oxathiolane-2-thione, with a conversion rate of up to 3.80 % at room temperature over 24 hours (Entry **6**, **Table 4.2**). This was found to be the lowest conversion rate for the reactions performed in MeOH. The conversion rate was seen to almost double from just MeOH (Entry **6**, **Table 4.2**) to when **C1** was used (Entry **2**, **Table 4.2**), with a conversion rate of up to 10.13 % achieved. This is low compared to when **C1** was paired with the co-catalysts. % Conversion of 34 %, 37 %, 58 % and 61 % were achieved when a catalyst system of **C1** was paired with TBAC, [PPN]Cl, DMAP and MeIm as co-catalysts, respectively (Entries **3** – **6**, **Table 4.2**). In comparing the conversion observed (**Figure 4.8**) when the catalyst system of **C1** + co-catalyst was used to when the co-catalysts on their own were used it was found that improved activity by a small margin for TBAC was observed. The difference was found to be 3 %. For DMAP, no difference was observed as DMAP on its own resulted in the exact same conversion rate as when DMAP was paired with **C1**. Improvements of 16 % and 14 % were observed from co-catalysts on their own to **C1** + co-catalysts for MeIm and [PPN]Cl, respectively. For the activity of the co-catalysts on their own, [PPN]Cl was found to be poorest performing co-catalyst.

### 4.2.3 Effect of reaction time in the coupling of carbon disulphide and propylene oxide in the presence of C1 and co-catalysts with MeOH

Upon observing that [PPN]Cl results in the least activity for the coupling of PO and $CS_2$ in the presence of MeOH and in the absence of co-catalyst, [PPN]Cl was used as a co-catalyst to investigate the conversion rate and the nature of the coupling reaction products as a function of time. These reactions were carried out in order to investigate if the cyclic products reported in **4.2.1** are formed at a certain point in time and as the reaction continues, they undergo some form of transformation to yield the methanol adducts of 5-methyl-1,3-oxathiolane-2-thione, 4-methyl-1,3-dithiolane-2-thione and 5-methyl-1,3-oxathiolan-2-one in the presence of MeOH. A method similar to the one described in **4.2.2** was employed for the time study reactions. To a stirring solution of **C1**, PO, $CS_2$ and [PPN]Cl, MeOH was added. The time study was carried out over a period of 12 hours, with the reactions stopped in 2hour intervals. After each 2hour interval, the respective reactions were stopped, and all volatiles were removed under vacuum. After work-up, $^1$H NMR spectra of the yellow oil-like products were obtained in $CDCl_3$.

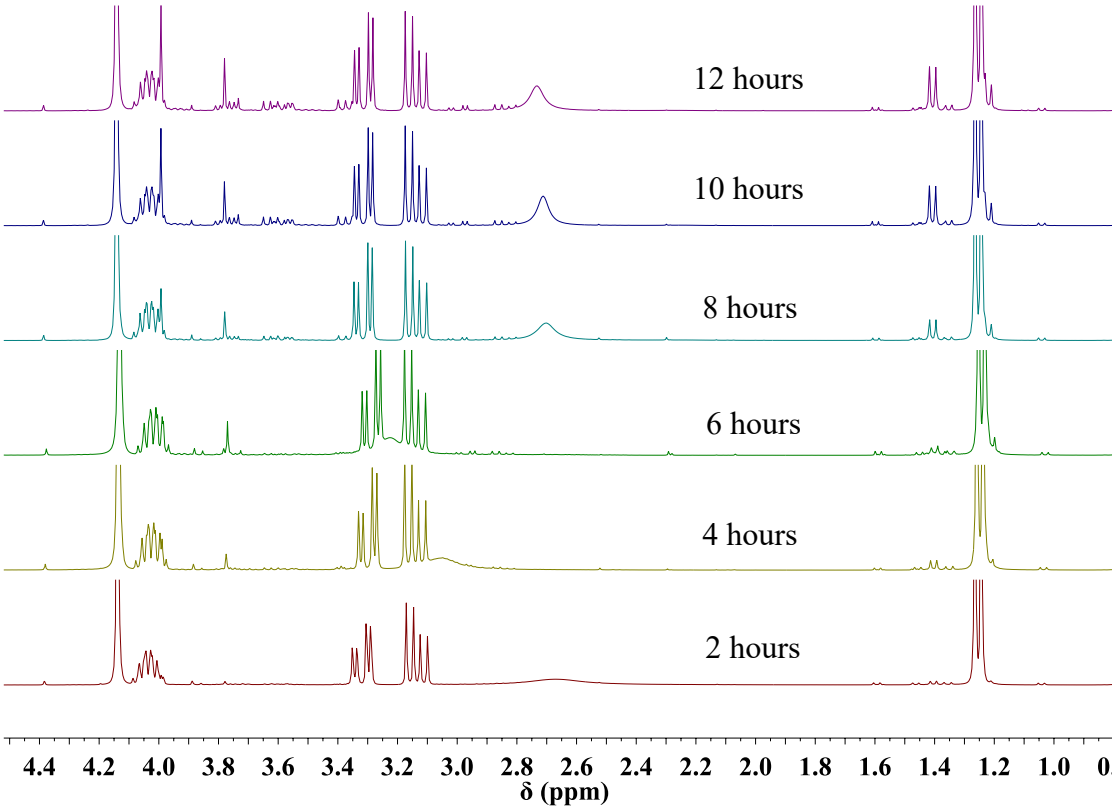



**Figure 4.10** *Stacked $^1$H NMR spectra obtained for the yellow oil-like products obtained in the time study ($CDCl_3$, 300 K)*

In the $^{1}$H NMR spectra obtained for the time study reaction products, signals corresponding to the methanol adduct of cyclic product (**a**) (**Figure 4.10**), was observed. Additional signals described suspected to be isomers of (**a**) produced due to oxygen/sulphur scrambling also gradually start to appear. The intensity of the additional signals is seen to increase with an increase in reaction time. This observation suggests that beyond 6 hours, the selectivity for the formation of the cyclic product (**a**) (**Figure 4.8**) is impeded. This observation is illustrated in the stacked $^{1}$H NMR spectra (**Figure 4.10**) for the coupling products obtained in time intervals of 2 hours, over a period of 12 hours. The time study revealed that the conversion rate is dependent on reaction time. The conversion rate went up from 2.4 % to 37 %, from 2 hours to 12 hours (Entries **1** & **6**, **Table 4.3**). This time dependence on conversion rate is in-line with literature reports [22].

**Table 4.3** *Effect of reaction time in the coupling of $CS_2$ and PO reaction data*

| Entry | Catalyst | Co-catalyst | Time (Hours) | Mass cyclic product (mg) | % PO conversion |
|---|---|---|---|---|---|
| **1** | **C1** | [PPN]Cl | 2 | 98.5 | 1.80 |
| **2** | **C1** | [PPN]Cl | 4 | 248 | 4.99 |
| **3** | **C1** | [PPN]Cl | 6 | 378.8 | 6.93 |
| **4** | **C1** | [PPN]Cl | 8 | 646.70 | 11.80 |
| **5** | **C1** | [PPN]Cl | 10 | 1305 | 23.86 |
| **6** | **C1** | [PPN]Cl | 12 | 1491 | 27.26 |

Time study reactions performed in MeOH (5.00 mL), PO (2.01 mL) and $CS_2$ (1.86 mL), mmol complex = co-catalyst = 30.00 mmol, ratio of complex:$CS_2$ = 1:1000:1000, temperature = 24 °C

### 4.2.4 Effect of MeOH quantity on the nature of the products formed in the coupling of $CS_2$ and PO

After observing that the presence of MeOH results in the formation of the methanol adduct, experiments were performed to determine if the amount of MeOH has an influence on the methoxylated cyclic product formation. This was done in order to investigate if the amount of MeOH would favour the formation of the methanol adduct or if the cyclic products observed in the neat reactions would also be produced. Two reactions were performed, an experiment with [PPN]Cl only in MeOH (0.50 mL) and an experiment using **C1** with [PPN]Cl in MeOH (0.5mL). These reactions were stirred over a period of 6 hours after which and all volatiles

were removed under vacuum. After work-up, $^1$H NMR spectra of the yellow oil-like products were obtained in $CDCl_3$.

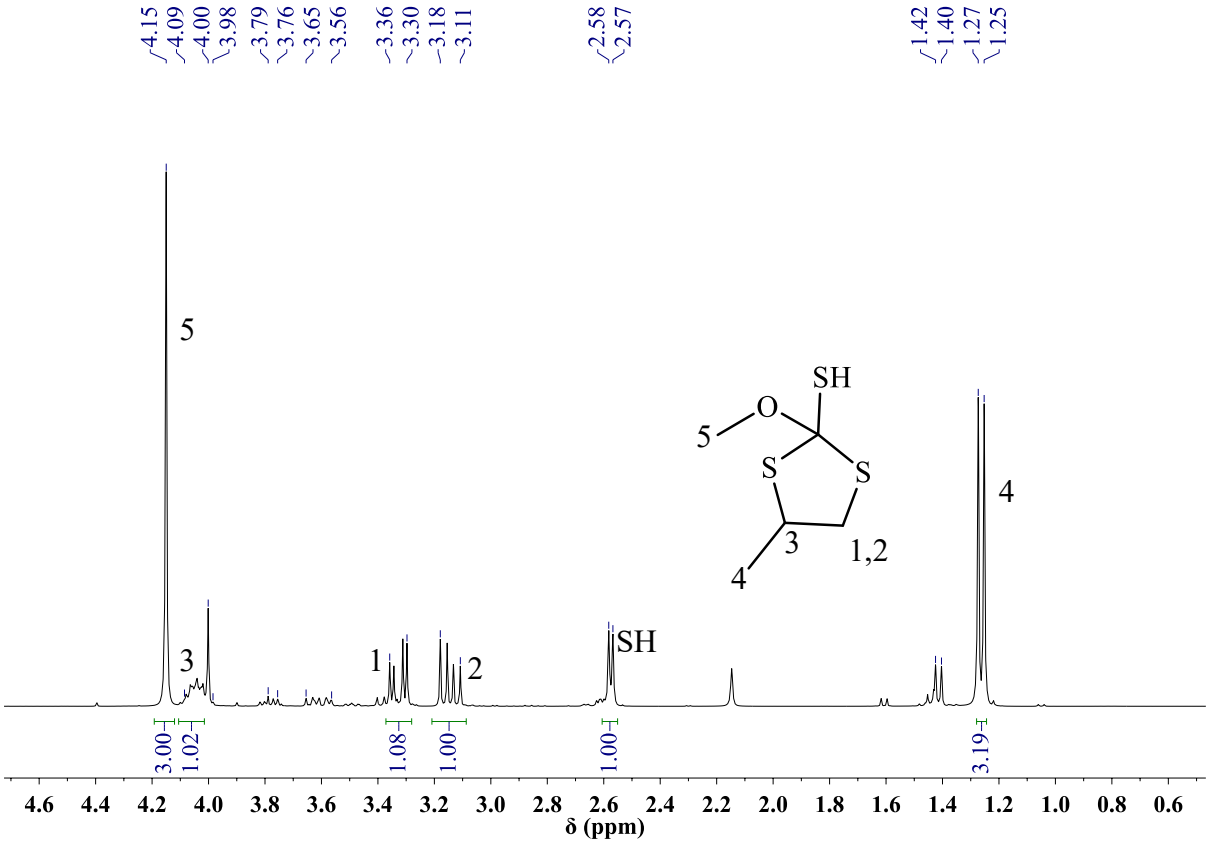



**Figure 4.11** *$^1$H-NMR spectrum for the reaction residue obtained in using C1 and [PPN]Cl in $CS_2/CO_2$ coupling using 0.5 mL MeOH for 6 hours (Entry **1**, **Table 4.4**) ($CDCl_3$, 300 K)*

**Table 4.4** *Effect of solvent volume in the coupling of $CS_2$ and PO reaction data*

| Entry | Catalyst | Co-catalyst | Mass cyclic product (mg) | % PO conversion |
|---|---|---|---|---|
| **1** | **C1** | [PPN]Cl | 337 | 6.93 |
| **2** | **-** | [PPN]Cl | 998.9 | 18.26 |

Reactions performed in MeOH (0.50 mL), PO (2.01 mL) and $CS_2$ (1.86 mL), mmol complex = co-catalyst = 30.00 mmol, ratio of complex:$CS_2$ = 1:1000:1000, temperature = 24 °C, time = 6 hours

In the $^1$H NMR spectrum (**Figure 4.11**) obtained for the yellow oil-like product signals corresponding to the methanol adduct of cyclic product (**a**) (**Figure 4.8**) are identified as the major product. The additional signals which are observed after 8 hours in the time study are also identified. Under the same reaction conditions, in the presence of MeOH (5.00 mL), the additional signals seen in the $^1$H NMR spectrum (**Figure 4.11**) of the product obtained when

the reaction was carried out in the presence of 0.50 mL of MeOH are not apparent. This is attributed to the difference in reaction mixture concentration.

Conversion rates of 6.16 % and 6.93 % were achieved for the reactions carried out in the presence of MeOH (0.50 mL) and MeOH (5.00 mL), respectively. From this finding, it can be seen that the activity of the catalyst system pair of **C1**/[PPN]Cl is slightly affected by MeOH volume in the coupling of $CS_2$/PO.

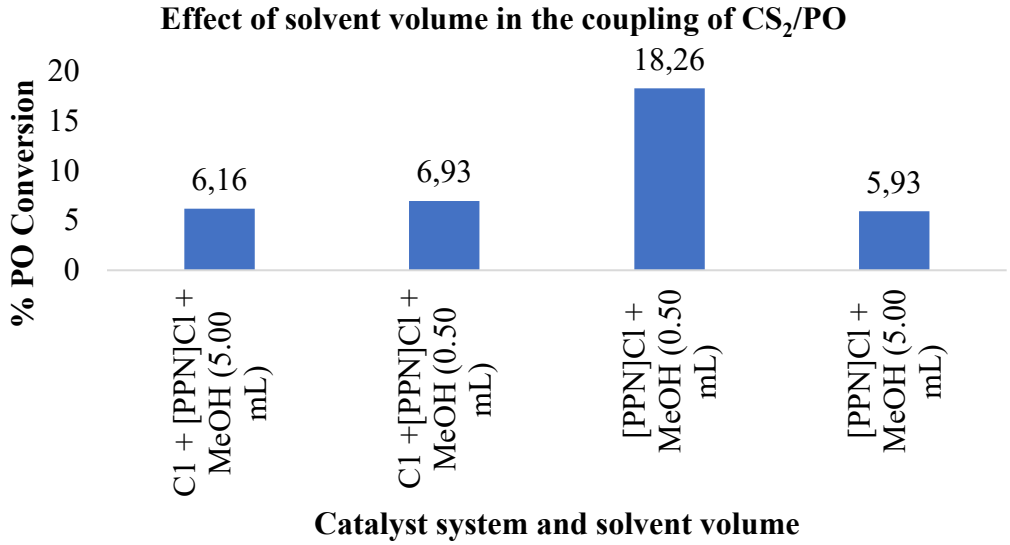



**Figure 4.12** *Effect of solvent volume on conversion rate in the coupling of carbon disulphide and propylene oxide*

However, the difference in conversion rates between the two is by a small margin, which can be considered insignificant. In the presence of [PPN]Cl only, conversion rates of 18.26 % and 5.93 % were achieved for the reactions carried out in MeOH (0.50 mL) and. (5.00 mL), respectively. This shows that the absence of **C1** results in a significant difference in the conversion rates for $CS_2$/PO coupling reactions carried out in the presence of 0.50 mL and 5.00 mL. This implies that in the absence of **C1**, the coupling reaction mixture concentration affects the conversion rate. A graphic comparison of the conversion rates as a function of solvent volume are illustrated in **Figure 4.12**. The conversion rates for the reactions carried out in the presence of MeOH (0.50 mL) were compared to the conversion rates for the reactions carried out in the presence of MeOH (5.00 mL). It was found that reducing the volume of solvent,

which results in a more concentrated reaction mixture does not affect the conversion rate over 6 hours.

### 4.2.5 Effect of catalyst in the coupling of carbon disulphide and propylene oxide

All 8 catalysts were screened for the coupling of $CS_2$ and PO in the presence of MeOH (5.00 mL). Upon observing that reducing the volume of MeOH lowers selectivity for the formation of the methanol adduct of 4-methyl-1,3-dithiolane-2-thione, all 8 catalysts were screened in the presence of MeOH (5.00 mL). The reactions were carried out following a procedure similar to that outlined in **4.2.2** whereby to a stirring solution of the respective catalyst, PO, $CS_2$ and [PPN]Cl, MeOH (5.00 mL) was added. The reaction mixtures were stirred for 12 hours at room temperature, after which the reactions were stopped. All volatiles were removed under vacuum and $^1$H NMR spectra of the resulting crude residue were obtained in $CDCl_3$.

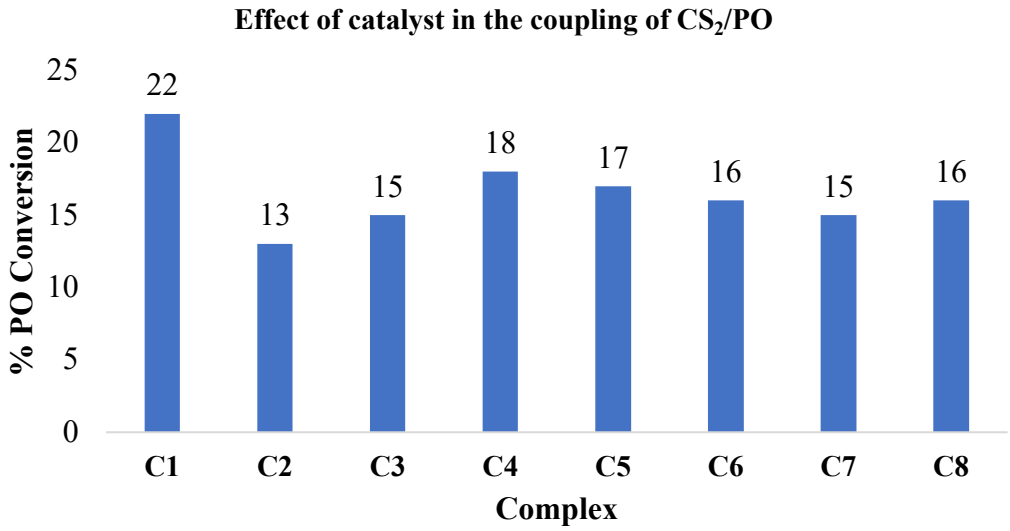



**Figure 4.13** *Effect of catalyst in the coupling of carbon disulphide and propylene oxide*

In the $^1$H-NMR spectra for the products obtained upon work-up, signals corresponding to the methanol adduct, cyclic product (**a**) (**Figure 4.8**) was identified as the major product. The presence of signals suggesting the formation of a cyclic isomers as minor products was also observed. In terms of conversion rate, **C1** + [PPN]Cl (Entry **1**, **Table 4.5**) showed the highest activity and resulted in a conversion rate of 30.9 %. **C2** + [PPN]Cl (Entry **2**, **Table 4.5**) showed the least activity and resulted in a conversion rate of 17.6 %. In fact, this was found to be lower than the conversion rate that was achieved when [PPN]Cl was screened under the same reaction conditions, however, in the absence of a catalyst. This observation suggests that **C2** hampers

the activity of [PPN]Cl for the coupling of $CS_2$ and PO in the presence of MeOH (5.00 mL) at room temperature, over 12 hours. **C2** and **C3** have been shown to readily decompose to **L2** and **L3**, respectively, in the presence of MeOH. This could explain why the two catalysts resulted in the lowest conversion rates.

**Table 4.5** *Effect of catalyst in the coupling of $CS_2$ and PO reaction data*

| Entry | Catalyst | Co-catalyst | Mass cyclic product (mg) | % PO conversion |
|---|---|---|---|---|
| **1** | **C1** | [PPN]Cl | 1223.8 | 22 |
| **2** | **C2** | [PPN]Cl | 687.7 | 13 |
| **3** | **C3** | [PPN]Cl | 812.7 | 15 |
| **4** | **C4** | [PPN]Cl | 979.7 | 18 |
| **5** | **C5** | [PPN]Cl | 908.6 | 17 |
| **6** | **C6** | [PPN]Cl | 851.3 | 16 |
| **7** | **C7** | [PPN]Cl | 835.8 | 15 |
| **8** | **C8** | [PPN]Cl | 857.4 | 16 |

Reactions performed in MeOH (0.50 mL), PO (2.01 mL) and $CS_2$ (1.86 mL), mmol complex = co-catalyst = 30.00 mmol, ratio of complex:$CS_2$ = 1:1000:1000, temperature = 24 °C, time = 12 hours

No trend between ligand architecture and conversion rate could be established. This is attributed to the varying degree of stability from **C1** – **C8**. That is, the anticipated effect of sterics is masked by how the stability of the 8 complexes differs. Although a trend between ligand architecture and conversion rate could not be established, an interesting observation is made with the Co(II) complexes, **C5** – **C8**. A difference of 1.90 % in conversion rate from the highest to the lowest is observed. This suggests that the activity of the cobalt complexes is almost identical, which begs the question; do these metal complexes decompose instantaneously to their respective neutral ligands and a similar species of cobalt. The species of cobalt the 4 metal complexes are suspected to decompose to what could be the agent that induces activity for this coupling reaction, which then explains why there isn't a stark difference in the conversion rates.

### 4.2.6 Effect of neutral ligand and cobalt chloride as catalyst systems in the coupling of carbon disulphide and propylene oxide

To investigate the speculation made in **4.2.5**, that the cobalt complexes (**C5** – **C8)** decompose to their respective ligands and a similar species of cobalt, a series of experiments were carried out. **L1** and **L3** were selected as the representative ligands as their steric demands vary considerably and this would allow for a reasonable study. These experiments were carried out in order to investigate if using equimolar quantities of the respective neutral ligand and $CoCl_2$ with [PPN]Cl in the coupling of $CS_2$ and PO, in the presence of MeOH would yield similar results to those obtained in **4.2.5**. These experiments were carried out by adding MeOH (5.00 mL) to a stirring solution of the respective ligand, $CoCl_2$, PO and $CS_2$, [PPN]Cl. The reaction mixtures were stirred for a period of 12 hours at room temperature. After 12 hours, the reactions were stopped, and all volatiles were removed under vacuum., however no significant residue for analysis was obtained indicating that these experiments did not yield any coupling products.

From the above observation, it can be concluded that $CoCl_2$ paired with either **L1** or **L3**, in the presence of [PPN]Cl are not active for the coupling of $CS_2$ and. PO over 12 hours. This was seen as odd as a combination of [PPN]Cl and MeOH, as well as MeOH own its own were observed to be active for this coupling reaction. In fact, conversion rates of 5.93 % and 3.8 % were achieved, respectively. This observation suggests that either $CoCl_2$, the neutral ligands or a combination of both retard the activity induced by [PPN]Cl and MeOH in this coupling reaction.

This observation does very little to shed light on the speculation made in **4.2.6** that the cobalt complexes (**C5** – **C8**) decompose to their respective ligands and a similar species of cobalt, which could explain why the conversion rates achieved when **C5** – **C8** + [PPN]C1 (Entries **5** – **8**, **Table 4.5**) were used as the catalyst systems differ by a small to negligible margin. Not all is in vain as another speculation can be made based on the results from this investigation. That is; **C5** – **C8** + [PPN]Cl catalyse the coupling of $CS_2$ and PO, however, due to their poor stability in solution, the metal complexes decompose to their respective neutral ligands and $CoCl_2$. As the metal complexes further decompose, the increased molar quantities of neutral ligands and $CoCl_2$ retard further catalysis, thereby capping the conversion rate. At this point, this is merely speculation and extensive studies would need to be carried out to confirm why this is so.

### 4.2.7 Effect of catalyst in the coupling of carbon dioxide and propylene oxide

After observing that bis-(pyrrole-aldimine) Zn(II) and Co(II) complexes, **C1** – **C8** show activity for the coupling of $CS_2$ and PO. Their catalytic activity was evaluated in the coupling of $CO_2$ and PO. The experiments were carried out following a procedure adapted from literature [26]. PO, the respective catalyst and [PPN]Cl were added to carrousel tubes. All 8 metal complexes and [PPN]Cl dissolved in PO. The reaction mixtures were stirred while the systems were flushed with a stream of $CO_2$ gas. After 15 minutes, the gas flow was stopped. The reactions were then allowed to stir for the specified period of time before stopping them. Once this was done, the reactions were worked up. The products obtained were quantified by mass difference and analysed by $^1$H NMR spectroscopy in $CDCl_3$.

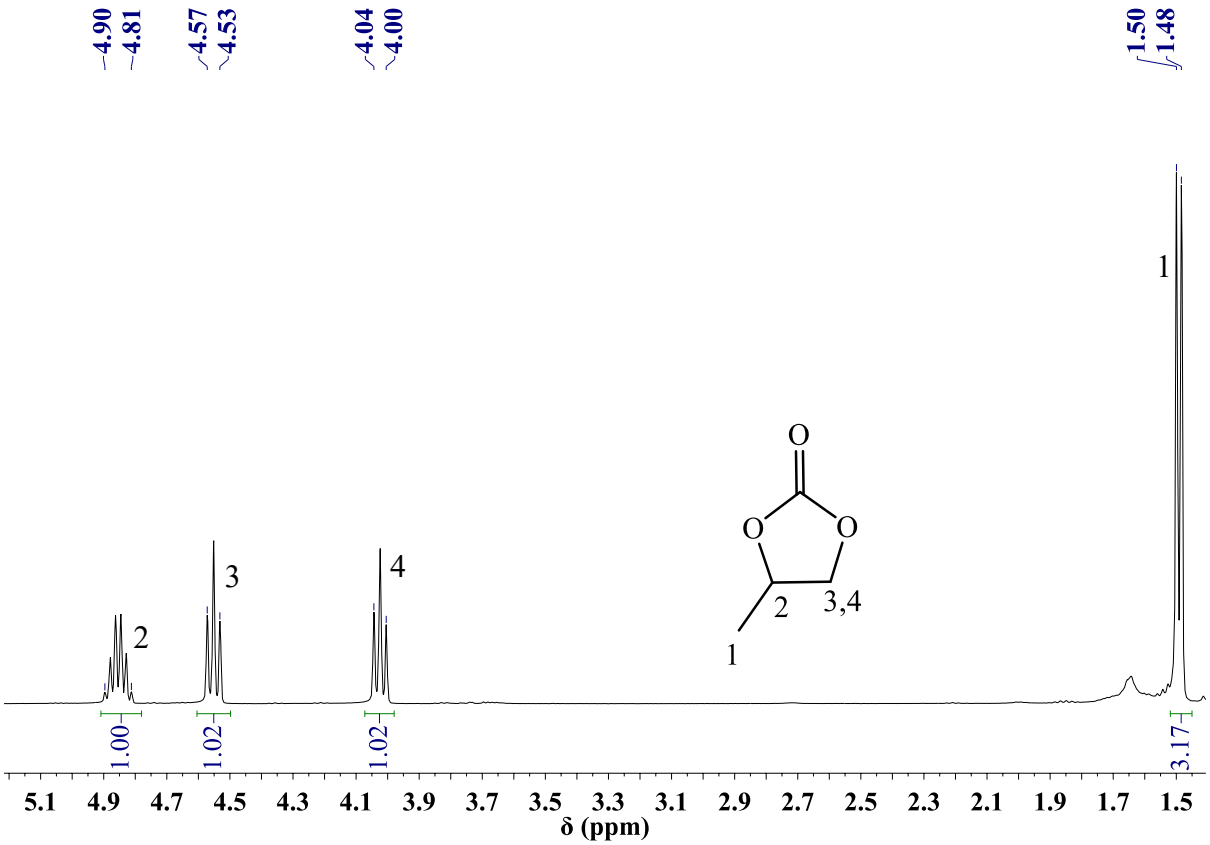



**Figure 4.14** *$^1$H NMR spectrum for the reaction residue obtained in using **C5** and [PPN]Cl in carbon dioxide and propylene oxide coupling for 12 hours (Entry **6**, **Table 4.6**) ($CDCl_3$, 300 K)*

In the $^1$H NMR spectrum (**Figure 4.14**) obtained for the residue in the reaction carried out in the presence of [PPN]Cl in the absence of a catalyst (Entry **28**, **Table 4.6**), signals corresponding to those expected for cPC are observed. These appear at 1.48 – 1.50 ppm as a

doublet, 4.00 – 4.04 ppm as a triplet, 4.53 – 4.57 ppm as a triplet and 4.82 ppm – 4.49 ppm as a sextet. These are assigned to the C$\underline{H}_3$ group, C$\underline{H}_2$, C$\underline{H}_2$ and C$\underline{H}$ protons, respectively, as shown in **Figure 4.14**. No additional signals corresponding to the co-polymer, PPC are observed. This suggests that all catalysts are highly selective for the formation of cPC at room temperature and over a period of 12 hours. This observation is made in all 9 $^1$H NMR spectra obtained for entries **1** – **9** (**Table 4.6**).

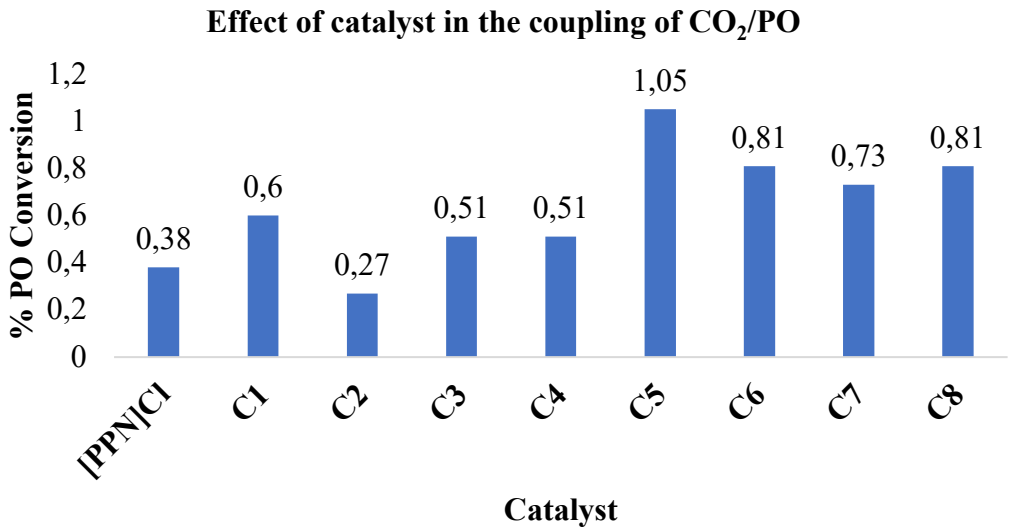



**Figure 4.15** *Effect of catalyst in the coupling of carbon dioxide and propylene oxide*

Although the 8 catalysts favoured the formation of exclusively cPC, low yields were obtained. The catalysts system pair of **C5** and [PPN]Cl resulted in the highest conversion of PO to cPC at 1.05 % (Entry **33**, **Table 4.6**). The lowest conversion was achieved with the catalyst system pair of **C2** and [PPN]Cl at 0.27 % (Entry **3**, **Table 4.6**). This was found to be lower than that achieved when [PPN]Cl was used as the catalysts system in the absence of a catalyst. Generally, the Co complexes (Entries **6** – **9**, **Table 4.6**) performed better than the Zn complexes (Entries **3** – **5**, **Table 4.6**), however, by a very small margin. A graphic illustration of the conversion rates achieved with each catalyst is shown (**Figure 4.15**).

**C1** and **C5** bear no substituents on the phenyl rings and these complexes were observed to perform better than the other Zn and Co complexes when in the presence of [PPN]Cl as a co-catalyst, respectively. This observation is consistent with the observation made by Shi *et al.* when then group evaluated the catalytic activity of Cu(II), Zn(II), and Co(II) salen-type complexes derived from binaphthyldiamino Schiff bases in the coupling of $CO_2$ and PO. The

group reported that the introduction of substituents on the phenyl rings of the Cu(II), Zn(II), and Co(II) salen-type complexes hampered the conversion of PO to cPC. Contrary to the observation in this study, the best performing catalyst was the unsubstituted Zn(II) complex in the presence of trimethylamine as a co-catalyst [27].

**Table 4.6** *Effect of catalyst in the coupling of PO/$CO_2$ reaction data*

| Entry | Catalyst | Co-catalyst | Mass cyclic product (mg) | % PO conversion |
|---|---|---|---|---|
| **1** | – | [PPN]Cl | 11.70 | 0.38 |
| **2** | **C1** | [PPN]Cl | 18.30 | 0.60 |
| **3** | **C2** | [PPN]Cl | 8.13 | 0.27 |
| **4** | **C3** | [PPN]Cl | 15.6 | 0.51 |
| **5** | **C4** | [PPN]Cl | 15.6 | 0.51 |
| **6** | **C5** | [PPN]Cl | 32.2 | 1.05 |
| **7** | **C6** | [PPN]Cl | 24.8 | 0.81 |
| **8** | **C7** | [PPN]Cl | 22.45 | 0.73 |
| **9** | **C8** | [PPN]Cl | 24.8 | 0.81 |

Reactions performed in PO (2.01 mL), mmol complex = co-catalyst = 30.00 mmol, ratio of mmol complex:PO = 1:1000, atmospheric pressure of $CO_2$, temperature = 24 °C, time = 12 hours

### 4.2.8 Effect of reaction time in the coupling of $CO_2$/PO

In light of the results in **4.2.7**, the catalyst system pair of **C5**/[PPN]Cl was selected as the representative catalyst system for the study on effect of increasing the reaction time to 24 hours on conversion of PO to cPC, as it resulted in the highest conversion of PO to cPC over a period of 12 hours. For comparison purposes, [PPN]Cl was screened on its own under the same reaction conditions. These reactions were carried out following a similar procedure to that highlighted in **4.2.7**, however, the reaction time was increased to 24 hours. Upon work up, the products obtained were quantified by mass difference and analysed by $^1$H NMR spectroscopy in $CDCl_3$.

In the $^1$H NMR spectrum (**Figure 4.16**) of the product obtained for the catalysts system pair of **C5**/[PPN]Cl (Entry **2**, **Table 4.7**), signals corresponding the presence of cPC are observed. As

with spectra obtained for entries **1** – **9** (**Table 4.6**), no additional signals that would suggest the formation of PPC as a side-product are observed.

**Table 4.7** *Effect of increasing reaction time in the coupling of carbon dioxide and propylene oxide reaction data*

| Entry | Catalyst | Co-catalyst | Mass cyclic product (mg) | % PO conversion |
|---|---|---|---|---|
| **1** | – | [PPN]Cl | 39.70 | 1.30 |
| **2** | **C5** | [PPN]Cl | 55.40 | 1.81 |

Reactions performed in PO (2.01 mL), mmol complex = co-catalyst = 30.00 mmol, ratio of mmol complex:PO = 1:1000, atmospheric pressure of $CO_2$, temperature = 24 °C, time = 24 hours

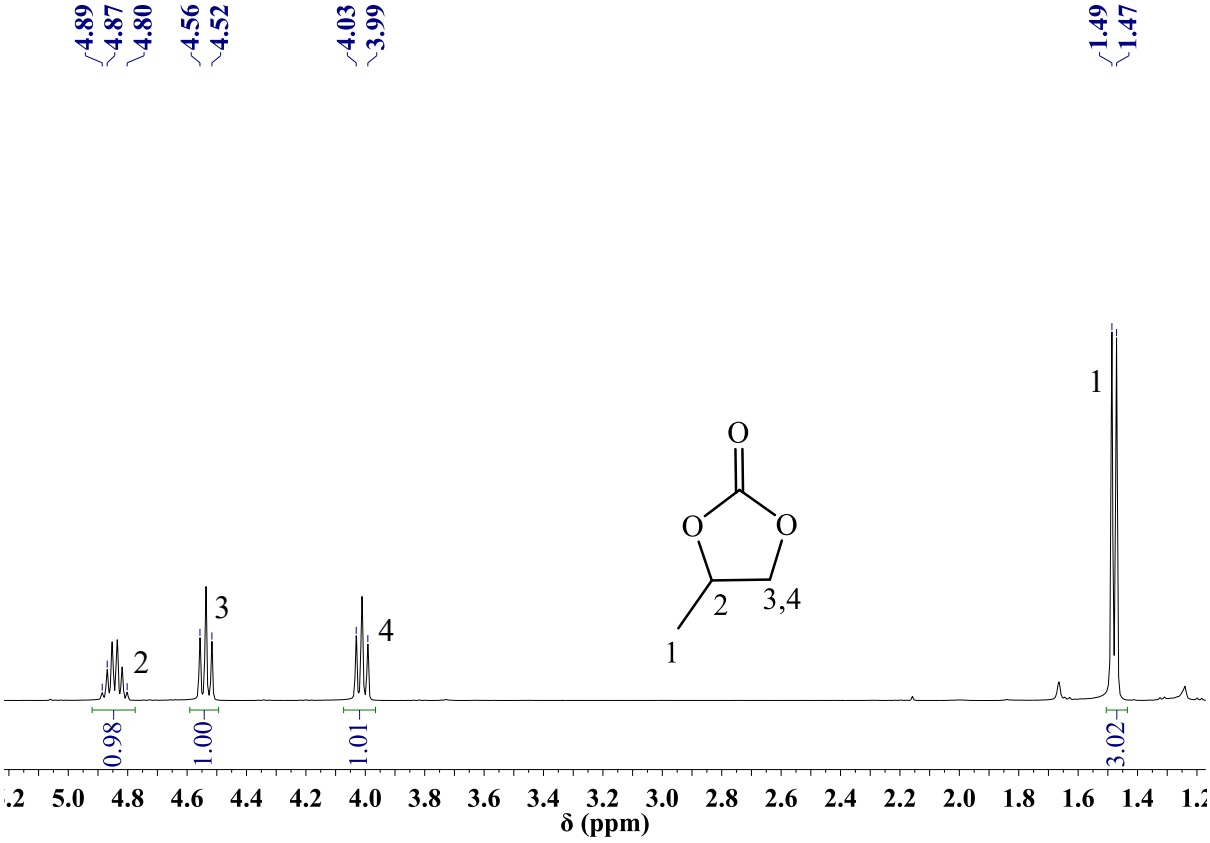



**Figure 4.16** *$^1$H NMR spectrum for the reaction residue obtained in using **C5** and [PPN]Cl in PO/$CO_2$ coupling for 12 hours (Entry **2**, **Table 4.6**) ($CDCl_3$, 300 K)*

Increasing the reaction time from 12 hours to 24 hours resulted in a 0.92 % increase in conversion rate for [PPN]Cl on its own and an increase of 0.76 % for the catalyst system pair of **C5**/[PPN]Cl. Even though an improvement in yield resulted from increasing the reaction time in the coupling of PO/$CO_2$ at atmospheric pressure of $CO_2$ and at room temperature, it is

insignificant. There are several reports highlighting the significance of reaction time in the conversion of PO to cPC in the coupling of $CO_2$ and PO. The conversion rate has been shown to increase significantly with an increase in reaction time [19], [28], [29]. This contradicts the observation made in this study, as increasing the reaction time from 12 hours to 24 hours had an insignificant effect in PO conversion.

### 4.2.9 Effect of solvent in the coupling of carbon dioxide and propylene oxide

A study on solvent effect in the coupling of PO/$CO_2$ was conducted at ambient pressure of $CO_2$, at a temperature of 24 °C and over a period of 24 hours. Solvents of varying polarities were selected for a comprehensive study. These are hexane, which is non-polar, DCM, which is borderline polar aprotic, acetonitrile, which is polar aprotic and MeOH which is polar protic. The catalyst system pair of **C5**/[PPN]Cl was selected as the representative catalyst system. In order to validate that the activity achieved in this study is not induced by the co-catalyst on its own, these experiments were also conducted in the presence of [PPN]Cl in the absence of a catalyst, under the same reaction conditions. Upon work up, the products obtained were analysed by $^1$H NMR spectroscopy in $CDCl_3$.

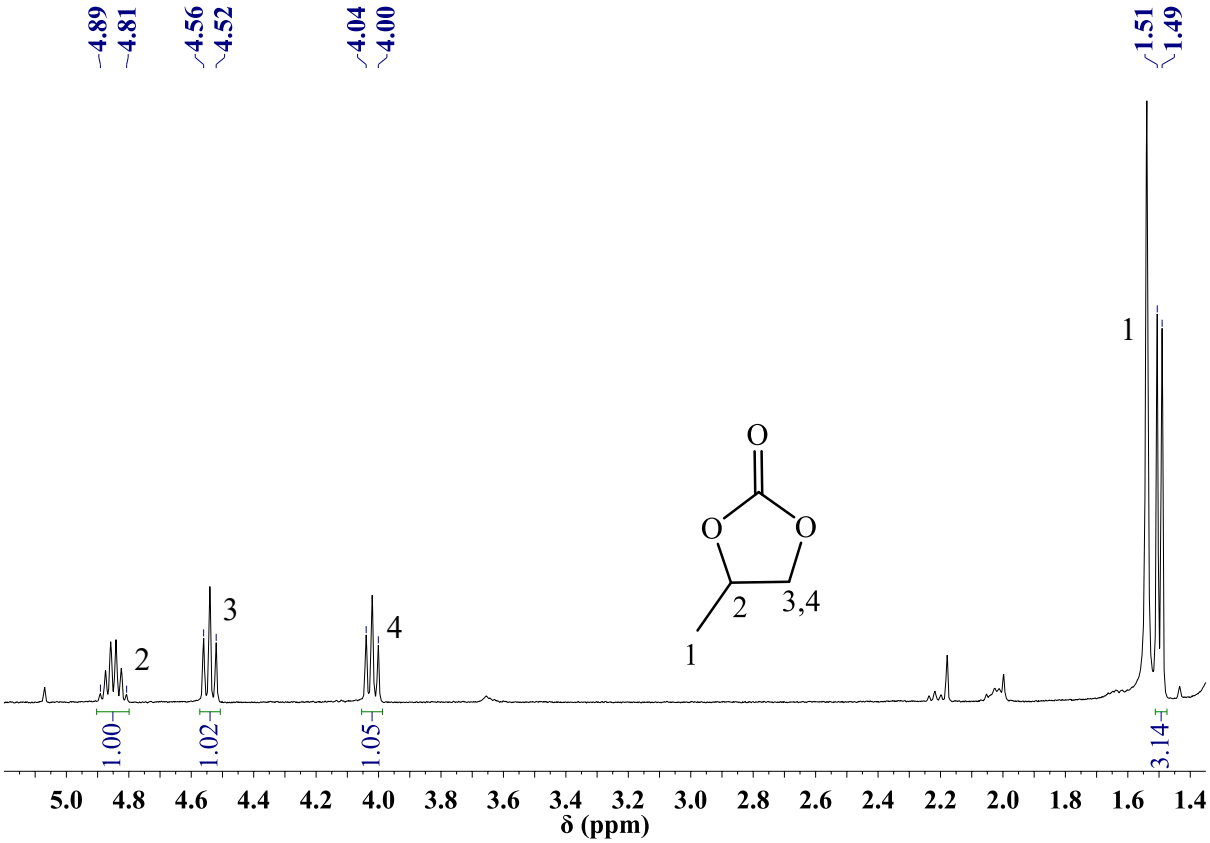



**Figure 4.17** *$^1$H NMR spectrum for the reaction residue obtained in using **C5** and [PPN]Cl in PO/$CO_2$ coupling for 24 hours (Entry **3**, **Table 4.8**) ($CDCl_3$, 300 K)*

In the $^{1}$H NMR spectra obtained for entries **2** – **8** (**Table 4.7**), signals corresponding to the presence of cPC are observed. These are assigned in the spectrum (**Figure 4.17**) obtained for the residue in which the reaction was carried out in the presence of **C5**/[PPN]Cl as the catalyst system and acetonitrile as the solvent. No additional signals that would suggest the formation of PPC as a side-product are observed. This observation suggests that the presence of hexane, DCM, acetonitrile and MeOH does not affect the selectivity for cPC as cPC is the only product obtained.

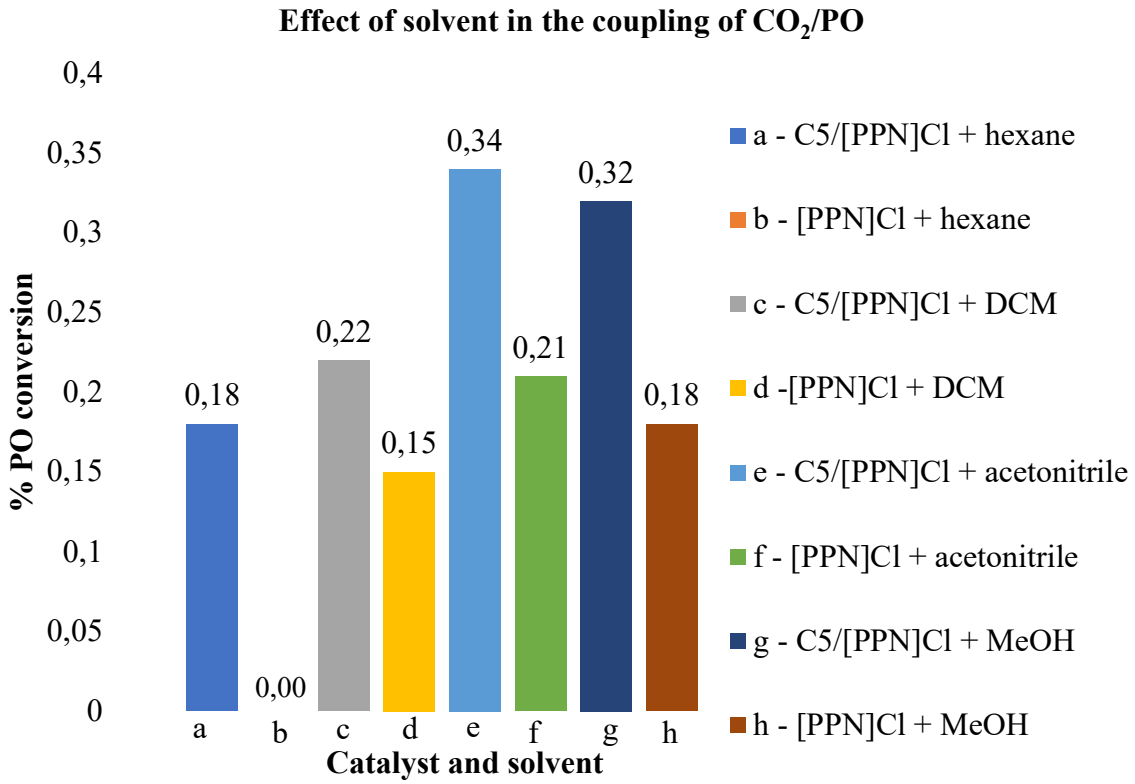



**Figure 4.18** *Effect of solvent in the coupling of carbon dioxide and propylene oxide*

In terms of conversion, [PPN]Cl on its own showed no activity in the coupling of PO and $CO_2$ at ambient $CO_2$ pressure, in the presence of hexane, at a temperature of 24 °C and over a period of 24 hours (Entry **4**, Table **4.8**). This is attributed to the poor solubility of [PPN]Cl in hexane. [PPN]Cl on its own (Entries **1** – **4**, **Table 4.8**) resulted in conversions lower than those achieved when it was paired with **C5**. This shows that activity and conversion of PO to cPC achieved in the presence of **C5**/[PPN]Cl as the catalyst system is not induced by the co-catalyst on its own. The highest conversion was achieved in acetonitrile with the catalyst system pair of **C5**/[PPN]Cl (Entry **3**, **Table 4.8**).

**Table 4.8** *Effect of solvent in the coupling of $CO_2$/PO reaction data*

| Entry | Catalyst | Co-catalyst | Solvent (2.00 mL) | Mass cyclic product (mg) | % PO conversion |
|---|---|---|---|---|---|
| **1** | **C5** | [PPN]Cl | Hexane | 5.4 | 0.18 |
| **2** | **C5** | [PPN]Cl | DCM | 6.8 | 0.22 |
| **3** | **C5** | [PPN]Cl | Acetonitrile | 10.3 | 0.34 |
| **4** | **C5** | [PPN]Cl | MeOH | 9.6 | 0.32 |
| **5** | - | [PPN]Cl | Hexane | - | - |
| **6** | - | [PPN]Cl | DCM | 4.5 | 0.15 |
| **7** | - | [PPN]Cl | Acetonitrile | 6.3 | 0.21 |
| **8** | - | [PPN]Cl | MeOH | 5.6 | 0.18 |

Reactions performed in PO (2.01 mL), mmol complex = co-catalyst = 30.00 mmol, ratio of mmol complex:PO = 1:1000, atmospheric pressure of $CO_2$, temperature = 24 °C, time = 24 hours

This was found to be 0.34 %. Although this was the highest conversion achieved in the solvent study, it was found to be lower than that achieved under the same reaction conditions, however, in the absence of solvent (Entry **2**, **Table 4.7**). As a matter of fact, the presence of hexane, DCM, acetonitrile and MeOH (Entries **1** – **4**, **Table 4.8**) resulted in conversions lower than those achieved when the same reaction conditions were applied neat (Entry **3**, **Table 4.8**). **Figure 4.18** shows a graphic illustration of the conversion rates achieved for the coupling of $CO_2$/PO in the presence of solvent.

### 4.2.10 Effect of $CO_2$ pressure in the coupling of carbon dioxide and propylene oxide

Upon observing that the presence of solvent (hexane, DCM, acetonitrile and MeOH) has a negative effect on the conversion rate in the coupling of $CO_2$/PO at ambient $CO_2$ pressure, in the presence of hexane, at a temperature of 24 °C and over a period of 24 hours. The activity of **C5**/[PPN]Cl was evaluated at $CO_2$ pressure of 25 bar, a temperature of 24 °C, under solventless conditions and over a period of 24 hours. A control reaction in which [PPN]Cl on its own was used as the catalyst system was carried out under the same reaction conditions for comparison. Upon work up, the residues obtained were analysed by $^1$H NMR spectroscopy in $CDCl_3$.

In the $^1$H NMR spectrum (**Figure 4.18**) obtained for the residue obtained for the reaction in which the catalyst system pair of **C5**/[PPN]Cl was used (Entry **1**, **Table 4.9**), signals

corresponding to the presence of PO are observed. These signals are also observed in the $^{1}$H NMR spectrum obtained for the residue that resulted from the reaction in which [PPN]Cl on its own was used as the catalyst (Entry **2**, **Table 2.9**). The assignment of these signals is made in the $^{1}$H NMR spectrum (**Figure 4.18**). No additional signals that would suggest the presence of PPC are observed. This observation suggests that increase the pressure of $CO_2$ to 25 bar does not affect the selectivity for cPC over PPC.

In terms of conversion, an increase of 0.26 % from ambient $CO_2$ pressure (Entry **2**, **Table 4.7**) to 25 bar of $CO_2$ (Entry **1**, **Table 4.9**) is observed. From this observation, it can be seen that increasing $CO_2$ pressure shows no significant change in the conversion rate in the presence of **C5**/[PPN]Cl as the catalyst, at room temperature and over a period of 24 hours. A 0.21 % increase in conversion rate from ambient $CO_2$ pressure (Entry **1**, **Table 4.7**) to 25 bar of $CO_2$ (Entry **2**, **Table 4.9**) is observed for when [PPN]Cl on its own is used as the catalyst at room temperature over 24 hours.

**Table 4.9** *Effect of $CO_2$ pressure in the coupling of $CO_2$/PO reaction data*

| Entry | Catalyst | Co-catalyst | Mass cyclic product (mg) | % PO conversion |
|---|---|---|---|---|
| **1** | **C5** | [PPN]Cl | 63.29 | 2.07 |
| **2** | - | [PPN]Cl | 46.34 | 1.51 |

Reactions performed in PO (2.01 mL), mmol complex = co-catalyst = 30.00 mmol, ratio of mmol complex:PO = 1:1000, 25 bar pressure of $CO_2$, temperature = 24 °C, time = 24 hours

This observation is in-line with an observation made by Aouissi *et al*. when the group utilized a gallosilicate zeolite catalysts in the coupling of $CO_2$ and PO. The group found that increasing the pressure of $CO_2$ results in an increase in the conversion of PO to cPC until the optimal pressure point is reached. After which, increasing the pressure starts to have a negative impact on the conversion of PO to cPC. This phenomenon is explained by the variance in $CO_2$ concentration in the reaction medium. That is, the coupling reaction vessel is a 2 phase system in which there is a bottom and top phase. The bottom phase is epoxide rich and the top phase is $CO_2$ rich. The coupling reaction occurs in the bottom phase as this is where the catalyst is present. Increasing $CO_2$ pressure up to the optimal pressure point increases the concentration of $CO_2$ in the bottom phase, which results in an increase in conversion of PO to cPC. However, increasing $CO_2$ pressure beyond the optimal pressure point shows a negative effect on the

conversion rate as this results in a decrease in epoxide concentration in the bottom phase due to $CO_2$ saturation [28]. Although conversion rate can be dependent of $CO_2$ pressure, it has been shown that the effect is by a small margin, as observed in this study.

## 4.3 CONCLUSION

The catalytic activity of bis-(pyrrole-aldiminato) Zn(II) and Co(II) complexes, **C1** – **C8** was evaluated in the coupling of $CS_2$ and PO as well as in the coupling of $CO_2$ and PO. In the coupling of $CS_2$ and PO, **C1**, which was selected as the representative catalyst for establishing the baseline reaction conditions was observed to be inactive for this coupling process over 24 hours at room temperature. The pairing of **C1** with 4 co-catalysts; TBAC, DMAP, [PPN]Cl and MeIm resulted in poor conversions of PO to a mixture of 3 cyclic products. These were identified as 4-methyl-1,3-dithiolane-2-thione, 5-methyl-1,3-oxathiolane-2-thione and 4-methyl-1,3-oxathiolane-2-thione using $^1$H NMR spectroscopy. The screening of C1 in the presence of the 4 co-catalysts and MeOH as a solvent resulted in an improvement in the conversion of PO. In these reactions, a new cyclic product which is speculated to be a methoxylated species of 4-methyl-1,3-dithiolane-2-thione as suggested by $^1$H NMR spectroscopy was obtained as the major product. A time study conducted using **C1**/[PPN]Cl, as the catalysts system and in the presence of MeOH at room temperature revealed that the conversion of PO to the methoxylated species of 4-methyl-1,3-dithiolane-2-thione increases with an increase in reaction. It also revealed that the selectivity of the methoxylated species is hampered beyond 6 hours. In the presence of MeOH as a solvent and [PPN]Cl as a co-catalyst, all 8 catalysts showed activity in the coupling of $CS_2$ and PO. The highest conversion rate was achieved with **C1**/[PPN]Cl and the lowest conversion rate was achieved with **C2**/[PPN]Cl.

The screening of the 8 metal complexes in the coupling of $CO_2$ and PO showed that they are poorly active for this coupling process over 12 hours and under mild conditions when paired with [PPN]Cl as a co-catalyst. **C5**/[PPN]Cl resulted in the highest conversion of PO and **C2**/[PPN]Cl resulted in the lowest conversion of PO. These were calculated to be 1.05 % and 0.27, respectively. Increasing the reaction time to 24 hours and the same reaction conditions, the conversion of PO increased to 1.81 % when **C5**/[PPN]Cl was used as the catalyst system. The addition of organic solvents was found to have a negative effect in PO conversions. % PO conversions of 0.18, 0.22, 0.34 and 0.32 were achieved in the presence of hexane, DCM, acetonitrile and MeOH, respectively, when **C5**/[PPN]Cl as the catalyst system at room temperature, over 24 hours and atmospheric pressure of $CO_2$. These % PO conversion values

are lower than those achieved under the same reactions but in the absence of solvents. Increasing $CO_2$ pressure from atmospheric pressure to 25 bar of $CO_2$ was shown to have a slight positive influence in PO conversion over 24 hours at room temperature and in the presence of **C5**/[PPN]Cl as the catalyst system.

All eight complex have been shown to be active in the coupling of $CS_2$ and PO as well as in the coupling of $CO_2$ and PO in the presence of co-catalysts. Although active in both coupling processes and showing selectivity for the exclusive conversion of PO to cPC in the latter, the poor conversion of PO is not economical.

## 4.4 EXPERIMENTAL

### 4.4.1 Materials and instrumentation

All chemical reactions and manipulations were performed on a dual vacuum/gas line using standard Schlenk techniques unless otherwise stated. Reagent grade chemicals were obtained from Sigma Aldrich and used as received. All solvents were dried under appropriate drying reagents and distilled prior to use with the exception of $CS_2$ and PO, which were used as acquired. $^1$H NMR spectra were recorded on a Varian 300 MHz spectrometer using tetramethylsilane as an internal standard. Chemical shifts are reported in (ppm) and referenced to residual proton in $CDCl_3$.

### 4.4.2 General procedure for the coupling of carbon disulphide and propylene oxide

A 12 place RADLEYS Carrousel Reaction Station fitted with a reflux unit as well as a gas distribution system was used to perform the coupling reactions. In a typical experiment, PO (30.0 mmol, 2.01 mL), $CS_2$ (30.0 mmol, 1.86 mL) and the respective catalyst and/or co-catalyst were added to glass reaction tubes. The reaction mixtures were stirred for the stipulated period of time at room temperature under Ar atmosphere. After the desired time had lapsed, the reactions were stopped. The reaction mixtures were transferred to round bottom flasks and DCM was used to extract what remained in the carrousel tubes. All volatiles were removed under vacuum; after which they were taken up in DCM. The DCM solutions were passed through a short silica column and collected in round bottom flasks. All volatiles were removed under vacuum and the resulting residue was analysed by $^1$H NMR spectroscopy in $CDCl_3$.

### 4.4.3 General procedure for the coupling of carbon dioxide and propylene oxide

A 12 place RADLEYS Carrousel Reaction Station fitted with a reflux unit as well as a gas distribution system was used to perform the coupling reactions at atmospheric $CO_2$ pressure. In a typical experiment, the respective catalyst and/or co-catalyst and PO (30.0 mmol, 2.01 mL) was added to a glass reaction tube. The reaction mixtures were stirred for 15 minutes under a steady stream of $CO_2$. After 15 minutes, the carrousel tubes were sealed, and the flow of $CO_2$ gas was stopped. Stirring was continued until the desired reaction time was reached. The reactions were stopped, and the reaction mixtures were transferred to round bottom flasks. DCM was used to extract what remained in the carrousel tubes. All volatiles were removed under vacuum; after which they were taken up in DCM. The DCM solutions were passed through a short silica column and collected in round bottom flasks. All volatiles were removed under vacuum and the resulting residue was analysed by $^1H$ NMR spectroscopy in $CDCl_3$

For the reactions carried out at 25 bar $CO_2$ pressure: PO (30.0 mmol, 2.01 mL) was added to the respective catalyst and co-catalyst in a Berghof 150 mL autoclave containing a stirrer bar. The autoclave was sealed and pressurized to 25 bar with $CO_2$ gas. The reaction mixtures were stirred for the desired period of time after which they were stopped. The reaction mixtures were transferred to round bottom flasks and DCM was used to extract what remained in the autoclave. All volatiles were removed under vacuum, after with they were taken up in DCM. The DCM solutions were passed through a short silica column and collected in round bottom flasks. All volatiles were removed under vacuum and the resulting residue was analysed by $^1H$ NMR spectroscopy in $CDCl_3$.

## 4.5 REFERENCES


[1] J. D Diebler, H. Komber, L. Häußler, A. Lederer, and T. Werner, *Macromolecules*, 2016, 49, 13, 4723–4731.

[2] S. Inoue, H. Koinuma, and T. Tsuruta, *J. Polym. Sci. Part C Polym. Lett.*, 1969, 7, 287–292.

[3] W.M. Ren, T.J. Yue, M.R. Li, Z.Q. Wan, and X.B. Lu, *Macromolecules*, 2017, 50, 1, 63–68.

[4] M. Luo, Y. Li, Y.Y. Zhang, and X.H. Zhang, *Polymer (Guildf).*, 2016, 82, 406–431.

[5] N. D. SZE and M. K.. Ko, *Nature*, 1979, 278, 5706, 731–732.

[6] A. W. DeMartino, D. F. Zigler, J.M. Fukuto, and P.C. Ford, *Chem. Soc. Rev.*, 2017, 46, 1, 21–39.

[7] J. Wang, C.-S. Jia, C.-J. Li, X.-L. Peng, L.-H. Zhang, and J.-Y. Liu, *ACS Omega*, 2019, 4, 21, 19193–19198.

[8] Y.M. Wang, B. Li, H. Wang, Z.C. Zhang, and X.B. Lu, *Appl. Organomet. Chem.*, 2012. 26, 11, 614–618.

[9] D. Tian, B. Liu, L. Zhang, X. Wang, W. Zhang, L. Han and D.W. Park, *J. Ind. Eng. Chem.*, 2012, 18, 4, 1332–1338.

[10] X. B. Lu, Y. J. Zhang, B. Liang, X. Li, and H. Wang, *J. Mol. Catal. A Chem.*, 2004, 210, 1-2, 31–34.

[11] N. Gautier, F. Dumur, V. Lloveras, J.V. Gancedo, J. Veciana, C. Rovira and P. Hudhomme, *Angew. Chemie Int. Ed.*, 2003, 42, 24, 2765–2768.

[12] A. Ishii, S. Asami, Y. Fujiwara, A. Ono, and N. Nakata, *Heteroat. Chem.*, 2011, 22, 3–4, 388–396.

[13] T. F. Baumann and J. G. Reynolds, *Chem. Commun.*, no.1998, 16, 1637–1638

[14] Y. Zhang and R. Munday, *Mol. Cancer Ther.*, 2008, 7, 11, 3470–3479.

[15] W. Choi, F. Sanda, and T. Endo, *Macromolecules*, 1998, 31, 8, 2454–2460.

[16] G. Rokicki, W. Kuran, and B. Pogorzelska-Marciniak, *Monatshefte for Chemie Chem. Mon.*, 1984, 115, 2, 205–214.

[17] N. Aoyagi, Y. Furusho, and T. Endo, *J. Polym. Sci. Part A Polym. Chem.*, 2013, 51, 5, 1230–1242.

[18] X.B. Lu, Y.J. Zhang, B. Liang, X. Li, and H. Wang, *J. Mol. Catal. A Chem.*, 2004, 210, 1–2, 31–34.

[19] X.B. Lu, B. Liang, Y.J. Zhang, Y.Z. Tian, Y.M. Wang, C.X. Bai, H. Wang and R. Zhang, *J. Am. Chem. Soc.*, 2004, 126, 12, 3732–3733.

[20] D. J. Darensbourg, W. C. Chung, and S. J. Wilson, *ACS Catal.*, 2013, 3, 12, 3050–3057.

[21] B. Li, R. Zhang, and X.B. Lu, *Macromolecules*, 2007, 40, 7, 2303–2307.

[22] J. Diebler, A. Spannenberg, and T. Werner, *Org. Biomol. Chem.*, 2016, 14, 31, 7480–7489.

[23] W. Clegg, R. W. Harrington, M. North, and P. Villuendas, *J. Org. Chem.*, 2010, 75, 18, 6201–6207.

[24] I. Yavari, M. Ghazanfarpour-Darjani, Z. Hossaini, M. Sabbaghan, and N. Hosseini, *Synlett*, 2008, 6, 889–891.

[25] D.J. Darensbourg, S.J. Wilson, and A.D. Yeung, *Macromolecules*, 2013, 46, 20, 8102–8110.

[26] X. Gao, M. Liu, J. Lan, L. Liang, X. Zhang, and J. Sun, *Cryst. Growth Des.*, 2017, 17, 1, 51–57.

[27] Y. M. Shen, W. L. Duan, and M. Shi, *J. Org. Chem.*, 2003, 68, 1559 –1562.

[28] A. Aouissi, D. Aldhayan, N. A. Y. Abduh, and A. Al Kahtani, *Green Process. Synth.*, 2020, 9, 1, 440–450.

[29] Y. Xiong, F. Bai, Z. Cui, N. Guo, and R. Wang, *J. Chem.*, 2013, 20, 1–9.

# Chapter 5:
# Summary

The synthesis and characterization of a range of neutral pyrrole-aldimine ligands with varying steric demands is reported. These were prepared by the Schiff-base condensation reaction to afford pyrrole-aldimine ligands in yields ranging from 75 % to 91 %. The successful preparation of the neutral ligands was confirmed by $^{1}$H NMR spectroscopy. In order to conclusively assign the $^{1}$H NMR spectra signals, COSY and NOESY spectroscopy were used. To further confirm the successful preparation of these ligands, $^{13}$C NMR spectroscopy was used. The $^{13}$C NMR spectra signals were conclusively assigned using HMBC and HSQC spectroscopy. ESI-MS, FT-IR and UV-Vis spectroscopy were used to further corroborate the preparation of these ligands and elemental analysis was used to confirm their purity.

The pyrrole-aldimine ligand were then utilized in the preparation of their corresponding bis-(pyrrole-aldiminato) Zn(II) and Co(II) complexes. The preparation of the bis-(pyrrole-aldiminato) Zn(II) and Co(II) complexes began with the treatment of the respective neutral ligand with NaH in THF to deprotonate the acidic pyrrole N-H proton. This yielded the respective neutral ligand's sodium ligand salt. The successful deprotonation of the neutral ligands was confirmed with $^{1}$H NMR spectroscopy. Two molar equivalence of the sodium ligand salts were reacted with 1 molar equivalence of either $ZnCl_2$ for the bis-(pyrrole-aldiminato) Zn(II) and $CoCl_2$ for the bis-(pyrrole-aldiminato) Co(II) complexes in THF. Upon work-up, the bis-(pyrrole-aldiminato) Zn(II) and Co(II) complexes were isolated as powders of varying colours and consistencies. Due to the paramagnetic nature of the bis-(pyrrole-aldiminato) Co(II) complexes, NMR spectroscopy was used to characterize only the bis-(pyrrole-aldiminato) Zn(II) complexes. As with the neutral ligands, COSY and NOESY spectroscopy were used to conclusively assign the $^{1}$H NMR spectra signals and HSQC and HMBC spectroscopy were used to conclusively assign the $^{13}$C NMR spectra chemical shifts. ESI-MS, FT-IR and UV-Vis spectroscopy were used to confirm the preparation of both bis-(pyrrole-aldiminato) Zn(II) and Co(II) complexes, and elemental analysis was used to confirm their purity.

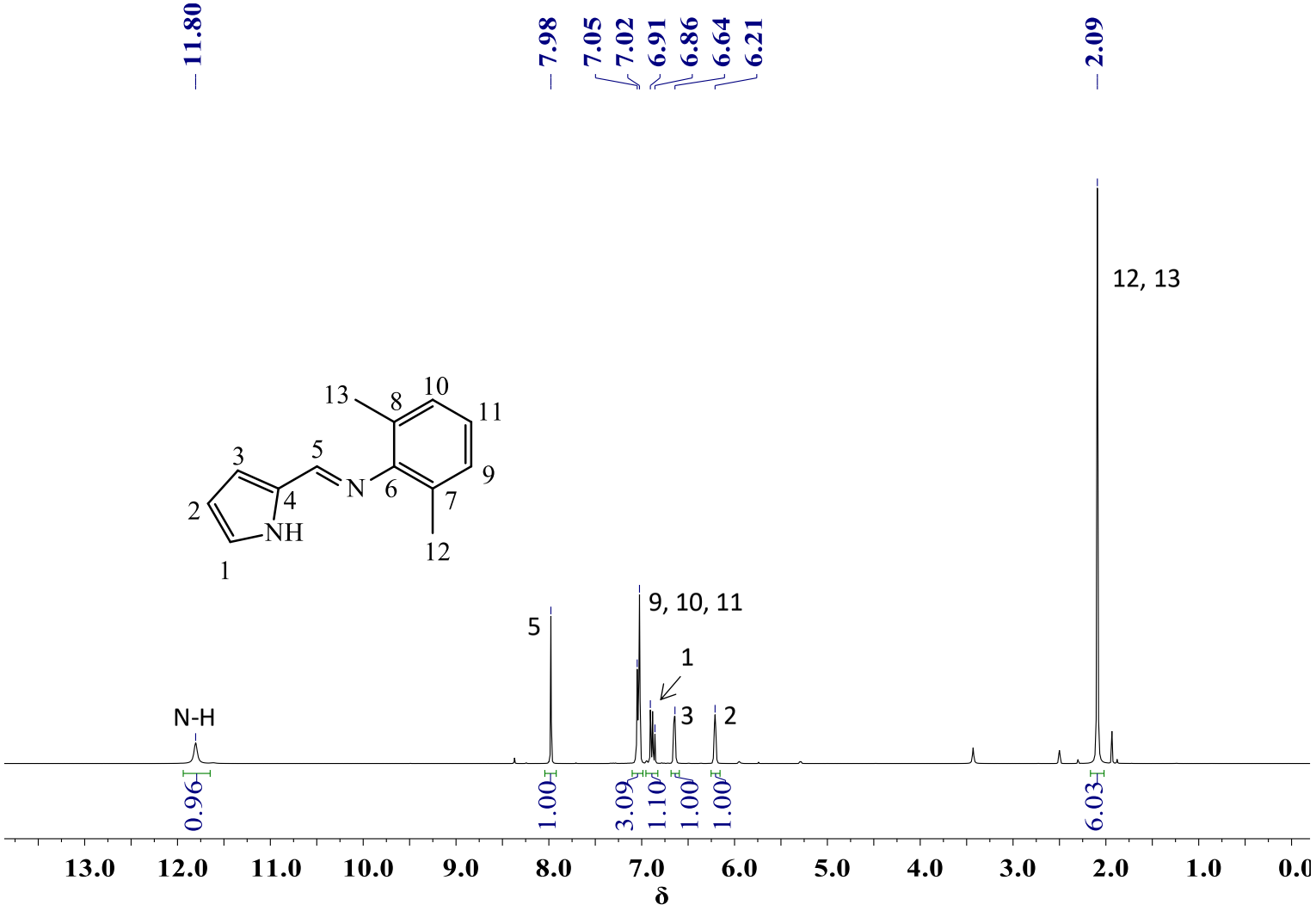
The activity of both bis-(pyrrole-aldiminato) Zn(II) and Co(II) complexes were evaluated in the coupling of $CS_2$/$CO_2$ with PO. The coupling of $CS_2$ and PO using **C1** as a catalyst was used

to establish the baseline coupling reaction conditions. **C1** on its own was inactive for this coupling process at room temperature, even after 24 hours. Pairing **C1** with co-catalysts such as TBAC, DMAP, [PPN]Cl and MeIm yielded 1 to 3 cyclic products. These were identified as 4-methyl-1,3-dithiolane-2-thione, 5-methyl-1,3-oxathiolane-2-thione and 4-methyl-1,3-oxathiolane-2-thione. In the presence of MeOH, **C1** on its own showed activity for the coupling of $CS_2$ and PO. However, a new cyclic product formed. The new cyclic product was identified as the methoxylated species of 4-methyl-1,3-dithiolane-2-thione. Pairing **C1** with TBAC, DMAP, [PPN]Cl and MeIm in the presence of MeOH improved the conversion of PO to the methoxylated species of 4-methyl-1,3-dithiolane-2-thione. MeOH on its own was also found to be active for the coupling of $CS_2$ and PO to yield the methoxylated species of 4-methyl-1,3-dithiolane-2-thione, however, the conversion was found to be poor. The co-catalysts on their own showed activity for the coupling of $CS_2$ and PO in the presence of MeOH. [PPN]Cl showed the lowest activity, and as such, it was selected as the representative co-catalyst. A time study was conducted using **C1**/[PPN]Cl as the catalyst system. The time study revealed that after 6 hours, the selectivity for the formation of the methoxylated species of 4-methyl-1,3-dithiolane-2-thione was hampered. This was seen by the emergence of signals in addition to the signals assigned to the methoxylated species of 4-methyl-1,3-dithiolane-2-thione in the $^1$H NMR spectra of the coupling reaction residues. All 8 catalysts were then screened in the coupling of $CS_2$ and PO using [PPN]Cl as the co-catalyst and in the presence of MeOH over 12 hours, at room temperature. **C1**/[PPN]Cl resulted in the highest conversion, whereas **C3**/[PPN]Cl resulted in the lowest conversion.

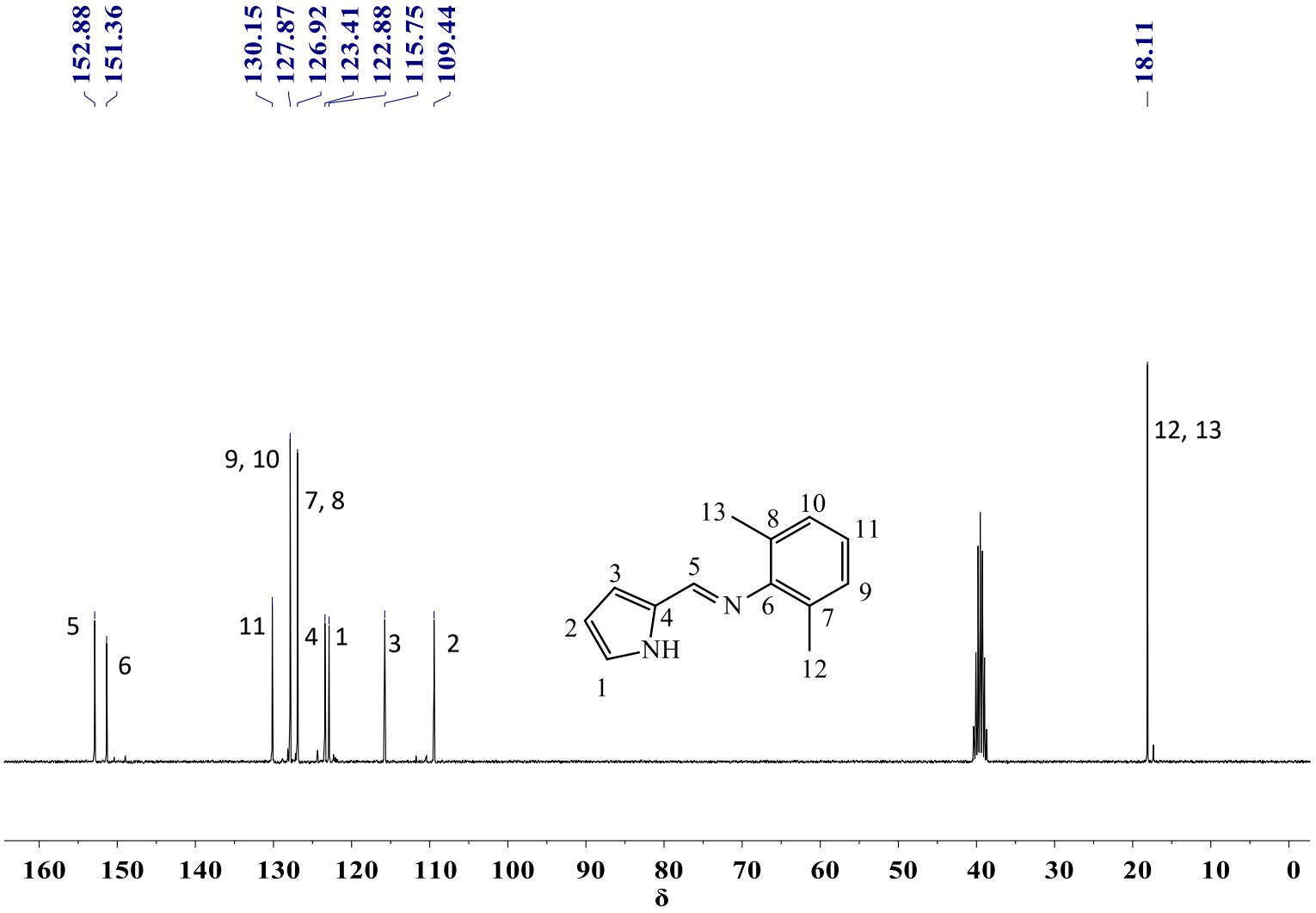
All 8 catalysts were screened for the coupling of $CO_2$ and PO. In the presence of [PPN]Cl, at room temperature under ambient $CO_2$ pressure, all eight catalysts showed activity for this coupling process over 24 hours. The catalyst system pair of **C5**[PPN]Cl resulted in the highest conversion of PO to cPC, the lowest conversion was achieved with **C3**/[PPN]Cl. With all 8 catalysts, the co-polymer PPC did not form as all eight catalysts showed selectivity for the conversion of PO to cPC. The catalysts system pair of **C5**/[PPN]Cl was used to investigate effect of solvent in this coupling process. Solvents of varying polarities (hexane, DCM, acetonitrile and MeOH) were selected. Acetonitrile resulted in the highest conversion of all solvents, with a conversion rate of 0.34 %; however, the conversion was lower than that achieved with **C5**/[PPN]Cl neat, which was 1.81 %. Using **C5**/[PPN]Cl and increasing the $CO_2$ pressure to 25 bar resulted in a slight increase in the conversion rate from 1.81 % to 2.07 %, however, by an insignificant margin.

The reaction conditions under which the bis-(pyrrole-aldiminato) Zn(II) and Co(II) complexes, **C1** – **C8** were evaluated for the coupling of $CS_2/CO_2$ with PO, yielded very low conversions of PO to cyclic products. The formation of the cyclic products which are reported in chapter 4 is known to be favoured under high reaction temperatures. A temperature study is proposed to be carried in future so as to investigate whether increasing temperature will improve the conversion of PO. The screening of co-catalysts other than those reported in **chapter 4** would also be necessary, so as to investigate the effect of nucleophile strength on the conversion rates.

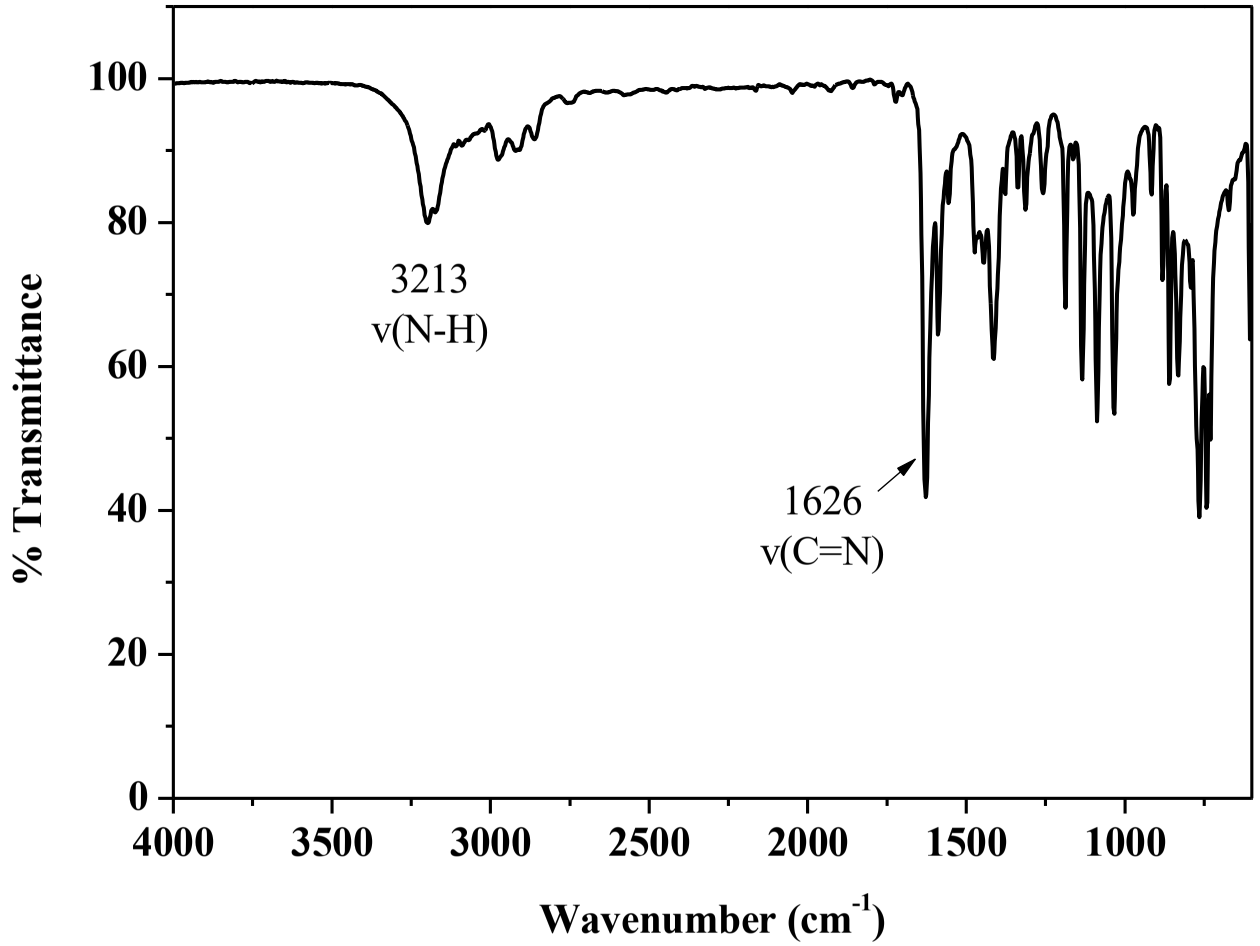
**L2**: $^{1}$H NMR spectrum (in DMSO-d6, 300 K)



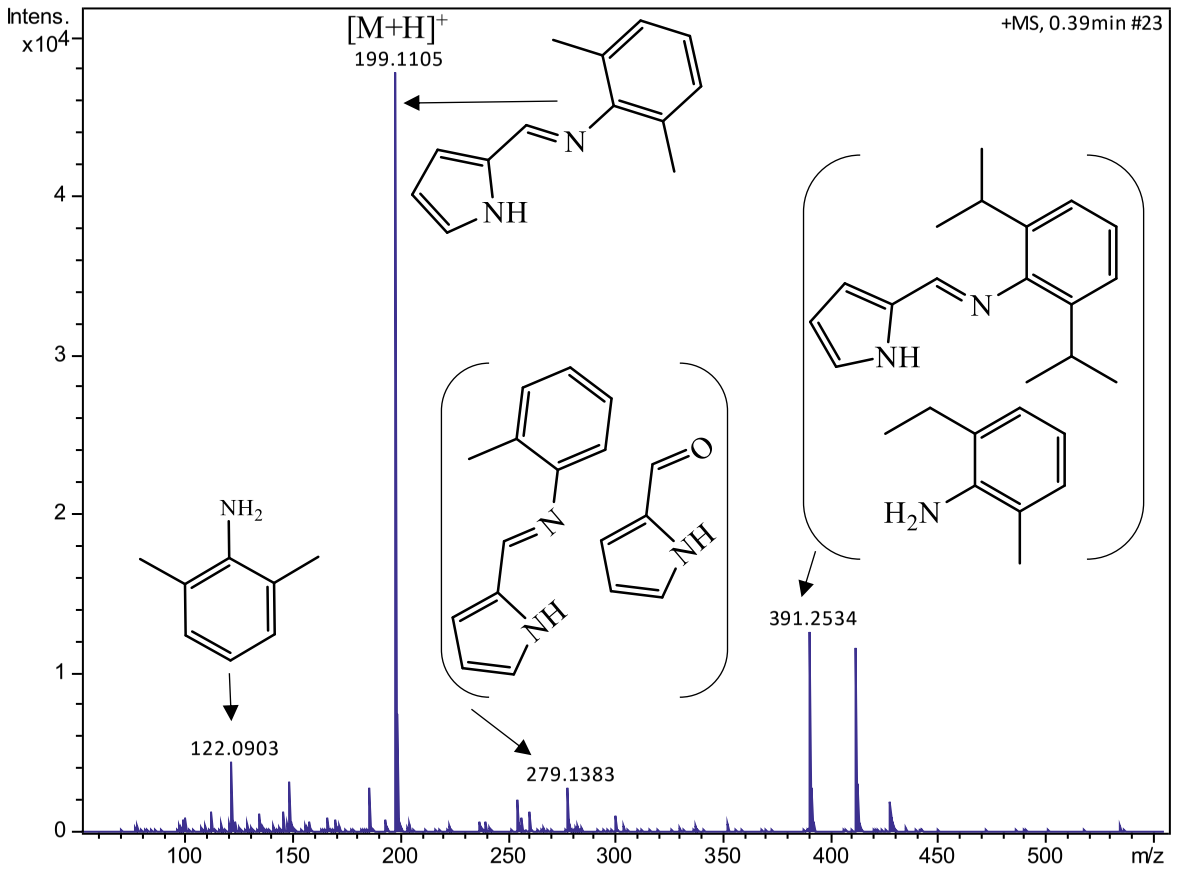
**L2**: $^{13}C$ NMR spectrum (in DMSO-d6, 300 K)



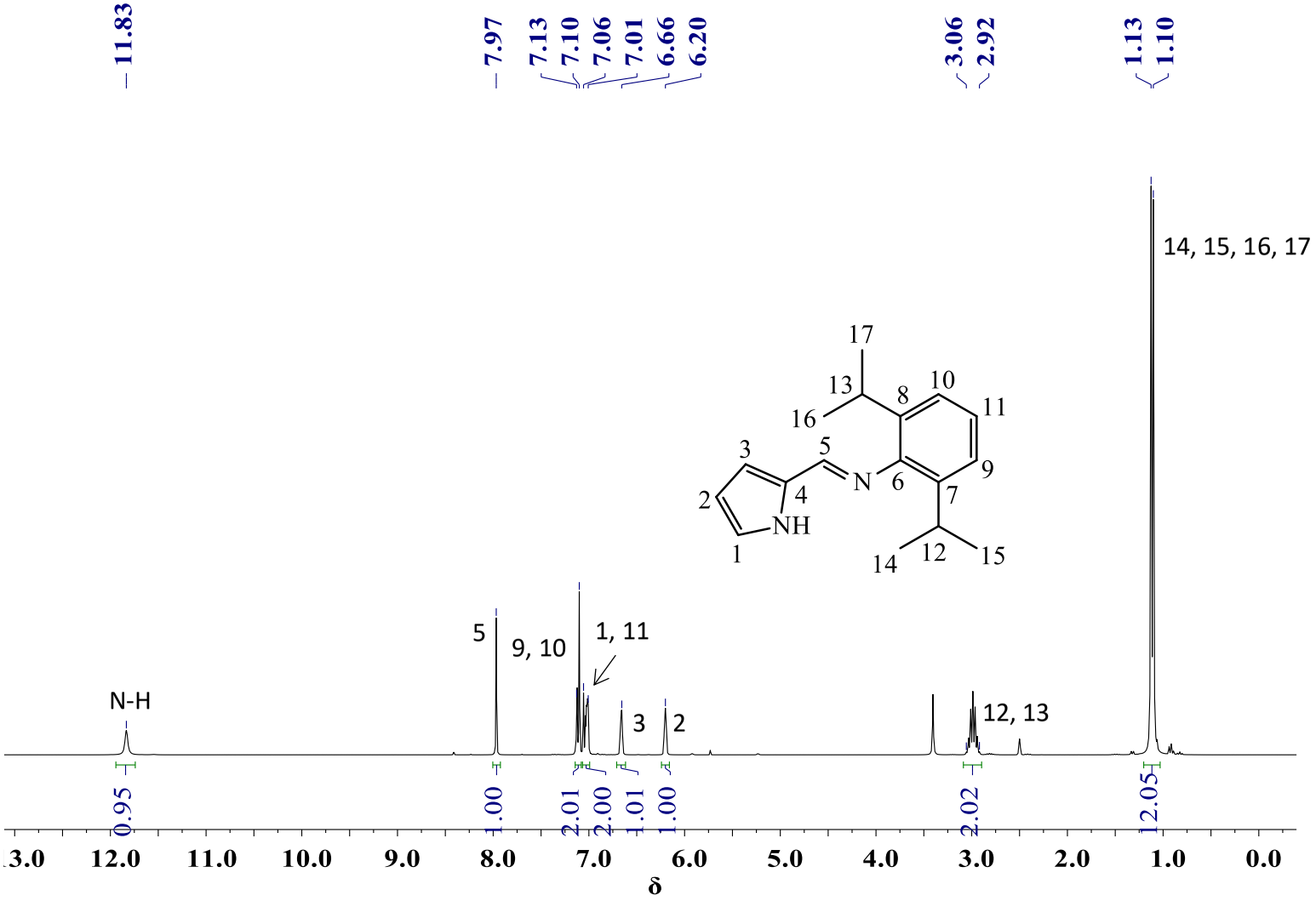
**L2: FT-IR spectrum**



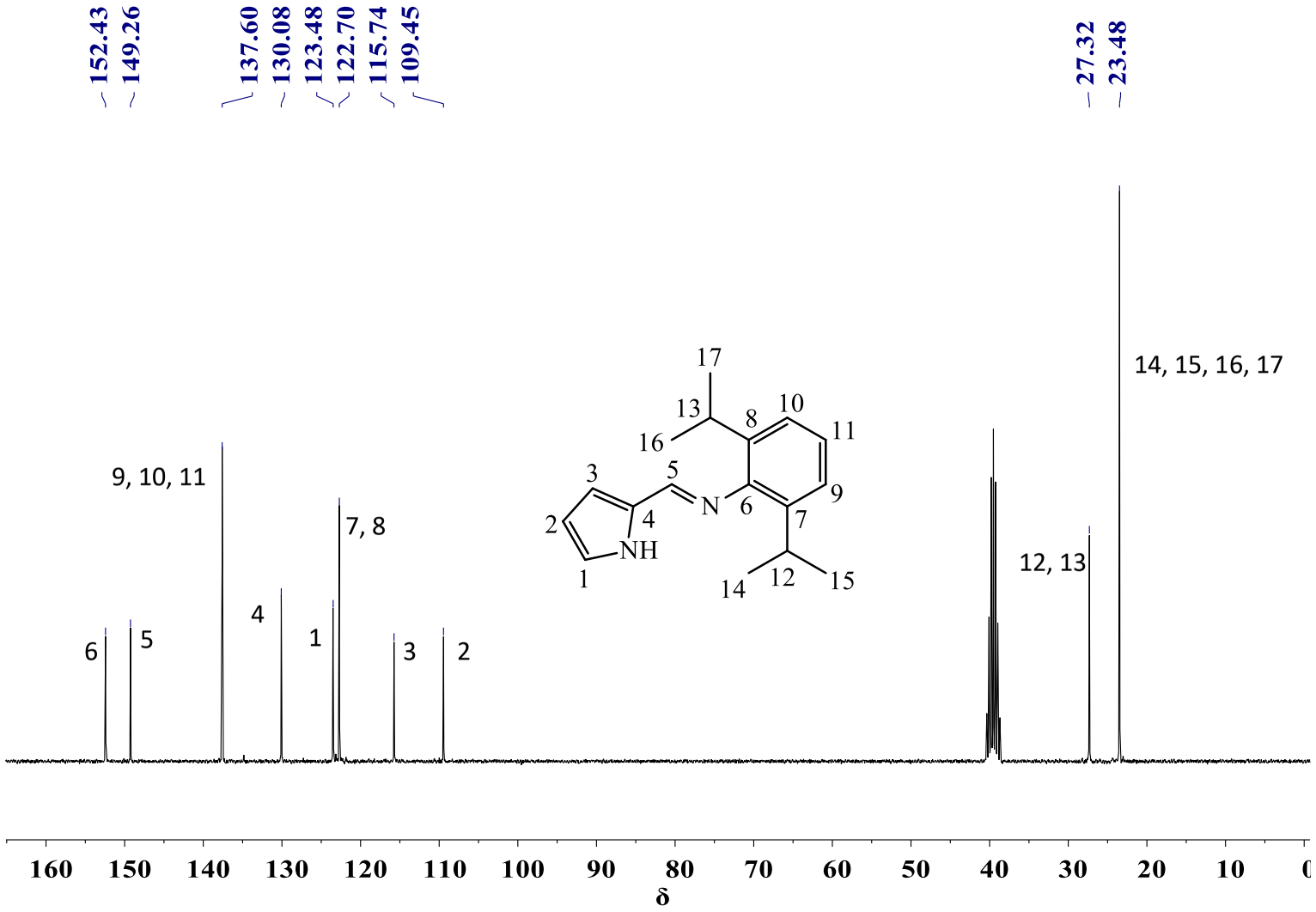
**L2**: ESI-MS (in MeOH)



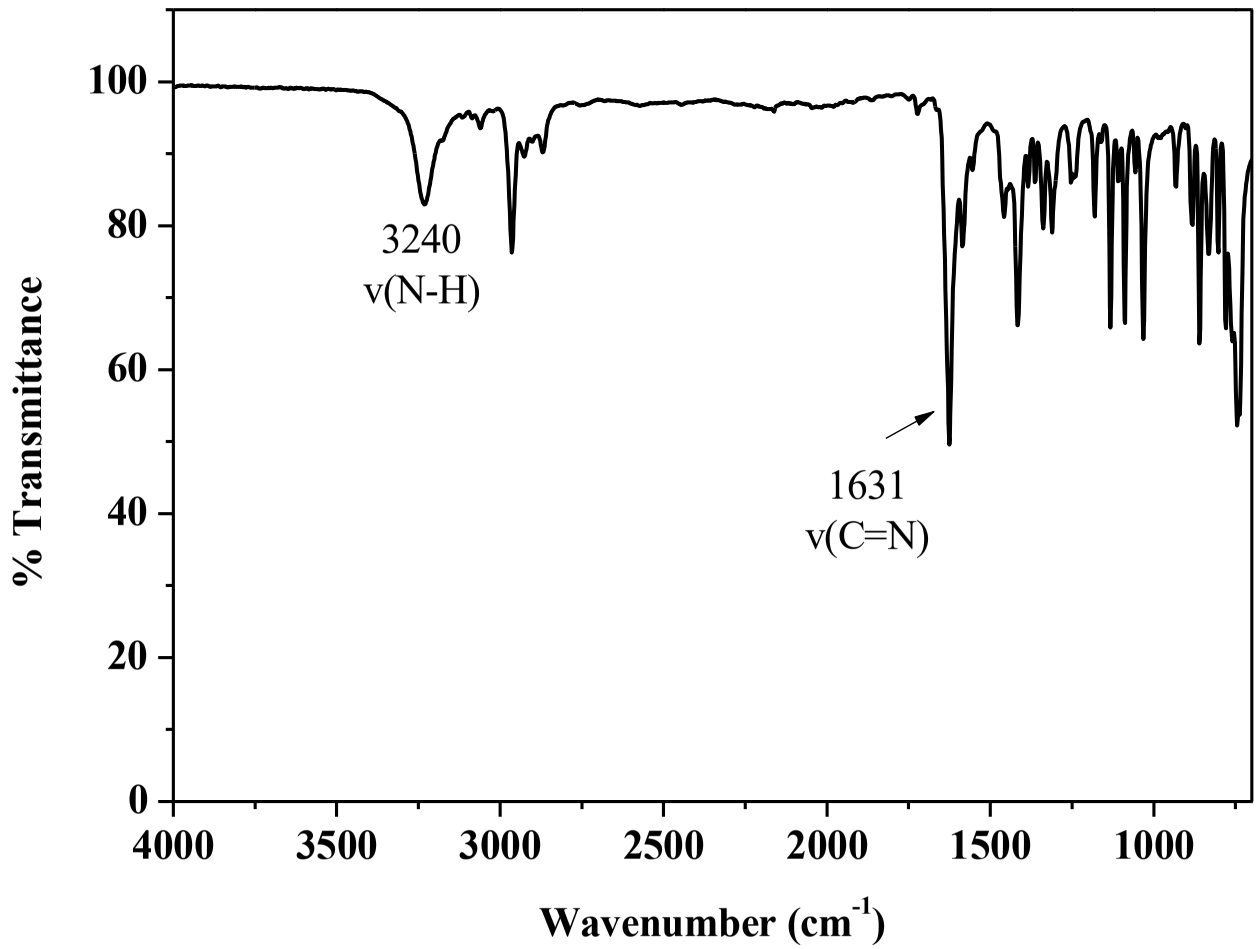
**L3**: $^{1}$H NMR spectrum (in DMSO-d6, 300 K)



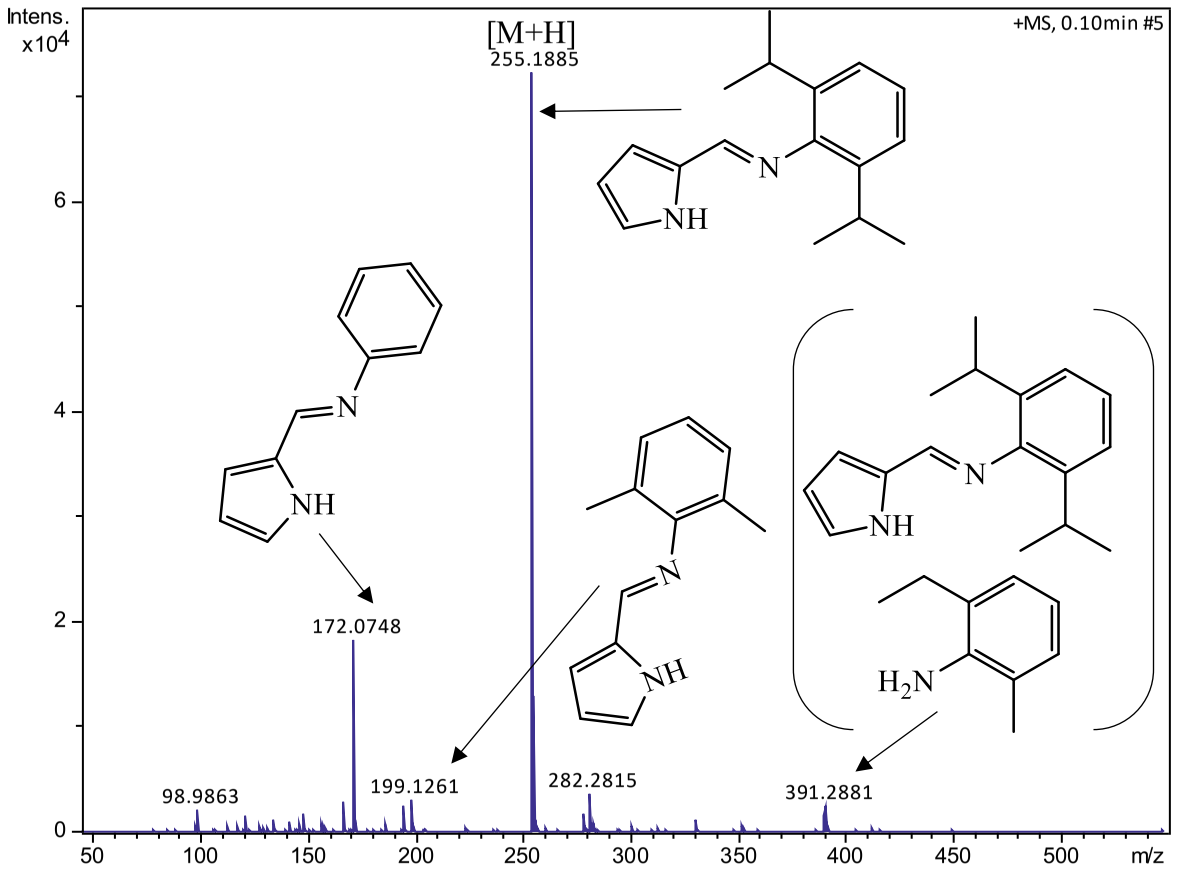
**L3**: $^{13}C$ NMR spectrum (in DMSO-d6, 300 K)



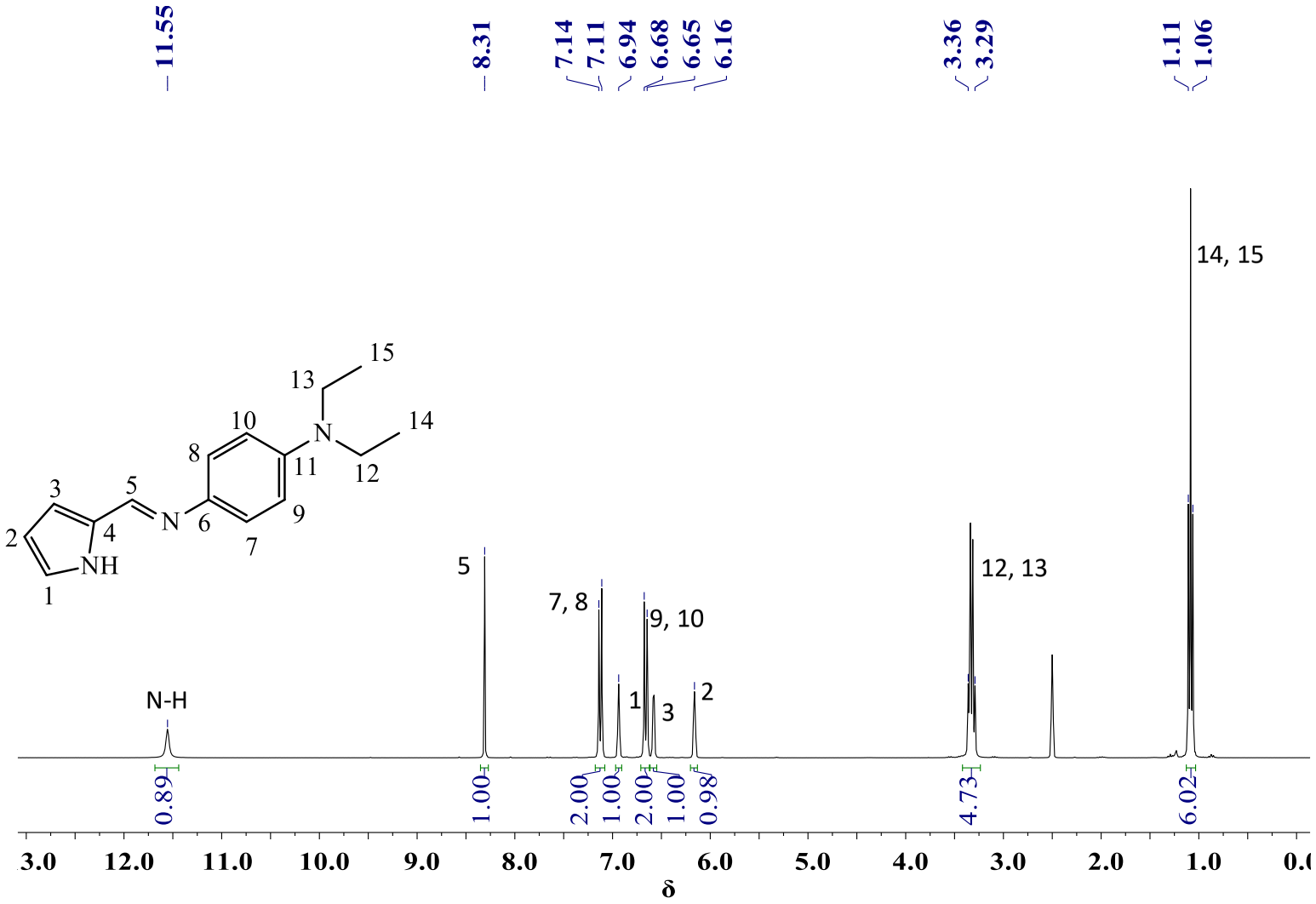
**L3: FT-IR spectrum**



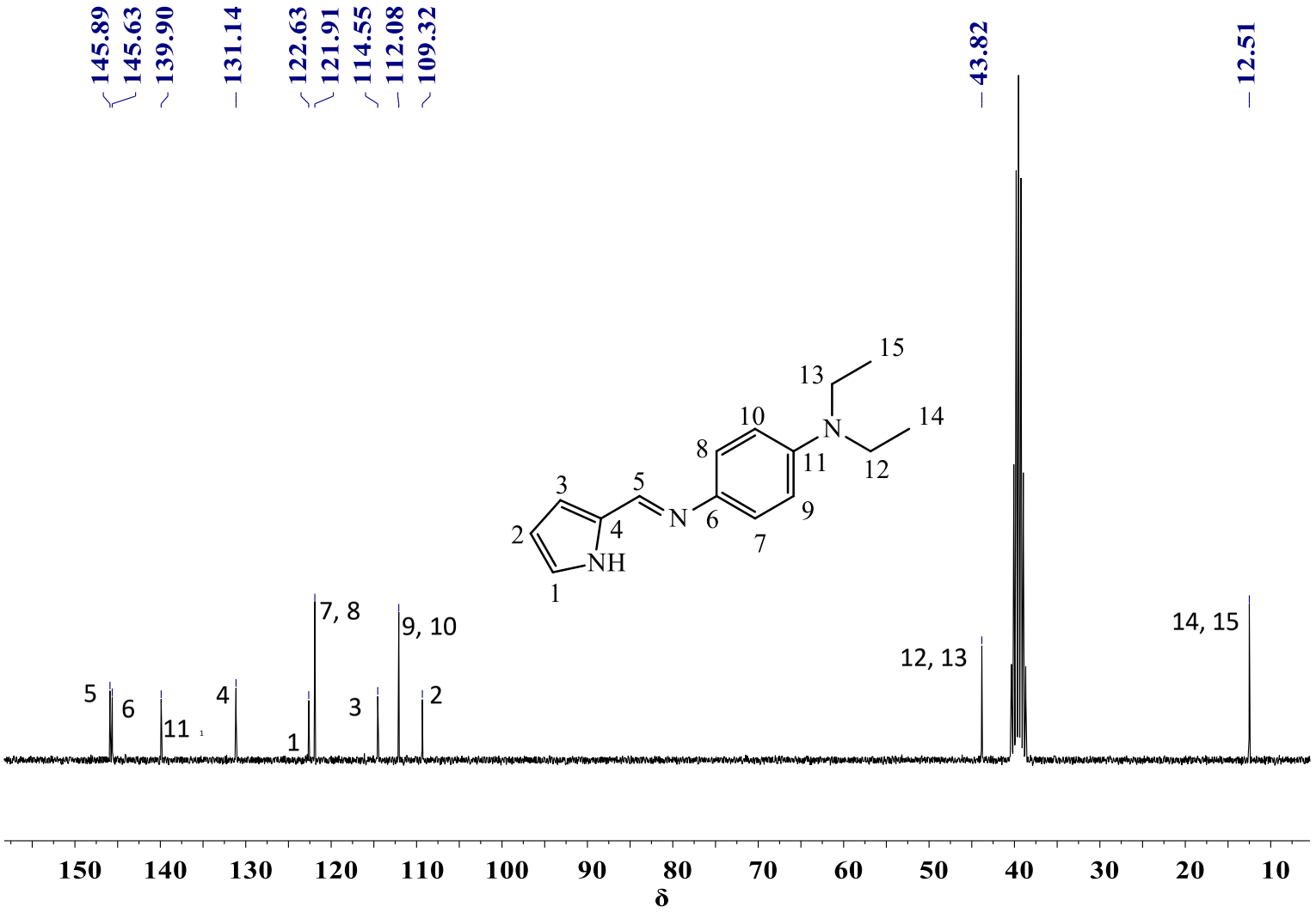
**L4:** ESI-MS (in MeOH)



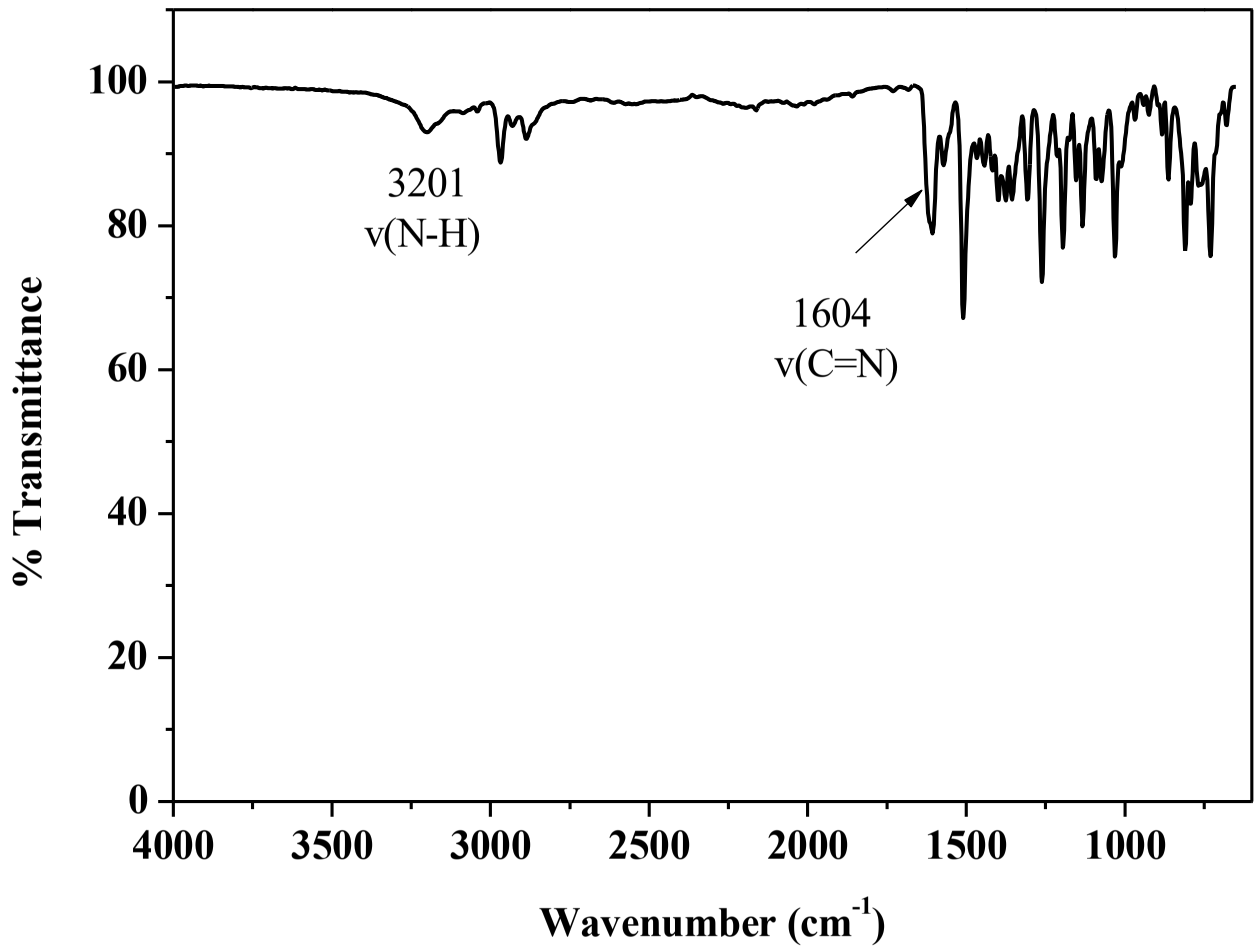
**L4**: $^{1}$H NMR spectrum (in DMSO-d6, 300 K)



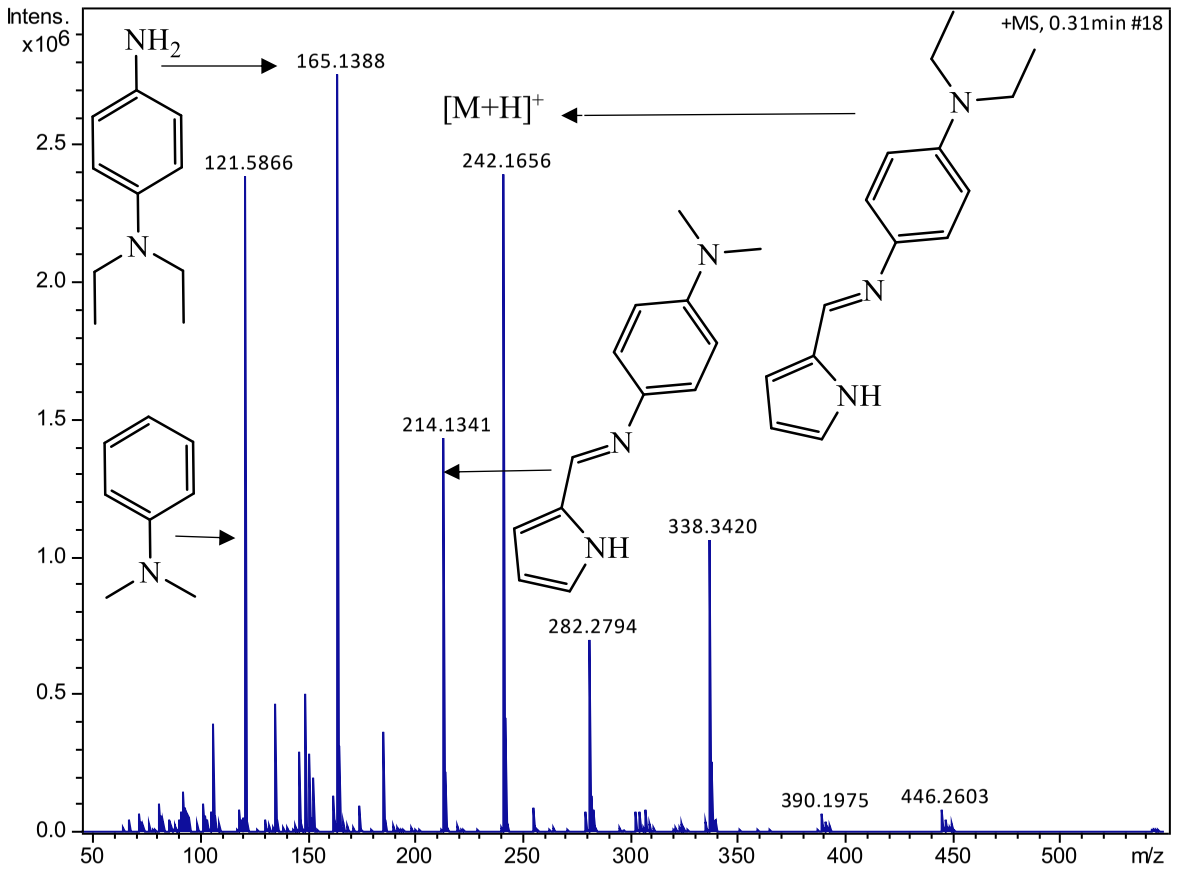
**L4**: $^{13}C$ NMR spectrum (in DMSO-d6, 300 K)



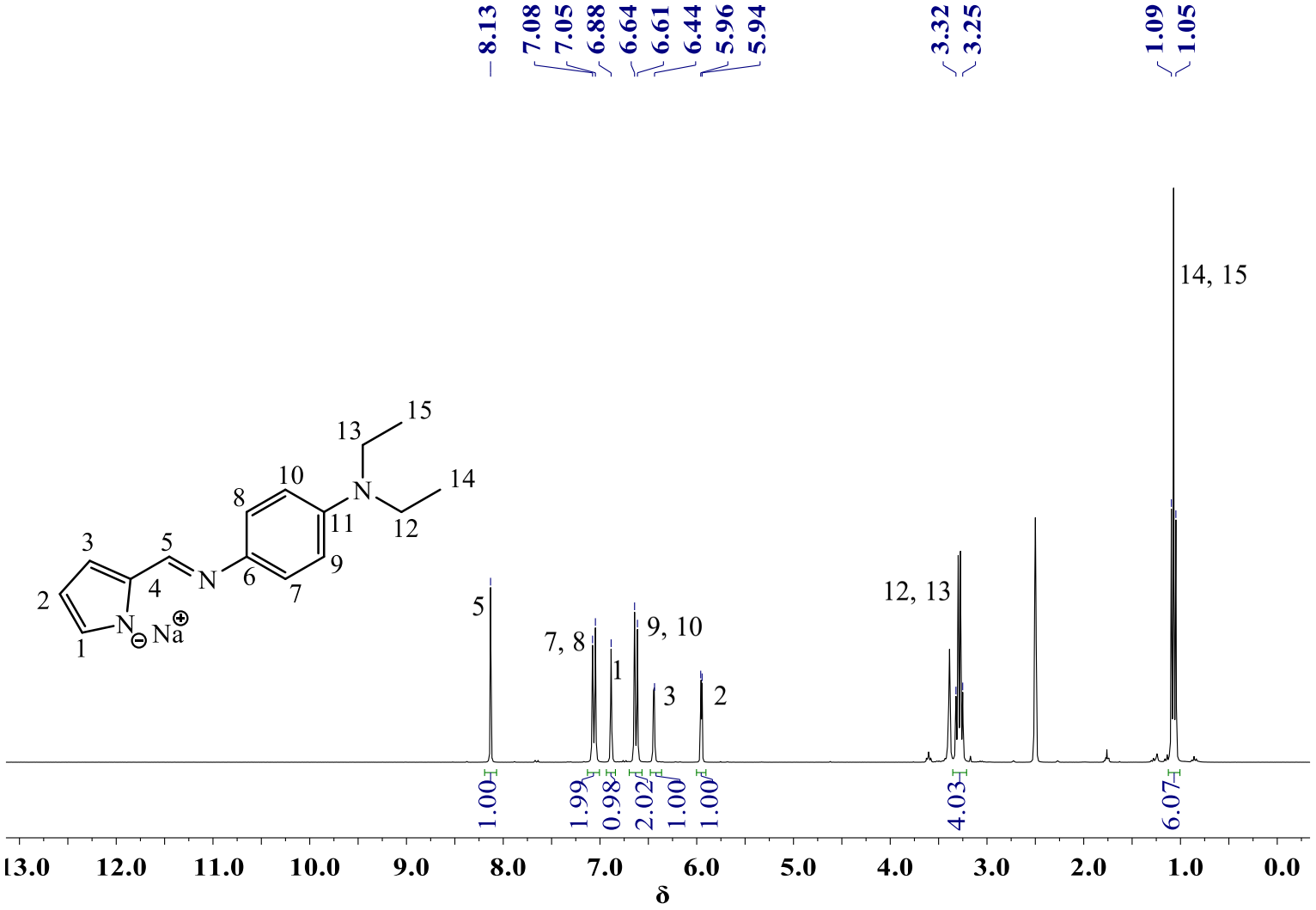
**L4:** FT-IR spectrum



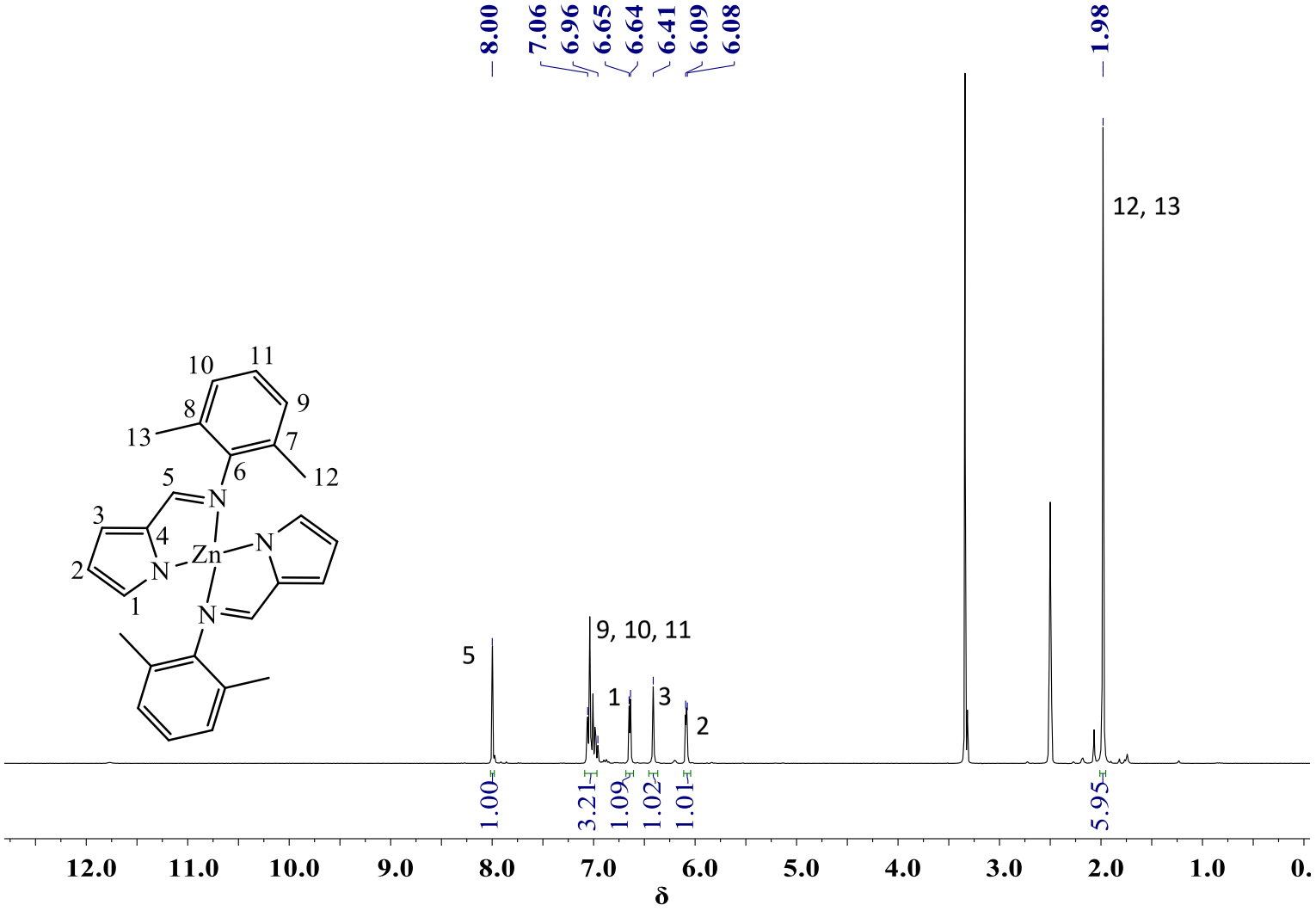
**L4**: ESI-MS (in MeOH)



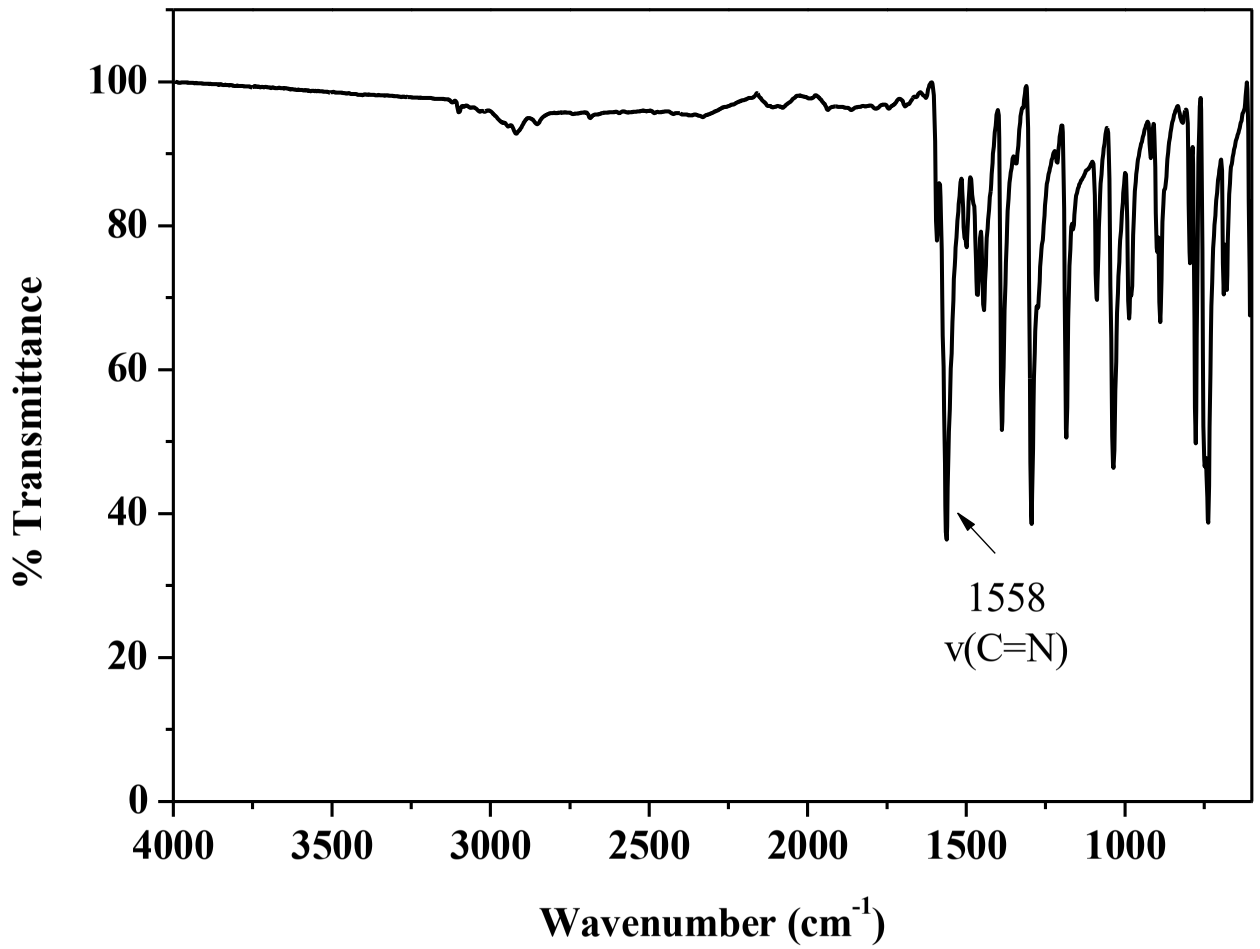
**L4$^{-}$Na$^{+}$:** $^{1}$H NMR spectrum (in DMSO-d6, 300 K)



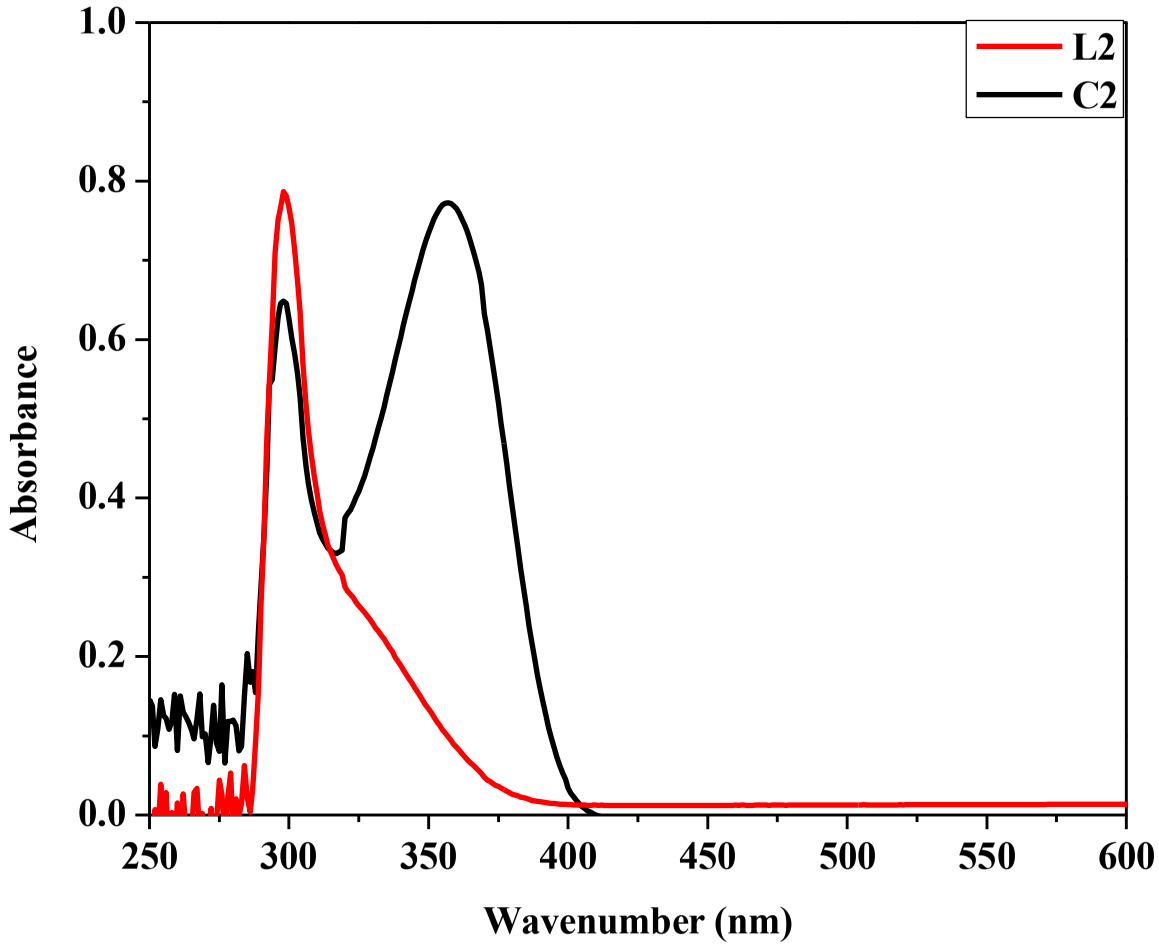
**C2:** $^{1}$H NMR spectrum (in DMSO-d6, 300 K)



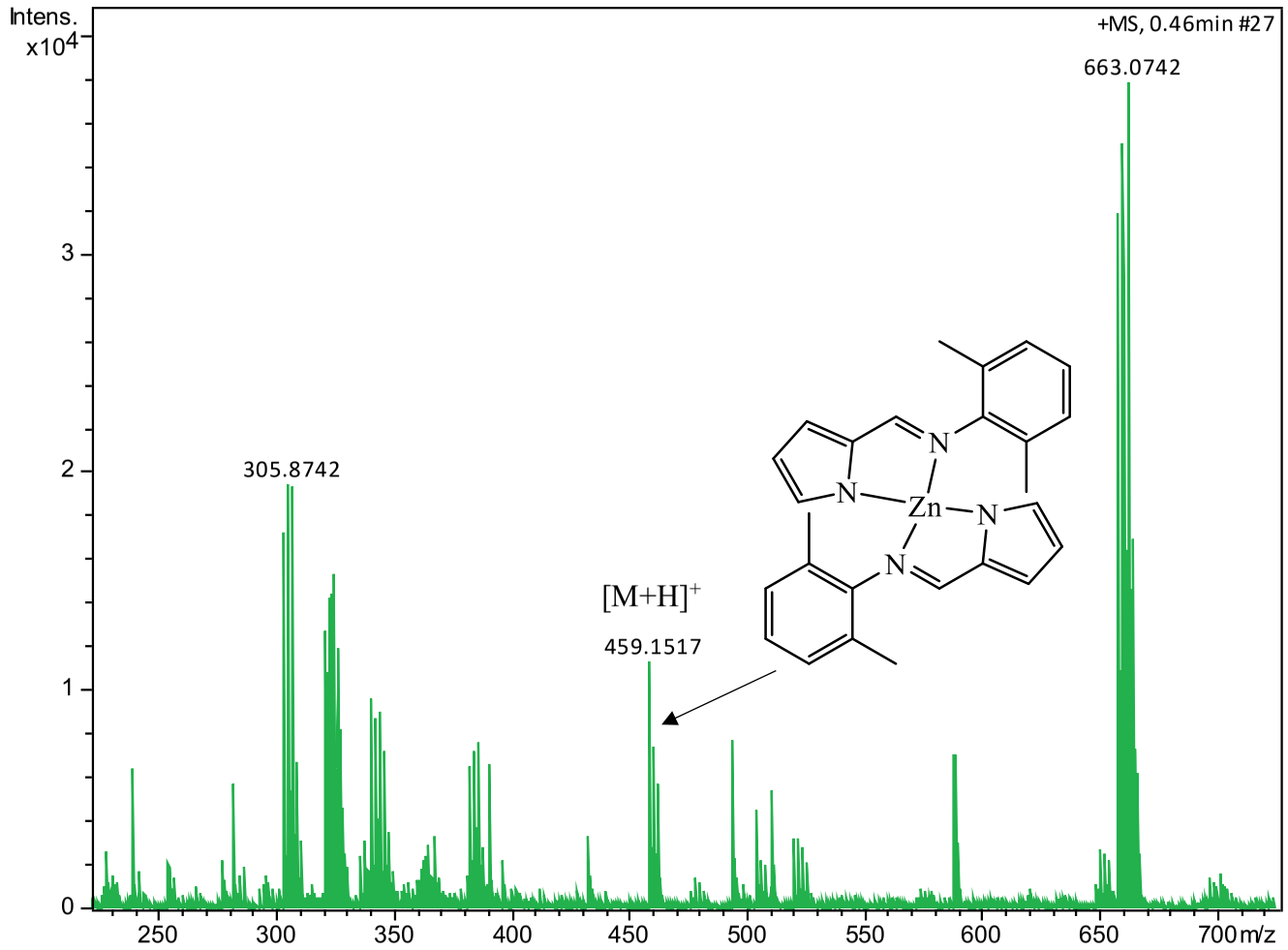
**C2:** FT-IR spectrum



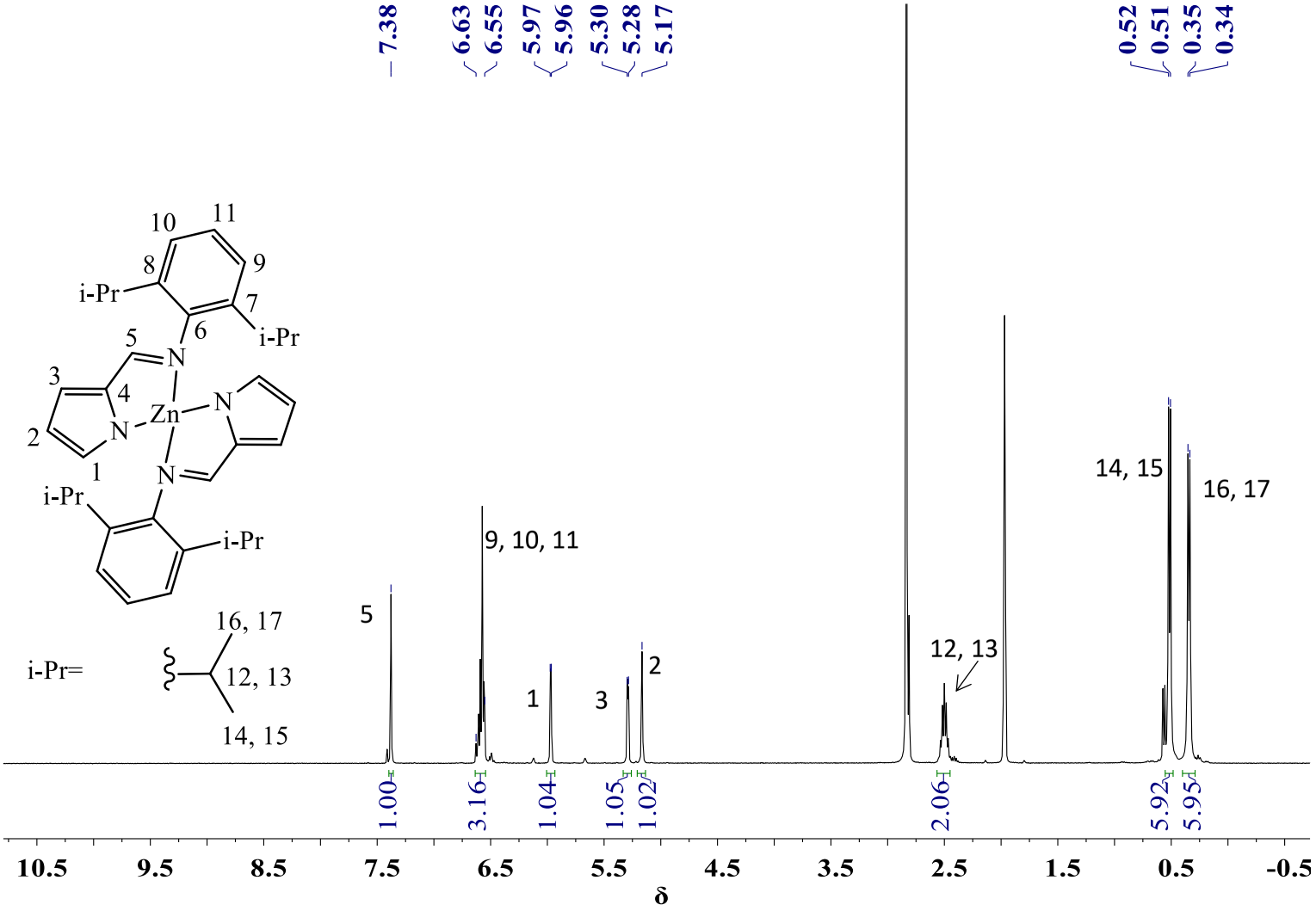
**C2:** UV-Vis spectrum (in Toluene)



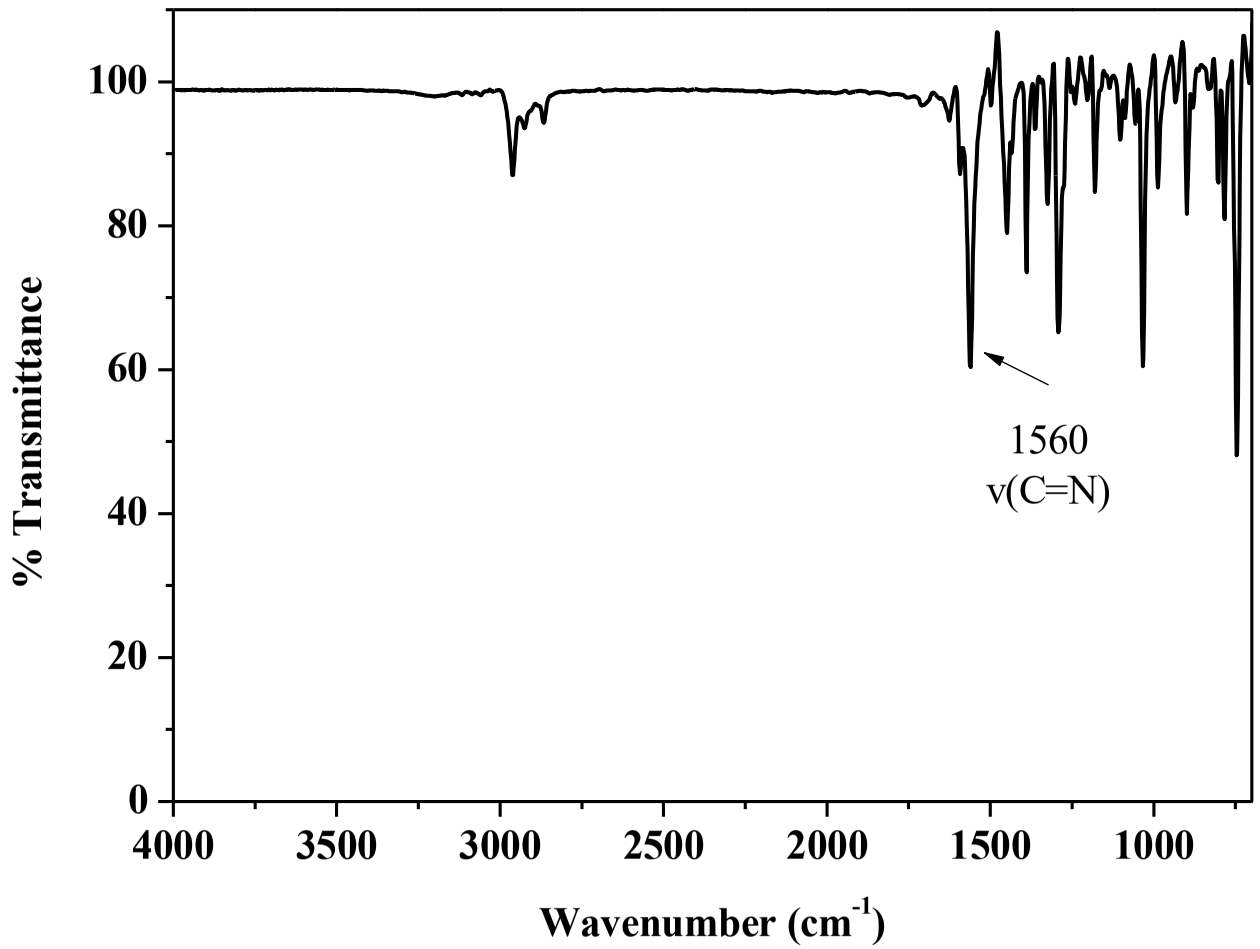
**C2:** ESI-MS (MeOH)



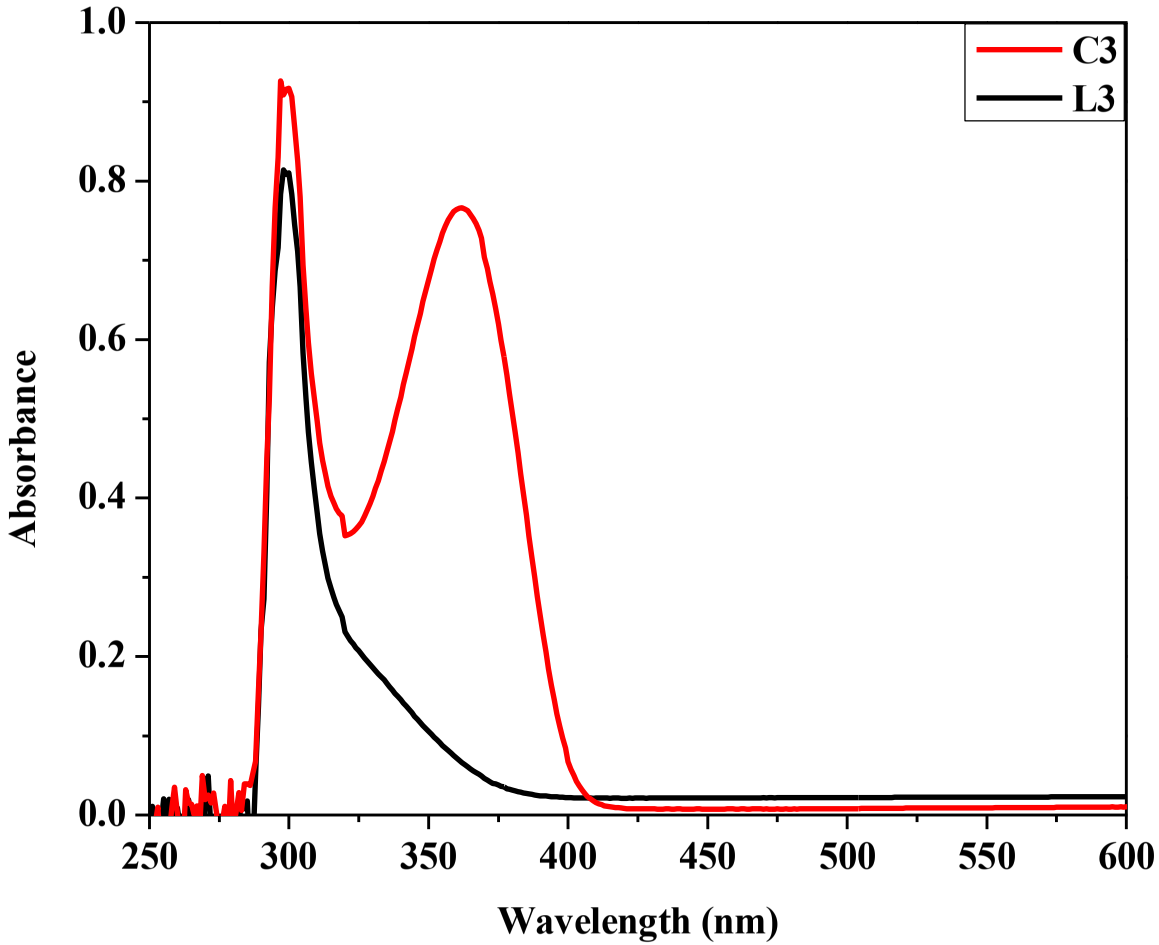
**C3:** $^{1}$H NMR spectrum (DMSO-d6, 300 K)



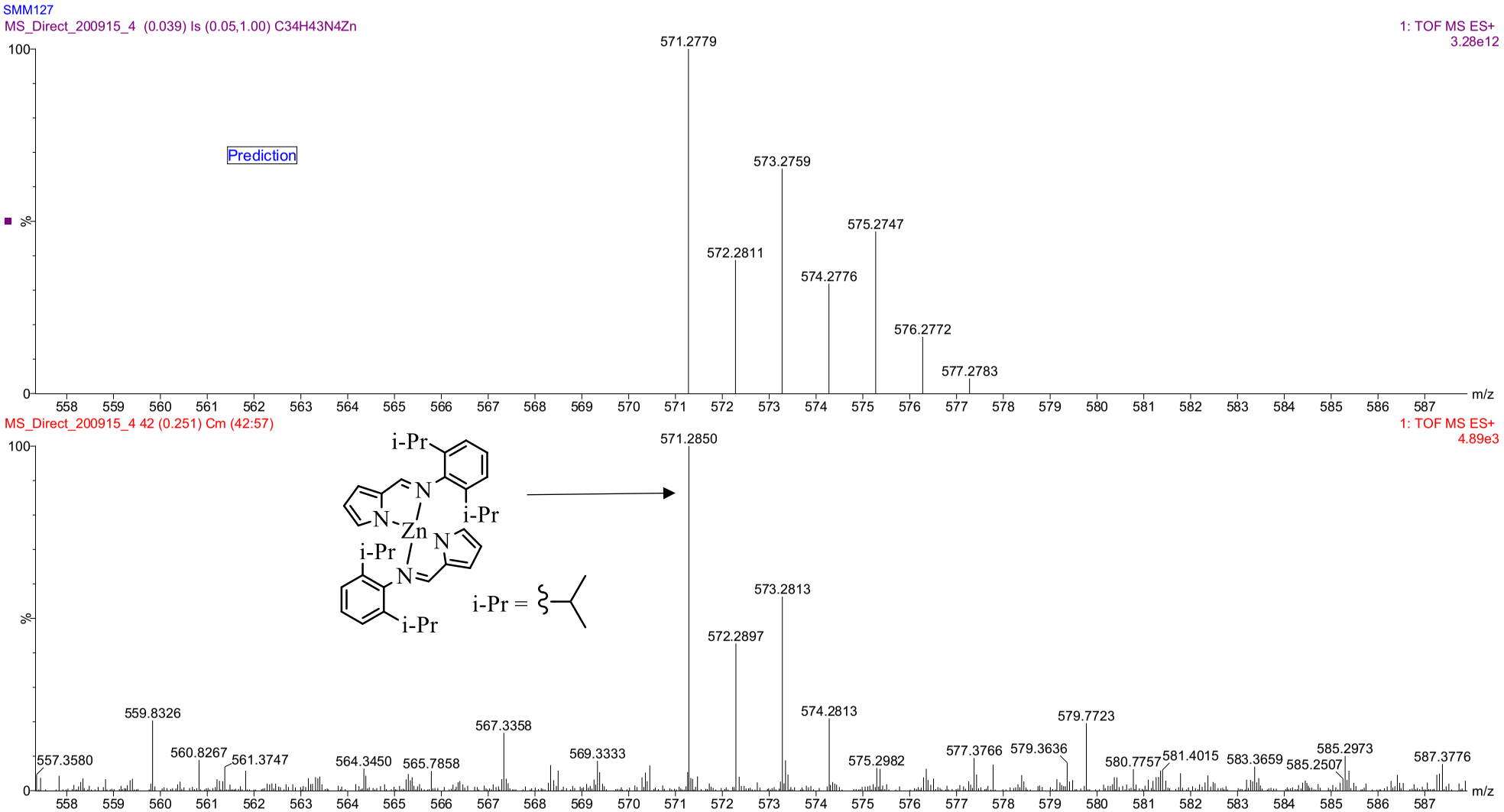
**C3:** FT-IR spectrum



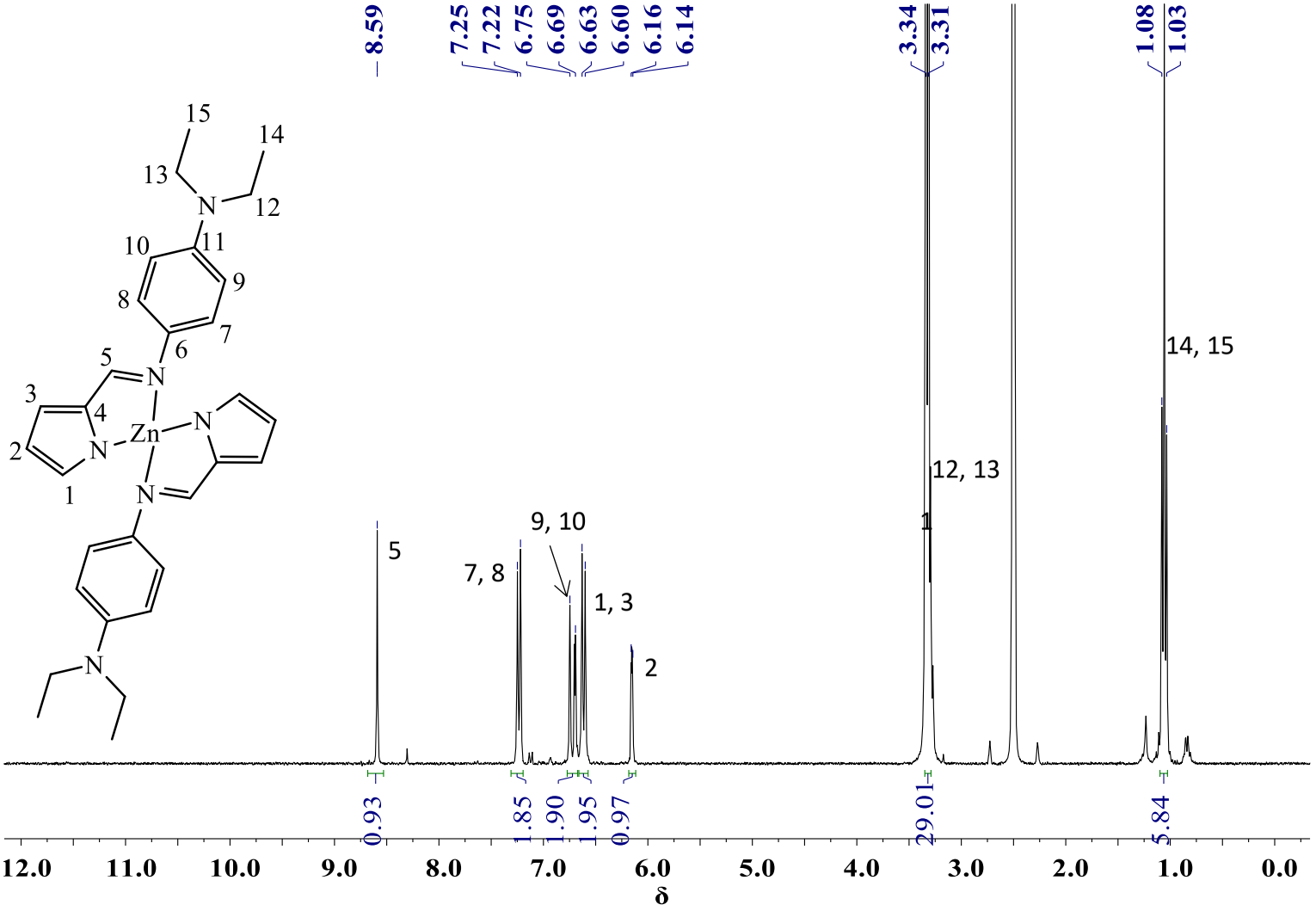
**C3:** UV-Vis spectrum (in Toluene)



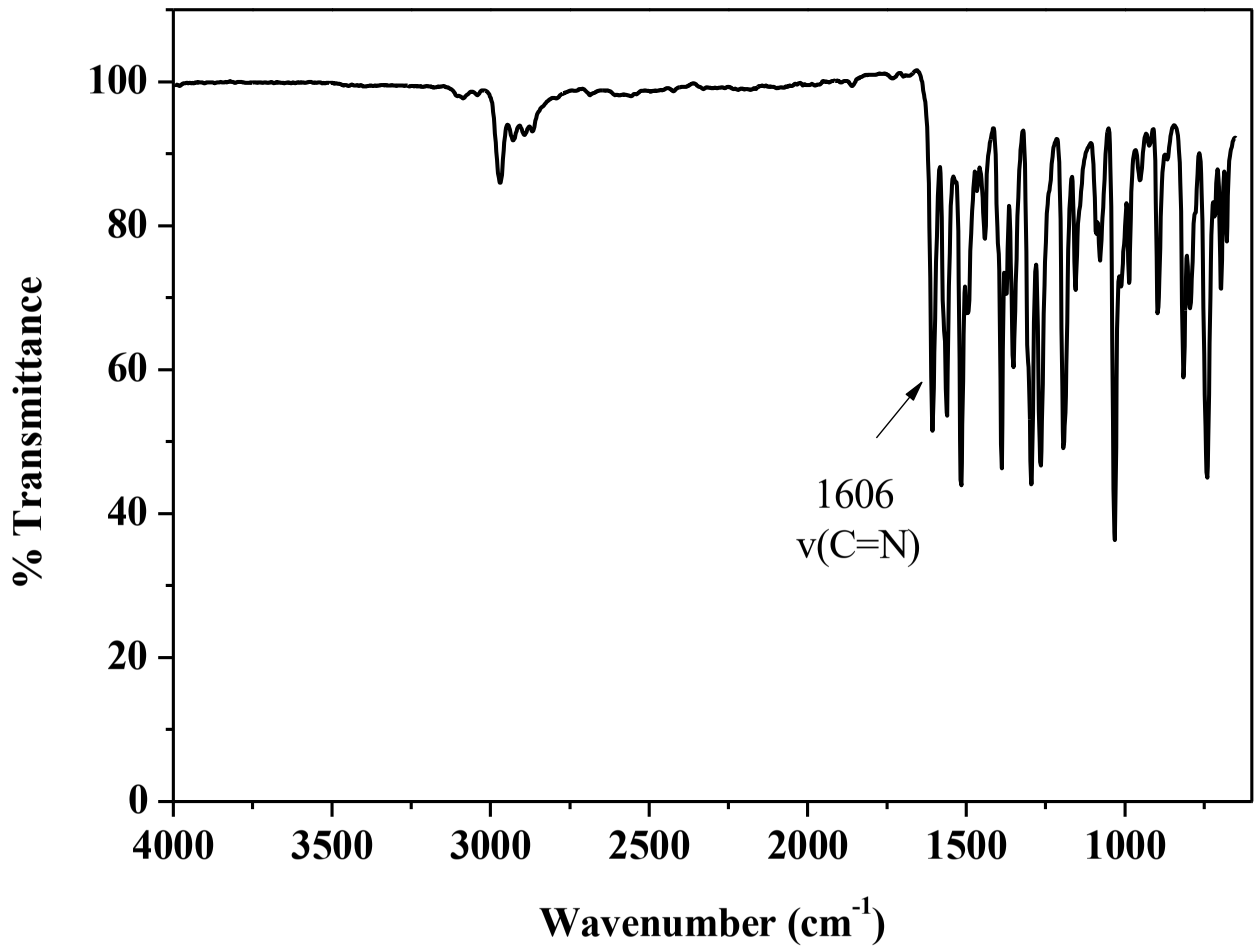
**C3:** ESI-MS (DMSO)



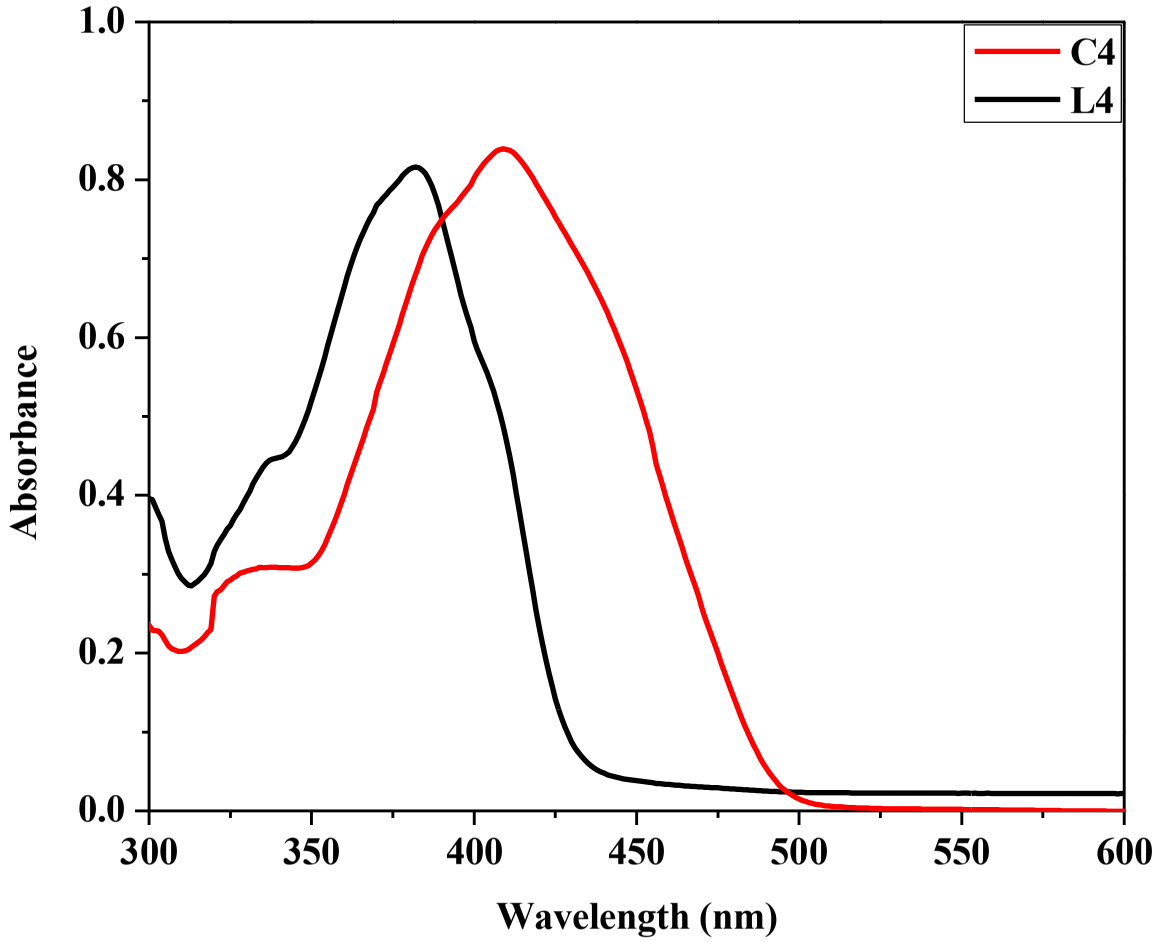
**C4:** $^{1}$H NMR spectrum (DMSO-d6, 300 K)



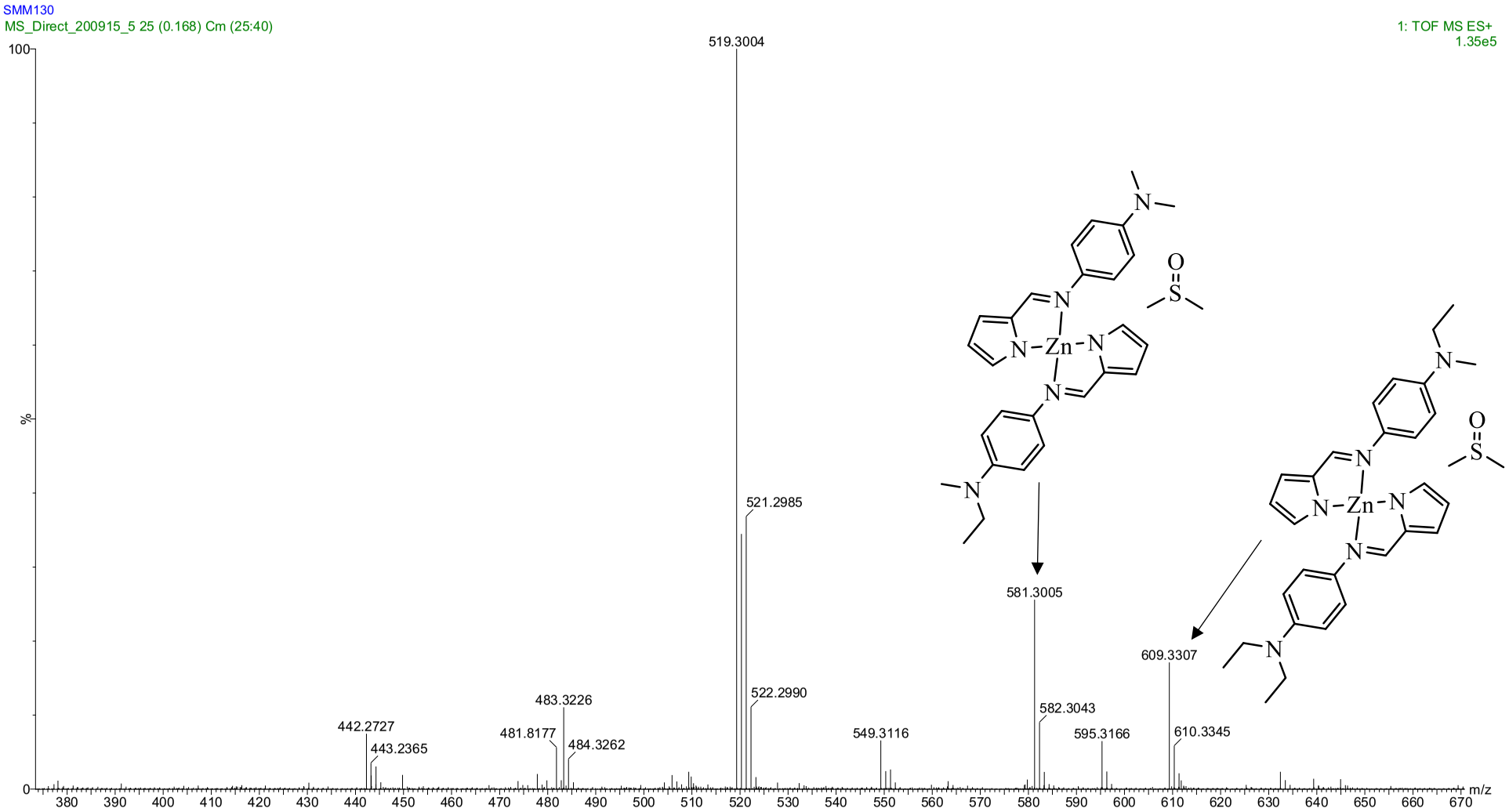
**C4: FTIR spectrum**



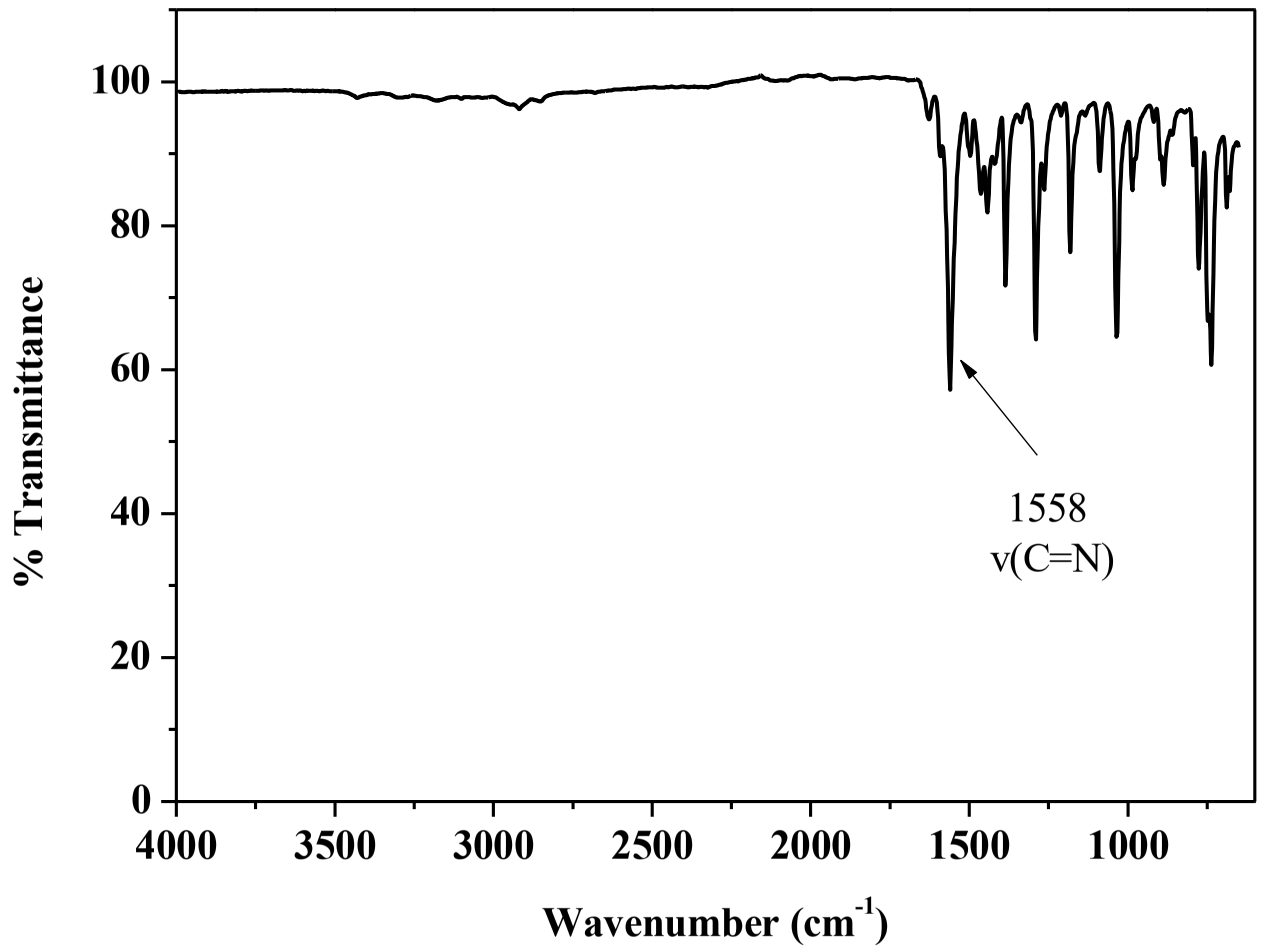
**C4:** UV-Vis spectrum (in Toluene)



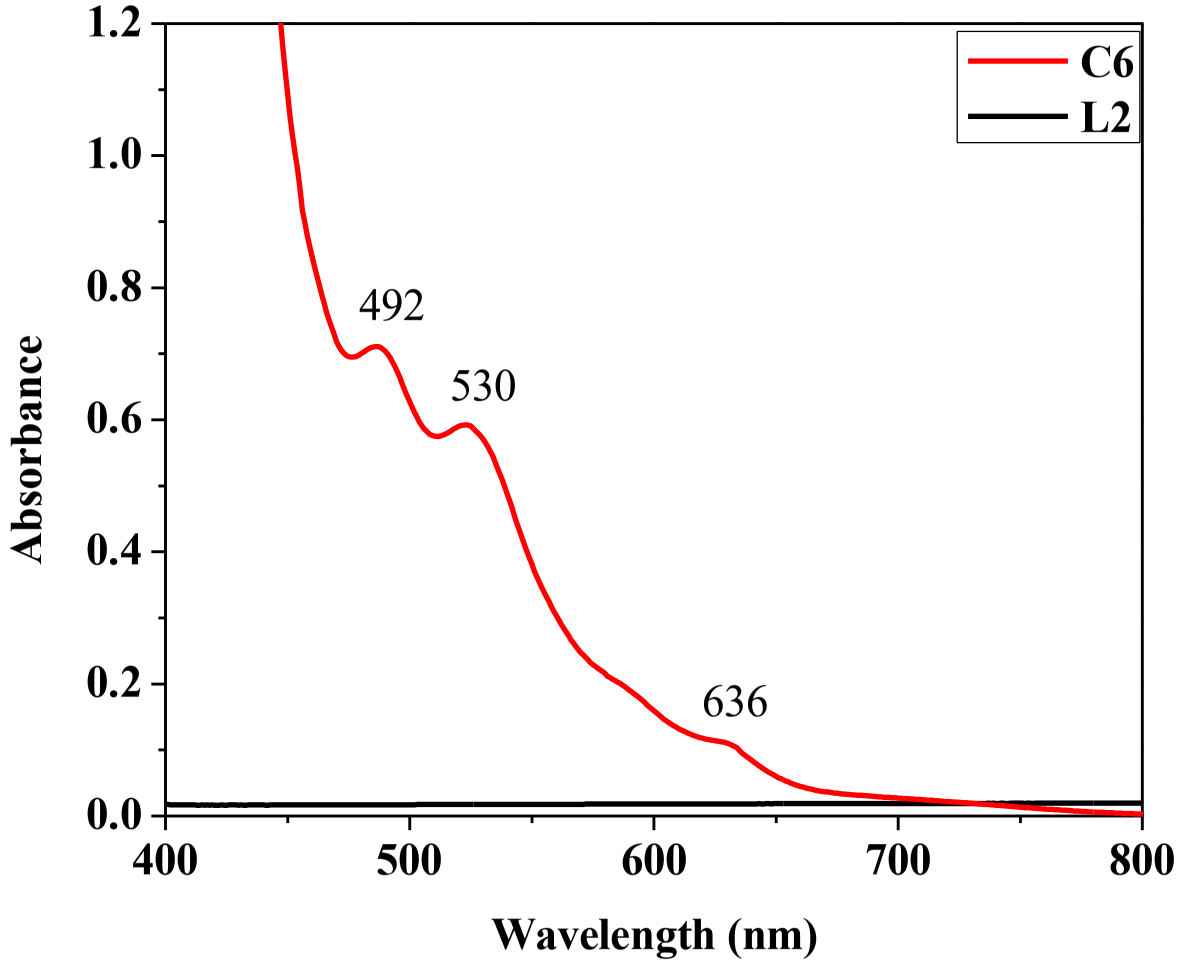
**C4:** ESI-MS (DMSO)



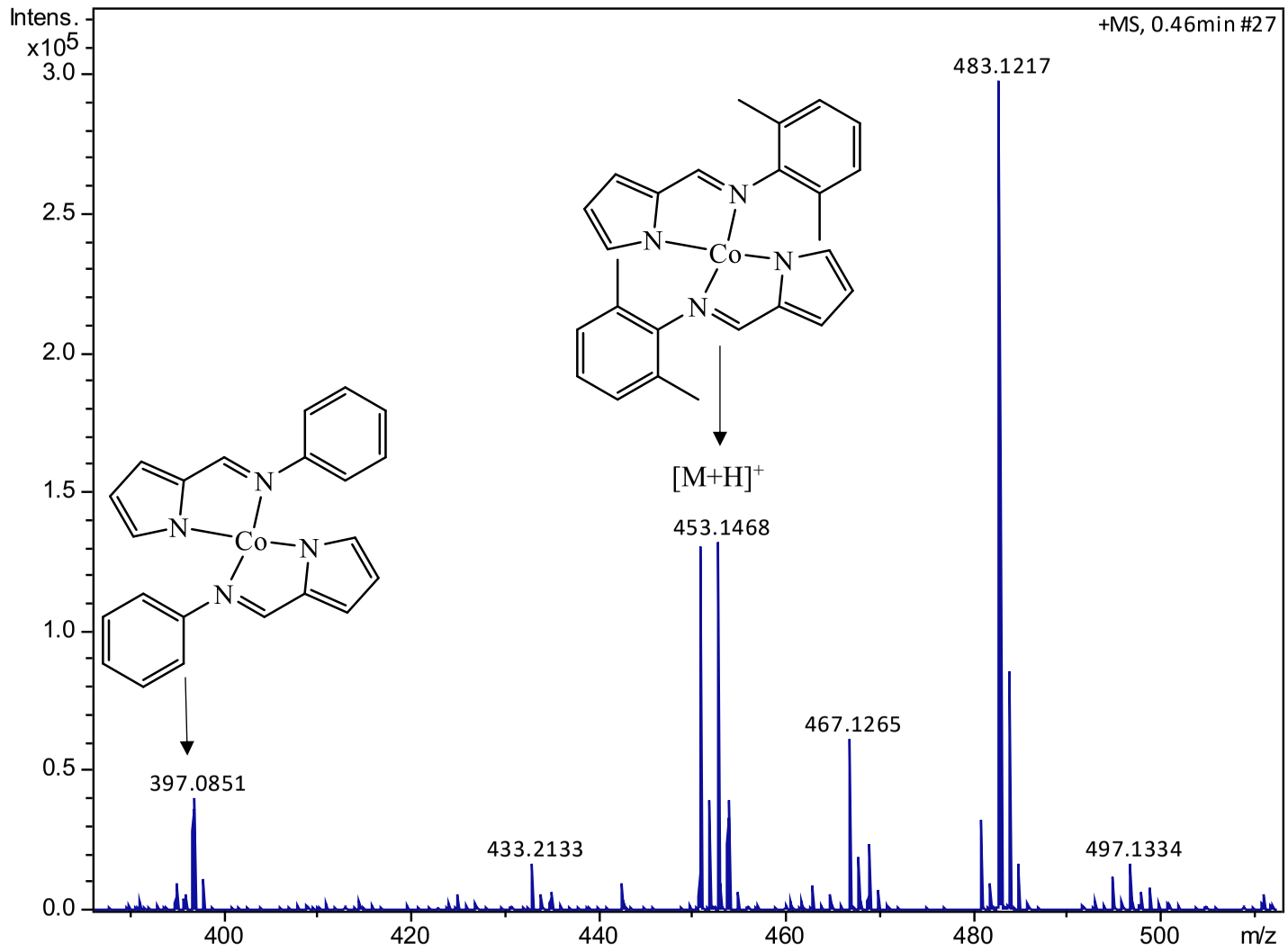
**C6:** FT-IR Spectrum



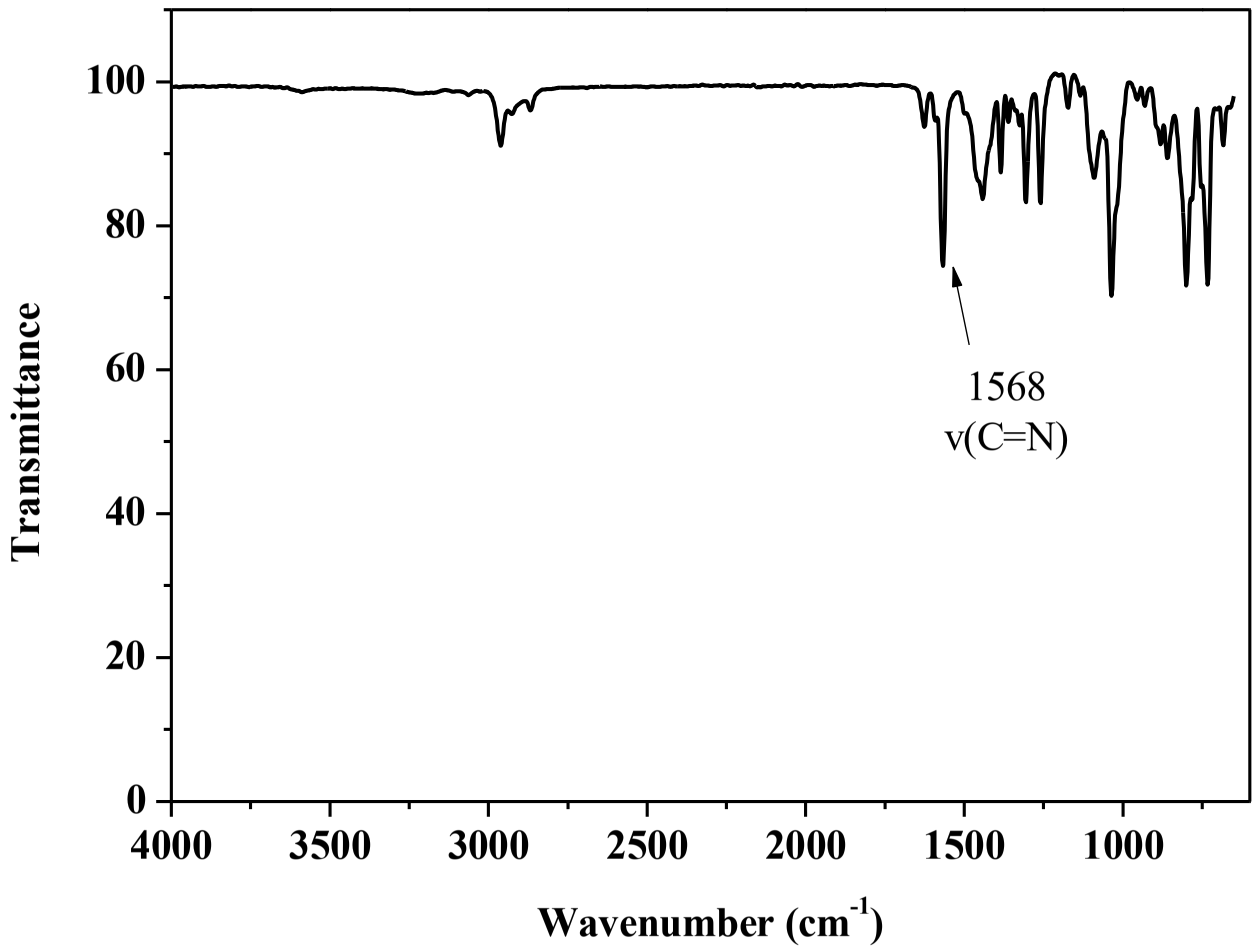
**C6:** UV-Vis spectrum (Toluene)



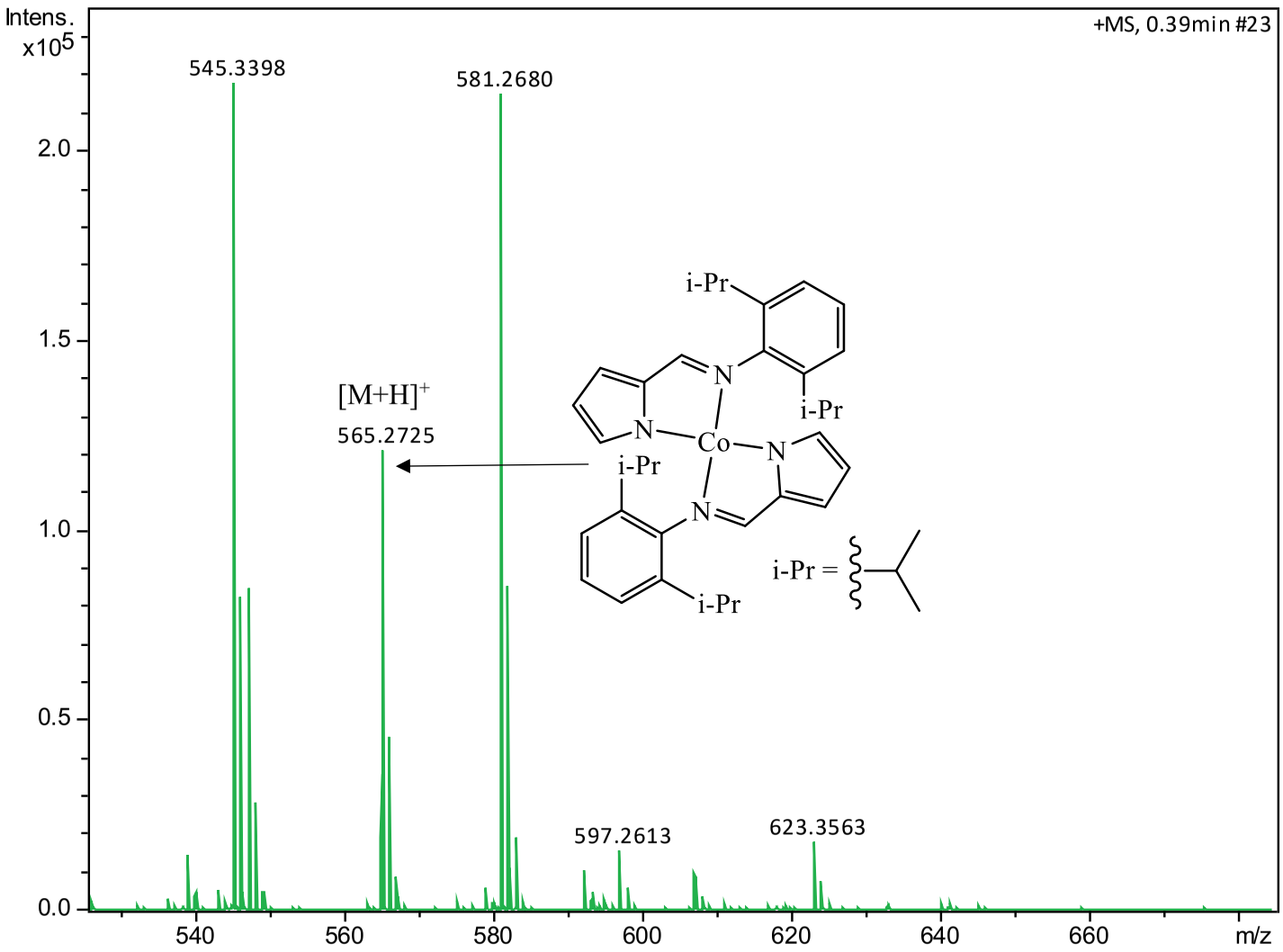
**C6:** ESI-MS (MeOH)



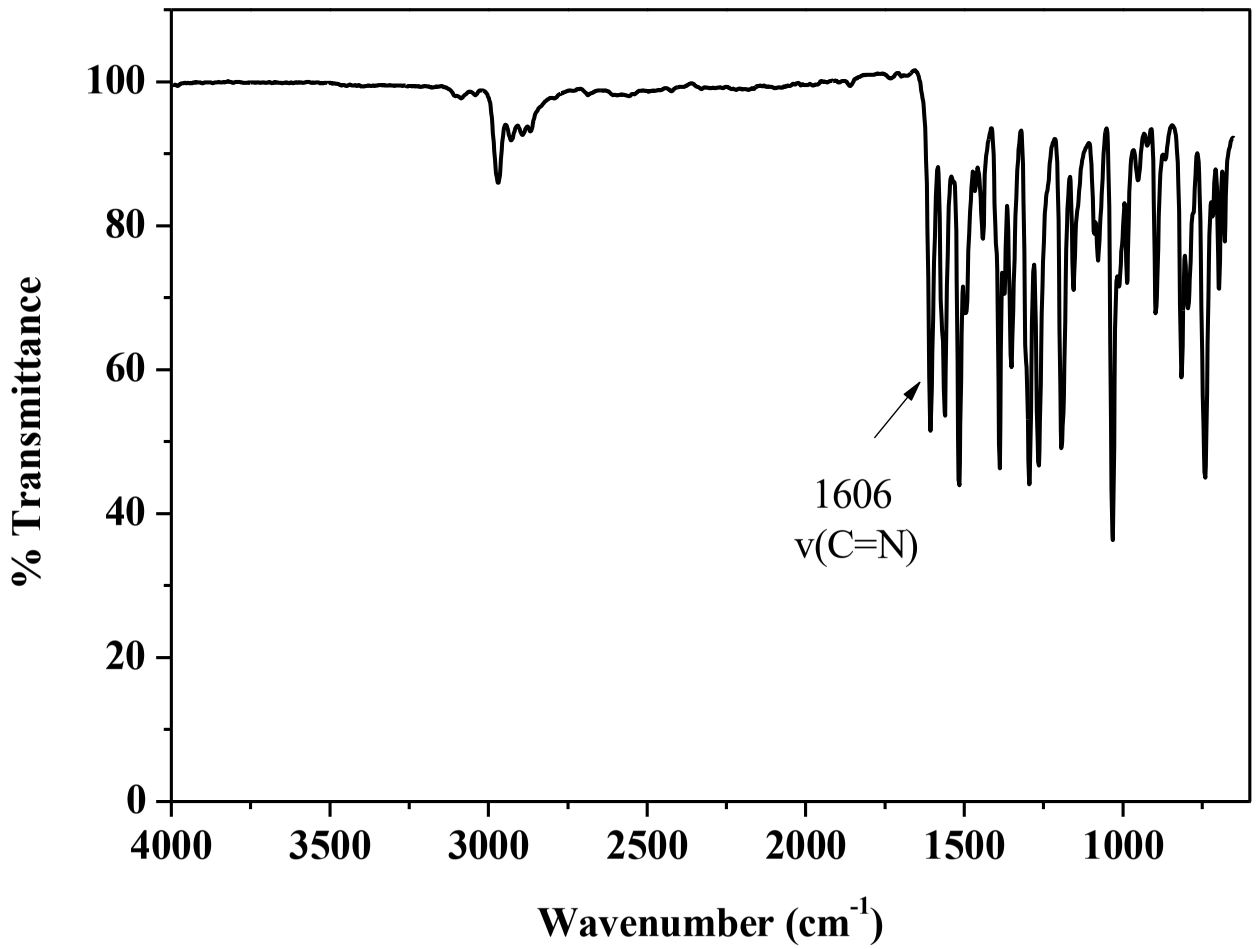
**C7:** FT-IR spectrum



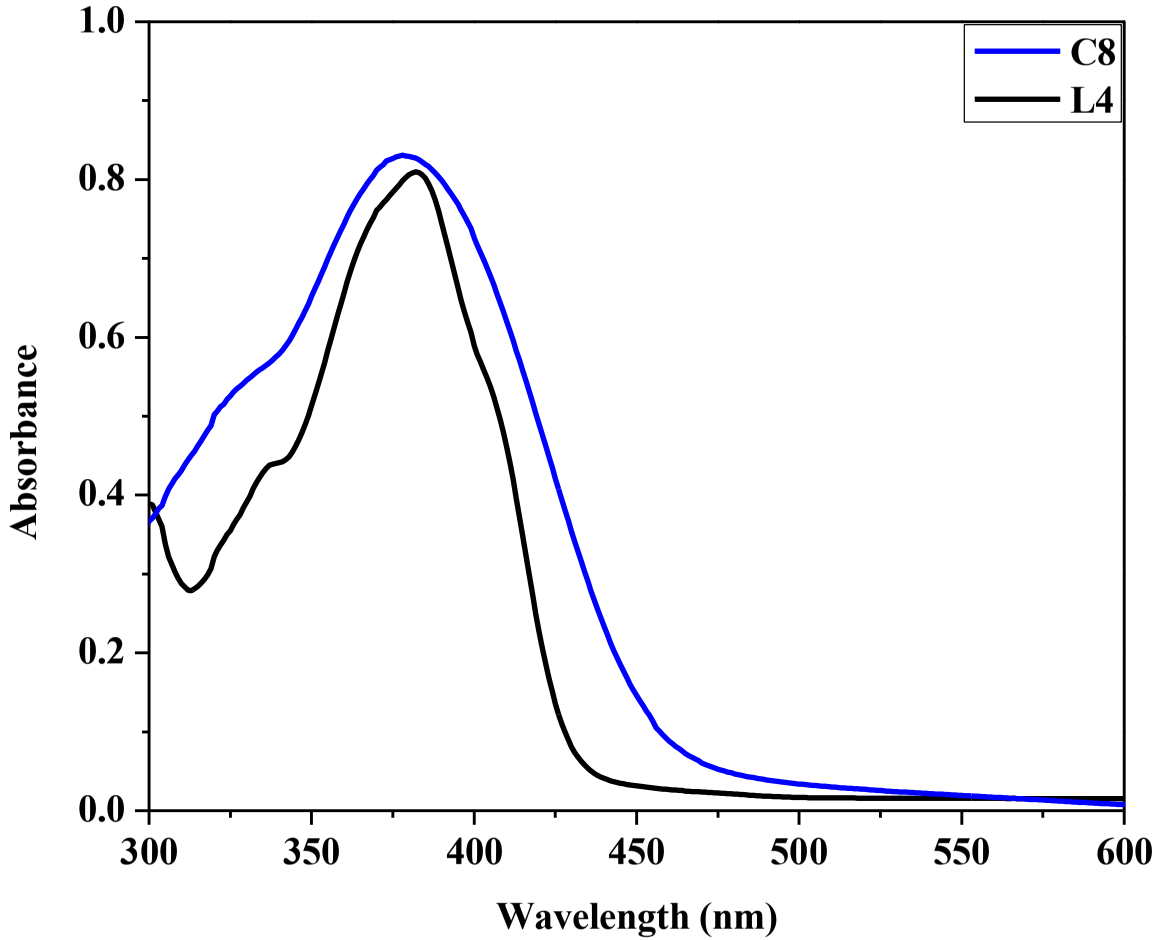
**C7:** ESI-MS (MeOH)



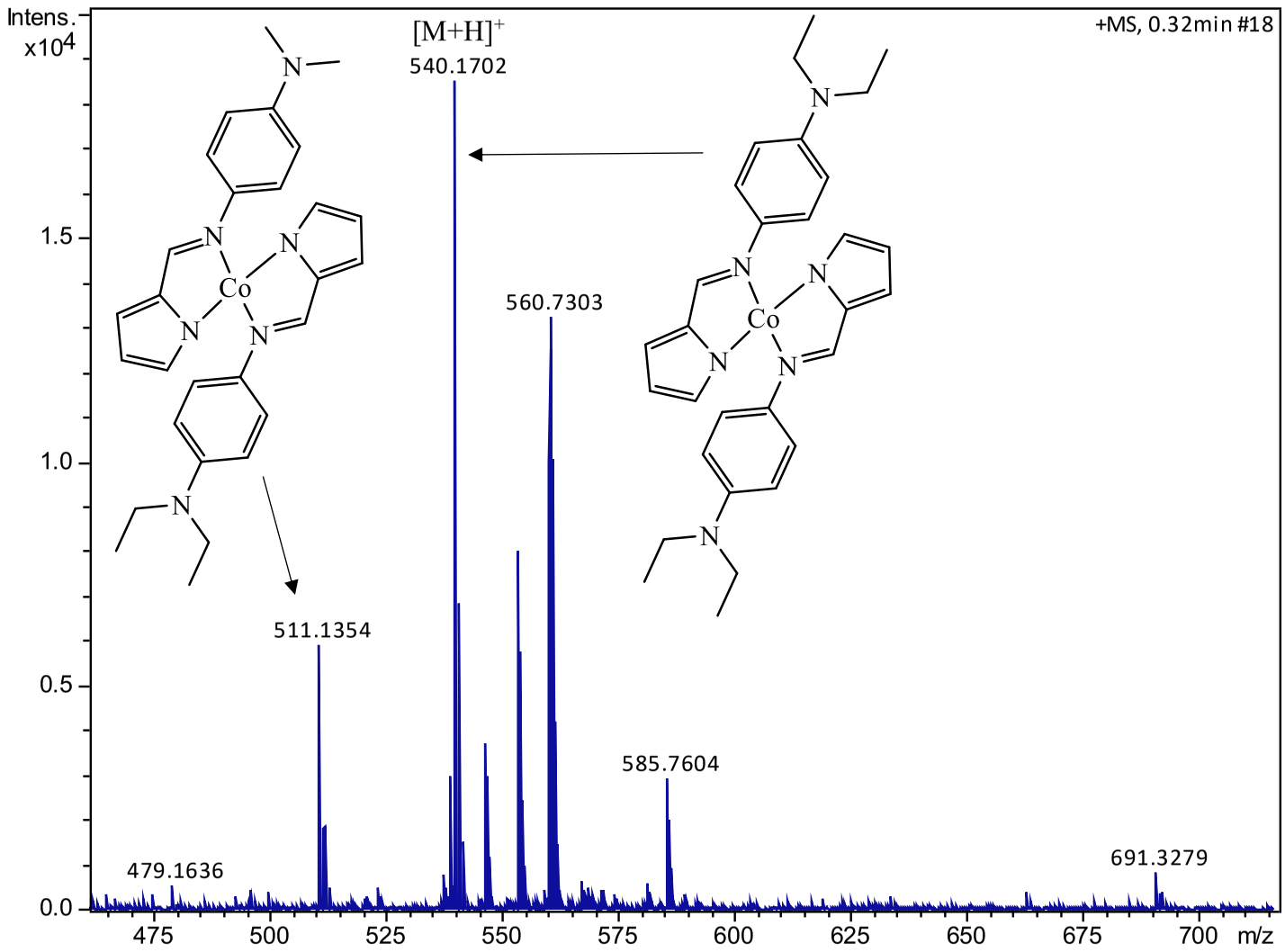
**C8:** FT-IR spectrum



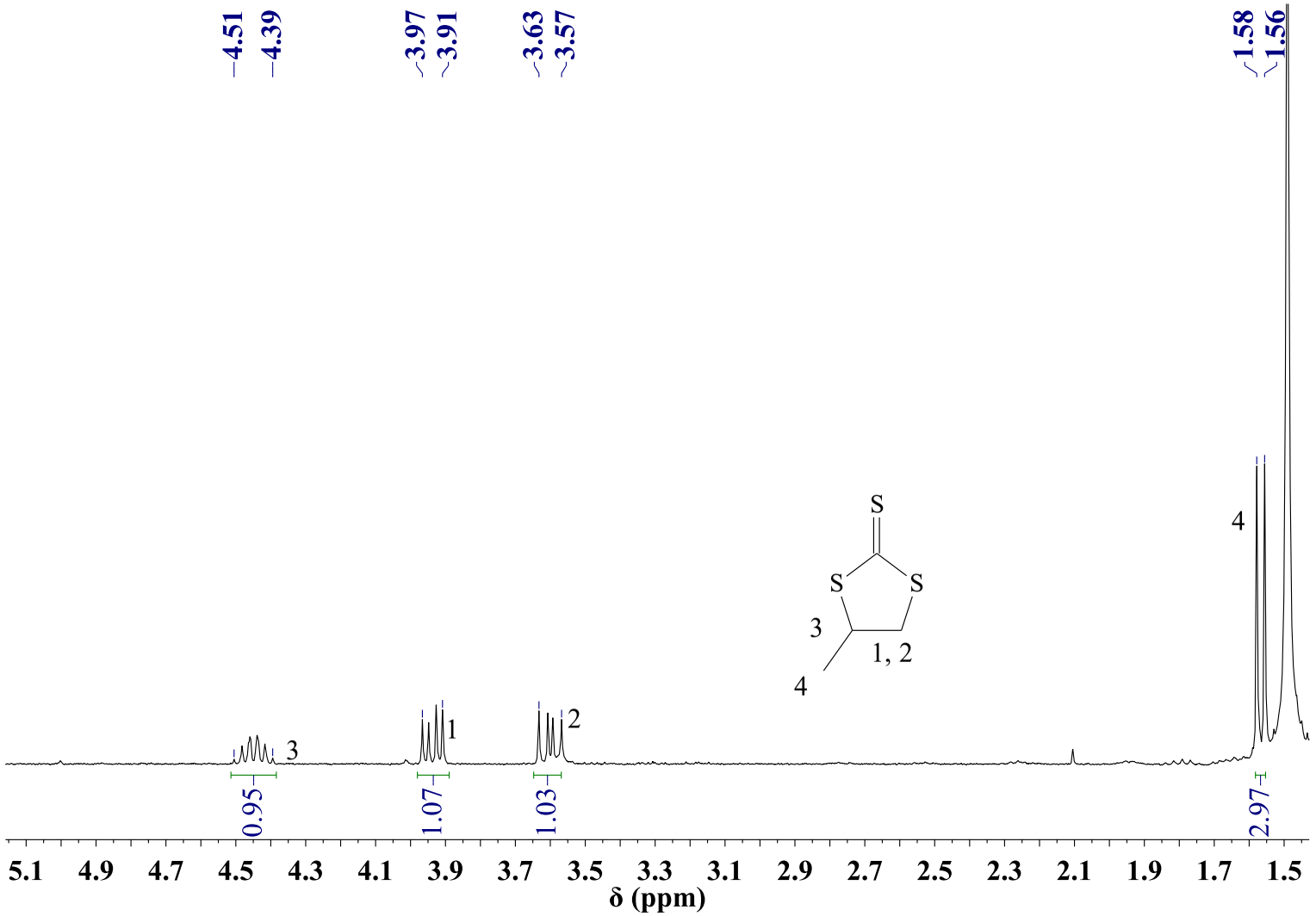
**C8:** UV-Vis spectrum (in Toluene)



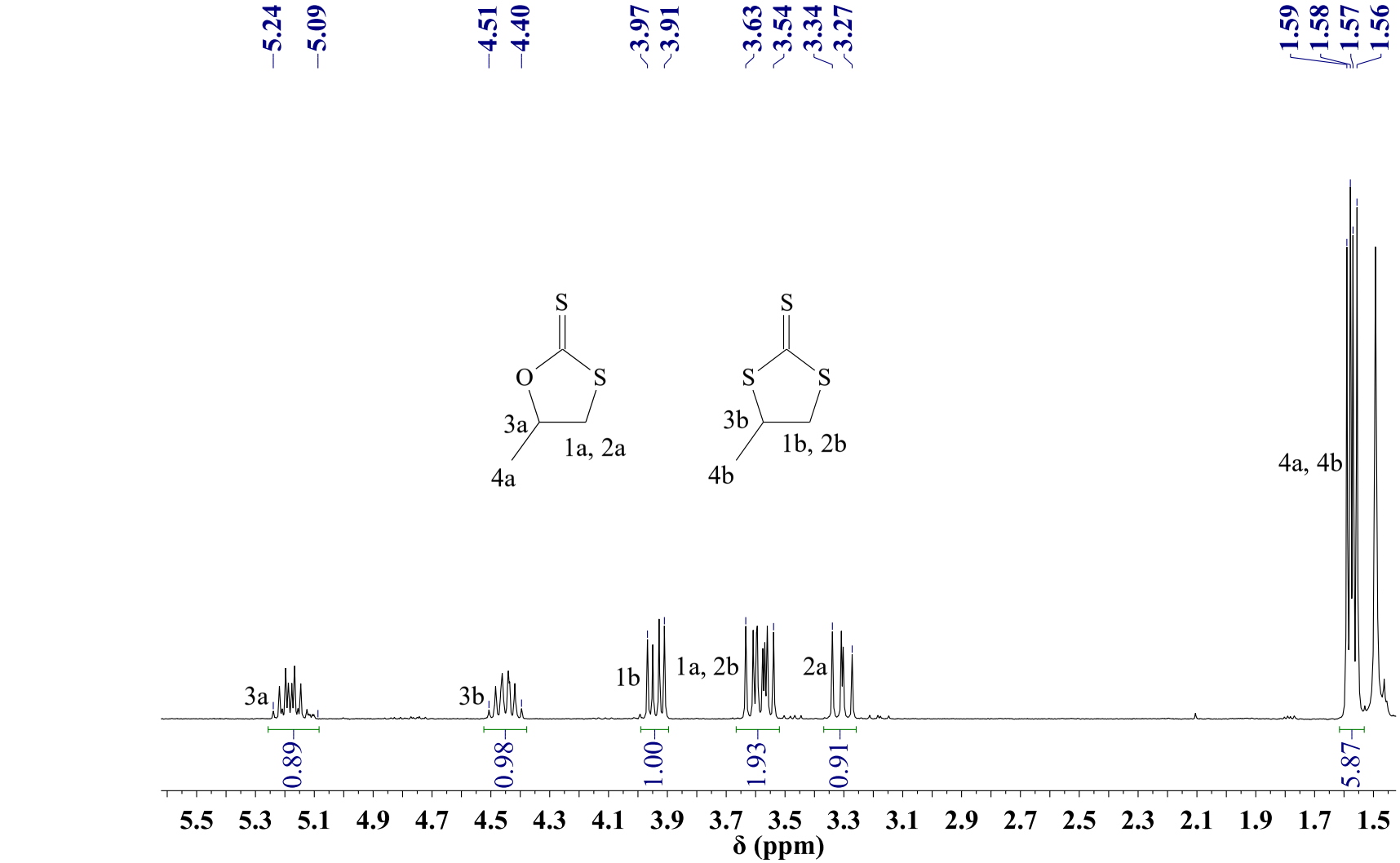
**C8:** ESI-MS (MeOH)



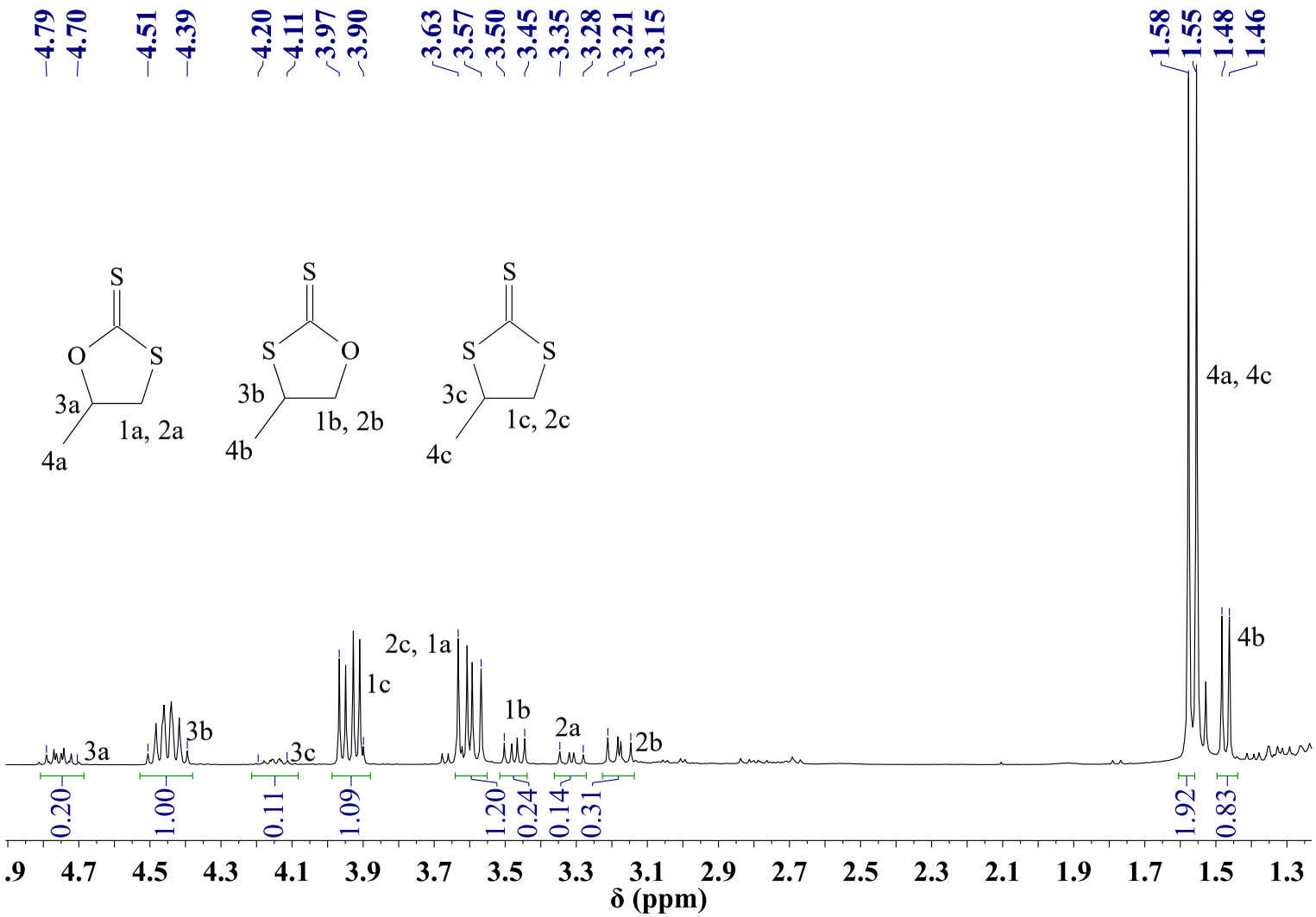
Entry **6**, **Table 2.1:** $^{1}$H NMR spectrum (yellow oil-like product obtained in the presence of [PPN]Cl) (in $CDCl_3$)



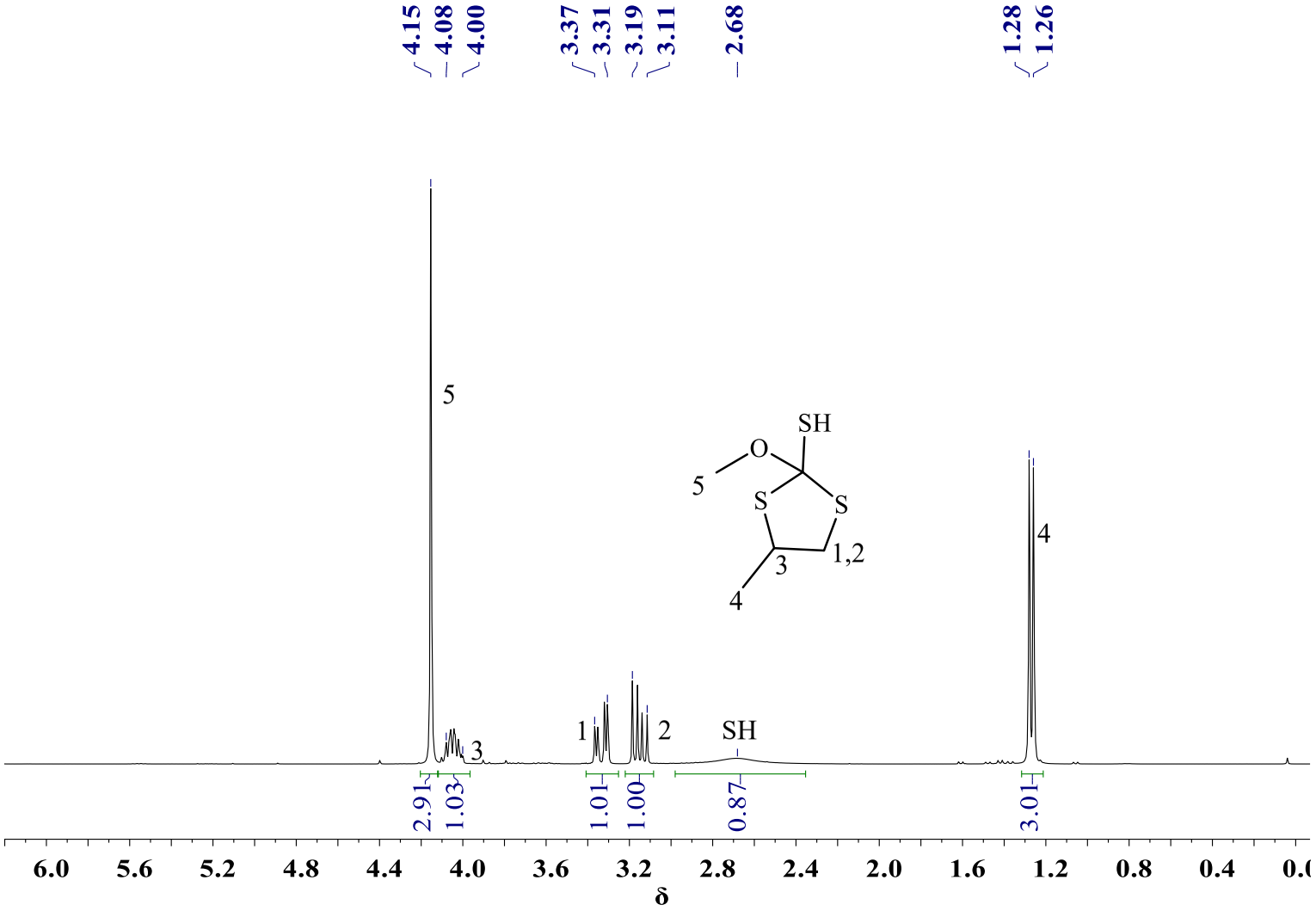
Entry **3**, **Table 2.1:** $^{1}$H NMR spectrum (yellow oil-like products obtained in the presence of **C1**/[PPN]Cl) (in $CDCl_3$)



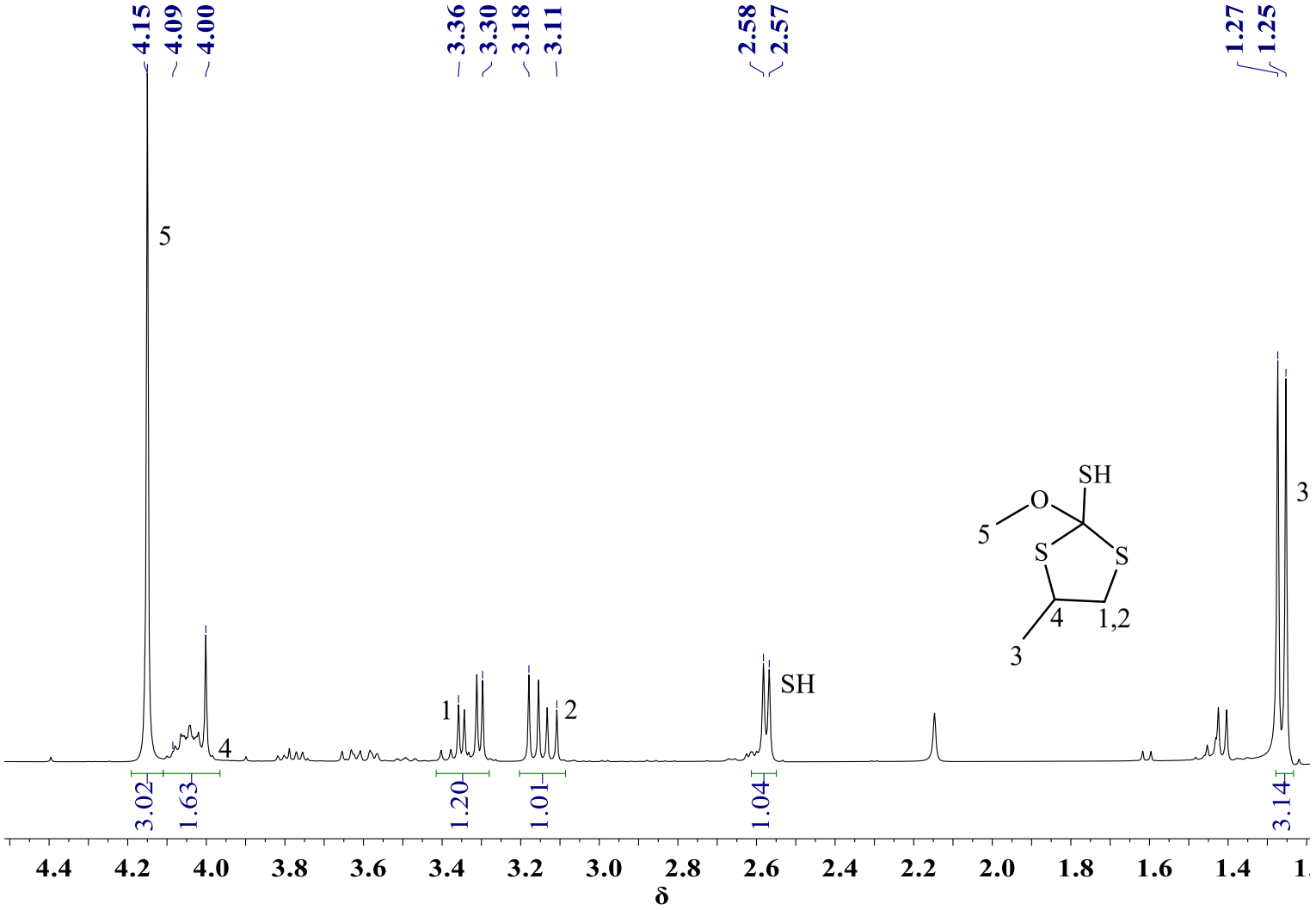
Entry **5**, **Table 2.1:** $^{1}$H NMR spectrum (yellow oil-like products obtained in the presence of **C1**/MeIm) (in $CDCl_3$)



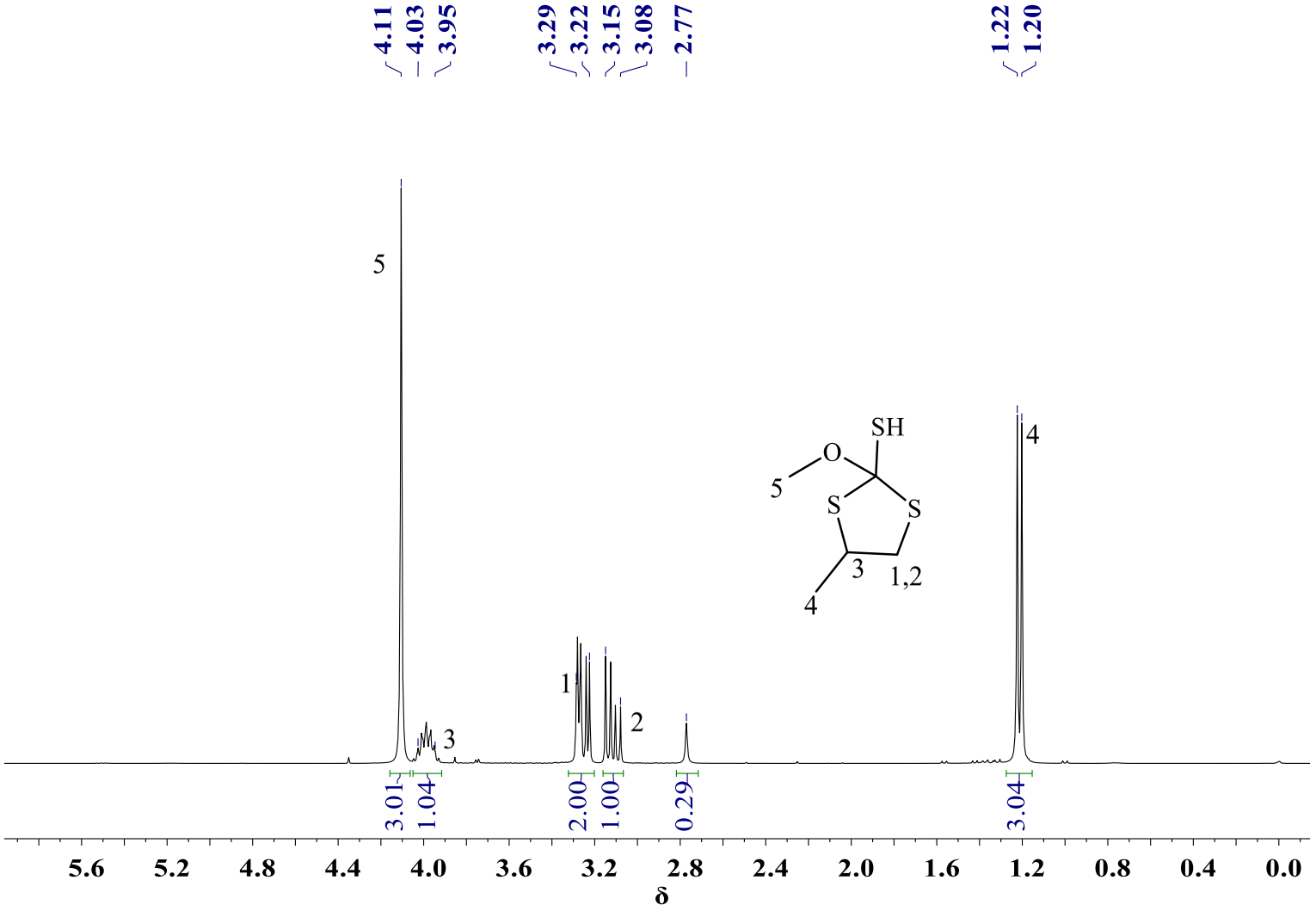
Entry **1**, **Table 2.2:** $^{1}H$ NMR spectrum (yellow oil-like products obtained in the presence of **C1**) (in $CDCl_3$)



Entry **2**, **Table 2.2:** $^{1}$H NMR spectrum (yellow oil-like products obtained in the presence of **C1**/TBAC) (in $CDCl_3$)



Entry **3**, **Table 2.2:** $^{1}$H NMR spectrum (yellow oil-like products obtained in the presence of **C1**/[PPN]Cl) (in $CDCl_3$)



Entry **4**, **Table 2.2:** $^{1}$H NMR spectrum (yellow oil-like products obtained in the presence of **C1**/DMAP) (in $CDCl_3$)

